Aus dem Institut für Pharmakologie und Toxikologie
Arbeitsgruppe: Prof. Dr. rer. nat. Kaomei Guan

Loss-of-function of leptin receptor impairs metabolism in human cardiomyocytes

DISSERTATIONSSCHRIFT

zur Erlangung des akademischen Grades

Doctor of Philosophy (Ph.D.)

vorgelegt

der Medizinischen Fakultät Carl Gustav Carus

der Technischen Universität Dresden

von

M. Sc. Anna Strano

aus Palermo, Italien

Dresden 2023

1. Gutachter: Prof. Dr. rer. nat. Kaomei Guan

   Medizinische Fakultät Carl Gustav Carus

   Technische Universität Dresden

2. Gutachter: Dr. Cynthia Andoniadou

   Centre for Craniofacial & Regenerative Biology

   King’s College London

Tag der mündlichen Prüfung:

gez.:

Anmerkung:

Die Eintragung der Gutachter und Tag der mündlichen Prüfung (Verteidigung) erfolgt nach Festlegung von Seiten der Medizinischen Fakultät Carl Gustav Carus der TU Dresden. Sie wird durch die Promovenden nach der Verteidigung zwecks Übergabe der fünf Pflichtexemplare an die Zweigbibliothek Medizin in gedruckter Form oder handschriftlich vorgenommen.

Contents

Abbreviations

a.a.	Amino acid
ACC	Acetyl coenzyme A carboxylase
ACS	Acyl coenzyme A synthetase
ADP	Adenosine diphosphate
AGEs	Advanced glycation end products
AgRP	Agouti-related protein
AKT	Protein kinase B
AMP	Adenosine monophosphate
AMPK	AMP-activated kinase
ARC	Hypothalamic arcuate nucleus
ATP	Adenosine triphosphate
cDNA	Complementary DNA
CM	Cardiomyocyte
c-Myc	V-myc myelocytomatosis avian viral oncogene homolog
CoA	Coenzyme A
CPT1	Carnitine palmitoyl transferase I
CRISPR	Clustered regularly interspaced short palindromic repeats
CRH	Cytokine receptor homology
Cas9	CRISPR-associated protein 9
crRNA	CRISPR RNA
cTnT	Cardiac troponin T
CVD	Cardiovascular disease
db	Diabetic
DHAP	Dihydroxyacetone phosphate
ECAR	Extracellular acidification rate
ECM	Extracellular matrix
ERK	Extracellular signal-regulated kinase
ESC	Embryonic stem cell
FABPpm	Fatty acid-binding protein
FAT/CD36	Fatty acid translocase
FATP	Fatty acid transporter protein
FCCP	Carbonyl cyanide 4-(trifluoromethoxy)phenylhydrazone
FNIII	Fibronectin type III

F16bP	Fructose 1,6-bisphosphate
gDNA	Genomic DNA
gRNA	Guide RNA
GLUT	Glucose transporter
GRB2	Growth factor receptor-bound protein 2
GSK3	Glycogen synthase kinase 3
G3PDH	Glyceraldehyde 3-phosphate dehydrogenase
G6P	Glucose 6-phosphate
HDL	High-density lipoprotein
HDR	Homologous-directed repair
hESC	Human embryonic stem cell
HF	Heart failure
HFpEF	HF with preserved ejection fraction
HFrEF	HF with reduced ejection fraction
HPRT	Hypoxanthine phosphoribosyltransferase
hiPSC	Human induced pluripotent stem cell
iPSC	Induced pluripotent stem cell
IgD	Immunoglobulin D
IL	Interleukin
iPSC-CM	IPSC-derived cardiomyocyte
IR	Insulin receptor
IRS	Insulin receptor substrate
ITRs	Inverted terminal repeats
IWP2	Inhibitor of WNT production 2
JAK2	Janus kinase 2
kDa	Kilodalton
KLF4	Krüppel-like factor 4
KOSR	Knockout serum replacement
LDL	Low-density lipoprotein
LEPR, OB-R	Leptin receptor
LEPROT	Leptin receptor overlapping transcript
LV	Left ventricular
MAPK	Mitogen-activated protein kinases
MCR	Melanocortin receptor
min	Minute

mTOR	Mammalian target of rapamycin
MVO_2	Mitochondrial O_2 consumption
NADH	Nicotinamide adenine dinucleotide
NHEJ	Nonhomologous end joining
NPY	Neurons co-expressing neuropeptide Y
NTD	N-terminal domain
ob	Obese
OB-RGRP	Leptin receptor gene-related protein
OCR	Oxygen consumption rate
OCT4	Octamer-binding transcription factor 4
Oligo	Oligomycin
PAM	Protospacer adjacent motif
PCR	Polymerase chain reaction
PDH	Pyruvate dehydrogenase
PDK	Pyruvate dehydrogenase kinase
PEP	Phosphoenolpyruvate
PI3K	Phosphoinositide-3-kinase
POMC	Pro-opiomelanocortin
PPAR	Proliferator-activated receptor
PTC	Premature termination codon
PTP1B	Protein tyrosine phosphatase 1B
qPCR	Quantitative real-time polymerase chain reaction
RAAS	Renin-angiotensin-aldosterone system
ROS	Reactive oxygen species
RT	Room temperature
RT-PCR	Reverse transcription polymerase chain reaction
Ser	Serine
SH2	Src homology 2
SOCS3	Suppressor of cytokine signalling 3
SOX2	Sex determining region Y box 2
SR	Sarcoplasmic reticulum
STAT	Signal transducer and activator of transcription
TCA	Tricarboxylic acid
Tet-On 3G	Tetracycline-inducible gene expression systems
TGF-β	Transforming growth factor beta 1

Thr	Threonine
TNFα	Tumor necrosis factor alpha
tracrRNA	Trans-activating CRISPR RNA
Tyr	Tyrosine
T2DM	Type 2 diabetes mellitus
VLDL	Very low-density lipoprotein
WNT	Wingless and int
WT	Wild type
ZDF	Zucker diabetic fatty
2-DG	2-Deoxy-D-glucose
3PG	3-phosphoglyceric acid

List of figures

List of tables

1 Introduction

1.1 Obesity and diabetes

1.1.1 Obesity-related type 2 diabetes

Obesity and diabetes are emerging pandemics in the 21st century. Patients defined as obese present a body mass index (BMI) of 30 kg/m^2 or higher. Since 1975, global obesity prevalence has nearly tripled in adults and has risen even more dramatically in children and adolescents. In 2016, almost 39% (1.9 billion) of adults worldwide were overweight and 13% (> 650 million) were obese. The prevalence of obesity in children and young adolescents (aged 5–19 years) has risen from 4% in 1975 to 18% in 2016 (WHO, 2021). A common co-morbidity of increased body weight and physical inactivity is type 2 diabetes mellitus (T2DM), which represents 90-95% of all diagnosed diabetes cases in adults. The frequency of diabetes is increasing in parallel with the increase in cases of obesity. According to Ford et al., for every kilogramme of weight gain, the risk of diabetes increases between 4.5 and 9% (Ford *et al.*, 1997). In 2021, diabetes was affecting 10.5% (536.6 million) among adults (aged 20–79) worldwide and potentially will affect 12.2% (783.2 million) in 2045 (Sun *et al.*, 2022). The relative risk for a given obese patient (BMI ≥ 35.0) to develop T2DM during a 10-year period is about 20 folds more likely for both women and men when compared to their same-sex peers with a BMI between 18.5 and 24.9 (Field *et al.*, 2001). Hence, to illustrate the interdependence of these diseases the term ‘diabesity’ has been coined (Zimmet *et al.*, 2001).

The mechanisms involved in obesity and T2DM development are quite complex. T2DM is mainly caused by two factors: the impairment of insulin secretion by pancreatic β-cells and the inability of insulin-sensitive tissue to respond appropriately to insulin, a condition also known as insulin resistance (Roden & Shulman, 2019). In an excessive nutritional state, such as obesity, hyperglycaemia and hyperlipidaemia are frequently present, favouring insulin resistance and chronic inflammation. Under these conditions, higher amounts of non-esterified fatty acids, glycerol, hormones, and pro-inflammatory cytokines are released by adipose tissue. On the one hand, pancreatic β-cells are subjected to toxic pressures including endoplasmic reticulum stress, hypoxia and metabolic/oxidative stress, which, at long last, result in loss of islet integrity (Christensen & Gannon, 2019; Wondmkun, 2020). Defects in insulin synthesis and secretion by pancreatic β-cells lead to the dysregulation of glucose homeostasis. On the other hand, insulin resistance contributes to increased

glucose production in the liver and decreased glucose uptake primarily in the muscle, liver, and adipose tissue, which are tissues responsible for energy storage. When β-cell dysfunction and insulin resistance are present, hyperglycaemia is amplified leading to the progression of obesity-associated T2DM (Galicia-Garcia *et al.*, 2020).

1.1.2 Leptin and its role in obesity-related type 2 diabetes

In 1949, the discovery of the autosomal recessive mutation in the so-called obese (*ob*) gene in mice revealed the existence of a gene essential for the control of feeding, metabolism, and body weight (Ingalls *et al.*, 1950). The *ob* gene was first isolated in 1994 and named leptin after the Greek word *leptós*, meaning “thin”. Positional cloning of the *ob* gene revealed the presence of a nonsense mutation in the coding region of the leptin protein in the *ob/ob* mouse (Zhang *et al.*, 1994). Leptin is a 16 KDa protein mainly produced by the adipose tissue in approximate proportion to their triglyceride stores, making more leptin circulating in the blood with the increased amount of body fat (Frederich *et al.*, 1995). Circulating leptin levels are correlated to body fat mass both in normoglycemic and in diabetic patients (Ahrén *et al.*, 1997; Haffner *et al.*, 1997). The potent effects of leptin on glucose homeostasis are mediated in large part by pro-opiomelanocortin (POMC)-expressing neurons within the hypothalamic arcuate nucleus (ARC) (Berglund *et al.*, 2012; Huo *et al.*, 2009). In addition, a bidirectional feedback loop that is also known as “adipoinsular axis” between adipose tissue and β-cells is mediated by insulin and leptin, respectively. Insulin stimulates adipogenesis and increases the production of leptin by the adipose tissue. On the other hand, leptin by negative feedback reduces both insulin synthesis and secretion. The role of leptin is mediated by the autonomic nervous system and by its direct action on β-cells. As a result, circulating insulin levels are reduced by leptin (Kieffer & Habener, 2000; Paz-Filho *et al.*, 2012). Leptin also diminishes hepatic glucose production, enhances insulin sensitivity, and diminishes glucagon levels (Seufert, 2004). Additionally, leptin prevents abnormal accumulation of triglycerides in non-adipose tissues, which leads to a deleterious condition known as lipotoxicity (Unger *et al.*, 2010). Given its ability to improve insulin sensitivity, lower plasma lipids, and reduce body weight, leptin was considered a suitable candidate for T2DM therapy. However, in obese subjects with T2DM, recombinant methionyl human leptin was ineffective in ameliorating insulin sensitivity (Mittendorfer *et al.*, 2011), nevertheless it did result in marginal improvements in HbA1c levels (Moon *et al.*, 2011). The failure of leptin to improve glucose homeostasis in these clinical trials may indicate leptin resistance since obese individuals are typically hyperleptinemic (Caro *et al.*, 1996; Sinha *et al.*, 1996). Mechanisms underlying the development of leptin resistance include mutations

in the genes encoding leptin and leptin receptor (LEPR), reduced expression of LEPR at the plasma membrane level, impaired LEPR function and signalling, or alterations in the transport of leptin across the blood-brain barrier (Gruzdeva *et al.*, 2019; Myers *et al.*, 2012). Currently, leptin therapy is only effective to treat obesity and the metabolic imbalance in patients who have congenital leptin deficiency (Farooqi *et al.*, 1999; Farooqi & O'Rahilly, 2009). Considering leptin resistance, pre-clinical studies in mice have shifted the focus from exogenous leptin therapy to strategies that enhance endogenous leptin sensitivity (Clemmensen *et al.*, 2014; Lee *et al.*, 2016; Liu *et al.*, 2015; Muller *et al.*, 2012; Roth *et al.*, 2008), suggesting that new therapeutic tools to restore leptin sensitivity could offer a new strategy to promote weight loss in obese patients and to treat obesity-related complications (Balland *et al.*, 2019; Zhao *et al.*, 2019).

1.1.3 Complications of type 2 diabetes

In the long run, T2DM is a disease that adversely affects the function of almost every organ in the human body. Thus, the biggest problem for diabetic patients is the long-term complications that accompany the disease (Turner *et al.*, 2010). The complications of T2DM can be distinguished into macrovascular and microvascular complications. Microvascular complications include eye damage (diabetic retinopathy), renal system disease (nephropathy), and nervous system disease (neuropathy). Macrovascular complications comprise cardiovascular disease (CVD), stroke, and peripheral arterial disease (Deshpande *et al.*, 2008). CVDs are the primary cause of death in diabetic patients, who have a 2–5 times higher risk of developing heart failure (HF) than age-matched non-diabetic patients, independent of other comorbidities (Schocken *et al.*, 2008). Diabetic patients frequently present atherosclerosis and hypertension both of which contribute to coronary artery disease and peripheral arterial disease, affecting ultimately the heart performance (Petrie *et al.*, 2018). However, there is another type of heart disease in T2DM patients, which is described as “diabetic cardiomyopathy” and is not associated with other cardiovascular risk factor that results in abnormal myocardial structure and impaired cardiac function. With an incidence of 19–26% to develop HF, cardiovascular remodelling processes resulting in diabetic cardiomyopathy are a major cause of disease-related deaths in patients with T2DM (Jia *et al.*, 2018).

1.2 Cardiac energy metabolism and diabetic cardiomyopathy

1.2.1 Metabolic flexibility in cardiomyocytes

Cardiomyocytes (CMs) with its continuous contraction require high energy demand for generating the necessary mechanical force, and for maintaining cellular homeostasis during the process. To perform their function, CMs rely on the use of multiple substrates, such as fatty acids, carbohydrates, and amino acids (Jia *et al.*, 2016; Lopaschuk *et al.*, 2010). The ability to switch between different substrates under physiological conditions is described as "metabolic substrate flexibility" (Vallerie & Bornfeldt, 2015). About 60–70% of the total amount of ATP required for adequate contraction of the heart is generated by mitochondrial oxidation of fatty acids (van der Vusse *et al.*, 1992). The remaining part is mainly obtained by oxidation of carbohydrates, such as glucose and lactate (Neely & Morgan, 1974; Taegtmeyer, 1985). Fatty acids can translocate into CMs through passive diffusion across the plasma membrane (Rose *et al.*, 1990), however, exogenous fatty acid uptake is mostly facilitated by protein-mediated carrier system consisting of three fatty acid transporters: fatty acid translocase (FAT/CD36), fatty ACS (acyl CoA synthetase) known also as FATP (fatty acid transporter proteins), and the plasma membrane form of fatty acid-binding protein (FABPpm) (van der Vusse *et al.*, 2000). The transport of fatty acids into CMs is regulated by both insulin and contraction (Schwenk *et al.*, 2008). Whereas the significant increase in fatty acid import is mainly CD36-dependent, insulin effect on fatty acid uptake is moderate (Luiken *et al.*, 2002). Cardiac performance induces intracellular increase of AMP/ATP ratio which activates the intracellular energy-sensing AMP-activated kinase (AMPK) (Hardie & Carling, 1997). Activation of AMPK promotes two different mechanisms: the translocation of CD36 to the sarcolemma (Habets *et al.*, 2007; Luiken *et al.*, 2003), and the phosphorylation and consequent inhibition of acetyl coenzyme A (acetyl-CoA) carboxylase (ACC) leading to reduced malonyl-CoA levels. The intracellular reduction of malonyl-CoA subsequently activates carnitine palmitoyl transferase I (CPT1) (Lopaschuk, 2001), the enzyme responsible for the first step in mitochondrial fatty acid import (Fig. 1). Contraction-mediated AMPK-activation results in an increase in exogenous fatty acid uptake, which are mainly used in mitochondrial β-oxidation. Upon fatty uptake into CMs, they are rapidly activated by fatty ACS-mediated esterification to acyl-CoA (Groot *et al.*, 1976) to prevent the potential toxicity due to the high intracellular accumulation of free fatty acids (Ellis *et al.*, 2011; Paul *et al.*, 2014). Finally, mitochondrial fatty acids undergo β-oxidation to produce acetyl-CoA, which is then utilized by the tricarboxylic acid (TCA) cycle for ATP production. Similar to fatty acid uptake, glucose uptake is facilitated by transmembrane transporters,

glucose transporters GLUT-1 and GLUT-4. These transporters are translocated from intracellular stores to the sarcolemma via vesicular trafficking and in response to insulin-mediated AKT activation and cardiac contraction (Mueckler, 1994; Schwenk *et al.*, 2008; Watson & Pessin, 2006). GLUT-4 is the insulin-sensitive transporter, which is responsible for the high increase in cardiac glucose uptake after insulin treatment or following a sudden increase of energy demand, while GLUT-1 is known as the basal cardiac glucose transporter due to its predominantly sarcolemma location (Abel, 2004; Zorzano *et al.*, 1997). Furthermore, AMPK activation can also enhance cardiac glucose uptake via GLUT-4 translocation (Russell *et al.*, 1999). In addition, an important role in cardiac fuel selection is played by metabolites derived from the catabolism of specific energy substrates. Thus, glycolysis leads to increased acetyl-CoA production from pyruvate and subsequent malonyl-CoA inhibition of CPT1, ultimately decreasing fatty acid β-oxidation (Awan & Saggerson, 1993; Lopaschuk, 2001; Saddik *et al.*, 1993). On the other hand, both the acetyl-CoA and nicotinamide adenine dinucleotide (NADH) products of fatty acid oxidation can allosterically activate pyruvate dehydrogenase kinase (PDK) (Orfali *et al.*, 1993) and directly inhibit pyruvate dehydrogenase (PDH) activity (Cooper *et al.*, 1975; Kerbey *et al.*, 1976), reducing PDH flux and glucose oxidation. The TCA metabolism of the fatty acid-derived acetyl-CoA to citrate blocks glycolysis by allosterically inhibiting phosphofructokinase 1 (Garland *et al.*, 1963). Thus, in the presence of fatty acid oxidation, glucose oxidation, glycolysis, and glucose uptake are inhibited (Randle *et al.*, 1964; Wheeler *et al.*, 1994). Therefore, the inherent flexibility of the heart to switch and use different types of energy substrate is critical for maintaining consistent ATP production with ever changing fuel availability (Pascual & Coleman, 2016) (Fig. 1).

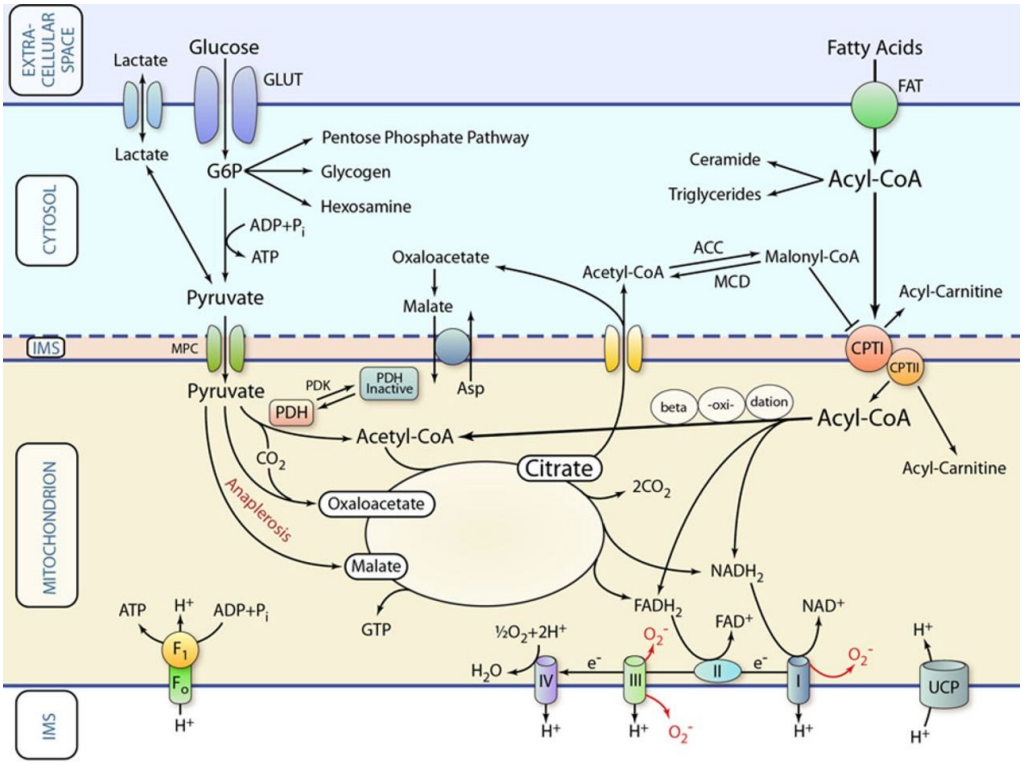

Figure 1. Schematic representation of classic pathways of cardiac metabolism. Energy substrates are transported across the extracellular membrane into the cytosol and are metabolized in different ways. For oxidation, the respective metabolic intermediates, such as pyruvate or acyl-coenzyme A (acyl-CoA), are transported across the inner mitochondrial membrane by specific transport systems. Inside the mitochondria, substrates are oxidized or carboxylated (anaplerosis) and used by the tricarboxylic acid cycle for the generation of reducing equivalents such as reduced nicotinamide adenine dinucleotide ($NADH_2$), reduced flavin adenine dinucleotide ($FADH_2$). The reducing equivalents are utilized by the electron transport chain to generate a proton gradient, which in turn is used for the production of ATP. The figure is taken from (Doenst *et al.*, 2013).

1.2.2 Functional and structural changes of the heart in diabetic cardiomyopathy

Although diabetic cardiomyopathy is usually asymptomatic in very early stages, its progression results in pathological cardiac remodelling. Patients with diabetic cardiomyopathy show left ventricular (LV) diastolic dysfunction and/or reduced ejection fraction, LV hypertrophy, and increased interstitial fibrosis (Jia *et al.*, 2016; Jia *et al.*, 2018; Lourenco *et al.*, 2018). The pathogenesis starts at a subcellular level with CM hypertrophy and develops as a clinical manifestation of LV hypertrophy (Bluemke *et al.*, 2008). The next pathophysiological change is an increase in interstitial and perivascular fibrosis which promotes the thickening of the myocardial capillary basement membrane (Velic *et al.*, 2013; Voulgari *et al.*, 2010). The combined effect of hypertrophy and fibrosis causes LV stiffness and impaired LV relaxation. This pathophysiological condition progresses in diastolic, but not systolic dysfunction at early stages, which gradually develops into severe diastolic HF

with preserved ejection fraction (HFpEF). At later stages, these patients develop systolic dysfunction and HF with reduced ejection fraction (HFrEF) (Poetsch *et al.*, 2020).

1.2.3 Mechanisms involved in diabetic cardiomyopathy development

Although the diabetic heart is clinically well characterized presenting diastolic dysfunction with HFpEF, the underlying pathogenic mechanisms of diabetic cardiomyopathy development remain unclear. Various mechanisms are proposed to explain the pathogenesis of diabetic cardiomyopathy. These factors include metabolic dysfunction, cardiac fibrosis, increase in oxidative stress and inflammation, CM death, and activation of the renin-angiotensin-aldosterone system (RAAS) (Fig. 2) (Jia *et al.*, 2016).

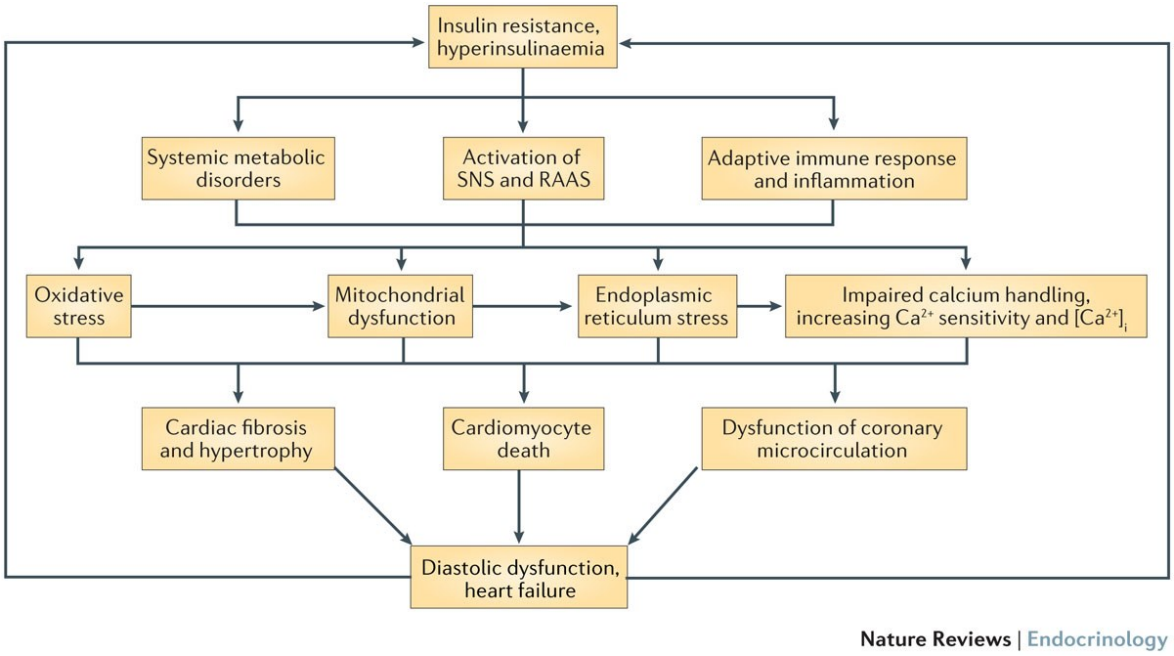

Figure 2. The development and progression of diabetic cardiomyopathy. Insulin resistance and hyperinsulinemia increase systemic metabolic disorders, activate RAAS (renin-angiotensin-aldosterone system), enhance oxidative stress, mitochondrial dysfunction and endoplasmic reticulum stress and impair calcium homeostasis. These effects result in cardiac fibrosis, hypertrophy, dysfunction, cardiomyocyte (CM) death, and eventually heart failure. Furthermore, these pathophysiological conditions in CMs underlie the risk factors for insulin resistance and hyperinsulinemia, which can result in a potentially vicious cycle. The figure is taken from (Jia *et al.*, 2016).

During diabetic cardiomyopathy development, upregulation in the expression of profibrotic factors, such as transforming growth factor beta 1 (TGF-β) and connective tissue growth factor, can promote the increased extracellular matrix (ECM) protein deposition (D'Souza *et al.*, 2011; Mizushige *et al.*, 2000; Way *et al.*, 2002). At the same time, a decrease in the activity of ECM-degrading enzyme metalloproteinase can lead to ECM accumulation

causing fibrosis (Westermann *et al.*, 2007). In addition to ECM protein deposition, metabolic dysfunction is one of the prevalent causes for increased LV mass in diabetic patients leading to heart failure (Regan, 1983).

Under normal physiological conditions, the adult heart utilizes fatty acids as its primary source and increasingly relies on glucose during periods of ischemia or increased workload maintaining a metabolic flexibility (Mishra & Rath, 2005). Hyperglycemia and insulin resistance lead to loss of metabolic flexibility, thus altered substrate supply and utilization by CMs could be the primary injury in the pathogenesis of diabetic cardiomyopathy (Rodrigues *et al.*, 1998). A major restriction to glucose utilization in the diabetic heart is the diminished glucose uptake due to reduced GLUT-1 and GLUT-4 expression and translocation to the plasma membrane (Russell *et al.*, 1998). Another mechanism of reduced glucose oxidation is driven by high circulating fatty acids which increase fatty acid uptake in CMs reducing PDH flux (Harmancey *et al.*, 2012; Liedtke *et al.*, 1988). This switch in energy source is accompanied by impaired oxidative phosphorylation and enhanced mitochondrial reactive oxygen species (ROS) generation. This increase in mitochondrial uncoupling leads to augmented mitochondrial O_2 consumption (MVO_2), however, this process is not accompanied by a proportional increase in ATP synthesis, leading to a decrease in cardiac energy efficiency (Bugger & Abel, 2010; Rider *et al.*, 2013). Furthermore, the inability to switch to glucose oxidation makes the heart susceptible to damage and dysfunction under condition with increased energy demand or hypoxia such as in myocardial ischemia (Lopaschuk & Stanley, 1997).

Persistent hyperglycemia, which is a common aspect in patients with T2DM, impairs cardiac structure and function, resulting in increased ROS production, DNA damage and inhibition of glyceraldehyde 3-phosphate dehydrogenase (G3PDH) activity, ultimately leading to the formation of advanced glycation end products (AGEs) (Avendano *et al.*, 1999). This various group of compounds is produced by a non-enzymatic reaction between carbonyl groups of reducing sugars and free amino groups of proteins, lipids, and nuclei acids. Cross-bridge formation between AGEs and structural proteins including collagen promotes myocardial fibrosis and impaired passive relaxation (Regan, 1983).

Patients with T2DM often present hyperlipidemia due to increased lipid synthesis in hepatocytes and increased lipolysis in adipocytes promoting high circulating fatty acid levels and triglycerides. Excessive accumulation of fatty acids is detrimental to CMs, as it can directly influence CM metabolism and contractility. Moreover, CMs are not equipped to store lipids. This highlights the concept of lipotoxicity as a mechanism for promoting diabetic cardiomyopathy development through a decrease in CM physiological autophagy and an

increase in apoptosis (Levelt *et al.*, 2018; Mandavia *et al.*, 2013). Thus, impaired glycolysis, pyruvate oxidation, lactate uptake, and a greater dependence on fatty acids as a source of acetyl-CoA lead to a perturbation of myocardial bioenergetics and contraction/relaxation coupling (Rodrigues *et al.*, 1998). Increased levels of free fatty acid storage and visceral adipose tissue lead to systemic and cardiovascular inflammatory cytokine expression. Upregulation of several proinflammatory cytokines, such as tumor necrosis factor (TNFα), interleukins 6 (IL-6) and 8 (IL-8), and monocyte chemotactic protein 1, is characteristic of the diabetic heart. These cytokines not only affect CMs but also other cardiac cell populations, including endothelial cells, fibroblasts, and smooth muscle cells which all contribute to pathological remodeling of the diabetic heart (Jia *et al.*, 2018). Cardiac oxidative stress, lipotoxicity, inflammation, and the accumulation of misfolded proteins cause endoplasmic reticulum stress, inducing the unfolded protein response, which ultimately increase cell apoptosis and autophagy (Jia *et al.*, 2016). Moreover, hyperglycaemia activates RAAS that has various detrimental effects on CMs. High intracellular angiotensin II levels result in hypertrophy and proliferation of cardiac fibroblasts (Kumar *et al.*, 2012), contributing in combination with oxidative stress and inflammation to myocardial damage (Kurdi & Booz, 2011). Despite great research efforts, the precise mechanism by which the altered cardiac metabolism is linked to the pathophysiology of the diabetic heart is still unresolved. One of the major events appears to be the increased reliance of the heart on lipid substrates. This may be a result of increased availability of fatty acids in circulation in T2DM. Elevated levels of free fatty acids in the CM directly and indirectly impact multiple signalling pathways, including inhibition of insulin signalling, suppression of glycolysis, and activation of the enzyme important for fatty acid oxidation, all of which force the heart in a metabolically rigid condition. The diabetic heart thus can no longer efficiently use glucose in response to elevated workload demand, making it more vulnerable to external insults. Moreover, oxidation of fat results in other maladaptive changes, including generation of toxic fatty acid intermediates, and accumulation of lipids in the myocardium. As a consequence of these changes, cardiac function gradually impairs, finally manifesting itself as diabetic cardiomyopathy.

1.3 Leptin signalling

1.3.1 Distribution and identification of LEPR isoforms

The leptin receptor (LEPR, or OB-R) is a single trans-membrane spanning receptor belonging to the class I cytokine receptor family (Tartaglia *et al.*, 1995). The gene encoding

the leptin receptor, both in mice (*db*) and in humans (*LEPR*), is regulated by a dual promoter: the *B219/OB-R* promoter generates *db*/*LEPR* transcripts only, while the *OB-RGRP* promoter initiates transcription of both *db*/*LEPR* and *OB-RGRP*/*LEPROT* (leptin receptor gene-related protein/leptin receptor overlapping transcript) genes (Mercer *et al.*, 2000). *LEPR* is highly expressed in the brain but also in most other tissues in humans and rodents: heart, placenta, lung, liver, muscle, kidney, pancreas, spleen, thymus, prostate, testes, ovary, small intestine, and colon (Kielar *et al.*, 1998). LEPR is mainly localized in intracellular compartments which include endosomes, the trans-Golgi apparatus, the endoplasmic reticulum, and the cell membrane (Belouzard *et al.*, 2004). In addition, the expression of OB-RGRP/LEPROT (also known as endospanin-1) negatively affected the expression of LEPR on the cell membrane (Seron *et al.*, 2011).

LEPR is found in six distinct isoforms that have been classified as secreted (LEPRe or OB-Re), short (LEPRa, c, d, and f, also known as OB-Ra, c, d, and f) and long isoforms (LEPRb or ORB-Rb) and present different biological activity. In mouse models, all of them are generated by alternative mRNA splicing (Lee *et al.*, 1996). In humans, LEPRa-d and f are derived from alternative mRNA splicing whereas the soluble isoform LEPRe is derived by post-translational cleavage of the *LEPR* gene (Ge *et al.*, 2002). All LEPR isoforms share an identical, highly glycosylated extracellular domain of 840 amino acids, while they differ for the length of the intracellular domain (Fig. 3).

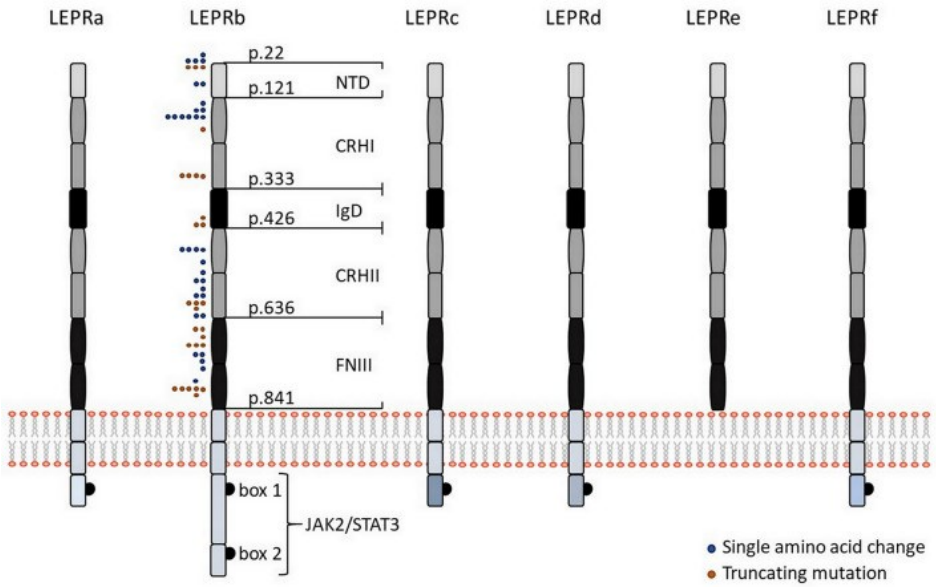

Figure 3. Schematic representation of the six different isoforms of LEPR in humans (LEPRa, b, c, d, e, and f). All isoforms share identical extracellular domains. In the intracellular domain, LEPRa-d and f share the first 29 amino acids including box 1 motif for binding of JAK2, but with the different lengths and sequences of the C-terminal domain. The intracellular domain of LEPRb

contains another JAK binding domain (“box 2”) in addition to a STAT binding site, making LEPRb the predominant isoform responsible for signal transduction. Colored dots indicate positions of human LEPR mutations, which result in single amino acid changes (blue dots), or a truncated protein (orange dots). The figure is taken from (Poetsch *et al.*, 2020).

The LEPR extracellular domain presents six subdomains: a N-terminal domain of undefined function (NTD), two cytokine receptor homologous domains (CRHI, CRHII) harbouring a Trp-Ser-X-Trp-Ser motif, an immunoglobulin-like domain (IgD), and two fibronectin type 3 domains (FNIII). CRHII and IgD domains are fundamental for the leptin binding and LEPR activation. All the membrane-bound LEPR isoforms present the same spanning trans-membrane domain with 23 amino acids as well as the first 29-amino acid intracellular domain containing box 1 motif, which is required for binding of Janus family tyrosine kinase 2 (JAK2). LEPR short isoforms comprise a short tail of 32-40 amino acids with the unique C-termini and are fundamental for internalization and lysosomal-dependent degradation of leptin (Uotani *et al.*, 1999). LEPRb presents the longest intracellular domain including ~306 amino acids (shorter in mice than in humans) and contains another JAK binding domain (“box 2”) and a STAT binding site, making LEPRb the only isoform containing a fully signalling-competent intracellular domain (Sweeney, 2002) (Fig. 3). The soluble LEPRe isoform is important for the leptin transport across the brain barrier (Kastin *et al.*, 1999). In addition, LEPRe modulates the leptin levels by forming complex with free leptin and by reducing its degradation and clearance (Huang *et al.*, 2001).

1.3.2 Role of LEPR in the hypothalamus

The most important role of LEPR in the hypothalamus is the regulation of energy expenditure and food intake. The area of the hypothalamus that presents the higher number of leptin-responsive neurons is the tuberal hypothalamus where LEPR is mainly located in the ARC, the ventromedial nucleus, the dorsomedial nucleus, and the lateral area (Elmquist *et al.*, 1998; Fei *et al.*, 1997; Mercer *et al.*, 1996; Schwartz *et al.*, 1996). Besides other neuronal nuclei expressing the LEPR, two populations of LEPR-expressing neurons in the ARC play a major role and exert opposite effects in feeding behaviour: the orexigenic GABAergic neurons co-expressing neuropeptide Y (NPY) and the agouti-related protein (AgRP) and the anorexigenic POMC neurons (Aponte *et al.*, 2011; Krashes *et al.*, 2011; Zhan *et al.*, 2013).

Binding of leptin to LEPRb promotes a conformational change that leads to LEPRb homo-oligomerization and activation of JAK2 through auto-phosphorylation (Nakashima *et al.*, 1997). After activation, JAK2 phosphorylates LEPRb at three different tyrosine residues (Tyr985, Tyr1077, Tyr1138), each comprising a Src homology 2 (SH2)-binding motif (Dunn

et al., 2005; Gong *et al.*, 2007; Hekerman *et al.*, 2005). Phosphorylation of Tyr1077 promotes recruitment and activation of STAT5 (Gong *et al.*, 2007; Hekerman *et al.*, 2005), whereas phosphorylation on Tyr1138 results in recruitment and activation of STAT1/5 and STAT3, which determine auto-phosphorylation of STAT proteins (Hekerman *et al.*, 2005). Phosphorylated STAT3 dimerizes and translocates to the nucleus to activate transcription of target genes, including suppressor of cytokine signalling 3 (SOCS3), which is important for LEPR-induced JAK/STAT signalling negative feedback. Phosphorylation of Tyr985 activates SOCS3 contributing to the inhibition of LEPR activity (Dunn *et al.*, 2005). In addition, leptin signalling is negatively regulated by phosphatases, such as protein tyrosine phosphatase 1B (PTP1B), which binds and inhibits JAK2 (Kaszubska *et al.*, 2002). By activating the JAK2/STAT3 pathway, leptin suppresses food intake by inhibiting the NPY/AgRP neurons and activating the POMC neurons which produce the α-melanocyte hormone. The interaction between α-melanocyte hormone and the downstream neurons expressing melanocortin receptor (MCR) 3 and MCR4 determines satiety and favours energy expenditure (Kim *et al.*, 2014; Waterson & Horvath, 2015). Alternatively to canonical JAK2/STAT3 pathway, leptin can activate phosphatidylinositol 3-kinase (PI3K)/AKT signalling pathway by recruiting the insulin receptor substrates IRS1 and IRS2, which are key mediators for regulation of glucose homeostasis, lipid metabolism, protein synthesis as well as cell proliferation and survival (Ren *et al.*, 2005). Another signalling branch promoted by leptin is the mitogen-activated protein kinase (MAPK) pathway. Here, the SH2 domain of the phosphatase SHP2 (SH2-containing protein tyrosine phosphatase 2) binds to phosphorylated Tyr985 of LEPRb and is phosphorylated by JAK2, which ultimately activates MAPK extracellular signal-related kinase (ERK1/2) via recruitment of growth factor receptor-bound protein 2 (GRB2), contributing to the regulation of energy homeostasis in the hypothalamus (Bjorbaek *et al.*, 2001; Rahmouni *et al.*, 2009). In addition, leptin binding to LEPR also inhibits AMPK activity in the hypothalamus, hence reducing food intake and body weight (Claret & Schneeberger, 2012) (Fig. 4).

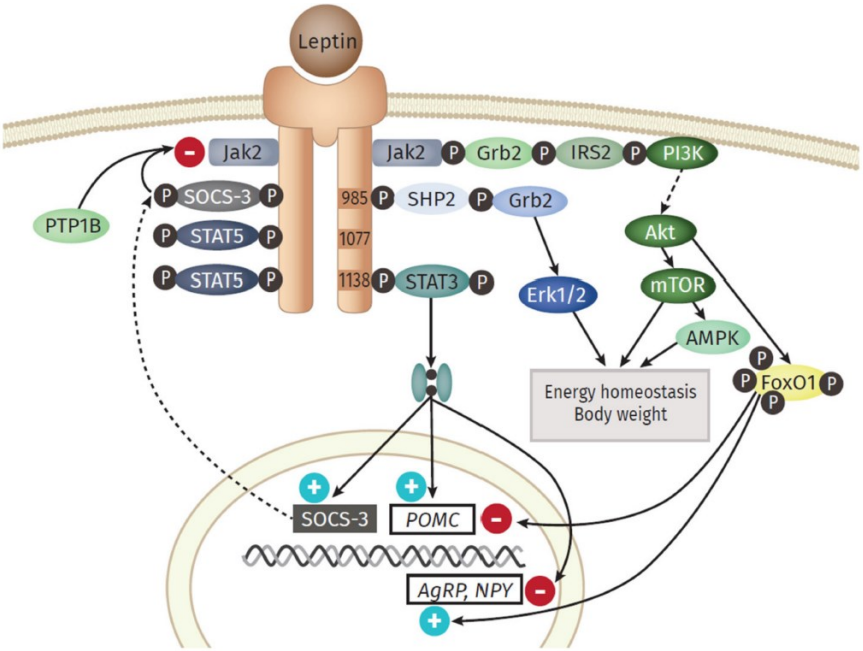

Figure 4. Overview of leptin signalling pathway. LEPRb presents the whole intracellular domain with three tyrosine residues (Y985, Y1077, Y1138). After binding of leptin, subsequent dimerization of the receptor and the following activation of JAK2 occur, followed by the recruitment of STAT3. Hereinafter, STAT3 translocates to the nucleus and regulates the expression of different genes. One prominent downstream gene is the suppressor of cytokine signalling 3 (SOCS3), which itself acts as a potent negative regulator of the leptin signalling, by binding to Y985 domain and following inhibition of JAK2. Protein tyrosine phosphatase 1 B (PTP1B), produced in the endoplasmic reticulum, is further able to inhibit leptin signalling by dephosphorylating JAK2. Besides STAT3, STAT5 is also known to be activated and phosphorylated. Other signalling pathway activated by leptin are MAPK and PI3K/AKT pathways which contribute to the regulation of energy homeostasis and body weight. The figure is taken from (Hornung *et al.*, 2021).

1.3.3 LEPR mutations in obese patients

Obesity-related LEPR mutations are usually inherited in an autosomal-recessive manner (Clement *et al.*, 1998). Most patients belong to a population in which consanguineous marriages are common. To date, 57 cases with 38 distinct LEPR mutations have been described and no differences in sex distribution have been reported (Nunziata *et al.*, 2018). The majority of LEPR mutations occur in the extracellular domain and particularly in the leptin-binding (CRHII) or activation domain (FNIII) (Lopez *et al.*, 2007). Based on *in silico* analysis, most of the mutations have been predicted to result in truncated LEPR proteins. Up to now, not a single LEPR mutation has been identified in the intracellular domain (Nunziata *et al.*, 2018). LEPR is encoded by a 20-exon transcript, however its translation starts only at exon 3 of the transcript. In 1998, the first LEPR mutation linked to severe obesity was described as a G to A substitution in the splice donor site of exon 16 (c.2597 +1G>A), which results in the exon 16 (or exon 18 considering the complete LEPR 20-exon transcript) skipping, and a formation of a premature stop codon (Clement *et al.*, 1998). In

2013, a novel homozygous mutation which involved a G>T base substitution in the splice acceptor site of exon 15 (or exon 17 considering the complete LEPR 20-exon transcript; c.2396-1G>T) was found in a 1.2-year-old girl, resulting in abnormal splicing of LEPR transcript by the skipping of exon 15 (Saeed *et al.*, 2014). In addition, the same mutation (c.2396-1G>T) have been reported in three unrelated probands between the ages of 0.6-2.0 years (Saeed *et al.*, 2015). Functional *in silico* analyses have been reported for 35 LEPR mutations, but functional *in vitro* data have only been described for four mutations (Lopez *et al.*, 2007; Nunziata *et al.*, 2018). Within these four mutations, only patients carrying the compound heterozygous LEPR mutation R612H (together with a non-sense mutation) showed residual LEPR-leptin signalling activation. The missense mutations A409E, W664R, and H684P promoted a complete loss of leptin-LEPR dependent pathway activation. However, all patients with these four mutations were characterized by hyperphagia, severe early-onset obesity, alterations in immune function, and delayed puberty (Lopez *et al.*, 2007). Obesity-related LEPR mutations have also been linked to insulin resistance and T2DM development. In fact, all patients carrying an obesity-related LEPR mutation (aged 4 to 55 years) show hyperinsulinemia, but T2DM was only described in two adults (41- and 55-year-old) (Lopez *et al.*, 2007). These data, together with other published data in humans, suggest that patients with obesity-related LEPR mutations present high risk for early-onset insulin resistance and T2DM (Poetsch *et al.*, 2020).

1.3.4 Role of LEPR in the heart

The role of LEPR in the heart remains controversial. It has not been completely understood whether leptin directly affects cardiac function or acts indirectly through a leptin-regulated neurohumoral pathway. Several leptin effects have been reported in the heart including regulation of fatty acid and glucose metabolism, cardiac remodelling, and protection against apoptosis (Hall *et al.*, 2015), which represent important mechanisms involved in diabetic cardiomyopathy development.

Leptin was able to exert an insulin-like effect on glucose uptake in Wistar rat hearts perfused in the Langendorff mode with a low concentration (1 ng/mL), however, this effect may have been caused by the absence of fatty acids in the perfusate (Haap *et al.*, 2003). On the contrary, working hearts of male Sprague Dawley rats perfused with both glucose and palmitate, glucose oxidation was unaltered upon leptin treatment (60 ng/mL). However, oxidation of both endogenous and exogenous fatty acids was increased by 82% independently of AMPK activation (Atkinson *et al.*, 2002). This study is corroborated by Sharma and colleagues using similar experimental conditions and showing an increase in

exogenous palmitate oxidation in combination with an unaltered rate of glucose oxidation mediated through a STAT3/nitric oxide/p38-MAPK-dependent mechanism (Sharma *et al.*, 2009). Experiments performed with an immortalized mouse CM line (HL-1) partially confirmed these results showing an increase in AMPK activation and palmitate oxidation with unaffected glucose uptake and oxidation upon 1 hour leptin incubation. However, leptin-dependent increase in fatty acid oxidation was diminished after 24 hours (Palanivel *et al.*, 2006). In addition to these findings, it has been reported that neonatal rat ventricular CM incubated with leptin for 72 hours revealed the induced expression of peroxisome proliferator-activated receptor alpha (PPARα), which is an important player in cardiac metabolism (Hou *et al.*, 2010).

Clinical studies have reported associations of plasma leptin levels with increased LV mass (Tritos *et al.*, 2004), thus different studies have been conducted to further understand the leptin role in cardiac hypertrophy development. Cultured neonatal rat ventricular CMs treated with leptin showed a significant increase in cell surface area after 24 or 72 hours (Rajapurohitam *et al.*, 2003), and a similar result was observed in cultured human CMs (Madani *et al.*, 2006; Xu *et al.*, 2004). Moreover, leptin treatment leaded to an increase in matrix metalloproteinase-2 activity and collagen III and IV mRNA expression although no change in total collagen synthesis was observed (Madani *et al.*, 2006). However, leptin treatment of murine HL-1 CMs did not increase the cell surface area (Pinieiro *et al.*, 2005). Moreover, the leptin role in the heart during cardiac remodelling under stress condition has been explored. Direct effect of leptin on CM apoptosis has been investigated after induced hypoxia-reoxygenation or treated with H_2O_2, showing cardiac protection of leptin against apoptosis (Eguchi *et al.*, 2008; Shin *et al.*, 2009). Apoptosis induced by chronic ischemia *in vivo* can also be attenuated by leptin (McGaffin *et al.*, 2009). Leptin administration has also been shown to reduce the infarct area after ischemia-reperfusion injury *ex vivo* (Smith *et al.*, 2006), conferring a cardioprotective role of leptin via attenuating CM apoptosis.

Taken together, although numerous studies regarding the role of LEPR in the heart have been reported, the intrinsic difference between the animal and human model as well as the systems (*in vivo, ex vivo, in vitro*) used in different investigations make the leptin role in cardiac function still unresolved (Hall *et al.*, 2015; Poetsch *et al.*, 2020).

1.3.5 Leptin- and LEPR-deficient rodent models

To explore the role of leptin in physiological and pathophysiological conditions, the leptin-deficient *ob/ob* mouse represents a widely used model. *Ob/ob* mice have a homozygous nonsense mutation (C to T) in the *ob* gene, which leads to the formation of a premature stop

codon causing premature termination (R105X). This results in a truncated leptin protein biologically inactive (Zhang *et al.*, 1994). *Ob/ob* mice show hyperphagia, hyperinsulinemia, insulin resistance and increased accumulation of adipose tissue, resembling the phenotype known in patients with congenital leptin deficiency. Leptin replacement almost completely reversed this phenotype (Seufert *et al.*, 1999). However, as insulin secretion remains high throughout the life and hyperglycaemia is decreased after 6 months of age, the *ob/ob* mouse model presents some drawbacks to study the role of leptin in T2DM in humans (Lindström, 2007; Wang *et al.*, 2014).

Lepr-deficient *db/db* mice are among the most useful models to investigate LEPR role in obesity-related T2DM. *Db/db* mice present an autosomal recessive G>T mutation in the splice acceptor at Arg 890 in the *db* gene, which leads to OB-Rb abnormal splicing and subsequent replacement of the OB-Rb long isoform by the OB-Ra short isoform (Lee *et al.*, 1996). OB-Ra lacks most of the intracellular domain, resulting in impaired leptin receptor signal transduction in the *db/db* mouse. The phenotype of *db/db* mice is similar to *ob/ob* mice, displaying severe and early-onset obesity as well as hyperinsulinemia. However, *db/db* mice show normal glucose tolerance by 4 weeks of age and insulin resistance and hyperglycaemia only by 8 weeks of age. Moreover, *db/db* mice show elevated cholesterol levels due to an increase in high-density lipoprotein (HDL) cholesterol. On the contrary, T2DM patients are characterized by reduced HDL cholesterol, elevated triglycerides and very low-density lipoprotein (VLDL) cholesterol, normal or even higher low-density lipoprotein (LDL) cholesterol and total cholesterol, making the *db/db* mice not the best model to study the contribution of leptin to T2DM development and its related complication in humans (Nishina *et al.*, 1994; Poetsch *et al.*, 2020).

Similar to mouse models, Zucker fatty (*fa/fa*) rats and Zucker diabetic fatty (ZDF) rats represent genetically induced diabetes models, which show obese phenotype by 5 weeks of age. The *fa/fa* rat is characterized by the homozygous missense mutation Q269P in the CRH1 domain in all Lepr isoforms, leading to loss of receptor function. The ZDF rat is an inbred sub-strain of the *fa/fa* rat, which, in addition to the genetic modification in Lepr, presents an inherited autosomal recessive genetic defect in β-cell transcription. Although hyperphagia and obesity are characteristics similar to T2DM-related human phenotype, both *fa/fa* and ZDF rats display high levels of LDL and HDL cholesterol as well as increased activity of lipoprotein lipase, which are not comparable to those of T2DM patients. Moreover, both *fa/fa* and ZDF rats develop insulin resistance at different ages. *Fa/fa* rats are not hyperglycaemic although they present high circulating insulin levels at 3-4 weeks of age, and plasm insulin levels return to normal by 30 weeks of age. On the contrary, plasma

insulin levels in ZDF rats are highly elevated from 6 to 8 weeks of age and decreased afterwards. In addition, ZDF rats display insufficient secretion of insulin at 14 weeks of age due to pancreatic β-cell dysfunction and male rat develop gender-specific hyperglycaemia by 10-12 weeks of age (Griffen *et al.*, 2001; Wang *et al.*, 2014), resembling a different phenotype compared to the human system.

1.3.6 Pathophysiological mechanism of diabetic cardiomyopathy associated with LEPR deficiency

The pathophysiological mechanisms of diabetic cardiomyopathy associated with LEPR deficiency have been mainly investigated in *db/db* mice or *fa/fa* and ZDF rats (Jia *et al.*, 2016). *Db/db* mice develop systolic and diastolic dysfunctions and contractile inefficiency although cardiac output was preserved by favourable loading conditions (increased preload and decreased afterload) at 12 weeks of age (Semeniuk *et al.*, 2002; Van den Bergh *et al.*, 2006). Similar to mouse models, ZDF rats with Lepr deficiency reveal LV hypertrophy and defects in cardiac contractility such as reduced fractional shortening, while these effects are less pronounced in *fa/fa* rats (Golfman *et al.*, 2005; Wang *et al.*, 2005). Moreover, *db/db* mice and ZDF rats are more susceptible to cardiac stress conditions as they show impaired recovery of cardiac function after myocardial infarction induced by coronary artery ligation at stages when animals have developed diabetes (Boudina & Abel, 2007). CM-specific deletion of *Lepr* (*Lepr−/−*) in mice, in the presence of increased Cre recombinase expression, resulted in significant wall thinning and severely impaired systolic function, which was associated with impaired ATP production via AMPK and mTOR signalling. After myocardial infarction, CM-specific *Lepr−/−* mice revealed greater cardiac dysfunction and increased lethal heart failure compared to wild-type mice, which were associated with attenuated cardiac STAT3, PI3K, and AKT activity and loss of energy substrate flexibility (Hall *et al.*, 2012). Moreover, these studies showed that impaired cardiac leptin signalling in *Lepr−/−* mice resulted in impaired glucose utilization under cardiac stress conditions (Hall *et al.*, 2012). In addition to these findings, global overexpression of the glucose transporter GLUT-4 in *db/db* mice resulted in improved glucose homeostasis and prevented cardiac dysfunction (Belke *et al.*, 2000; Semeniuk *et al.*, 2002), while another study showed that high levels of insulin and glucose ameliorated cardiac metabolism, restored cardiac efficiency, and enhanced post cardiac recovery in the same mouse model (Hafstad *et al.*, 2007). In addition, *db/db* mice present increased MVO_2 and increased ROS, which are linked to increased fatty acid oxidation, mitochondrial uncoupling, and oxidative stress in the heart (Boudina *et al.*, 2007). Comparable to *db/db* mice, *fa/fa* rats show highly active

oxidative stress response, as indicated by increased levels of lipid peroxide and elevated activity of the superoxide dismutase (Vincent *et al.*, 2001), while ZDF rats show elevated triglyceride levels and lipid accumulation in the myocardium, which may promote lipotoxicity and impaired cardiac function (Christoffersen *et al.*, 2003; Lee *et al.*, 2001; Sharma *et al.*, 2004; Zhou *et al.*, 2000). Administration of a peroxisome proliferator-activated receptor γ (PPARγ) agonist in ZDF rats resulted in improved glucose metabolism, reduced lipid accumulation in the myocardium, and restored cardiac function (Golfman *et al.*, 2005). However, although chronic administration of the PPARγ agonist in *db/db* mice restored insulin sensitivity and energy substrate flexibility, it failed to restore cardiac function (Carley *et al.*, 2004). In addition, CM-specific re-expression of *Lepr* in *db/db* mice decreased triglyceride accumulation in myocardium independent of triglyceride plasma levels and these mice showed lower heart weight and reduced LV wall thickness in comparison to *db/db* mice (Hall *et al.*, 2014). Apart from metabolic inflexibility and lipotoxicity, another mechanism involved in the pathogenesis of diabetic cardiomyopathy development associated with Lepr-deficiency in rodent models is perturbed intracellular Ca^{2+} handling. In *db/db* mice, systolic and diastolic Ca^{2+} levels, sarcoplasmic reticulum Ca^{2+} load, Ca^{2+} transient decay, and L-type Ca^{2+} current are all reduced while Ca^{2+} leakage from the sarcoplasmic reticulum is enhanced, suggesting that perturbations in cardiac Ca^{2+} handling contribute to contractile dysfunction (Belke *et al.*, 2004; Pereira *et al.*, 2006). Moreover, *db/db* mice present increased CM apoptosis and decreased survival compared with wild-type controls suggesting that abnormal leptin signalling is involved in myocardial dysfunction development (Barouch *et al.*, 2006). Overall, these studies show that the absence of a functional LEPR signalling leads to alteration in metabolic energy substrate utilization, increased MVO_2 and ROS production, impairment in Ca^{2+} handling and increased apoptosis, all contributing to impairment of cardiac efficiency and performance (Fig. 5). Although the important knowledge has been acquired from the animal studies, existing differences in the underlying mechanisms and pathways between animal models and patients with obesity and T2DM still make data interpretation challenging (Poetsch *et al.*, 2020).

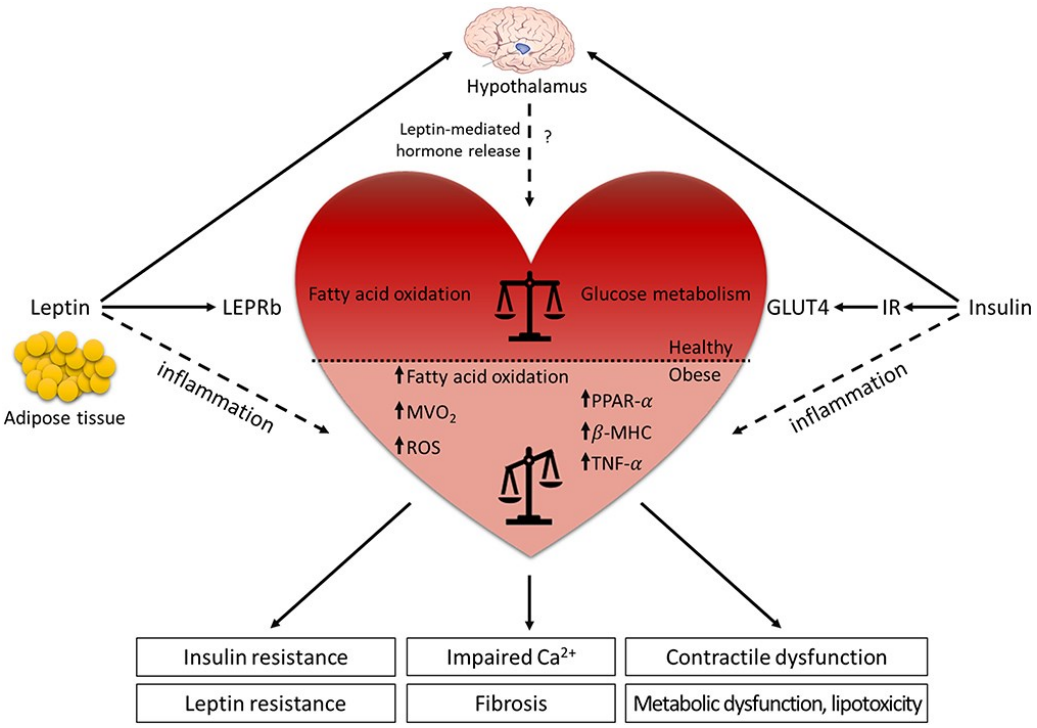

Figure 5. Leptin and LEPR signalling in the (dys-)regulation of the heart. Leptin is mainly secreted from the adipose tissue and binds to the LEPR in the ARC of the hypothalamus where it regulates food intake, energy expenditure and hormone release. The actions of leptin and insulin are interconnected and contribute to the switch of metabolic energy substrates. Although leptin role in the heart is still controversial, *db/db* and *ob/ob* mice demonstrate that leptin has beneficial effects on cardiac metabolism. Under physiological condition, leptin signalling supports the balance between glucose metabolism and fatty acid oxidation in the heart, while the absence of leptin or LEPR results in the loss of metabolic flexibility. The impaired metabolic substrate utilization contributes to systemic metabolic disorders (insulin resistance, leptin resistance, metabolic dysfunction, and lipotoxicity), leading to decreased cardiac efficiency (impaired Ca^{2+} handling, contractile dysfunction, and fibrosis). On the other hand, elevated leptin levels in obese patients contribute to the low-grade systemic inflammation, which enhances the risk to develop cardiovascular diseases. Horizontal black line demarcates differences between the healthy heart and the heart in obesity/diabetes. The figure is taken from (Poetsch *et al.*, 2020).

1.4 Modelling of cardiac disease with human induced pluripotent stem cells

1.4.1 Human induced pluripotent stem cell technology

The generation of human-induced pluripotent stem cells (hiPSCs) from somatic cells offers great potential and since their discovery, the stem cell field has achieved significant milestones and opened several gateways in the area of disease modelling, drug discovery, and regenerative medicine (Deinsberger *et al.*, 2020; Rowe & Daley, 2019). Similar to human embryonic stem cells (ESCs), hiPSCs are characterized by the ability to undergo long-term self-renewal and the potential to differentiate into numerous amounts of any differentiated cells in the human body (Takahashi *et al.*, 2007; Yu *et al.*, 2007). However,

obtaining ESCs is associated with the destruction of the human embryo at the blastocyst-stage, which give rise to two main obstacles: the ethical concerns generated by the use of the inner cell mass of developing embryos in clinical application (de Wert & Mummery, 2003) and the transplant rejection by the immune system of the host due to the non-autologous origin of ESCs. Generation of hiPSCs from patient-specific somatic cells represents a solution to overcome these issues. In 2006, Yamanaka and colleagues generated for the first time iPSCs from mouse adult fibroblasts by introducing only four transcription factors (Takahashi & Yamanaka, 2006), while adult human fibroblast-reprogrammed iPSCs were subsequently established in 2007 (Takahashi *et al.*, 2007). The first set of retrovirally transfected reprogramming factors, also called Yamanaka's factors, was composed of *OCT4* (octamer-binding transcription factor 4), *SOX2* (sex determining region Y box 2), *KLF4* (Krüppel-like factor 4) and *C-MYC* (v-Myc myelocytomatosis avian viral oncogene homolog) (Takahashi & Yamanaka, 2006). Besides, other combinations such as *OCT4*, *SOX2*, *NANOG*, and *LIN28* were also sufficient to induce pluripotency (Yu *et al.*, 2007). HiPSCs present several features in common with human ESCs (hESCs) in terms of morphology, proliferation ability, surface marker, gene expression, and telomerase activities. In addition, hiPSCs have potential to differentiate into derivatives of three germ layers (ectoderm, mesoderm, and endoderm) *in vitro*, and form teratoma in immunodeficient mice *in vivo*, which is another common aspect with hESCs (Takahashi et al., 2007). In the last decade, several reprogramming techniques were developed including viral-mediated transgene overexpression and or virus-free approaches, using adenoviruses (Zhou & Freed, 2009), plasmids (Okita *et al.*, 2010), minicircle vectors (Narsinh *et al.*, 2011), episomal vectors (Yu *et al.*, 2009), Sendai viruses (Yang *et al.*, 2008), synthetic mRNAs (Warren *et al.*, 2010), or recombinant proteins (Zhou *et al.*, 2009). Cells from various sources have been effectively reprogrammed into iPSCs, including skin fibroblasts, hair keratinocytes, mononuclear cells from peripheral or umbilical cord blood, and urine cells containing renal tubular epithelial cells and fibroblast-like or urothelial cells. Even cells obtained from biological waste materials were successfully used for reprogramming, including bone marrow cells, mesenchymal stem cells derived from fat tissue and teeth, liver and stomach cells, β-cells, melanocytes, or neural stem cells and progenitors (Poetsch *et al.*, 2022). Hence, the introduction of iPSCs has presented great potential and iPSCs are giving rise to a wide range of therapeutic possibilities, considering that treatment-specific target cells differentiated from iPSCs, such neurons or CMs, can be directly transplanted into patients. In 2014, the pioneering work of Takahashi and colleagues in the field of clinical trials demonstrated the successful use of iPSC-derived retinal pigment epithelial cells to treat

retinal degenerative diseases (Kim *et al.*, 2022). Several further clinical trials involving iPSCs have been conducted in last years. For instance, a clinical trial conducted by Domae and colleagues demonstrated that iPSC-derived tissue sheets transplanted into a human heart might promise functional recovery and good clinical outcome in selected patients with non-ischemic dilated cardiomyopathy, in addition to safety and feasibility (Domae *et al.*, 2021).

1.4.2 CRISPR-Cas9 technology in the iPSC system

The development of genome-editing technologies has revolutionized biomedical research, thanks to the introduction of clustered regularly interspaced short palindromic repeats (CRISPR)-associated protein 9 (CRISPR-Cas9), allowing the generation of patient-specific genetically modified cell lines (Jang & Ye, 2016). The first description of CRISPR loci appeared in 1987, after the sequencing of the *iap* gene of *Escherichia coli* (Ishino *et al.*, 1987). CRISPR loci were then recognised in archaea and bacteria representing with Cas9 genes a unique defence mechanism against genetic material from virus by specific DNA sequence recognition and cleavage (Barrangou *et al.*, 2007; Marraffini & Sontheimer, 2008). In 2011, Charpentier and colleagues discovered that trans-activating CRISPR RNA (tracrRNA) is necessary for the maturation of CRISPR RNAs (crRNAs) in studies with *S. pyogenes* (Deltcheva *et al.*, 2011). The simplicity of the CRISPR–Cas9 system has made genome editing more accessible and easier than traditional DNA editing techniques (Ding *et al.*, 2013). As a genome editing tool, the CRISPR–Cas9 system consists of two components, the endonuclease Cas9 and a single guide RNA (gRNA). Whereas the Cas9 enzyme cleaves double strand DNA, the gRNA contains a specific sequence to recognise the target gene in the region of interest. The gRNA is generated by the fusion of two components: the crRNA that provides target specificity (20 bases), and the tracrRNA that is used as a scaffold between crRNA and Cas9 endonuclease. The gRNA binds the complementary sequence in the target region in close proximity to the protospacer adjacent motif (PAM) that presents a 5'-NGG-3' sequence. After binding to the target region, Cas9 introduces a double-strand break. The cell repairs the double-strand break through either nonhomologous end joining (NHEJ) in the absence of a repair template, creating random insertion and deletion (indel) mutations, or homologous-directed repair (HDR) in the presence of a donor template, resulting in knock-in modification near the nuclease cutting site (Ran *et al.*, 2013) (Fig. 6).

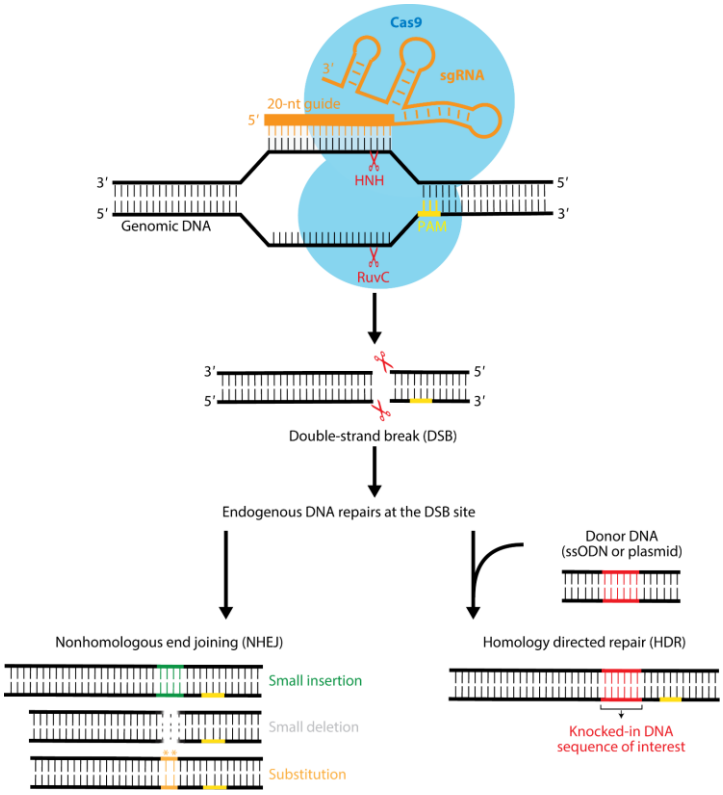

Figure 6. The mechanism of CRISPR/Cas9-mediated genome engineering. In the CRISPR/Cas9 system, a guide RNA hybridizes a 20-nt DNA sequence immediately preceding an "NGG" DNA motif (protospacer-associated motif or PAM), resulting in a double-strand break (DSB) 3 bp upstream of the NGG. In the absence of a repair template, the prevalent error-prone nonhomologous end joining (NHEJ) pathway is activated and causes random insertions and deletions (indels) or even substitutions at the DSB site. In the presence of a donor template containing a sequence of interest flanked by homology arms, the homology directed repair (HDR) pathway can be initiated to create desired mutations through homologous recombination. HNH and RuvC nuclease domains represent Cas9 catalytic residues. Figure modified from (Jiang & Doudna, 2017).

The efficiency of targeted genome modification by deep sequencing analysis was initially reported between 2% and 4% in hiPSCs (Mali *et al.*, 2013). With this low efficiency, recovery of properly targeted clones without positive selection is labour-intensive. Low efficiency of target genome is mainly due to low transfection efficiency of the relatively large Cas9 expression construct (Li *et al.*, 2014). Knock-in of inducible Cas9 into the adeno-associated virus integration site 1 locus, known as a safe harbour locus, increases the genome-editing efficiency, however, the Cas9 transgene was not excisable (Gonzalez *et al.*, 2014). To overcome these issues, the PiggyBac system became a promising tool for non-viral genetic engineering of hiPSCs. This system comprises the PiggyBac transposon vector and transposase vector, which transiently expresses transposase enzyme. PiggyBac transposon is a mobile genetic element that efficiently inserts copy of DNA into the genome by a "cut-and-paste" mechanism. PiggyBac transposition requires transposase enzyme that recognizes transposon specific inverted terminal repeats (ITRs) and efficiently integrates the transposon vector into a specific chromosome site sequence (TTAA) in the genome. The great strength of this system consists in its large cargo capacity suitable for the delivery of up to several hundred kilobases of DNA (Li *et al.*, 2011; Rostovskaya *et al.*, 2012), and most importantly the system is reversible. In fact, genomes harbouring an inserted piggyBac vector can be transiently re-transfected with the transposase expression vector to remove

the transposon from the genome avoiding any possible frameshift (Park *et al.*, 2018; Woodard & Wilson, 2015; Yusa *et al.*, 2011). In 2017, a new strategy was defined to perform foot print-free, highly efficient and consistent genome modification in hiPSCs, by generating a stable cell line that harbours a inducible Cas9 transgene and a puromycin resistant cassette encapsulated on a piggyBac transposon (Wang *et al.*, 2017). Selection of Cas9 genome integrated clones followed by Cas9 doxycycline induction and transfection with gRNA efficiently have been reported to result in mutant iPSC clones (Wang *et al.*, 2017). Furthermore, a novel plasmid that combines the PiggyBac transposon and tetracycline-inducible gene expression systems (Tet-On 3G) has demonstrated the ability to temporally modulate gene expression in hiPSCs and to precisely control the amount of gene expression (Randolph *et al.*, 2017). The combination of CRISPR and Tet-On 3G inducible PiggyBac system represents a powerful toolkit for studying gene functions in hiPSCs (Ben Jehuda *et al.*, 2018; Jiang *et al.*, 2022).

1.4.3 Modelling of diabetes using iPSC-CMs

To investigate the pathological mechanisms of cardiovascular diseases, adult human CMs could be used as a tool, however neither survive nor proliferate well when isolated from the heart *in vivo*. In light of this, mouse models are used as an alternative. In addition, because of differences in electrophysiological properties and in gene expression patterns, these models do not fully recapitulate human heart disease (Nerbonne, 2004; Shanks *et al.*, 2009). In the last decade, disease modelling using hiPSC have emerged as a promising platform to influence modern cardiovascular medicine on several fronts: molecular understanding of pathological mechanisms, early diagnosis, drug development, and effective treatment (Moretti *et al.*, 2013). Thus far, a wide range of cardiac diseases have been modelled using hiPSC technology, including long QT syndrome (Itzhaki *et al.*, 2011), short QT syndrome (Shinnawi *et al.*, 2019), Brugada syndrome (Li *et al.*, 2020; Liang *et al.*, 2016), catecholaminergic polymorphic ventricular tachycardia (Park *et al.*, 2019), dilated cardiomyopathy (Shah *et al.*, 2019), and hypertrophic cardiomyopathy (Li *et al.*, 2018). Besides the advantages of iPSC-based disease models, one of the major challenges in using hiPSC-CMs as disease model is represented by their immature state. In fact, the selection of energetic substrates in CMs for the constant generation of ATP depends on the stage of cardiac development (Lopaschuk & Jaswal, 2010). During early cardiac development, glycolysis is the principal source of energy for CMs. As CMs mature and become terminally differentiated, mitochondrial oxidative capacity enhances, with fatty acid β-oxidation turning in a major source of energy for the heart (Lopaschuk & Jaswal, 2010),

therefore cellular metabolism and alterations therein play an important role. Accordingly, metabolism has been shown to be central in maturing hiPSC-CMs (Batho *et al.*, 2020). Moreover, perturbations in cellular metabolism are central in the pathogenesis of cardiac disease, such as diabetic cardiomyopathy in which impaired cardiac insulin sensitivity, increased fatty acid oxidation and decreased glycolysis are emerging as predominant molecular and metabolic mechanisms for cardiac dysfunction (Mandavia *et al.*, 2013). In recent years, different approaches were used to improve the maturation state of iPSC-CMs such as the addition of fatty acid species (Feyen *et al.*, 2020), supplementation of glucose with galactose or lactate (Correia *et al.*, 2017; Feyen *et al.*, 2020; Yang *et al.*, 2019), an increase of Ca^{2+} levels (Feyen *et al.*, 2020; Shen *et al.*, 2022), or addition of hormones or small molecules (Funakoshi *et al.*, 2021; Parikh *et al.*, 2017).

The healthy heart obtains its energy from a combination of fatty acids, glucose, amino acids, and ketone bodies, and has the flexibility to shift between substrates according to the underlying conditions. On the contrary, the diabetic heart is exposed to hyperglycaemia, hyperinsulinemia and hyperlipidaemia, no longer presents metabolic flexibility, and relays predominantly on fatty acids, while glucose metabolism only contributes a small amount to the overall energy production (Lopaschuk & Jaswal, 2010). Therefore, another crucial challenge in modelling diabetic cardiomyopathy *in vitro* is the creating of a diabetic medium resembling the hallmarks of T2DM. In addition, the culture period of iPSC-CMs under the diabetic-like conditions plays a fundamental role in the molecular and metabolic change, which aims to mimic diabetic cardiomyopathy development in iPSC-CMs. To use iPSC-CMs for modelling diabetic cardiomyopathy, in a previous study iPSC-CMs were cultured in a maturation medium containing fatty acids but not glucose for 3 days, followed by cultivation of iPSC-CMs in the maturation medium supplemented with 10 mM glucose, 10 nM endothelin-1, and 1 µM cortisol for additional 2 days to mimic diabetic conditions. Subsequently, the iPSC-CMs presented increased lipid accumulation and peroxidation, decreased frequency of calcium transients, cellular hypertrophy, and loss of sarcomere integrity (Drawnel *et al.*, 2014). Graneli and colleagues, used fatty acids to improve iPSC-CM maturation and they induced insulin resistance by 4 days of culture with fatty acids but no glucose, followed by 6 days with 20 mM glucose and 50 µM palmitate supplemented with 15 mg/100 ml uric acid and 10 nM endothelin-1 (Graneli *et al.*, 2019). They demonstrated an increase in basal respiration but a decrease in maximal respiration suggesting the development of mitochondrial dysfunction. The study from Geraets and colleagues showed that 30-day-old hESC-derived CMs incubated with 250 µM palmitate and 50 nM insulin for 16 hours resulted in lipid-induced insulin resistance. However, they

commented that the hESC-CMs were structurally and functionally immature (Geraets *et al.*, 2018). A study from Fialho and colleagues demonstrated induced insulin resistance using a staged approach of culture for a week in maturation media containing 5 mM glucose supplemented with 0.4 mM oleic acid, followed by glucose-free insulin resistance media containing 0.3 mM palmitic acid and 50 nM insulin, and then a further 3 days with 12 mM glucose added to the insulin resistance medium (Sousa Fialho *et al.*, 2021), demonstrating that the insulin-resistant iPSC-CM present impaired hypoxic response. Given the multiples studies, iPSC-CMs show great potential to study the effects of diabetes in CMs, however further studies are needed to improve iPSC-CM maturation and to resemble the diabetic conditions known in diabetic patients to more deeply understand the underlying mechanism in diabetic cardiomyopathy development.

2 Aims of this study

The role of LEPR in heart has been investigated for decades mainly in animal models which provide useful insights into the role of LEPR in CM metabolic function under physiological and pathophysiological conditions. However, none of the animal models used so far can fully recapitulate the phenotypes of patients with obesity or T2DM, making data interpretation challenging. In fact, the alteration of lipid profile in *ob/ob* or *db/db* animal models cannot fully recapitulate the phenotypes of patients with T2DM. Therefore, the role of LEPR in the human heart, and whether leptin-LEPR signalling affects cardiac function directly or acts through a leptin-regulated neurohumoral pathway, remain unravelled. Human iPSC-based technology combined with the CRISPR/Cas9 technique allows us studying and better understanding abnormal leptin signalling in CMs *in vitro*, which could be related to obesity- and T2DM-associated cardio-metabolic remodelling processes. To verify this hypothesis, the scientific aims of this study are to assess the effect of LEPR mutations on the leptin-mediated signalling pathways, and to investigate glucose and fatty acid metabolism in iPSC-CMs with LEPR mutations ($LEPR^{\Delta/\Delta}$-iPSC-CMs) compared to wild-type iPSC-CMs (WT-iPSC-CMs). Following objectives were included in this study:

1. Investigation of the LEPR expression and function in cardiac differentiation of hiPSCs;
2. Generation of $LEPR^{\Delta/\Delta}$-iPSC lines;
3. Investigation of leptin/LEPR signalling pathway activation;
4. Investigation of leptin/LEPR and insulin signalling regulation;
5. Study of the metabolic profile of $LEPR^{\Delta/\Delta}$-iPSC-CMs;
6. Study of leptin effect on energy metabolism of WT- and $LEPR^{\Delta/\Delta}$-iPSC-CMs;
7. Study of the effect of pathophysiological culture conditions on metabolic flexibility of WT- and $LEPR^{\Delta/\Delta}$-iPSC-CMs.

3 Materials and methods

3.1 Materials

3.1.1 Cells

WT- and LEPR$^{\Delta/\Delta}$-iPSC lines used in this study are listed in Table 1. For the generation of WT cell lines isWT1.14 and isWT7.22 (UMGi014-C clone 14, and UMGi020-B clone 22, respectively), dermal fibroblasts obtained from two healthy individuals were reprogrammed into iPSCs by ectopic expression of the Yamanaka factors using the non-integrative Sendai virus and kindly provided by the Stem Cell Unit at the Universitätsmedizin Göttingen (Göttingen, 2019a, b). The cell lines were characterized as pluripotent by expression of pluripotency markers. To generate a stable cell line expressing Cas9, a piggyBac transposon that harbours an inducible Cas9 transgene was used (Wang *et al.*, 2017). Briefly, a piggyBac transposon containing the reverse tet activator, a tet-activator-responsive promoter driving humanized Cas9, and a puromycin resistance cassette was integrated into the genome of WT-iPSCs. The piggyBac transposon construct was stably introduced into the WT-iPSCs by co-transfection with a plasmid encoding the piggyBac transposase. To select puromycin-resistant clones, iPSCs were incubated in E8 medium with 1000 ng/ml puromycin for 48 hours. After selection, two LEPR$^{\Delta/\Delta}$-iPSC lines (1B2 and 1E6) were generated from inCas9-iPSC lines isWT1.14 and isWT7.22, respectively, in this study using the CRISPR/Cas9 gene-editing technology to investigate the physiological and pathophysiological role of LEPR in iPSC-CMs.

Table 1: WT- and LEPR$^{\Delta/\Delta}$-iPSC lines used in this study

iPSC lines	Donors	a.a. changes	Somatic cells	Virus used
isWT1.14	Male donor	Unknown	WT1.14	Sendai
isWT7.22	Female donor	Unknown	WT7.22	Sendai
inCas9-isWT1.14	isWT1.14	Unknown	--	--
inCas9-isWT7.22	isWT7.22	Unknown	--	--
1B2	inCas9-isWT1.14	p.Asp799Glu	--	--
1E6	inCas9-isWT7.22	p.Asp799Glu	--	--

3.1.2 Chemicals, solutions, and buffer used for cell culture

Table 2: List of components for cell culture

Components	Provider
Albumax	Thermo Fisher Scientific #11020021
Albumin, rice-derived human recombinant	Sigma-Aldrich #A9731
B-27 supplement, serum free (50 ×)	Thermo Fisher Scientific #17504044
B-27 supplement, serum free (50 ×) w/o insulin	Thermo Fisher Scientific #A1895601
Biotin	Sigma-Aldrich #B4639
CHIR99021	Merck Millipore #361559
Collagenase B	Worthington Biochemical #CLS-AFB
Creatine-monohydrate	Sigma Aldrich #C3630
D-glucose	Sigma Aldrich #G7021
D-glucose (U-$^{13}C_6$, 99%)	Cambridge Isotope Laboratories #CLM-1396-1
DMEM (Dulbecco's modified Eagle medium)/F12	Thermo Fisher Scientific #31331028
DMEM (Dulbecco's modified Eagle medium) w/o glucose	Thermo Fisher Scientific #11966025
Dimethyl sulfoxide (DMSO)	Thermo Fisher Scientific #D12345
DPBS (Dulbecco's phosphate buffered saline)	Sigma-Aldrich #D1408
Doxycycline	Sigma-Aldrich #D3447
Essential 8 (E8) basal medium	Thermo Fisher Scientific #A1516901
E8 supplement (50 ×)	Thermo Fisher Scientific #A1517101
Fetal bovine serum (FBS)	Sigma-Aldrich #F7524
Formic acid 98-100%	Sigma-Aldrich #1002640100
Geltrex	Thermo Fisher Scientific #A1413301
HEPES (1 M)	Sigma-Aldrich #H0887
Human Stem Cell Nucleofector Kit 2	Lonza #VPH-5022
Insulin	Sigma-Aldrich #I9278
IWP2	Merck Millipore #681671
Knockout serum replacement (KOSR)	Thermo Fisher Scientific #10828028
L-arginine	Sigma-Aldrich #A5006
L-ascorbic acid 2-phosphate	Sigma-Aldrich #A8960

L-carnitine-hydrochloride	Sigma-Aldrich #C0283
Sodium L-lactate (≥ 99%)	Sigma-Aldrich #71718
L-lysine hydrochloride	Sigma-Aldrich #W384712
L-phenylalanine	Sigma-Aldrich #P5482
Non-essential amino acids (NEAA, 100 ×)	Thermo Fisher Scientific #11140035
Puromycin	Thermo Fisher Scientific #A1113803
RPMI 1640 SILAC Flex Media	Thermo Fisher Scientific #A2494201
RPMI 1640 with HEPES with GlutaMax	Thermo Fisher Scientific #72400021
RPMI 1640 with L-glutamine w/o glucose	Thermo Fisher Scientific #11879020
Recombinant human leptin	Peprotech #300-27
Seahorse XF DMEM	Agilent #103575-100
Seahorse XF glucose (1.0 M)	Agilent #103577-100
Seahorse XF glutamine (200 mM)	Agilent #103579-100
Seahorse XF pyruvate (100 mM)	Agilent # 103578-100
Sodium DL-lactate solution (60%)	Sigma-Aldrich #L4263
Sodium pyruvate solution (100 mM)	Sigma-Aldrich #S8636
Taurine	Sigma-Aldrich #T0625
Thiazovivin (TZV)	Millipore # 420220
Trypsin-EDTA (0.25%)	Thermo Fisher Scientific #25200056
Versene solution (0.48 mM EDTA)	Thermo Fisher Scientific #15040066
Vitamin B12	Sigma-Aldrich #V6629

Table 3: List of buffers and solutions for cell culture

Substance	**Preparation**
Biotin (0.818 mM)	2 mg biotin in 10 ml MilliQ water, stored at –20°C
CHIR (12 mM)	5 mg CHIR99021 dissolved in 0.894 ml DMSO, stored at –20°C
Collagenase B	Working concentration: 1 mg/ml Dissolved in B27 medium, sterile filtered, stored at –20°C
Geltrex	2 mg Geltrex per 15 ml falcon tube, stored at –80°C
IWP2 (5 mM)	10 mg IWP2 dissolved in 4.28 ml DMSO, incubated for 10 minutes at 37°C, stored at –20°C

Recombinant human leptin for F3+ medium (100 µM)	5 mg leptin dissolved in 3.125 ml sterile filtered MilliQ water, stored at –20°C
Recombinant human leptin for F2+ medium (1.24 µM)	18.6 µl of 100 µM leptin dissolved in 1.481 ml sterile filtered MilliQ water, stored at –20°C
Sodium DL-lactate (1 M)	3 ml of 60% sodium DL-lactate diluted in 18 ml 1 M HEPES, stored at –20°C
TZV (2 mM)	10 mg TZV dissolved in 6.8 ml DMSO, stored at –20°C
Vitamin B12 (36.89 µM)	2.5 mg vitamin B12 in 50 ml MilliQ water, stored at –20°C

Table 4: List of media for cell culture experiments

Medium	**components**
B27 medium	RPMI 1640 with Glutamax and HEPES; 1 × B27 supplement, serum free
F2 medium	DMEM with 0.8 mM Sodium L-lactate (≥ 99%); 1.6 mM L-carnitine; 5 mM Creatine-monohydrate; 2 mM Taurine; 0.48 mM L-ascorbic acid 2-phosphate; 0.5% Albumax; 50 nM Insulin; 1 x NEAA; 7 mM Glucose; 1% KOSR; 0.082 µM Biotin; 0.369 nM Vitamin B12; 1 × B27 supplement w/o insulin, serum free
F2+ medium	F2 medium with 1.24 nM leptin
F3+ medium	DMEM with 0.8 mM Sodium L-lactate (≥ 99%); 1.6 mM L-carnitine; 5 mM Creatine-monohydrate; 2 mM Taurine; 0.48 mM L-ascorbic acid 2-phosphate; 0.5% Albumax; 700 nM Insulin; 1 x NEAA; 11 mM Glucose; 1% KOSR; 0.082 µM Biotin; 0.369 nM Vitamin B12; 100 nM Leptin; 1 × B27 supplement w/o insulin, serum free
Cardio differentiation medium	RPMI 1640 with Glutamax and HEPES; 0.5 mg/ml Albumin; 0.2 mg/ml L-ascorbic acid 2-phosphate
CM digestion medium	80% B27 medium; 20% FBS; 2 µM TZV

E8 medium	E8 basal medium; 1 × E8 Supplement
iPSC cryopreservation medium	80% E8 medium; 20% DMSO; 2 µM TZV
CM cryopreservation medium	80% FBS; 20% DMSO; 2 µM TZV
Starvation medium	RPMI 1640 with L-glutamine w/o glucose; 4 mM Sodium DL-lactate; 25 mM HEPES; 1 × B27 supplement w/o insulin, serum free

Table 5: List of media for analysis of glycolytic and respiratory capacity

Medium	**components**
Glycolysis stress test medium	Seahorse XF DMEM with 1 mM Pyruvate; 2 mM Glutamine; 10 mM Glucose
Cell Mito stress test medium	Seahorse XF DMEM with 2 mM Glutamine

Table 6: Medium for ^{13}C-isotope labelling studies

Medium	**components**
Basal medium	RPMI 1640 SILAC Flex Media with 25 mM HEPES; 0.27 mM L-lysine; 1.14 mM L-arginine; 2 mM Glutamine; 0.1 mM Pyruvate; 0.9 mM 60% Sodium DL-lactate

3.1.3 Disposable items

Table 7: List of laboratory disposable items

Name	**Types**	**Provider**
Cell culture plate	6-well plate, TC-treated; 12-well plate, TC-treated; 48-well plate, TC-treated; 96-well plate, TC-treated	CytoOne Starlab
Cell culture plate for cell harvesting in labelling studies	96-well plate, not treated, V-bottom	Falcon
Cell culture plate for lipid droplets accumulation studies	24-well plate, clear bottom, polymer coverslip	Ibidi

Cell scraper	2-Posit. Blade 25	Sarstedt
Cell strainer	40 µm, 100 µm Nylon	Corning
Centrifuge tube	0.2 ml, 0.5 ml, 1.5 ml, 2 ml	Eppendorf
Cryo tube	2 ml Cryo S.	Greiner Bio-One GmbH
Falcon tube	15 ml, 50 ml	BD Biosciences
Filter pipette tip	0.1-1000 µl	Corning
Glass coverslips	25 mm, round	Engelbrecht Medizin und Labortechnik
Gloves	Micro-touch coated	Ansell
Nitrocellulose blotting membrane	0.45 µm NC	Amersham™ Protran™
Parafilm	Parafilm	Amcor
Plastic pipette	5 ml, 10 ml, 25 ml, 50 ml	Costar
Real-Time PCR plate	96-well plate	Biozym

3.1.4 Chemicals, solutions, and buffers for molecular and metabolic experiments

Table 8: List of chemicals used for molecular and metabolic experiments

Substance	**Provider**
Agarose	Biozym #840004
Ammonium persulfate (APS)	Bio-Rad #1610700
AmpliTaq DNA polymerase with buffer II	Thermo Fisher Scientific #N808-0167
Albumin bovine, Fraction V	Serva #11922
Boric acid	VWR Chemicals #20185.297
Bromophenol blue	Fluka #18040
cOmplete tablets, mini	Roche #04693124001
Dithiothreitol (DTT)	PanReac AppliChem #A1101
dNTP mix	Bioline #BIO-39029
Ethylenediaminetetraacetic acid (EDTA)	Sigma-Aldrich #E6758
Fluoromount-G	eBioscience #00-4958-02
GeneRuler 100 bp Plus DNA Ladder	Thermo Fisher Scientific #0321
Glycerol	Roth #3783.1
Glycine	PanReac AppliChem #131340.1211

GoTaq G2 DNA polymerase	Promega #M7845
HDGreen plus safe DNA dye	Intas Science Imaging #ISII-HDGreen plus
HEPES	Serva #25245.05
Hoechst 33342, trihydrochloride, trihydrate	Invitrogen #H3570
Lipid (Oil Red O) Staining Kit	Invitrogen #MAK194
Methanol	VWR Chemicals #20847.307
MuLV reverse transcriptase (200 U/µl)	Thermo Fisher Scientific #28025-013
Non-fat dry milk	PanReac AppliChem #A0830,1000
Nonidet P 40 substitute (NP-40)	Sigma-Aldrich #74385
NucleoSpin Gel and PCR Clean-up	Thermo Fisher Scientific #11992242
Oligo $d(T)_{16}$ (50 µM)	Thermo Fisher Scientific #N808-0128
Paraformaldehyde (PFA)	Sigma-Aldrich #158127
PhosSTOP	Roche #04906837001
Pierce BCA protein assay kit	Thermo Fisher Scientific #23225
Phenylmethylsulfonyl fluoride (PMSF)	Roth #6367.1
PureLink Genomic DNA Mini Kit	Thermo Fisher Scientific #K182002
RNase inhibitor (20 U/µl)	Thermo Fisher Scientific #N808-0119
Rotiphorese gel 30	Roth #3029
Seahorse FluxPak	Agilent #102416-100
Seahorse XF Cell Mito Stress Test Kit	Agilent #103015-100
Seahorse XF Glycolysis Stress Test Kit	Agilent # 103020-100
Sodium chloride	Carl Roth #3957.1
Sodium deoxycholate	Sigma-Aldrich #D6750
Sodium dodecyl sulfate (SDS)	Serva #20765.03
Sodium fluoride (NaF)	Roth #4503.1
SV total RNA isolation system	Promega #Z3105
SYBR™ Green PCR Master Mix	Applied Biosystems #4309155
Tetramethylethylenediamine (TEMED)	Bio-Rad #161-0801
Tris base	Sigma-Aldrich #T1503
Tris hydrochloride (Tris-HCl)	Roth #9090.2
Triton X-100	Sigma-Aldrich #3051.3
Tween 20	Serva #37470.01
West Femto maximum sensitivity substrate	Thermo Fisher Scientific #34096

Table 9: List of buffers and solutions for molecular analyses

Solution/Buffer	Preparation
1 × Running buffer	192 mM Glycine, 0.1% SDS, 25 mM Tris base, pH 8.3
1 × TBS-T buffer	50 mM Tris, 150 mM NaCl, 0.1% Tween 20
1 × Transfer buffer	25 mM Tris base, 192 mM Glycine, 20% Methanol, 0.05% SDS, pH 8.3
5 × TBE buffer	54 g Tris base, 27.5 g Boric acid, 20 ml 0.5 M EDTA dissolved in 1 L MilliQ water, pH 8.0
6 × Laemmli buffer	12% SDS, 0.06% bromophenol blue, 60% glycerol, 60 mM Tris (pH 6.8), 0.6 M DTT
10% APS	10 g APS dissolved in 100 ml MilliQ water, filtered
5% BSA	12.5 g BSA dissolved in 250 ml 1 x TBS-T buffer
5% milk	5 g Non-fat dry milk dissolved in 100 ml 1 × TBS-T buffer
Cell lysis RIPA buffer	150 mM NaCl, 1% NP-40, 0.5% Sodium deoxycholate, 0.1% SDS, 50 mM Tris-HCl (pH 8.0), 1 mM EDTA, 10 mM NaF, 1 mM PMSF, 1 Tablet PhosStop per 10 ml, 1 Tablet cOmplete per 10 ml, prepared freshly
Enhanced chemiluminescent (ECL) mix	Kit: Western Femto maximum sensitivity substrate; 1 ml luminol/enhancer, 1 ml stable peroxide, mixed freshly
Hoechst 33342	Stock solution: 10 mg/ml Working solution: 1:1000 in MilliQ water, prepared freshly
10% SDS	10 g SDS dissolved in 100 ml MilliQ water, filtered
Stripping buffer (pH 2.2)	200 mM Glycine; 0.1 % SDS; 1% Tween 20 dissolved in MilliQ water

Table 10: Buffer for glycolytic flux analysis

Buffer	Preparation
Quenching buffer	20% Methanol (HPLC grade), 0.1% Formic acid (HPLC grade), 3 mM NaF, 1 mM Phenylalanine, 100 µM EDTA

3.1.5 Antibodies

Primary and secondary antibodies, listed in Tables 11 and 12, respectively, were used for immunofluorescence (IF), flow cytometry (FC), and western blot (WB) analyses.

Table 11: List of primary antibodies

Antigen	Host	Dilution	Provider
AKT	Rabbit (IgG)	WB: 1:1000	Cell Signaling #9272
AMPK	Rabbit (IgG)	WB: 1:1000	Cell Signaling #2532
cTNT-APC conjugate	Human cell line (IgG1)	FC: 1:50	Miltenyi Biotec #130-120-543
GAPDH	Mouse (IgG)	WB: 1:1000	Santa Cruz #sc-365062
JAK2	Mouse (IgG1)	WB: 1:1000	Cell Signaling #74987
LEPR	Rabbit (IgG)	WB: 1:1000	Proteintech #20966-1-AP
LIN28	Goat (IgG)	IF: 1:300	R&D systems #AF3757
NANOG	Goat (IgG)	IF: 1:200	Abcam #PA5-18406
OCT4	Goat (IgG)	IF: 1:40	R&D systems #AF1759
p-AKT (Ser473)	Rabbit (IgG)	WB: 1:1000	Cell Signaling #9271
p-AMPKα (Thr172)	Rabbit (IgG)	WB: 1:1000	Cell Signaling #2535
p-JAK2 (Tyr1007, Tyr1008)	Rabbit (IgG)	WB: 1:500	Thermo Fisher Scientific #44-426G
Isotype Control Antibody, human IgG1, APC conjugate	-	FC: 1:50	Miltenyi Biotec #130-113-446
SOX2	Mouse (IgG)	IF: 1:50	R&D systems #MAB2018
SSEA-4	Mouse (IgG)	IF: 1:200	Abcam #MC813
TRA-1-60	Mouse (IgM)	IF: 1:200	R&D systems #MAB4770

Table 12: List of secondary antibodies

Antigen	Host	Dilution	Provider
Alexa fluor 488-anti-mouse IgG	Donkey	IF: 1:500	Invitrogen #A21202
Alexa fluor 555-anti-goat IgG	Donkey	IF: 1:1000	Thermo Fisher Scientific #A21432
Anti-mouse IgG HRP	Goat	WB: 1:1000	Sigma-Aldrich #A3682
Anti-rabbit IgG HRP	Goat	WB: 1:1000	Sigma-Aldrich #A0545

FITC-anti-mouse IgM	Goat	IF: 1:200	Jackson ImmunoResearch #115-095-020
Cy3-anti-mouse IgG+IgM	Goat	IF: 1:300	Jackson ImmunoResearch #115-165-068

3.1.6 Primers

Forward (for) and reverse (rev) primers used for LEPR sequencing analysis, reverse transcription polymerase chain reaction (RT-PCR) and quantitative real-time polymerase chain reaction (qPCR) of different genes with exact annealing temperature (T_A) or melting temperature (T_m), number of cycles and size of products (F) are listed in Table 13 and Table 14, and Table 15, respectively.

Table 13: List of primers for sequencing analysis

Name	Target	Sequence	F (bps)	T_A (°C)	Cycles
LEPR (introns 16 -17)	gDNA	For: AAAGCTCATACACCCTGCACTT Rev: TCCTTTGGAACCTCACCATGAAAA	545	60	35
LEPR (exons 15-19)	cDNA	For: ATTCACTTTCCTGTGGACAGAGC Rev: CAGGAACAATTCTTGGGGTTCG	549	60	35
NA Chr8	gDNA	For: AGCTGAGTTCAAAATGGTTGGC Rev: CTTAGTGAGCCTACGTGTTCTATTT	414	59	35
PIEZO2, Chr18	gDNA	For: GAATGAGGGATGGAGATGAGGAGGA Rev: CCATCCCTCCCACTCATCCTTAATC	475	60	35

RP13-258O15, ChrX	gDNA	For: AAGTTAGTTCAGCCTATGCCCAGC Rev: TCCCACCTGTAACCTCCATTAGAACT	407	59	35

NA: gene not assigned. gDNA: genomic DNA. cDNA: complementary DNA. *LEPR (introns 16-17):* For: from +65619625 to +65619646; Rev: from +65620149 to +65620172. *LEPR* (*exons 15-19*) For: from +65422936 to +65422958; Rev: from +65423463 to +65423484. *NA*, Chr8 For: from +116189084 to +116189105; Rev: from +116189473 to +116189497; *PIEZO2*, Chr18 For: from +10756856 to +10756880; Rev: from +10757306 to +10757330; *RP13-258O15,* ChrX For: from +90634 to +90657; Rev: from +91015 to +91040.

Table 14: List of primers for reverse transcription polymerase chain reaction (RT-PCR)

Name	Sequence	F (bps)	T_A (°C)	Cycles
HPRT	For: CCTGGCGTCGTGATTAGTG Rev: ACAGAGGGCTACAATCTGATGG	183	60	35
LEPR (exons 9-11)	For: GCTGCAATGAACATGAATGCC Rev: AAAGGCTGCTCCTATGATACCTC	180	59	35

Table 15: List of primers for quantitative real-time polymerase chain reaction (qPCR)

Name	Sequence	F (bps)	T_m (°C)	Cycles
CD36	For: TCTTTCCTGCAGCCCAATG Rev: AGCCTCTGTTCCAACTGATAGTGA	60	79.5	45
CPT1-B	For: ACATCTCTGCCCAAGCTTCC Rev: ACCATGACTTGAGCACCAGG	175	85.5	45
GLUT-1	For: CTGGCATCAACGCTGTCTTC Rev: TGACGATACCGGAGCCAATG	96	84.5	45
GLUT-4	For: CATTCCTTGGTTCATCGTGGC Rev: ATAGCCTCCGCAACATACTGG	132	87	45
HPRT	For: CCTGGCGTCGTGATTAGTG Rev: ACAGAGGGCTACAATCTGATGG	183	82	45
LEPR (exons 9-11)	For: GCTGCAATGAACATGAATGCC Rev: AAAGGCTGCTCCTATGATACCTC	180	59	45
LEPR (exons 15-17)	For: ATTCACTTTCCTGTGGACAGAGC Rev: CAGGAACAATTCTTGGGGTTCG	549	81	45

3.1.7 Laboratory devices and experimental hardware

Table 16: List of laboratory devices and tools

Description	Name	Provider
Analytical balance	MCBA100; BP3100S	Satorius
Autoclave	Vakulab HP	Müchener Medizin Mechanik GmbH
Centrifuges	Heraeus Fresco 21; Heraeus Megafuge 8R	Thermo Fisher Scientific
Chemiluminescence camera for Western blot and PCR	FusionFX	Vilber Lourmat
Counting chamber	Neubauer	Marienfeld Superior
Electrophoresis chamber	41-2025	Peqlab
Electrophoresis power supply	Power Pac HC	Bio-Rad
Flow cytometer	FACS Canto™ II	BD
Freezing box	Mr. Frosty	Thermo Fisher Scientific
Gel casting chamber	40-1515	Peqlab
Incubation hood	Uni hood 650	Biotech
Incubator (CO2-free)	Heratherm IMH180-S	Thermo Fisher Scientific
Incubators	BBD 6220	Thermo Fisher Scientific
Lyophilizer	FreeZone 2.5 Liter	Labconco
MS analyser	QTRAP 5500	Sciex
Microscopes	IX50; IX70 BZ-X710	Olympus Keyence
Microwave	HF 22023	Siemens
PCR cycler	Mastercycler nexus	Eppendorf
pH meter	IonLab® pH Level 2	WTW
Photometer	Nanodrop ND-1000	Peqlab
Pipette controller	Pipetus	Hirschmann
Plate reader	Synergy HTX	BioTek
Real-time PCR detection system	CFX96	Bio-Rad
Rotator	IKA™ 0004016000	Thermo Fisher Scientific
Seahorse XFe96 analyser	XFe96 Analyzer	Agilent
Sterile work bench	HeraSafe KSP15	Thermo Fisher Scientific

Thermomixer	5350 mixer	Eppendorf
Transfection unit	Amaxa Nucleofector II device	Lonza
Vacuum pumps	Scroll Vacuum Pump	Labconco
Vortexer	MS2 Minishaker	IKA Labortechnik
Water preparation system	Q-Pod Milli-Q	Millipore
Western blot Criterion™ blotter	1704071	Bio-Rad
Western blot electrophoresis cell	1656001	Bio-Rad
Western blot gel casting chamber	Mini-PROTEAN®	Bio-Rad
Western blot precast gel	Criterion™ TGX™	Bio-Rad

3.1.8 Software

Table 17: List of software

Name	Purpose	Company
Benchling	Sequence analysis	Benchling
Bio-Rad CFX Manager	Data analysis	Bio-Rad
CCTOP	Data analysis	Uni-Heidelberg
El-Maven	Processing MS data	Elucidata
FlowJo	Single-cell flow cytometry analysis	BD-Biosciences
FUSION CAPT Version V17.04	Image processing	VILBER LOURMAT
Graphpad Prism 9	Data analysis and graph design	Graphpad Software, Inc.
MSConvert	MS analysis	Proteowizard
Seahorse Wave	Data analysis	Agilent
Unipro UGENE v. 45.0	Sequence visualization and alignment	UGENE

3.2 Methods

3.2.1 Cell culture

Cells were cultivated in an incubator under humidified conditions at 37°C and 5% carbon dioxide. Cell culture was performed under sterile conditions using a laminar airflow cabinet to avoid microbiological contamination.

3.2.1.1 Coating of plates

Geltrex, a basement membrane extract that contains mainly laminin, collagen IV, entactin, and heparin sulphate proteoglycans, was used as a coating matrix for iPSC and iPSC-CM cultivation. Geltrex was defrosted on ice, aliquoted in 15 ml Falcon tubes (2 mg/tube) and stored at –80°C. Ready to use aliquots were diluted in 12 ml of cold DMEM/F12 medium. Hereafter, Geltrex volume was transferred into plates as shown in Table 18. The coated plates were incubated for 1 h at 37°C or overnight at 4°C before use.

Table 18: Geltrex volume for coating plates

Plate	Volume
6-well plate	1 ml/well
12-well plate	0.5 ml/well
24-well plate	0.5 ml/well
48-well plate	0.3 ml/well
96-well plate	0.1 ml/well

3.2.1.2 Cultivation of iPSCs

iPSCs were cultivated in Geltrex-coated plates with E8 medium. When the cell confluence reached 85%, cells were passaged into new plates. In Brief, E8 medium supplemented with 2 µM TZV (E8 + TZV medium), Versene, and Geltrex-coated plates were warmed up to 37°C. Cells were washed once and then incubated in Versene for 6 min at room temperature (RT). After removal of Versene, cell cluster or single cells were resuspended with E8 + TZV medium and divided into new plates with a splitting ratio ranging from 1:6 to 1:10. On the next day, the medium was changed to E8 medium without TZV and refreshed daily until next splitting.

3.2.1.3 Cryopreservation and thawing of iPSCs

To cryopreserve iPSCs, E8 + TZV medium and iPSC cryopreservation medium were prewarmed to RT, and Versene was warmed up to 37°C. Cells were washed once with Versene and incubated with Versene for 6 min. After Versene removal, cells from one well of a 6-well plate were resuspended in 0.75 ml of E8 + TZV medium and transferred into a 2 ml cryo tube. After this step, 0.75 ml of iPSC cryopreservation medium was added into the tube drop-wisely and the content was mixed gently. The cells were kept overnight at –80°C in a freezing box, containing isopropanol, allowing controlled freezing at –1°C per min. The following day, the cryo tubes were stored in a liquid nitrogen tank vapor for extended storage.

To thaw iPSCs, frozen cells were transferred from the liquid nitrogen tank in a water bath at 37°C. The cell suspension was added slowly into a 15 ml Falcon tube containing 10 ml cold E8 medium and centrifuged at 200 × *g* for 5 min. After aspiration of the supernatant, the cell pellet was resuspended in 3 ml prewarmed E8 + TZV medium and divided into two wells (1 ml for one well and 2 ml for another well). Another 1 ml medium was added into each well. Daily E8 medium change was performed until splitting was needed.

3.2.1.4 Directed differentiation of iPSCs into cardiomyocytes

For direct differentiation of iPSCs into ventricular CMs, the standardized protocol was used as previously described (Cyganek *et al.*, 2018). In Brief, iPSCs cultured on Geltrex were transferred into 12-well plates and homogeneously distributed. When the confluence of iPSCs reached approximately 90%, directed differentiation was initiated (d0) by changing the medium from E8 to the cardio differentiation medium supplemented with 4 µM CHIR99021, a glycogen synthase kinase 3 (GSK3) inhibitor that induces activation of canonical WNT signalling. According to the protocol shown in Fig. 7, 48 hours after initiation of the differentiation, the medium was replaced by the cardio differentiation medium supplemented with 5 µM of the WNT pathway inhibitor IWP2 and changed again after 48 hours with cardio differentiation medium. At day 8, medium was replaced by B27 medium und refreshed daily until day 15. First beating CMs were observed at day 8-10.

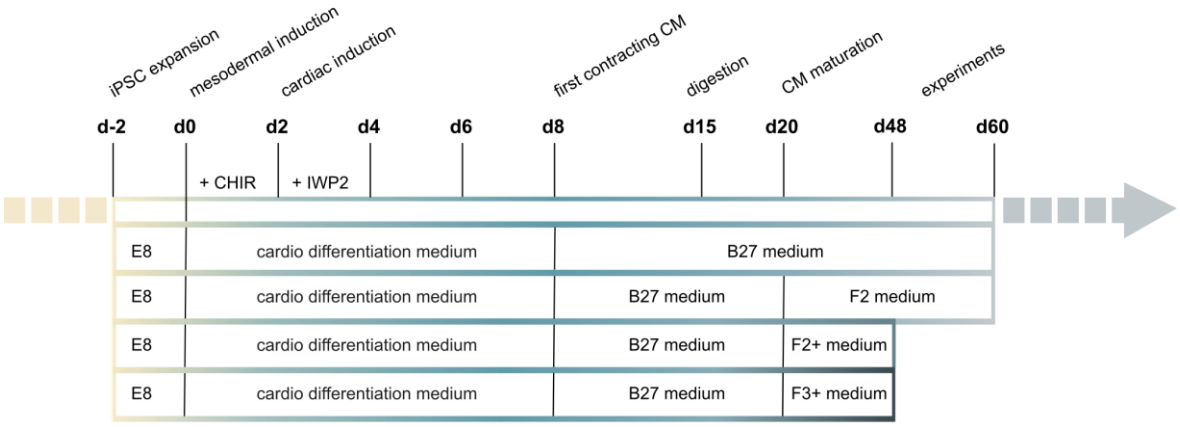

Figure 7. Schematic illustration of iPSC differentiation into CMs. iPSCs were differentiated into CMs by manipulating the WNT pathway. 20 days post-differentiation, iPSC-CMs were cultured in either B27 or F2 medium for additional 40 days or in F2+ or F3+ medium for additional 28 days.

3.2.1.5 First digestion of iPSC-CMs

For further maturation, iPSC-CMs were replated into 6-well plates at a low density (Fig. 7). At day 15 (d15) post-differentiation, iPSC-CMs were first incubated with collagenase II (46 U/ml) for 2-3 hours to allow cell detachment from the plates and dissociated into single cells by adding 0.25% Trypsin/EDTA. Next, trypsination was neutralized by adding the double amount of CM digestion medium, and the cell suspension was pelleted by centrifugation at 200 × *g* for 5 min. Finally, cells were resuspended in CM digestion medium, filtered through a 100 µm cell strainer and seeded at a density of 1,000,000 cells/well onto Geltrex-coated 6-well plates. At day 16, the CM digestion medium was changed to B27 medium and the iPSC-CMs were cultured in B27 medium until day 20, with the medium change every other day.

3.2.1.6 Cryopreservation and thawing of iPSC-CMs

iPSC-CMs with high purity were cryopreserved at day 15 post-differentiation. As previously described in 3.2.1.5, iPSC-CMs were detached with collagenase II and dissociated into single cells with 0.25% trypsin/EDTA. After centrifugation, the supernatant was removed, and the cell pellet was resuspended at a density of 4 million cells per 0.75 ml in FBS. Next, cell suspension was transferred into cryo tubes (0.75 ml/tube), and another 0.75 ml of CM cryopreservation medium was added dropwise into every tube. Finally, the cryo tubes containing the cells were kept overnight at –80°C in a freezing box and then transferred into liquid nitrogen tank. To thaw the cells, the cryo tube was warmed up in a water bath (37°C) until only a small part of ice remained and the cell suspension was added into a 15-ml Falcon tube containing 10 ml of cold B27 medium. Next, DMSO containing supernatant was

removed by centrifugation and the cell pellet was resuspended in 4 ml of CM digestion medium and replated into two wells of a Geltrex-coated 6-well plate. On the next day, the CM digestion medium was replaced with B27 medium, and the cells were cultured in B27 until day 20, with the medium change every second day.

3.2.1.7 Long-term culture of iPSC-CMs

To achieve CM maturation and to study the effect of different metabolic conditions, CMs were cultivated in different media from day 20 on, as shown in Fig. 7 and Table 19. To examine the long-term effect of leptin on CM metabolism, leptin (1.24 nM and 100 nM) was added to F2+ and F3+ medium, respectively, before use. In addition, half amount of medium was added freshly to the culture on the next day. The media of iPSC-CMs cultured under different conditions were replaced every second day until the cells were used for different experiments.

Table 19: List of components in different metabolic media

Components	B27	F2	F2+	F3+
Fatty acid	-	0.5% Albumax	0.5% Albumax	0.5% Albumax
KOSR	-	1%	1%	1%
Glucose	11 mM	7 mM	7 mM	11 mM
Insulin	700 nM	50 nM	50 nM	700 nM
Sodium L-lactate (≥ 99%)	-	0.8 mM	0.8 mM	0.8 mM
L-Glutamine	2 mM	4 mM	4 mM	4 mM
Leptin	-	-	1.24 nM	100 nM

3.2.1.8 Second digestion of iPSC-CMs

For the measurement of oxygen consumption rate (OCR) and extracellular acidification rate (ECAR), iPSC-CMs cultured under B27, F2, F2+, or F3+ medium conditions were digested again one week before the experiments. In Brief, iPSC-CMs cultured in different media were detached with collagenase II and dissociated with 0.25% trypsin/EDTA. Single-cell suspensions were obtained using a 100 µm strainer and iPSC-CMs were seeded at a density of 15,000 cells/well on a Geltrex-coated Seahorse XF 96-well plate in CM digestion medium. One day later, the medium was replaced with B27, F2, F2+ or F3+, respectively, and the cells were allowed to recover for seven days before starting the experiment. For the evaluation of lipid droplets accumulation, iPSC-CMs cultured under F2+ or F3+ medium

were digested again one week prior to the experiments as described above. iPSC-CMs were seeded at a density of 30,000 cells/well on a Geltrex-coated 24-well plate with glass bottom and polymer coverslip in CM digestion medium. One day later, the medium was replaced with F2+ or F3+, respectively, and the cells were allowed to recover for seven days before starting the experiment.

3.2.1.9 Collection of cell pellets for molecular experiments

To collect pellets of iPSCs or iPSC-CMs for the molecular analysis, cells were first washed twice with cold PBS and then carefully scraped off the plate. Next, cells were gently transferred into a 1.5 ml tube, centrifuged for 5 min at 2,000 × *g* and snap frozen in liquid nitrogen. Collected cell pellets were stored at –80°C until further use.

3.2.2 Gene expression analyses

3.2.2.1 RNA isolation

Total mRNA was isolated and purified using the SV total RNA isolation system according to the manufacturer's instructions. Depending on the cell pellet size, samples were lysed in 500-800 µl RNA lysis buffer. After purification, mRNA was eluted into 20 µl nuclease-free H_2O. The concentration of isolated RNA was measured with the Nanodrop and adjusted to 50 ng/µl. The RNA was used for reverse transcription reaction or stored at –80°C.

3.2.2.2 Reverse transcription reaction

To obtain single-stranded complementary DNA (cDNA), total mRNA was transcribed by reverse transcription reaction. Components used for one reverse transcription reaction are listed in Table 20.

Table 20: List of components for reverse transcription reaction

Components	20 µl final volume
10 × PCR buffer II	2 µl
25 mM $MgCl_2$	4 µl
100 mM dNTPs	1 µl
RNase inhibitor (20 U/µl)	1 µl
50 µM Oligo $d(T)_{16}$	1 µl
MuLV Reverse transcriptase (50 U/µl)	1 µl
200 ng RNA in nuclease-free H_2O	4 µl
Nuclease-free H_2O	6 µl

cDNA synthesis was performed in a PCR-cycler using the following program:

Temperature	Time
22°C	10 min
42°C	50 min
95°C	10 min
4°C	∞

Following the addition of 20 µl nuclease-free H_2O, synthesized cDNA (5 ng/µl) was stored at –20°C until further use for RT-PCR or qPCR.

3.2.2.3 Reverse transcription polymerase chain reaction (RT-PCR)

Components needed to amplify certain cDNA fragments are listed in Table 21.

Table 21: List of components for PCR

Components for PCR	25 µl final volume
cDNA (5 ng/µl)	1 µl
Nuclease-free H_2O	15.88 µl
5 × Green GoTaq reaction buffer	5 µl
10 mM dNTPs	1 µl
[1]Forward primer (10 µM)	1 µl
[1]Reverse primer (10 µM)	1 µl
GoTaq G2 DNA polymerase (5 U/µl)	0.13 µl

[1]Exact primer sequences for cDNA amplification are listed in Table 14.

The reaction was conducted in a PCR-cycler using the following program:

Step	Temperature	Time	Repeats
Denaturation	95°C	2 min	1
	95°C	30 sec	35
Annealing	60°C	30 sec	
Elongation	72°C	45 sec	
		10 min	1
Final step	4°C	∞	1

[1]Exact annealing temperature for cDNA amplification are listed in Table 14.

3.2.2.4 Quantitative real-time polymerase chain reaction (qPCR)

Quantitative real-time polymerase chain reaction (qPCR) was performed to quantify mRNA expression levels. qPCR reaction was performed in 96-well plates with three replicates of each sample. The qPCR reaction mixture was prepared as listed in Table 22.

Table 22: List of components for qPCR

Components	20 µl final volume
SYBR™ Green PCR Master Mix	10 µl
Nuclease-free H_2O	3 µl
Forward primer (1.67 µM)	3 µl
Reverse primer (1.67 µM)	3 µl
5 ng cDNA in nuclease-free H_2O	1 µl

After adding the reaction mixture to the 96-well plate, the plate was centrifuged at 200 rpm for 1 minute. Amplification of the targeted genes was achieved in a qPCR cycler using the following program:

Temperature	Time	Repeats
95°C	30 sec	1
95°C	15 sec	45
60°C	1 min	
65°C to 95°C	Melting curve	1
4°C	∞	1

[1]Exact melting temperatures for different genes are listed in Table 15.

The qPCR data including melting curve and cycle threshold value (C_T) were obtained using CFX manager software. Data were exported in MS Excel and normalized C_T values were calculated using the $2^{\Delta C_T}$ [$2^{\Delta C_T}$ of target gene = $2^{(\text{average } C_T \text{ value of target gene} - \text{average } C_T \text{ value of reference gene})}$] method to analyse the mRNA expression in iPSCs and iPSC-CMs.

3.2.3 Generation of LEPR$^{\Delta/\Delta}$-iPSC lines by using CRISPR/Cas9

Fig. 8 illustrates the procedure for generating and characterising iPSC lines with a mutation in LEPR using the CRISPR/Cas9 technology, which includes 7 steps described in more details below.

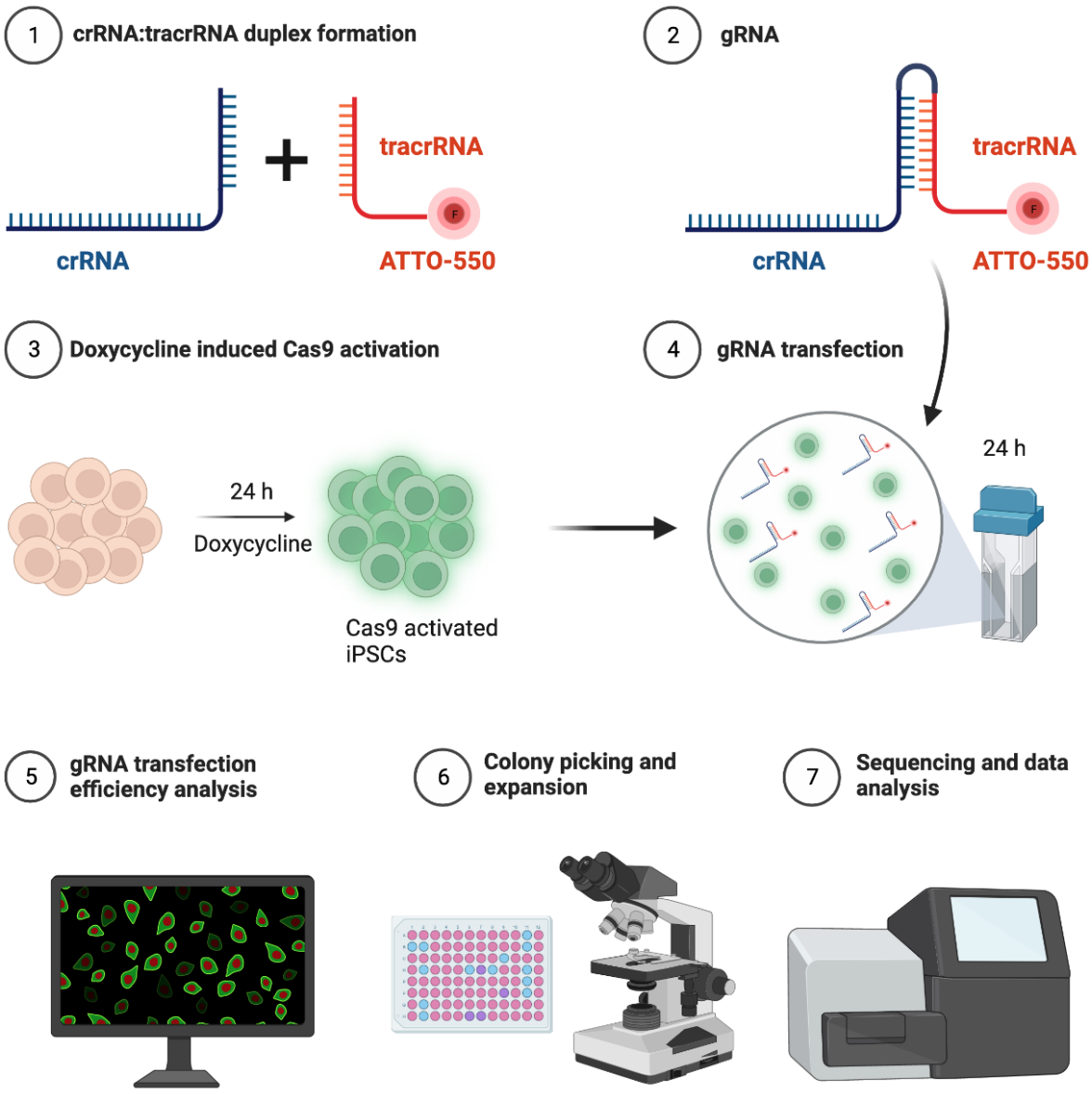

Figure 8. Workflow of LEPR$^{\Delta/\Delta}$-iPSC generation and characterization using the CRISPR/Cas9 technique. (1-2) Universal tracrRNA oligo fluorescently labelled with ATTO™-550 was mixed with

crRNA which contains a specific target region in the genome for the formation of crRNA:tracrRNA duplex (guide RNA). (3) Cas9 was activated by doxycycline in inCas9-iPSCs and, after 24 hours, (4) the guide RNA (gRNA) was transfected into inCas9-iPSCs by electroporation. (5) The gRNA transfection efficiency of inCas9-iPSCs was analysed by fluorescence microscopy. (6) iPSC colonies were picked mechanically and transferred into Geltrex-coated 96-well plates or 48-well plates, depending on the colony size. Cells were then expanded and a confluent well of each colony was used for pellet collection for DNA extraction. (7) Sequencing and data analysis was conducted to characterize the clones with specific *LEPR* mutations in exon 17.

3.2.3.1 Design and formation of a guide RNA specific for LEPR

To generate iPSCs with a patient-specific *LEPR* mutation, a guide RNA (gRNA) was designed with the sequence analysis online software Benchling and provided by a specialized company in genome editing (Integrated DNA Technologies, IDT). CCTOP, a CRISPR/Cas9 target online predictor software, was used to predict the gRNA efficiency and to check for off-target genes (Stemmer *et al.*, 2015). For this purpose, the sequence of human LEPR (ENSG00000116678, Ensembl) in the region of exon 17 (LEPR, CCDS631, Ensembl) was examined for available PAM (protospacer adjacent motifs). The crRNA was selected based on its proximity to the catalytic domain and the smallest possible number of off-targets (Table 23). The sequence specific CRISPR RNA (crRNA) and a conserved, transactivating crRNA (tracrRNA) were used to create crRNA:tracrRNA duplex following the manufacturer instruction. Briefly, 2 nmol crRNA was resuspended in 20 µl nuclease-free duplex buffer, while the 20 nmol trascrRNA was resuspended in 200 µl nuclease free duplex buffer, to obtain a final concentration of 100 µM for each oligonucleotide. The tracrRNA and the crRNA were mixed in equimolar concentration to create the crRNA:tracrRNA duplex with 50 µM final concentration.

Table 23: gRNA sequence and off-target prediction

Name	CRISPR-binding site	Calculated off-targets	Order number
Alt-R CRISPR-Cas9 crRNA-LEPR	AATGGGGATAAAATGATCTG AGG	3 at n=2 mismatches	IDT #3026685
Alt-R CRISPR-Cas9 tracrRNA, ATTO™ 550	Universal 67nt RNA sequence to form the gRNA		IDT #1075928

Alt-R CRISPR-Cas9 tracrRNA is labelled with a red fluorescent dye (ATTO™-550) to detect positive transfected cells. Off-targets with up to n=4 mismatches were calculated with CCTOP.

3.2.3.2 Transfection of human induced pluripotent stem cells

For generation of LEPR$^{\Delta/\Delta}$-iPSC lines, two indCas9-iPSC lines (inCas9-isWT1.14 and inCas9-isWT7.22) were thawed as previously described in 3.2.1.3 and expanded under puromycin (10 µg/ml) to select puromycin-resistant inCas9-iPSCs. Doxycycline (400 ng/ml) was added to the E8 medium 24 hours before transfection to induce Cas9 activation. InCas9-iPSCs were transfected with crRNA:tracrRNA duplexes of *LEPR* using the Human stem cell Nucleofection kit 2. Hereby, inCas9-iPSCs with confluence about 50-70% were washed once and incubated with Versene for 6 min until the cells detached. The cell number was counted using a cell counting chamber and 2x10^6 single cells were centrifuged at 200 x *g* for 5 min. After the supernatant was removed, the cell pellet was re-suspended in a mixture of nucleofection buffer A (82 µl) and B (18 µl) with the addition of 2 µl crRNA:tracrRNA duplexes of *LEPR* (50 µM) and transferred into the Nucleofector cuvette. The cuvette was placed in the Nucleofector II device and program B-016 was started. The transfected cells were transferred dropwise at 200, 300 or 500 cells/well into a 6-well plate containing E8 medium supplemented with TZV and doxycycline (400 ng/ml). After 24 hours the medium was changed with E8 medium.

3.2.3.3 Expansion of cell clones edited by CRISPR/Cas9

First colonies were observed five to seven days post-plating. iPSC colonies were picked mechanically and transferred into Geltrex-coated 96-well plates or 48-well plates, depending on the colony size. When colonies were large enough (usually after 5-7 days of culture), each colony was passaged into a well of a 48-well plate as described in 3.2.1.2. Confluent 48-well plates were transferred into two wells of a 24-well plate or in one well of a 12-well plate and were further expanded as described in 3.2.1.2. Confluent wells were used for pellet collection for DNA extraction or for cryopreservation as described previously in 3.2.1.6.

3.2.3.4 Genomic DNA isolation and purification

Genomic DNA (gDNA) from iPSCs was isolated and purified using the PureLink Genomic DNA Mini Kit following the manufacturer's instructions. After purification, gDNA was eluted into 25 µl nuclease-free H_2O and the concentration of the isolated gDNA was measured with the Nanodrop. The gDNA samples were stored at –80°C until further use.

3.2.3.5 gDNA and cDNA sequencing

To amplify the target gene, the gDNA or cDNA sequence was amplified by PCR using the components listed in Table 24.

Table 24: List of PCR components for gDNA or cDNA sequencing

Components	50 µl final volume
5 × Green GoTaq reaction buffer	10 µl
10 mM dNTPs	1 µl
[1]Forward primer (10 µM)	2.5 µl
[1]Reverse primer (10 µM)	2.5 µl
GoTaq G2 DNA polymerase (5 U/µl)	0.25 µl
DNA or cDNA	0.4 µg gDNA or 10 ng cDNA
Nuclease-free H_2O	Required volume to reach 50 µl

[1]Exact primer sequences for gDNA or cDNA amplification are listed in Table 13.

The reaction was conducted in a PCR-cycler using the following program:

Step	Temperature	Time	Repeats
Denaturation	95°C	2 min	1
	95°C	30 sec	35
[1]Annealing	59-60°C	30 sec	
Elongation	72°C	45 sec	
		10 min	1
Final step	4°C	∞	1

[1]Exact annealing temperatures and number of cycles for different genes are listed in Table 13.

The PCR product was electrophoretically separated on a 2% agarose gel and subsequently excised with a scalpel. The DNA fragment was then extracted from the agarose gel using the NucleoSpin Gel and PCR Clean-up extraction kit according to the manufacturer's instructions and the DNA concentration was measured using the Nanodrop. The isolated PCR product was used for gDNA or cDNA sequencing performed by a commercial sequencing facility (Seqlab-Microsynth, Dresden), for which the samples were prepared with the components shown in Table 25.

Table 25: List of components for gDNA or cDNA sequencing

Target region	PCR product	Final concentration of gDNA or cDNA	Primer For or Rev	Nuclease-free H_2O
[1]*LEPR (introns 16-17)*	~600 bp	9 ng/µl	3 µl	Required volume to reach 15 µl
[1]*LEPR (exons 15-19)*	~600 bp	9 ng/µl		
[1,2]*NA,* Chr8	~400 bp	6 ng/µl		
[1]*PIEZO2,* Chr18	~500 bp	7.5 ng/µl		
[1]*RP13-258O15, ChrX*	~400 bp	6 ng/µl		

[1]Exact primer sequences for the sequencing analysis of LEPR and off-target genes are listed in Table 13.

3.2.4 Protein expression analyses

3.2.4.1 Stimulation with leptin, insulin, and co-stimulation

To study activation of the leptin and insulin pathway, iPSC-CMs cultured in B27 or F2 medium were starved overnight with starvation medium. After starvation for 24 hours, iPSC-CMs cultured in B27 medium were acutely stimulated with leptin (1.24 nM) or insulin (50 nM) for 5-, 10- and 15-min, respectively, in starvation medium with the presence of 11 mM glucose, while iPSC-CMs cultured in F2 medium were stimulated with leptin (1.24 nM) or insulin (50 nM) for 5-, 10- and 15-min, respectively, in F2 medium without insulin. The crosstalk between insulin and leptin pathways were studied by co-stimulation with leptin (1.24 nM) and insulin (50 nM) for 10 min. After stimulation, cells were gently washed with cold PBS and frozen as described in 3.2.1.9.

3.2.4.2 Western blot

3.2.4.2.1 Lysis of cultured cells

To extract proteins from cultured cells, frozen or freshly collected cell pellets were resuspended in 80-150 µl cell lysis RIPA buffer. Following resuspension, the samples were

vortexed and incubated for 30 min on a rotator at 4°C. Afterwards, cell lysates were centrifuged at 14,000 × *g* for 20 min at 4°C. The supernatant was transferred into a new tube for following use. To determine the protein concentrations, 6 µl samples were diluted with 54 µl MiliQ water and measured using the Pierce BCA protein assay kit according to the manufacturer's instructions. Protein concentrations were determined using the best fit curve method of the loaded protein standards. The protein samples were directly used for SDS-polyacrylamide gel electrophoresis (SDS-PAGE) or aliquoted and stored at –80°C for further use. Before SDS-PAGE, a total amount of 30-40 µg protein was mixed with 6 × Laemmli loading buffer at a final volume of 25 µl and denatured for 5 min at 90°C.

3.2.4.2.2 SDS-polyacrylamide gel electrophoresis

SDS-PAGE was used to separate proteins according to their molecular weight. Precast or hand-casted gradient gels were used to better resolve a broad range of proteins. To prepare the hand-casted gel, a separation gel was mixed according to Table 26 and poured into the space between two glass plates separated by spacers and fixed with clamps. The gel was covered with a thin layer of isopropanol. After polymerization, isopropanol was removed, and the stacking gel was prepared accordingly to Table 26 and poured on top of the separation gel. Once the stacking gel was added, a comb was placed in it to shape the loading pockets. After polymerization of the stacking gel, the gel was assembled in an electrophoresis chamber and the chamber was filled with 1 × running buffer. At last, samples and markers were loaded into the pockets, the electrophoresis was run for 30 min at 80 V and afterwards for about 90 min at 120 V.

Table 26: Components used to prepare separation and stacking gels

Separation gel 2 Gels	**8%**	**15%**
Suitable for proteins with sizes	**>100 kDa**	**20-60 kDa**
Rotiphorese gel 30	2.6 ml	5 ml
1.5 M Tris pH 8.8	2.6 ml	2.6 ml
MilliQ water	4.55 ml	2.15 ml
10% SDS	100 µl	
10% APS	100 µl	
TEMED	10 µl	

Stacking gel 2 Gels	**5%**
Rotiphorese gel 30	0.67 ml
0.5 M Tris pH 6.8	1.25 ml
MilliQ water	2.975 ml
10% SDS	50 µl
10% APS	50 µl
TEMED	5 µl

3.2.4.2.3 Transfer and detection of proteins

Proteins previously separated by SDS-PAGE were transferred onto a nitrocellulose blotting membrane using a Wet/Tank blotting system. The gel was closely attached with a nitrocellulose blotting membrane, each side of which was coated with two Whatman paper and one sponge. Air bubbles between the layers were carefully removed using a roller. The prepared “sandwich” was fixed in a holder cassette and placed into a transfer apparatus with 1 × transfer buffer. The transfer took around 2 hours with a current of 0.25 A at 4°C. After the protein transfer, membranes were stained with ponceau S to check the protein loading and the equal transfer of all samples. To block unspecific binding, the successfully transferred nitrocellulose blotting membrane was washed three times with 1 x TBS-T buffer, and for the detection of phosphorylated proteins the membrane was then incubated in 5% BSA in 1 × TBS-T buffer for 1 hour at RT. For the detection of total proteins, the nitrocellulose membrane was blocked in 5% non-fat milk in 1 × TBS-T buffer for at least 1 hour at RT. After blocking, the membrane was incubated with the primary antibody diluted in 5% BSA (Table 11) overnight at 4°C. Thereafter, the membrane was washed three times with 1 × TBS-T buffer for 10 min and incubated with the HRP-coupled secondary antibody diluted in 1 x TBS-T for 1.5 hours at RT. After three washing steps with 1 × TBS-T buffer for 10 min, the membrane was incubated for 2 min with a luminol-based substrate (West Femto) to detect the protein of interest. Signals were detected by using the imaging Fusion FX system using the full resolution parameter.

To detect another antigen, the membrane was incubated with a mild stripping buffer for 20 min, washed three times with 1 x TBS-T buffer, and incubated with 5% non-fat milk in 1 × TBS-T buffer for at least 1 h at RT. After blocking, the membrane was incubated with the primary and secondary antibodies as described above.

3.2.4.3 Flow cytometry

To assess the purity of iPSC-CMs, flow cytometry was used to quantify the percentage of cTNT positive cells at day 60 post differentiation. Dissociated iPSC-CMs were fixed with 4% PFA at RT for 20 min and centrifuged at 500 × *g* for 5 min. After centrifugation, iPSC-CMs were blocked with 1% BSA in PBS for 1 hour at RT. Subsequently, cells were permeabilized with 0.1% Triton X-100 for 10 min at RT. After washing with PBS, iPSC-CMs were incubated with directly coupled cTNT-APC at 4°C for 1 hour or stored in 1% BSA for up to 5 days at 4°C. After incubation, samples were washed two times and resuspended in 1% BSA and analysed by flow cytometry. Negative controls were performed for all individual samples using isotype-controls. At least 10,000 events were recorded for each sample.

3.2.4.4 Immunofluorescence staining

Immunofluorescence staining was performed to study the expression of pluripotency associated proteins in iPSCs. Cells grown on coverslips were used when they reached approximately 30-40% confluency. After washing three times with PBS, iPSCs were fixed with 4% PFA for 20 min at RT, followed by washing another three times with PBS. Unspecific binding sites were blocked with 1% BSA overnight at 4°C. Samples used for nuclear- and cytoplasmic-protein analyses were permeabilized with 0.1% Triton X-100 for 10 min at RT. After washing three times with PBS, samples were then incubated with specific primary antibodies overnight at 4°C. Three washing steps were followed by incubation with the corresponding secondary antibodies in a humidified chamber protected from light for 1 hour at RT. Nuclei were co-stained with Hoechst 33342 for 10 min at RT. Immunostaining was visualized with a fluorescence microscope.

3.2.5 Cellular metabolism analyses

3.2.5.1 ^{13}C-isotope-assisted glucose metabolic flux studies

To determine the enrichment of the glycolytic intermediate, ^{13}C-isotopomer labelling studies were performed in iPSC-CMs at day 60 post differentiation. iPSC-CMs cultured in B27 medium were initially washed twice with the basal medium (Table 6). To this end, cells were incubated with 11 mM [U-$^{13}C_6$] glucose for 1-, 2- and 3-hours, respectively. To assess the glycolytic intermediate enrichments dependent from hormone stimulations, iPSC-CMs were incubated with leptin (1.24 nM), insulin (10 nM) or the combination of leptin (1.24 nM) and insulin (10 nM) for 1-, 2- and 3-hours, respectively. Cells were quenched at different time point by a rapid wash with ice-cold PBS and then collected in 150 µl of an ice-cold quenching solution (Table 10). All samples were lyophilized and resuspended in 50 µl of MilliQ water prior the LC-MS/MS analysis. The MS data were processed using the El-Maven software, as described previously (Avels et al., 2015).

3.2.5.2 Analysis of glycolytic and respiratory capacity

To study the glycolysis and oxidative metabolism, iPSC-CMs were digested and plated in a Seahorse XF 96-well plate from FluxPack as described in 3.2.1.8. Depending on the assay, cells were washed and incubated with either Cell Mito Stress or Glycolytic stress medium (Table 5) for 1 hour at 37°C in CO_2-free incubator. Afterwards, basal extracellular acidification rate (ECAR) and oxygen consumption rate (OCR) were measured using the Seahorse XFe96 Analyzer. To assess specific parameter of the mitochondrial function, the

Cell Mito stress test assay was used and, injection of 2.5 µM oligomycin, 2 µM carbonyl cyanide 4-(trifluoromethoxy)phenylhydrazone (FCCP), and 0.5 µM of rotenone and antimycin A was applied, as shown in Fig. 9 (left). Glycolytic stress test assay was used to evaluate key parameters of the glycolytic function by the injection of 10 mM Glucose, 2.5 µM oligomycin and 50 mM 2-DG, as demonstrated in Fig. 9 (right). Measurements were carried out in triplicate. Protein concentration was determined using the Pierce BCA protein assay kit according to the manufacturer's instructions to normalize the resulted OCR and ECAR measurements, respectively. Data analysis was performed according to the XF report generator user guide. Seahorse Cell Mito stress test and Glycolytic stress test parameter equations were calculated as shown in Table 27 and in Table 28, respectively.

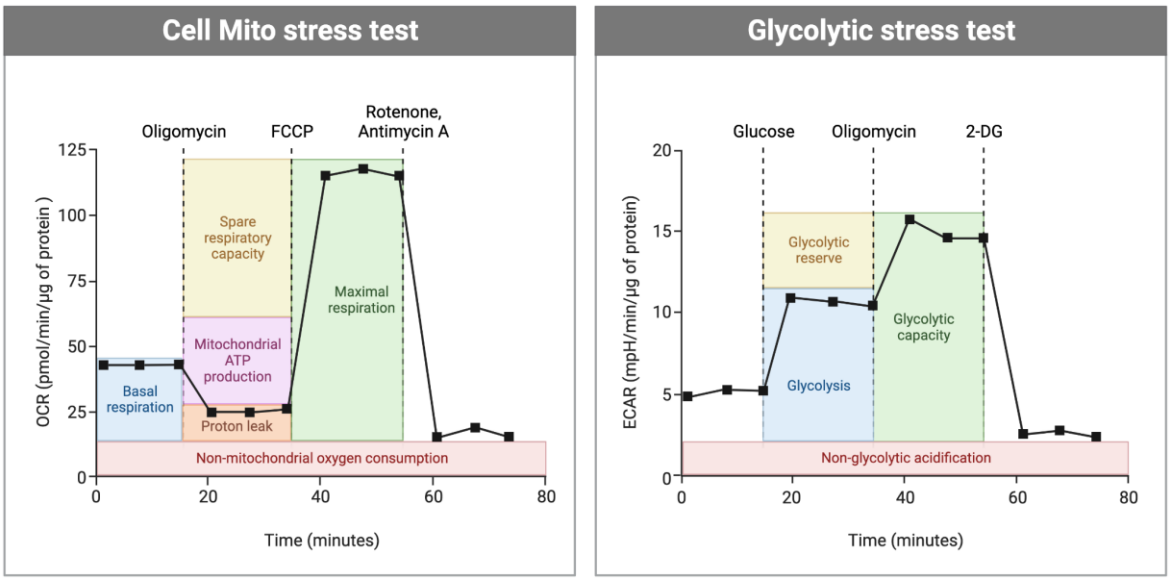

Figure 9. Seahorse Cell Mito stress test and glycolytic stress test profile. Representative Seahorse Cell Mito stress test assay (left side) and glycolytic stress test assay (right side) showing calculable parameters (adapted from Biorender template).

Table 27: Seahorse XF Cell Mito stress test parameter equations

Parameters	Equations
Non-mitochondrial oxygen consumption	Minimum rate measurement after Rotenone/antimycin A injection
Basal respiration	(Last rate measurement before oligomycin injection) – (Non-mitochondrial oxygen consumption)
Maximal respiration	(Maximum rate measurement after FCCP injection) – (Non-mitochondrial oxygen consumption)

Spare respiratory capacity	(Maximal respiration) – (Basal respiration)
Proton leak	(Minimum rate measurement after oligomycin injection) – (Non-mitochondrial oxygen consumption)
Mitochondrial ATP production	(Last rate measurement before oligomycin injection) – (Minimum rate measurement after oligomycin injection)

Table 28: Seahorse XF glycolysis stress test parameter equations

Parameters	Equations
Non-glycolytic acidification	Minimum rate measurement after 2-DG injection
Glycolysis	(Maximum rate measurement before oligomycin injection) – (Non-glycolytic acidification)
Glycolytic capacity	(Maximum rate measurement after oligomycin injection) – (Non-glycolytic acidification)
Glycolytic reserve	(Glycolytic capacity) – (Glycolysis)

3.2.5.3 Analysis of lipid droplet accumulation

Oil-Red-O staining was performed to analyse lipid droplet accumulation in iPSC-CMs using the lipid staining kit according to the manufacturer's instruction. iPSC-CMs were digested and plated in a 24-well plate with flat and clear bottom for high throughput microscopy as described in 3.2.1.8. After washing three times with PBS, iPSC-CMs were fixed with 10% formalin for 30 min at RT, followed by 5 min incubation and two washing steps in MilliQ water. The fixed iPSC-CMs were then incubated with 60% isopropanol for 5 min before adding 250 µl of Oil Red O staining solution for 20 min at RT. Stained iPSC-CMs were washed 3 times with MilliQ water until no excess of stain was observed. To stain the nuclei, iPSC-CMs were incubate with haematoxylin for 2 min, followed by 3 washing steps with tap water. Oil Red O staining was visualized with a light microscope.

3.2.6 Statistical analysis

Statistical analyses of the data obtained from all experiments were performed using GraphPad Prism 9 and results were presented as mean ± standard error of the mean (SEM). The sample size used for each experiment and the methods used for the statistical analysis were indicated in the figures or figure legends. *: $P < 0.05$, **: $P < 0.01$, ***: $P < 0.001$, ****: $P < 0.0001$.

4 Results

4.1 LEPR expression in iPSC-CMs

4.1.1 LEPR expression during cardiac development

To assess how LEPR is expressed during early cardiac development, directed differentiation of WT-iPSCs into ventricular CMs was initiated (d0) with cardio differentiation medium and CHIR which determined the activation of the WNT pathway and consequent mesodermal induction. After 48 hours (d2), inhibition of the WNT pathway with IWP2 induced the formation of cardiac mesoderm (d4-d6). First beating WT-iPSC-CMs were observed between day 8 and 10 after starting differentiation (Cyganek *et al.*, 2018). For maturation, WT-iPSC-CMs were cultured in B27 medium for 30, 60 or 90 days, respectively. LEPR expression was evaluated during the differentiation of iPSCs into spontaneously beating CMs, and during iPSC-CM maturation. *LEPR* (exons 9-11) relative expression showed comparable results among the different stages of cardiac development (d0-d90) (Fig. 10A, B). To assess whether the LEPR protein expression was enhanced during WT-iPSC-CM differentiation and maturation, a polyclonal antibody binding the intracellular region of LEPR (864-881 a.a., Proteintech, personal communication) was applied for western blot analysis. As shown in Fig. 10C, D, LEPR detection revealed increased LEPR expression at d30, d60 and d90.

As a summary of this part, *LEPR* mRNA was expressed already in iPSCs, and expression levels were not changed significantly during WT-iPSC-CM differentiation and maturation. In contrast, LEPR protein expression was almost no detectable in iPSCs and during early cardiac differentiation stages (till day 8) but was found in WT-iPSC-CMs at the maturation stages.

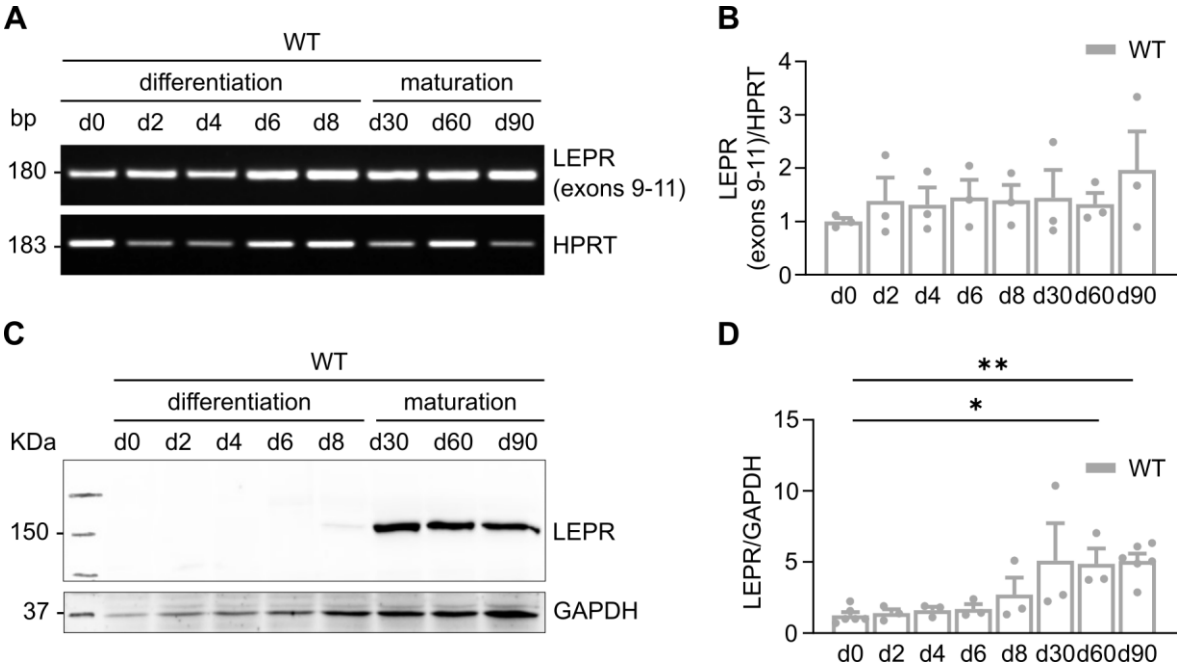

Figure 10. Characterization of LEPR expression during differentiation and maturation of WT-iPSC-CMs. (A, B) Reverse transcription-PCR analyses of WT-iPSCs and WT-iPSC-CMs showing *LEPR* (exons 9-11) expression during differentiation (d0-d8) and maturation (d30-d90). *LEPR* expression levels were normalized to *HPRT* (n = 3). (C, D) Western blot analysis of LEPR during differentiation (d0-d8) and maturation (d30-d90) of WT-iPSC-CMs. Protein levels of LEPR were normalized to GAPDH (d0: n = 6; d2-d4-d6-d8-d30-d60: n = 3; d90: n = 6). *P < 0.05; **P < 0.01 d30, d60 and d90 *vs*. d0 by using the Kruskal-Wallis with the Dunn's multiple comparison test.

4.2 Generation and characterisation of iPSC lines with LEPR mutations using CRISPR/Cas9 genome editing

4.2.1 LEPR-targeted gene editing in WT-iPSCs with the CRISPR/Cas9 system

To generate iPSC lines with mutations in LEPR, known in patients with early-onset obesity, CRISPR/Cas9 genome editing was used as a tool. The mutation c.2396-1G>T before the exon 17 results in an abnormal splicing of the *LEPR* transcript by the skipping of exon 17, based on *in silico* data (Farooqi *et al.*, 2007). To achieve this goal, two WT-iPSC lines (inCas9-isWT1.14; inCas9-isWT7.22) harbouring doxycycline inducible Cas9 coupled with GFP, previously generated in our lab, were used. A 20-nt crRNA was designed covering the position of c.2396-1 starting at the end of the intronic region and the beginning of *LEPR* exon 17 (position +65619925 to +65619944 of the genomic sequence). For gRNA formation, crRNA and ATTO^{TM}-550-labelled tracrRNA was prepared in nuclease-free duplex buffer. Both isWT1.14 and isWT7.22 were transfected with crRNA:tracrRNA duplexes using the Lonza nucleofection system. As shown in Fig. 11, the gRNA was efficiently introduced into

WT-iPSCs. In addition, doxycycline-dependent Cas9 induction (GFP+) in both inCas9-isWT1.14 and -isWT7.22 iPSCs was successfully demonstrated (Fig. 11A, B).

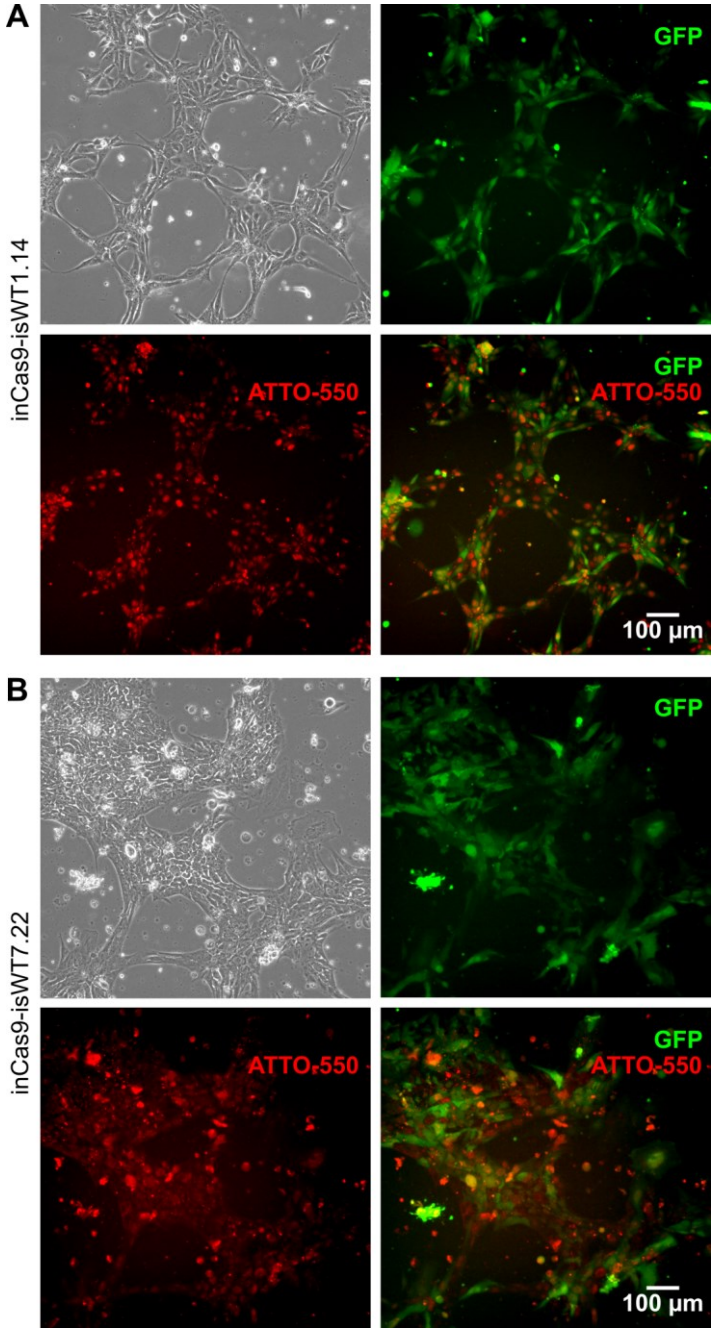

Figure 11. Transfection efficiency of gRNA in iPSCs. Representative fluorescence microscopy images probing for doxycycline (400 ng/ml) dependent Cas9 induction (GFP, green) and gRNA transfection (ATTO^{TM}-550, red) in inCas9-isWT1.14 (A) and -isWT7.22 (B) iPSCs. Scale bar, 100 µm.

To obtain single clones, iPSC colonies were picked mechanically. To assess the efficiency of editing of the CRISPR/Cas9 targeted region, genomic DNA was extracted from 24 and

11 colonies picked from the gRNA-transfected culture of inCas9-isWT1.14 and -isWT7.22 iPSCs, respectively. Afterwards, the CRISPR/Cas9 targeted LEPR region was amplified and sequenced. In total, 15 and 4 pure clones with *LEPR* mutations were obtained from inCas9-isWT1.14 and -isWT7.22 iPSCs, respectively. As shown in Fig. 12A, B, CRISPR/Cas9 targeted pure clones presented insertion or deletion in the gRNA-targeting region including the acceptor splicing site of exon 17. The CRISPR/Cas9 targeted clones 1B2, 3D4, 4B1 (1B2-, 3D4-, 4B1-LEPR$^{\Delta/\Delta}$) derived from inCas9-isWT1.14 (Fig. 11A) and 1E6 (1E6-LEPR$^{\Delta/\Delta}$) from inCas9-isWT7.22 (Fig. 11B) are homozygous with an insertion of "A" in exon 17 which led to a reading frameshift, a formation of a premature termination codon (PTC), and thus a truncated protein. Homozygous clone 1A2 displayed a 258-bp deletion in both alleles and was generated from inCas9-isWT1.14 iPSC line. Two clones obtained from inCas9-isWT1.14-iPSCs are with compound heterozygous deletions: 3D1 clone with a deletion of 17 bp in one allele and a deletion of 16 bp in the second allele, and 4E2 clone with a deletion of 5 bp in one allele and a deletion of 19 bp in the second allele. These three colonies derived from inCas9-isWT1.14 iPSCs (1A2-, 3D1-, 4E2- LEPR$^{\Delta/\Delta}$-iPSCs) included the deletion of the acceptor splicing site of exon 17, resulting in an abnormal splicing of the *LEPR* transcript by the skipping of exon 17 similar to the mutation known in early-onset obesity patients.

A

gRNA targeting region in ***LEPR***		**Sequence**
		Allele 1: 5'-TTCTCCTCAGATCATTTTATCCCCATT-3' Allele 2: 3'-AAGAGGAGTCTAGTAAAATAGGGGTAA-5'
Origin	**Clones**	**Sequence**
inCas9-isWT1.14	1A1; 1D4	Allele 1: 5'-TTCTCCTCAGAATCATTTTATCCCCATT-3' Allele 2: 3'-AAGAGGAGT- - - - -AAAATAGGGGTAA-5'
	1A2	Allele 1: 5'- 258 bp deletion ATT -3' Allele 2: 3'- 258 bp deletion TAA -5'
	1B2; 3D4;4B1	Allele 1: 5'- TTCTCCTCAGAATCATTTTATCCCCATT -3' Allele 2: 3'- AAGAGGAGTCTTAGTAAAATAGGGGTAA -5'
	1D2; 1E4	Allele 1: 5'- TTCTCCTCAGAATCATTTTATCCCCATT -3' Allele 2: 3'- AAGAGG - - - - - - - - - - - - - GGTAA -5'
	1D3	Allele 1: 5'- TTCTCCTCAGAATCATTTTATCCCCATT -3' Allele 2: 3'- AAGAGGAGT- - - GTAAAATAGGGGTAA -5'

	1E1	Allele 1: 5'- TTCTCCTCA - - - - - TTTTATCCCCATT -3' Allele 2: 3'- AAGAGGAGTCT - - - - - - - - - - - - GTAA -5'
	1F1	Allele 1: 5'- TTCTCCTCAGAATCATTTTATCCCCATT -3' Allele 2: 3'- AAGAGGAGTCTTTTTAGTAAAATAGGGG -5'
	1F2	Allele 1: 5'- TTCTCCTCAGAATCATTTTATCCCCATT -3' Allele 2: 3'- TT - - - - - - - - - - - - - - - - - TAGGGGTAA -5'
	3B2	Allele 1: 5'- TTCTCCTCAGAATCATTTTATCCCCATT -3' Allele 2: 3'- AAGAGGAGT - - - - - - - - - - - - - - - - AA -5'
	3D1	Allele 1: 5'- T- - - - - - - - - - - - - - - - - ATCCCCATT -3' Allele 2: 3'- TT- - - - - - - - - - - - - - - - - -TAGGGGTAA -5'
	4E2	Allele 1: 5'- TTCTCCTCA - - - - - TTTTATCCCCATT -3' Allele 2: 3'- 19 bp deletion AATAGGGGTAA -5'

B

Origin	Clones	Sequence
inCas9-isWT7.22	1A4	Allele 1: 5'- TTCTCCTCAGAAACATTTATCCCCATT -3' Allele 2: 3'- AAGAGGAGTCTTTGTAAATAGGGGTAA-5'
	1C4	Allele 1: 5'- TTCTCCTCAGAATCATTTTATCCCCATT -3' Allele 2: 3'- AAGAGGAGT - - AGTAAAATAGGGGTAA -5'
	1E6	Allele 1: 5'- TTCTCCTCAGAATCATTTATCCCCATT -3' Allele 2: 3'- AAGAGGAGTCTTAGTAAATAGGGGTAA -5'
	1F6	Allele 1: 5'- TTCTCCTCAGAATCATTTATCCCCATT -3' Allele 2: 3'- AAGAGGAGTCTTCATAAAATAGGGGTAA -5'

Figure 12. Screening of CRISPR/Cas9-edited cell clones. In total, 15 and 4 pure clones transfected with the gRNA targeting *LEPR* were sequenced from inCas9-isWT1.14 and -isWT7.22, respectively. (A, B) All clones presented homozygous or heterozygous mutations in the gRNA-targeted region including the splicing acceptor site of exon 17. The majority of the clones presented a heterozygous mutation with an insertion of an "A" in one allele and deletions in the second allele (1A1; 1D4; 1D2; 1E4; 1D3; 1F2; and 3B2 from inCas9-isWT1.14 and 1C4 from inCas9-isWT7.22). Two of the clones showed a heterozygous mutation with a different number of base pair insertions in one allele compared to the second (1F1 from inCas9-isWT1.14; and 1F6 from inCas9-isWT7.22). Three of the clones showed a heterozygous mutation with a different number of base pair deletions in one allele compared to the second (1E1; 3D1; and 4E2 from inCas9-isWT1.14). Five of the clones presented a homozygous mutation with a big deletion (1A2) or with a single base pair insertion (1B2; 3D4; 4B1; from inCas9-isWT1.14 and 1E6 from inCas9-isWT7.22). gRNA binding site (PAM) is showed in green, splicing site of the LEPR exon 17 is underlined and the exonic region is showed in blue, while the insertions are showed in red.

As confirmed by gDNA sequence chromatograms of 1B2 and 1E6 LEPR$^{\Delta/\Delta}$-iPSCs compared with inCas9-isWT1.14 and -isWT7.22, respectively, a homozygous mutation in LEPR with an insertion of "A" in exon 17 (c.2396insA) was observed (Fig. 13A, C).

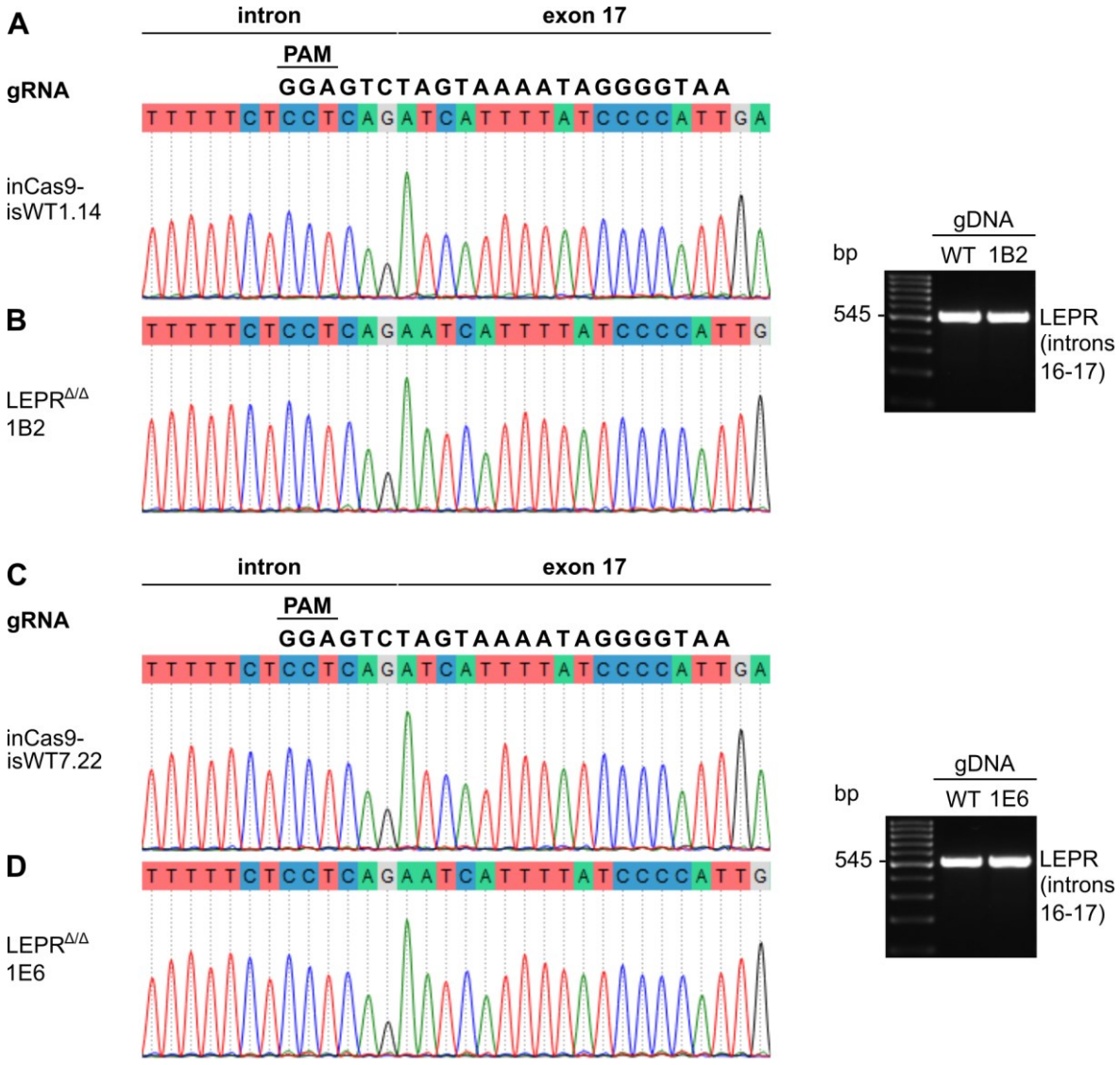

Figure 13. Verification of the single base insertion in exon 17 of *LEPR* in LEPR$^{\Delta/\Delta}$-iPSC lines using the gDNA sequencing. (A, B) Sequence chromatograms (A) of gDNA amplified using the primer set *LEPR* (introns 16-17) (B) in 1B2 LEPR$^{\Delta/\Delta}$-iPSCs compared with the isogenic control (inCas9-isWT1.14 iPSCs) revealed a homozygous mutation in *LEPR* with an insertion of "A" in exon 17 (c.2396insA). (C, D) An identical homozygous mutation in exon 17 of *LEPR* (c.2396insA) was obtained in 1E6 LEPR$^{\Delta/\Delta}$-iPSCs as showed by the comparison with the isogenic control (inCas9-isWT7.22 iPSCs).

To further confirm the insertion occurs within exon 17 and does influence the splicing of exon 17, cDNA sequence chromatograms of 1B2 and 1E6 LEPR$^{\Delta/\Delta}$-iPSCs were compared with the control sequences of inCas9-isWT1.14 and inCas9-isWT7.22, respectively. As expected, a nucleotide insertion of A in exon 17 of *LEPR* was observed in both 1B2 and 1E6 LEPR$^{\Delta/\Delta}$-iPSCs which leads to the conversion of aspartic acid (Asp) to glutamic acid (Glu) at position 799 of the protein and a formation of a PTC (D799Efs*7), thus a truncated protein (Fig. 14A, B). Reverse transcription-PCR analyses of cDNA using the primer set

designed for exons 15-19 demonstrate similar cDNA products between 1B2 and 1E6 LEPR$^{\Delta/\Delta}$-iPSCs and their respective isogenic controls (Fig. 14C, D).

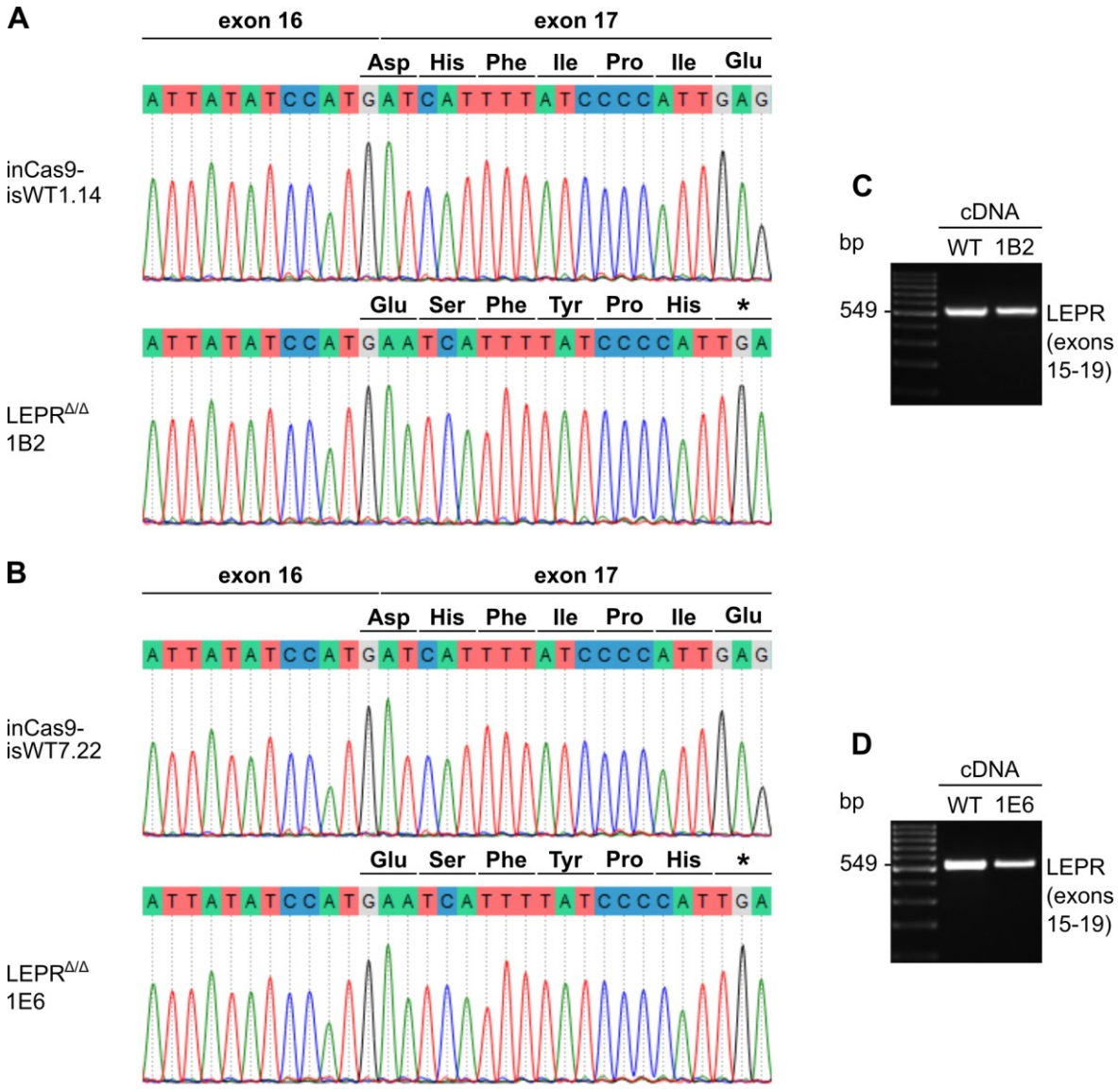

Figure 14. Verification of the single base insertion in the LEPR cDNA of 1B2 and 1E6 LEPR$^{\Delta/\Delta}$-iPSC lines. (A, B) Comparison of 1B2 and 1E6 LEPR$^{\Delta/\Delta}$-iPSC cDNA sequence chromatograms with the sequences of the isogenic controls inCas9-isWT1.14 and inCas9-isWT7.22, respectively, showed a nucleotide insertion of A in exon 17 of *LEPR* leading to a frameshift mutation. The resulted shift of the open reading frame leads to the conversion of aspartic acid (Asp) to glutamic acid (Glu) at position 799 of the protein and a formation of a premature stop codon (D799Efs*7). (C, D) Reverse transcription-PCR analyses of cDNA using the primer set targeting *LEPR* (exons 15-19) in 1B2 and 1E6 LEPR$^{\Delta/\Delta}$-iPSCs compared to their isogenic controls.

Since the designed gRNA was predicted to have potential off-target effects with n=2 mismatches in three regions of the human genome including Chr8 (gene *NA*), Chr18 (gene *PIEZO2*) and ChrX (gene *RP13-258O15.1*) using the CRISPR/Cas9 target online predictor

(CCTOP), gRNA potential off-target effects in 1B2 and 1E6 LEPR$^{\Delta/\Delta}$-iPSC lines were analysed by sequencing.

As shown in Figs. 15 to 17, sequence chromatograms of genomic DNA amplified for Chr8 (gene *NA*) (Fig. 15A, B), Chr18 (gene *PIEZO2*) (Fig. 16A, B), and ChrX (gene *RP13-258O15.1*) (Fig. 17A, B) in 1B2 and 1E6 LEPR$^{\Delta/\Delta}$-iPSCs were identical to the control sequences of inCas9-isWT1.14 and inCas9-isWT7.22, respectively, indicating no off-target effects. PCR analyses of genomic DNA using primer sets specific for Chr8 (gene *NA*) (Fig. 15C, D), Chr18 (gene *PIEZO2*) (Fig. 16C, D), and ChrX (gene *RP13-258O15.1*) (Fig. 17C, D) identify similar PCR products between 1B2 and 1E6 LEPR$^{\Delta/\Delta}$-iPSCs and their respective isogenic controls.

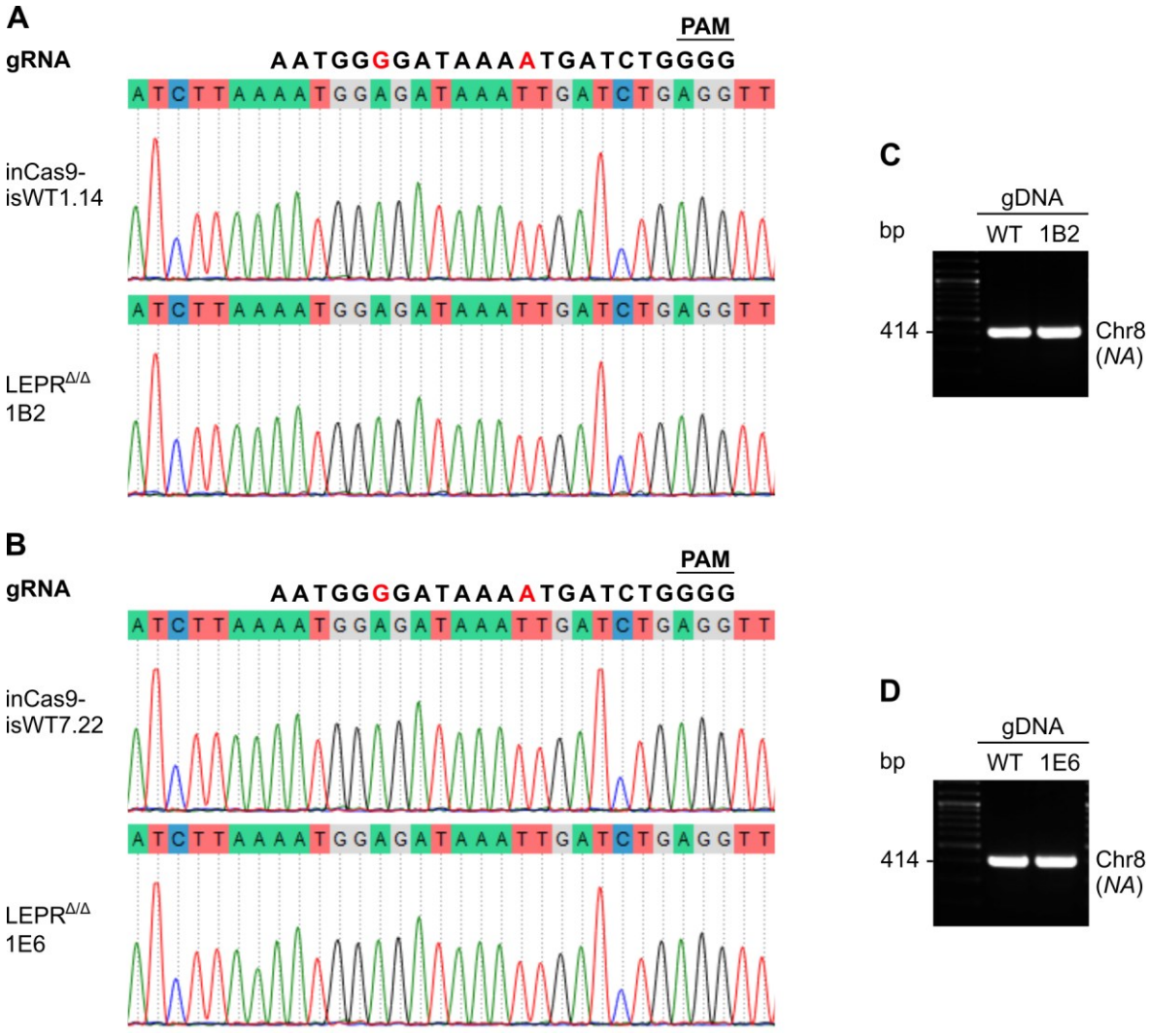

Figure 15. Genomic DNA sequencing analysis of gRNA potential off-target effects in Chr8. (A, B) 1B2 and 1E6 LEPR$^{\Delta/\Delta}$-iPSC sequencing chromatograms for Chr8 (gene *NA*) were aligned with inCas9-isWT1.14 and inCas9-isWT7.22, respectively. (C, D) PCR analyses of gDNA amplified for Chr8 (gene *NA*) in 1B2 and 1E6 LEPR$^{\Delta/\Delta}$-iPSCs showed no difference when compared with inCas9-isWT1.14 and inCas9-isWT7.22, respectively. Mismatches in the gRNA sequence are marked in red.

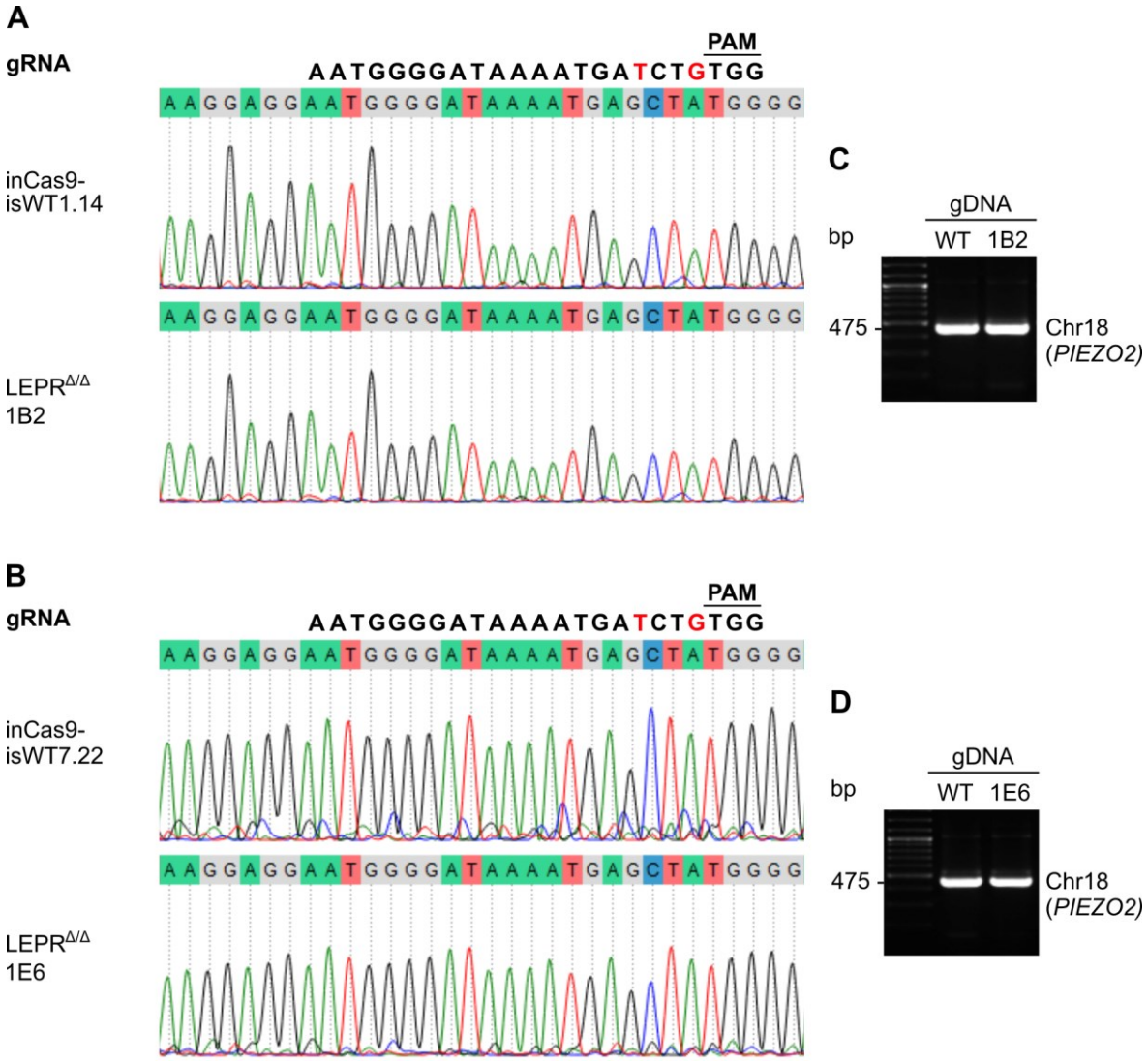

Figure 16. Genomic DNA sequencing analysis of gRNA potential off-target effects in Chr18. (A, B) 1B2 and 1E6 LEPR$^{\Delta/\Delta}$-iPSC sequencing chromatograms for Chr18 (gene *PIEZO2*) were aligned with inCas9-isWT1.14 and inCas9-isWT7.22, respectively. (C, D) PCR analyses of gDNA amplified for Chr18 (gene *PIEZO2*) in 1B2 and 1E6 LEPR$^{\Delta/\Delta}$-iPSCs showed no difference when compared with inCas9-isWT1.14 and inCas9-isWT7.22, respectively. Mismatches in the gRNA sequence are marked in red.

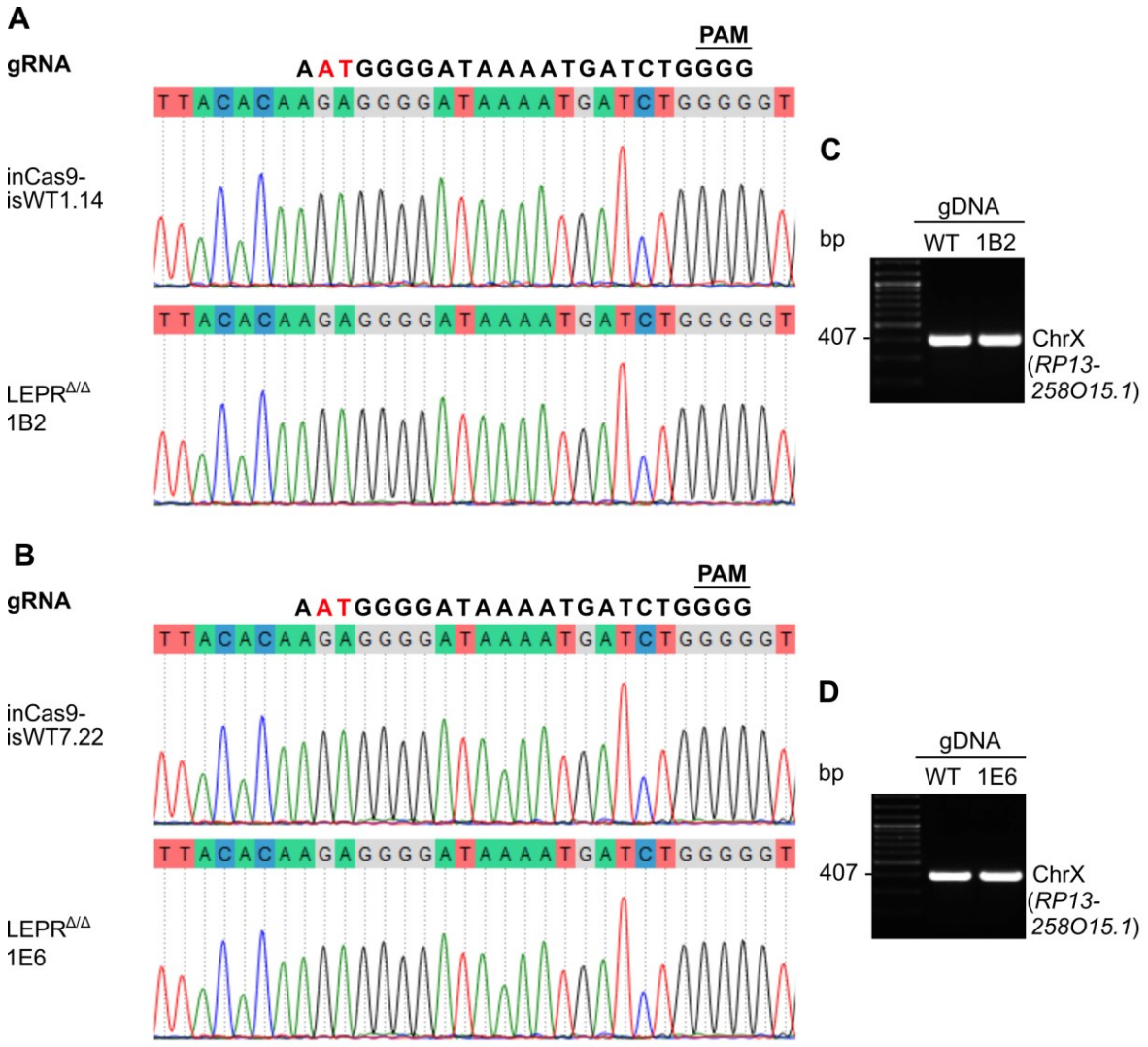

Figure 17. Genomic DNA sequencing analysis of gRNA potential off-target effects in ChrX. (A, B) 1B2 and 1E6 LEPR$^{\Delta/\Delta}$-iPSC sequencing chromatograms for ChrX (gene *RP13-258O15.1*) were aligned with inCas9-isWT1.14 and inCas9-isWT7.22, respectively. (C, D) PCR analyses of gDNA amplified for ChrX (gene *RP13-258O15.1*) in 1B2 and 1E6 LEPR$^{\Delta/\Delta}$-iPSCs showed no difference when compared with inCas9-isWT1.14 and inCas9-isWT7.22, respectively. Mismatches in the gRNA sequence are marked in red.

4.2.2 Loss of LEPR does not alter the pluripotency of LEPR$^{\Delta/\Delta}$-iPSCs

The generated LEPR$^{\Delta/\Delta}$-iPSC lines were first evaluated for their pluripotency. Both 1B2 and 1E6 LEPR$^{\Delta/\Delta}$-iPSC lines were positive for the pluripotency markers OCT4, SOX2, LIN28, NANOG, TRA-1-60, and SSEA4 as observed by immunostaining (Fig. 18A, B), similar to WT-iPSCs (Göttingen, 2019a, b).

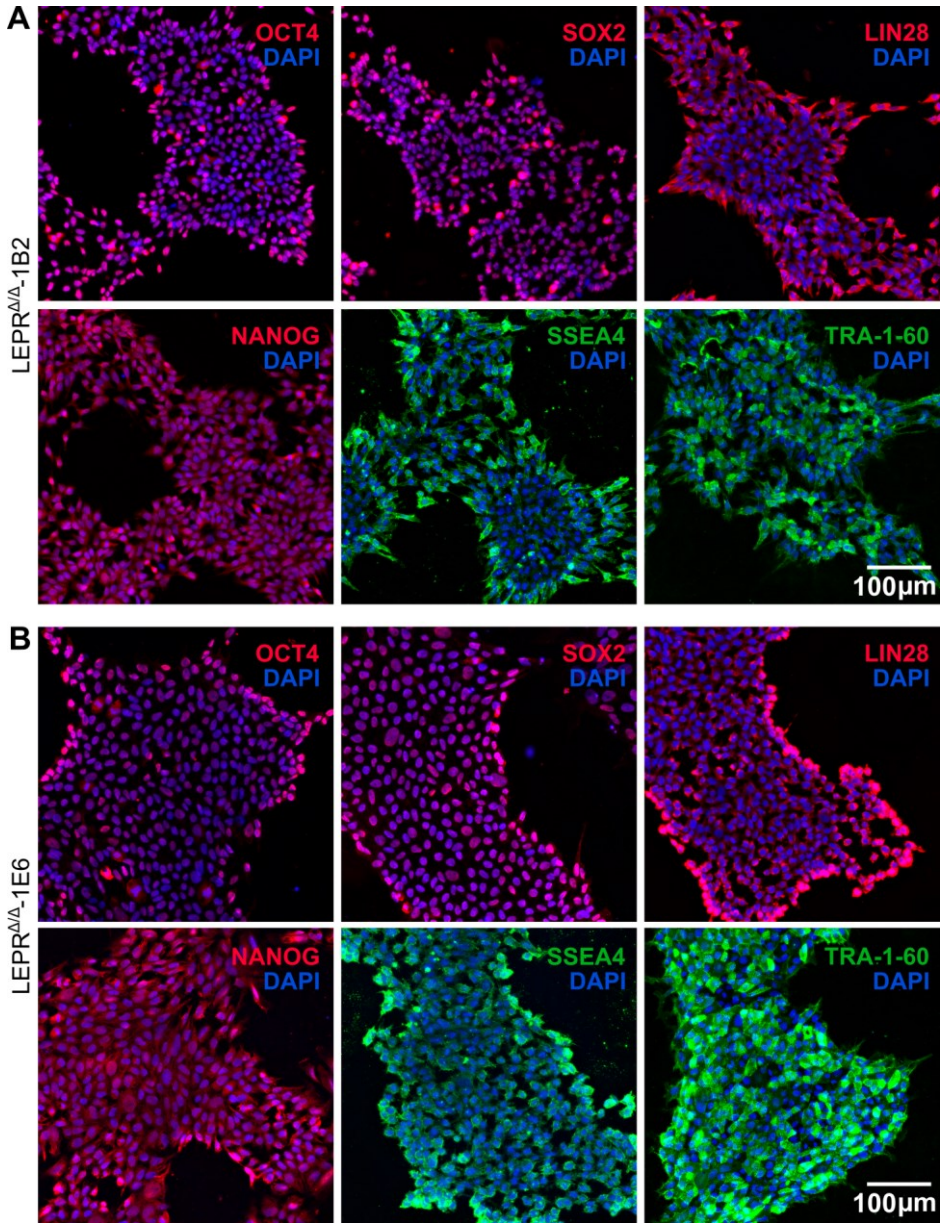

Figure 18. Pluripotency characterization of 1B2 and 1E6 LEPR$^{\Delta/\Delta}$-iPSC lines. Immunostaining for the pluripotent markers in 1B2 (A) and 1E6 (B) LEPR$^{\Delta/\Delta}$-iPSCs. Nuclei were stained with Hoechst 33342. Scale bar, 100 µm.

4.2.3 Loss of LEPR does not alter cardiac differentiation of LEPR$^{\Delta/\Delta}$-iPSCs

Importantly, using the standard directed differentiation protocol, 1B2 LEPR$^{\Delta/\Delta}$ -iPSCs were able to differentiate into spontaneously beating CMs similar to WT-iPSCs. The percentage of cTNT-positive CMs at day 60 post differentiation of 1B2 LEPR$^{\Delta/\Delta}$-iPSC-CMs was comparable to those in the WT groups under the B27 medium. Both WT- and LEPR$^{\Delta/\Delta}$-iPSC-CMs demonstrated high percentage of CMs (~90%) in B27 medium, indicating that loss of LEPR does not alter the differentiation efficiency into CMs.

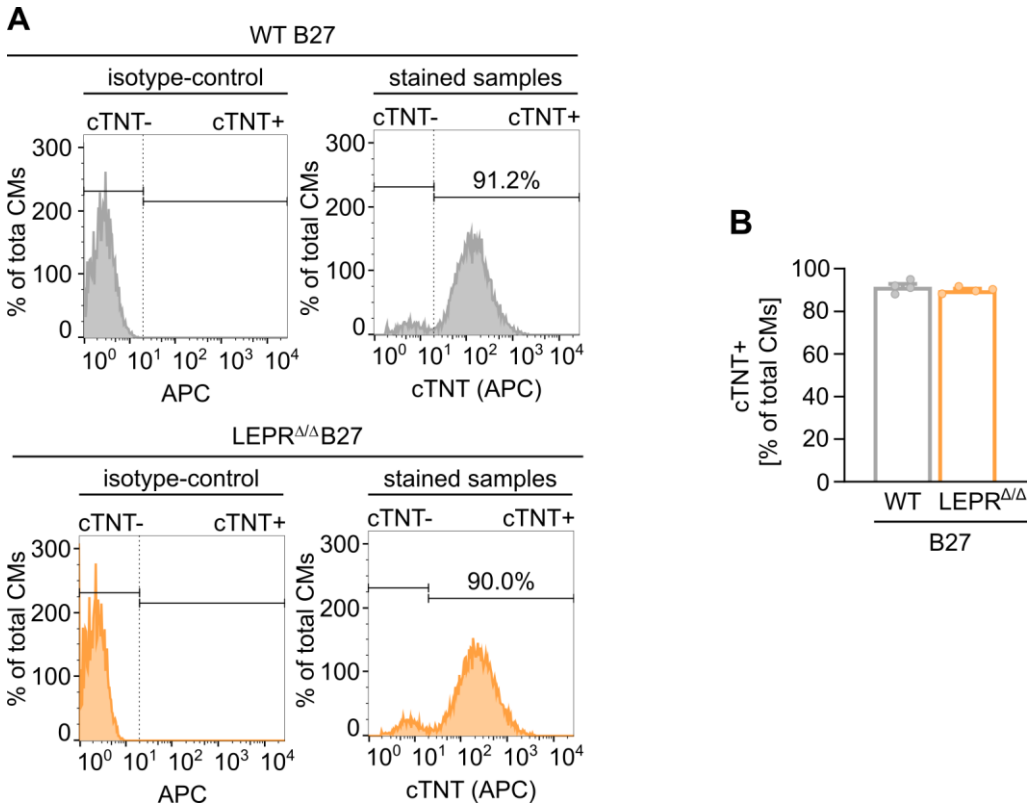

Figure 19. Analysis of cTNT-positive iPSC-CMs. (A) Representative flow cytometry histograms (left isotype-control; right cTNT-APC staining) show high population of cTNT-positive CMs in LEPR$^{\Delta/\Delta}$-iPSC-CMs comparable to WT-iPSC-CMs at day 60 post differentiation in B27 medium. (B) Quantification for cTNT-positive WT- and LEPR$^{\Delta/\Delta}$-iPSC-CMs (WT: n = 4; LEPR$^{\Delta/\Delta}$: n = 4).

Taken together, the generation of LEPR$^{\Delta/\Delta}$-iPSCs may provide a promising platform for the investigation of the molecular and metabolic mechanisms driven by LEPR in the heart. To explore LEPR function in iPSC-CMs, two LEPR$^{\Delta/\Delta}$-iPSC lines with a homozygous LEPR mutation leading to the formation of truncated LEPR similar to that observed in the patient were successfully generated and characterized. The data show that loss of function of LEPR does not affect the initiation of cardiac differentiation from human iPSCs.

4.3 Alterations of leptin and insulin signalling in 1B2 LEPR$^{\Delta/\Delta}$-iPSC-CMs

To study the role of LEPR in glucose and fatty acid metabolism of iPSC-CMs, we first analysed the changes in leptin and insulin signalling in 1B2 LEPR$^{\Delta/\Delta}$-iPSC-CMs compared to WT-iPSC-CMs.

4.3.1 Alterations of LEPR signalling in LEPR$^{\Delta/\Delta}$-iPSC-CMs

To assess the *LEPR* expression in LEPR$^{\Delta/\Delta}$-iPSCs and WT-iPSC-CMs, quantitative real-time polymerase chain reaction analysis was performed. LEPR (exons 9-11) and (exons

15-17) mRNA levels were decreased in LEPR$^{\Delta/\Delta}$-iPSC-CMs compared to WT-iPSC-CMs at d30, d60 and d90 cultured in B27 medium (Fig. 20A, B). To evaluate LEPR protein expression in LEPR$^{\Delta/\Delta}$-iPSC-CMs, the antibody targeting the cytoplasmic domain (Proteintech) was applied for western blot analysis. Although LEPR protein level expression was lower in LEPR$^{\Delta/\Delta}$-iPSC-CMs compared to WT-iPSC-CMs at d30 and d60 cultured in B27 medium, a band of the same molecular weight was observed.

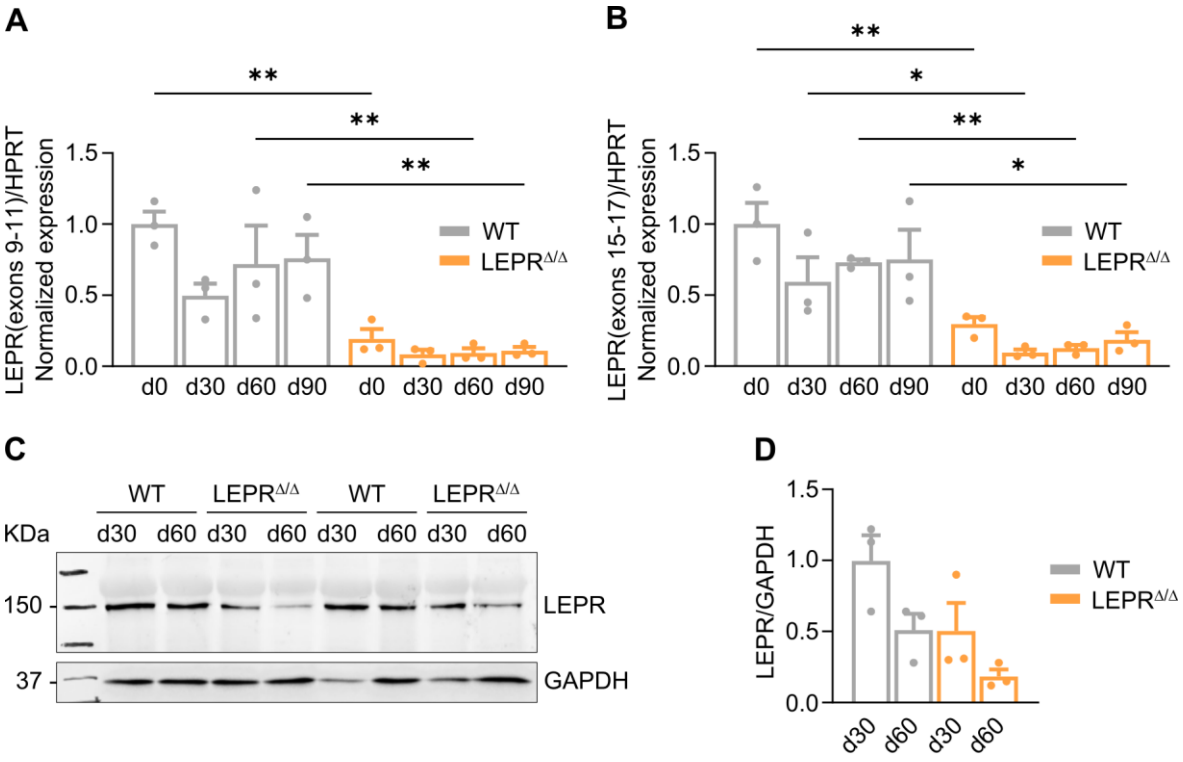

Figure 20. LEPR expression in LEPR$^{\Delta/\Delta}$-iPSC-CMs. (A) Quantitative real-time polymerase chain reaction analysis for *LEPR* (exons 9-11) in WT- and LEPR$^{\Delta/\Delta}$-iPSCs (d0) and -iPSC-CMs (d30-d90) cultured in B27 medium (WT: n = 3; LEPR$^{\Delta/\Delta}$: n = 3). (B) Quantitative real-time polymerase chain reaction analysis for *LEPR* (exons 15-17) in WT- and LEPR$^{\Delta/\Delta}$-iPSCs (d0) and -iPSC-CMs (d30-d90) cultured in B27 medium (WT: n = 3; LEPR$^{\Delta/\Delta}$: n = 3). mRNA levels were normalized to *HPRT*. *P < 0.05, **P < 0.01; d30, d60 and d90 *vs*. d0 WT; d30, d60 and d90 *vs*. d0 LEPR$^{\Delta/\Delta}$; LEPR$^{\Delta/\Delta}$ *vs*. WT by using the two-way ANOVA with the Šídák's multiple comparison test. (C, D) Representative western blot and quantification of LEPR in WT- and LEPR$^{\Delta/\Delta}$-iPSC-CMs cultured in B27 medium (WT: n = 3; LEPR$^{\Delta/\Delta}$: n = 3). Protein levels were normalized to GAPDH.

Although the B27 medium represent a well-established medium to cultivate iPSC-CMs, it discloses limitations for studying CM metabolism due to its high concentrations of insulin (700 nM) and glucose (11 mM), but a low concentration of fatty acid. Since leptin is known to play a critical role in regulating energy metabolism including glucose and fatty acid, to explore the physiological role of leptin, we generated a new medium (F2) with physiological concentrations of insulin (50 nM) and glucose (7 mM), and high concentrations of fatty acid

using Albumax (0.5%). Analysis of LEPR showed slightly lower LEPR expression (Fig. 21A, B) and reduced JAK2 phosphorylation in LEPR$^{\Delta/\Delta}$-iPSC-CMs in both B27 and F2 medium compared to those in the WT groups under the same conditions (Fig. 21C, D). These results indicate that JAK2 phosphorylation is decreased in LEPR$^{\Delta/\Delta}$-iPSC-CMs in comparison to WT-iPSC-CMs under basal conditions.

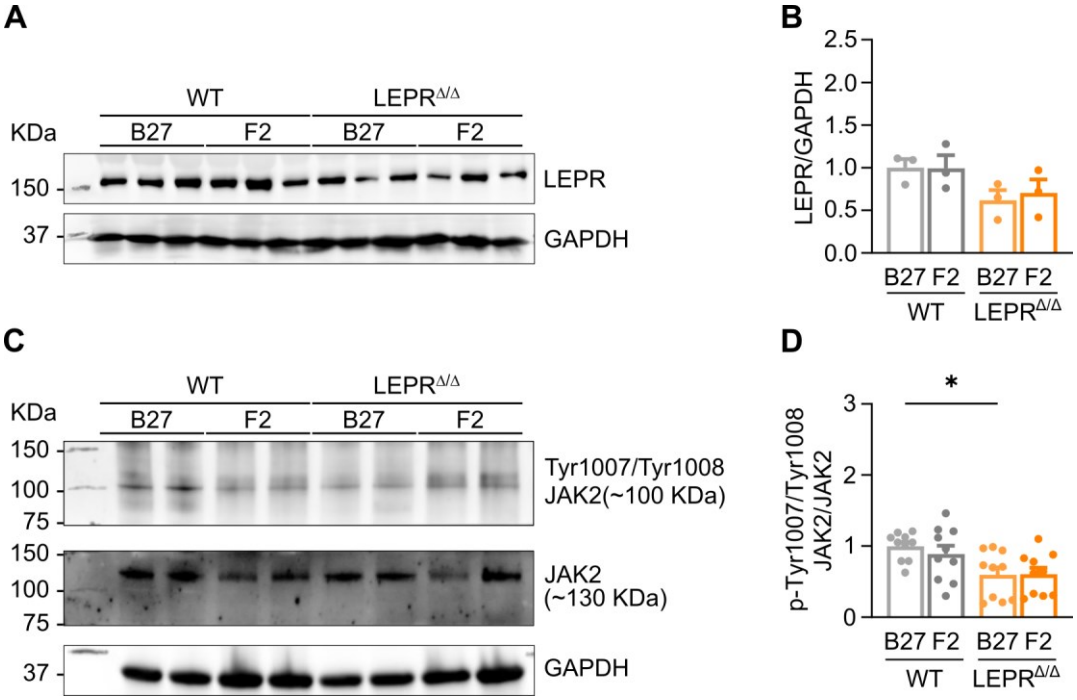

Figure 21. LEPR expression and phosphorylation of JAK2 in WT- and LEPR$^{\Delta/\Delta}$-iPSC-CMs in B27 or F2 medium. (A, B) Representative western blot and quantification of LEPR in WT- and LEPR$^{\Delta/\Delta}$-iPSC-CMs cultured in B27 or F2 medium (WT B27: n = 3; LEPR$^{\Delta/\Delta}$ B27: n = 3; WT F2: n = 3; LEPR$^{\Delta/\Delta}$ F2: n = 3). Protein levels were normalized to GAPDH. (C, D) Representative western blot and quantification of changes in the phosphorylation of JAK2 (Tyr1007/1008) in WT- and LEPR$^{\Delta/\Delta}$-iPSC-CMs cultured in B27 or F2 medium (WT B27: n = 10; LEPR$^{\Delta/\Delta}$ B27: n = 10; WT F2: n = 10; LEPR$^{\Delta/\Delta}$ F2: n = 10). *P < 0.05; LEPR$^{\Delta/\Delta}$ *vs.* WT for B27 and F2 as well as B27 *vs.* F2 for WT and LEPR$^{\Delta/\Delta}$ by using the two-way ANOVA with the Šídák's multiple comparisons test.

To investigate leptin-mediated LEPR signalling activation, 60-day-old WT- and LEPR$^{\Delta/\Delta}$-iPSC-CMs cultured in B27 medium were first applied. To this end, the cells were starved for 24 hours with the starvation medium (without glucose and without insulin, but with lactate) and then stimulated with leptin (1.24 nM) in starvation medium with the addition of 11 mM glucose for 5-, 10- and 15-minutes. LEPR expression in LEPR$^{\Delta/\Delta}$-iPSC-CMs was slightly reduced compared to that of WT-iPSC-CMs without leptin stimulation (Fig. 22A, B). However, there was no changes in LEPR expression after leptin stimulation either in WT- or in LEPR$^{\Delta/\Delta}$-iPSC-CMs after leptin stimulation (Fig. 22A, B). Leptin-dependent phosphorylation of JAK2 (Tyr1007/1008) was also not significantly changed either in WT-

or in LEPR$^{\Delta/\Delta}$-iPSC-CMs after leptin stimulation (Fig. 22C, D). The difference in phosphorylation of JAK2 between WT- and LEPR$^{\Delta/\Delta}$-iPSC-CMs cultured in B27 medium (Fig. 21D) was not observed when the cells were starved overnight, suggesting a different glucose- and/or lactate-regulated JAK2 phosphorylation in LEPR$^{\Delta/\Delta}$-iPSC-CMs compared to WT-iPSC-CMs.

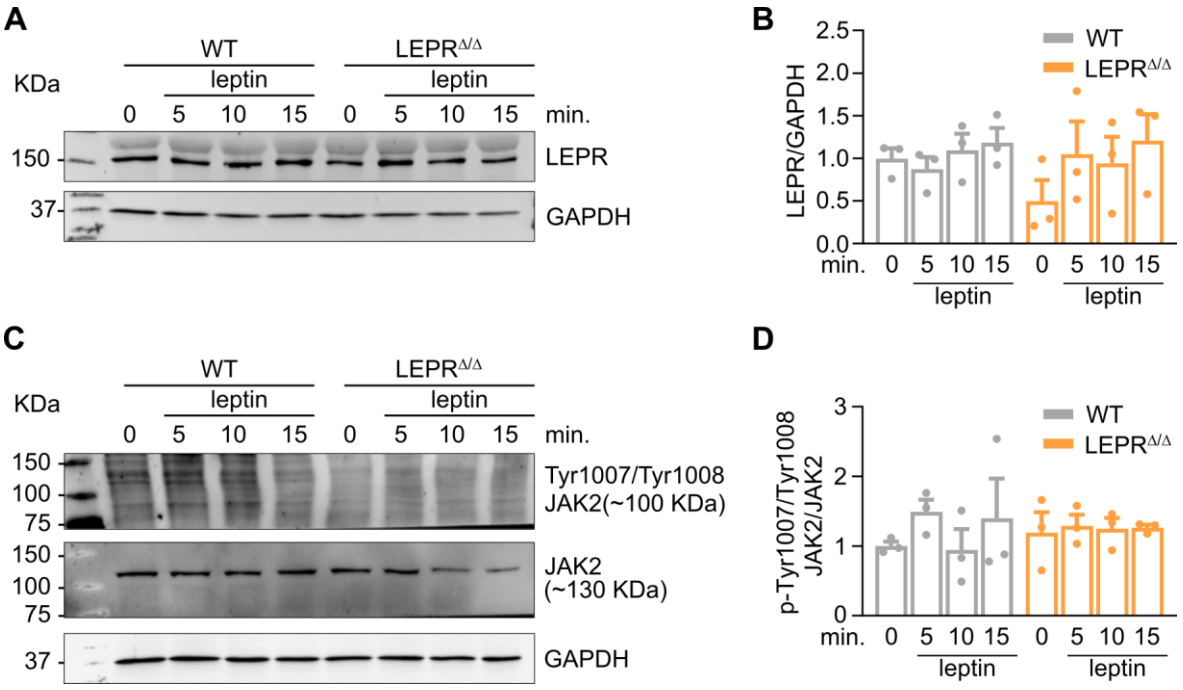

Figure 22. LEPR signalling in WT- and LEPR$^{\Delta/\Delta}$-iPSC-CMs in B27 medium upon acute leptin stimulation. (A, B) Representative western blot and quantification of LEPR and (C, D) p-JAK2 (Tyr1007/1008) in WT- and LEPR$^{\Delta/\Delta}$-iPSC-CMs cultured in B27 medium. WT- and LEPR$^{\Delta/\Delta}$-iPSC-CMs were starved overnight and stimulated with leptin (1.24 nM) for 5-, 10- and 15-minutes (min) (WT B27: n = 3; LEPR$^{\Delta/\Delta}$ B27: n = 3). LEPR protein levels were normalized to GAPDH, p-JAK2 (Tyr1007/1008) protein levels were normalized to total JAK2.

Given that LEPR signalling was not activated by leptin in WT-iPSC-CMs cultured in B27 medium before (Fig. 22D), changes in LEPR signalling pathway activation were then analysed in WT- and LEPR$^{\Delta/\Delta}$-iPSC-CMs cultivated in F2 medium upon starvation for 24 hours in starvation medium and acute leptin (1.24 nM) stimulation for 5-, 10- or 15-minutes. For the acute leptin stimulation, the starvation medium was changed to F2 medium without insulin. Significantly decreased LEPR expression was observed in starved and non-stimulated LEPR$^{\Delta/\Delta}$-iPSC-CMs compared to WT-iPSC-CMs (Fig. 23A, B). Whereas there are no any changes in LEPR expression in LEPR$^{\Delta/\Delta}$-iPSC-CMs after leptin stimulation, slight increases in LEPR protein expression levels were observed in leptin-stimulated WT-iPSC-CMs. Importantly, leptin stimulation significantly induced the activation of JAK2 in WT-iPSC-

CMs but not in LEPR$^{\Delta/\Delta}$-iPSC-CMs (Fig. 23C, D), indicating impaired leptin/LEPR-mediated signalling in LEPR$^{\Delta/\Delta}$-iPSC-CMs. Therefore, LEPR loss of function was demonstrated in LEPR$^{\Delta/\Delta}$-iPSC-CMs only under the physiological metabolic medium (F2) condition, but not under the B27 medium condition, indicating that the culture condition represents an important parameter to study LEPR role in iPSC-CMs.

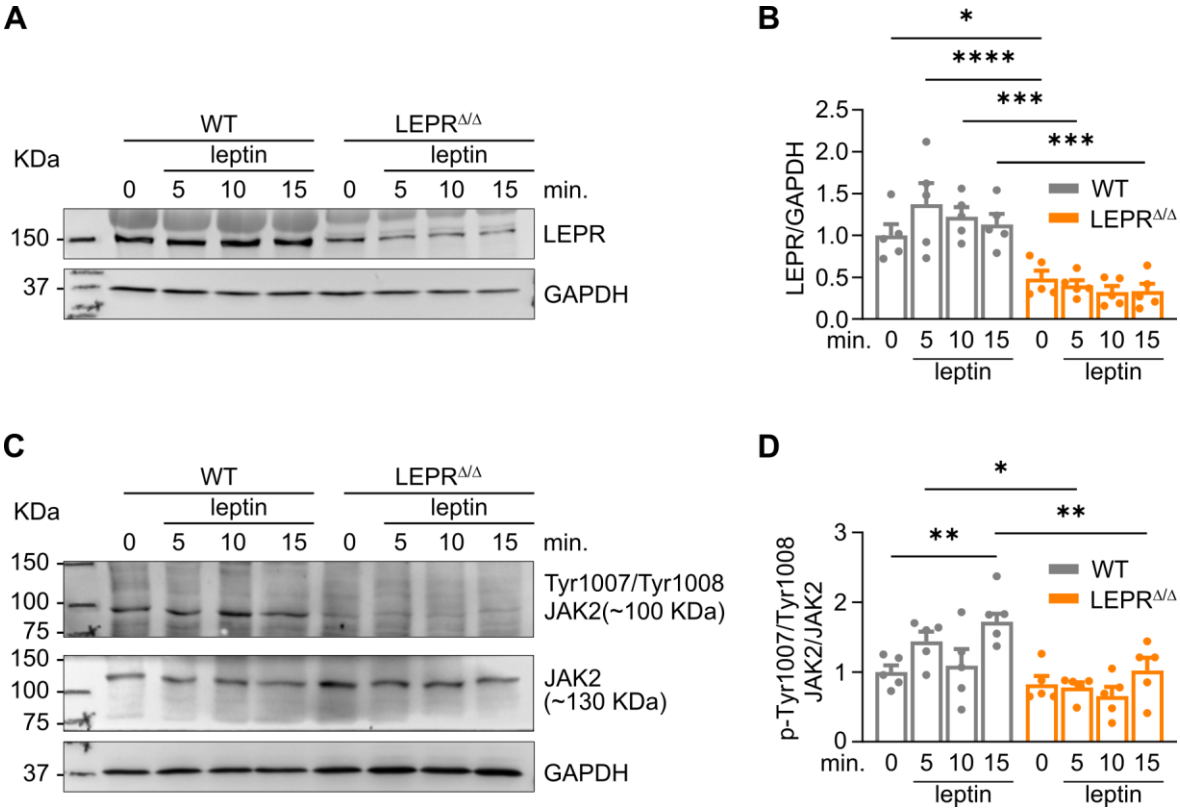

Figure 23. LEPR signalling activation in WT- and LEPR$^{\Delta/\Delta}$-iPSC-CMs upon acute leptin stimulation in F2 medium. (A, B) Representative western blot and quantification of LEPR and (C, D) p-JAK2 (Tyr1007/1008) in WT- and LEPR$^{\Delta/\Delta}$-iPSC-CMs cultured in F2 medium (WT F2: n = 5; LEPR$^{\Delta/\Delta}$ F2: n = 5). WT- and LEPR$^{\Delta/\Delta}$-iPSC-CMs were starved overnight and stimulated with leptin (1.24 nM) for 5-, 10- and 15-minutes (min). LEPR protein levels were normalized to GAPDH, p-JAK2 (Tyr1007/1008) protein levels were normalized to total JAK2. 5-, 10- and 15-min. *vs.* 0 min WT; 5-, 10- and 15-min *vs.* 0 min LEPR$^{\Delta/\Delta}$; LEPR$^{\Delta/\Delta}$ *vs.* WT; *P < 0.05; **P < 0.01; ***P < 0.001; ****P < 0.0001; by using the two-way ANOVA with the Šídák's multiple comparison test.

4.3.2 Alterations of Insulin signalling in LEPR$^{\Delta/\Delta}$-iPSC-CMs

As leptin and insulin are both known as major regulators of energy homeostasis and play fundamental roles in metabolic flexibility of CMs, insulin-mediated AKT activation was studied in iPSC-CMs. To figure out the optimal stimulation duration of insulin, WT-iPSC-CMs cultivated under F2 medium for 60 days were starved for 24 hours with starvation medium and then changed to F2 medium with the presence of insulin (50 nM) for 5, 10 and

15 minutes. Slight insulin-dependent rise in AKT phosphorylation (Ser473) was observed upon 10-minute insulin stimulation in iPSC-CMs (Fig. 24A, B).

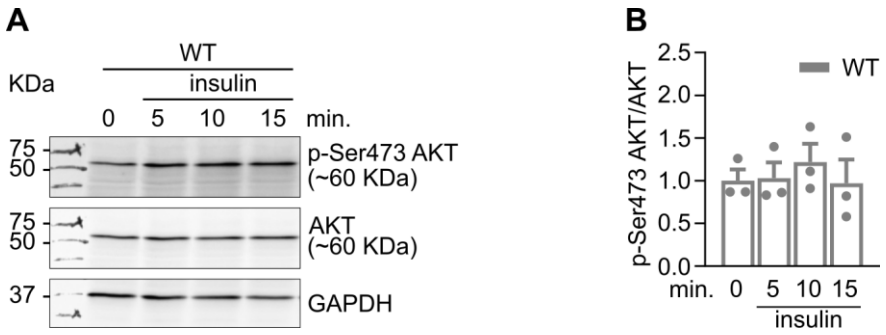

Figure 24. Assessment of AKT phosphorylation upon insulin stimulation. (A, B) Representative western blots and quantification of AKT phosphorylation (Ser473) in WT-iPSC-CMs cultured in F2 medium upon acute insulin stimulation (50 nM) for 5-, 10- and 15-minutes (WT F2: n = 3). Phosphorylated AKT levels were normalized to total AKT. WT-iPSC-CMs were starved overnight prior to stimulation.

Next, the crosstalk between leptin and insulin pathways was investigated in WT- and LEPR$^{\Delta/\Delta}$-iPSC-CMs maintained in B27 and F2 medium. Stimulation with leptin (1.24 nM), insulin (50 nM), and their combination was applied to WT- and LEPR$^{\Delta/\Delta}$-iPSC-CMs for 10 minutes. In general, LEPR expression was slightly lower in non-stimulated LEPR$^{\Delta/\Delta/}$-iPSC-CMs compared to non-stimulated WT-iPSC-CMs in B27 medium (Fig. 25A, B) and more pronounced in F2 medium (Fig. 26A, B), as also shown above (Fig. 22A, B; Fig. 23A, B). There is no significant influence of leptin, insulin, or their combination on LEPR expression in both WT- and LEPR$^{\Delta/\Delta/}$-iPSC-CMs cultured either in B27 (Fig. 25A, B) or F2 medium (Fig. 26A, B). Similar to the data shown in Figs. 22C, D and 23C, D, non-stimulated LEPR$^{\Delta/\Delta}$-iPSC-CMs demonstrated comparable AKT phosphorylation to non-stimulated WT-iPSC-CMs in B27 (Fig. 25C, D) or F2 medium (Fig. 26C, D) after starvation for 24 hours. Upon leptin stimulation, no significant changes in AKT phosphorylation were found either in LEPR$^{\Delta/\Delta}$-iPSC-CMs or in WT-iPSC-CMs in B27 (Fig. 25C, D) or F2 medium (Fig. 26C, D). However, insulin-dependent phosphorylation of AKT was significantly enhanced in both WT-iPSC-CMs and LEPR$^{\Delta/\Delta/}$-iPSC-CMs cultured in B27 medium before (Fig. 25C, D), and in WT-iPSC-CMs cultured in F2 medium before (Fig. 26C, D). A slight but not significant increase in AKT phosphorylation was observed in LEPR$^{\Delta/\Delta}$-iPSC-CMs, cultured in F2 medium before, after insulin stimulation (Fig. 26C, D). Leptin and insulin co-stimulation led to a significant increase in AKT phosphorylation in both WT-iPSC-CMs and LEPR$^{\Delta/\Delta/}$-iPSC-CMs in B27 (Fig. 25C, D) or F2 medium (Fig. 26C, D). Whereas their effects were slightly less than insulin stimulation alone in WT-iPSC-CMs in B27 (Fig. 25C, D) or F2 medium (Fig.

26C, D), this effect was also observed in LEPR$^{\Delta/\Delta}$-iPSC-CMs in B27 medium (Fig. 25C, D), but not in F2 medium (Fig. 26C, D).

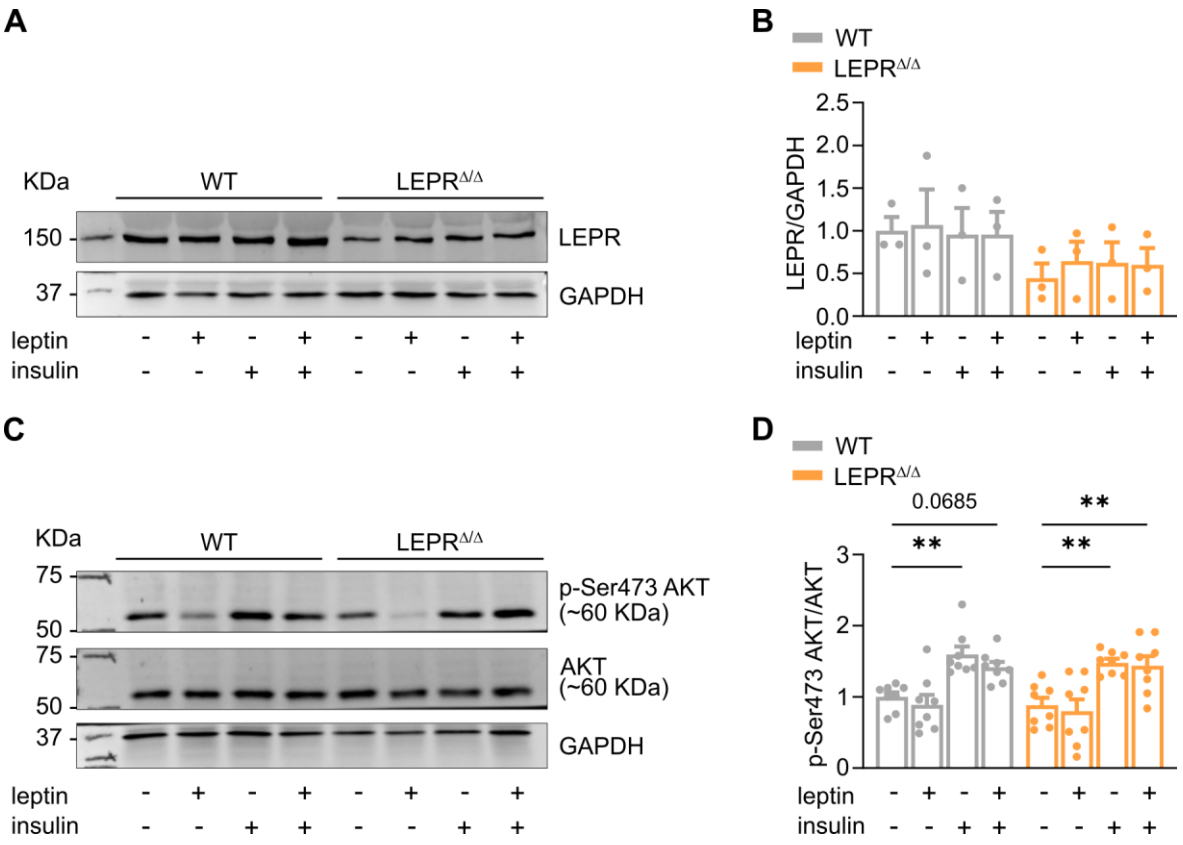

Figure 25. Insulin signalling activation in WT- and LEPR$^{\Delta/\Delta}$-iPSC-CMs upon acute stimulation with insulin, and leptin, and their co-stimulation in B27 medium. (A, B) Representative western blots and quantification of LEPR in WT- and LEPR$^{\Delta/\Delta}$-iPSC-CMs cultured in B27 medium upon acute stimulation with leptin (1.24 nM), insulin (50 nM) and their combination. Protein levels were normalized to GAPDH (WT B27: n = 3; LEPR$^{\Delta/\Delta}$ B27: n = 3). (C, D) Representative western blots and quantification of changes in the phosphorylation of AKT (Ser473) in WT- and LEPR$^{\Delta/\Delta}$-iPSC-CMs cultured in B27 medium upon acute stimulation with leptin (1.24 nM), insulin (50 nM) and their combination. Protein levels were normalized to total AKT (WT B27: n = 8; LEPR$^{\Delta/\Delta}$ B27: n = 8). **P < 0.01 leptin-, insulin- or leptin and insulin-stimulated WT *vs.* non-stimulated WT; leptin-, insulin- or leptin and insulin-stimulated LEPR$^{\Delta/\Delta}$ *vs.* non-stimulated LEPR$^{\Delta/\Delta}$; LEPR$^{\Delta/\Delta}$ *vs.* WT by using the two-way ANOVA with the Šídák's multiple comparison test.

Importantly, the activation of insulin pathway was more pronounced in WT-iPSC-CMs in F2 medium than in B27 medium, as shown by more significant increases in AKT phosphorylation upon insulin or insulin and leptin co-stimulation. However, insulin-dependent AKT phosphorylation in LEPR$^{\Delta/\Delta}$-iPSC-CMs was not as significantly increased as in WT-iPSC-CMs in F2 medium, implying an altered insulin signalling in LEPR$^{\Delta/\Delta}$-iPSC-CMs in F2 medium with the presence of glucose and fatty acids (Fig. 26C, D).

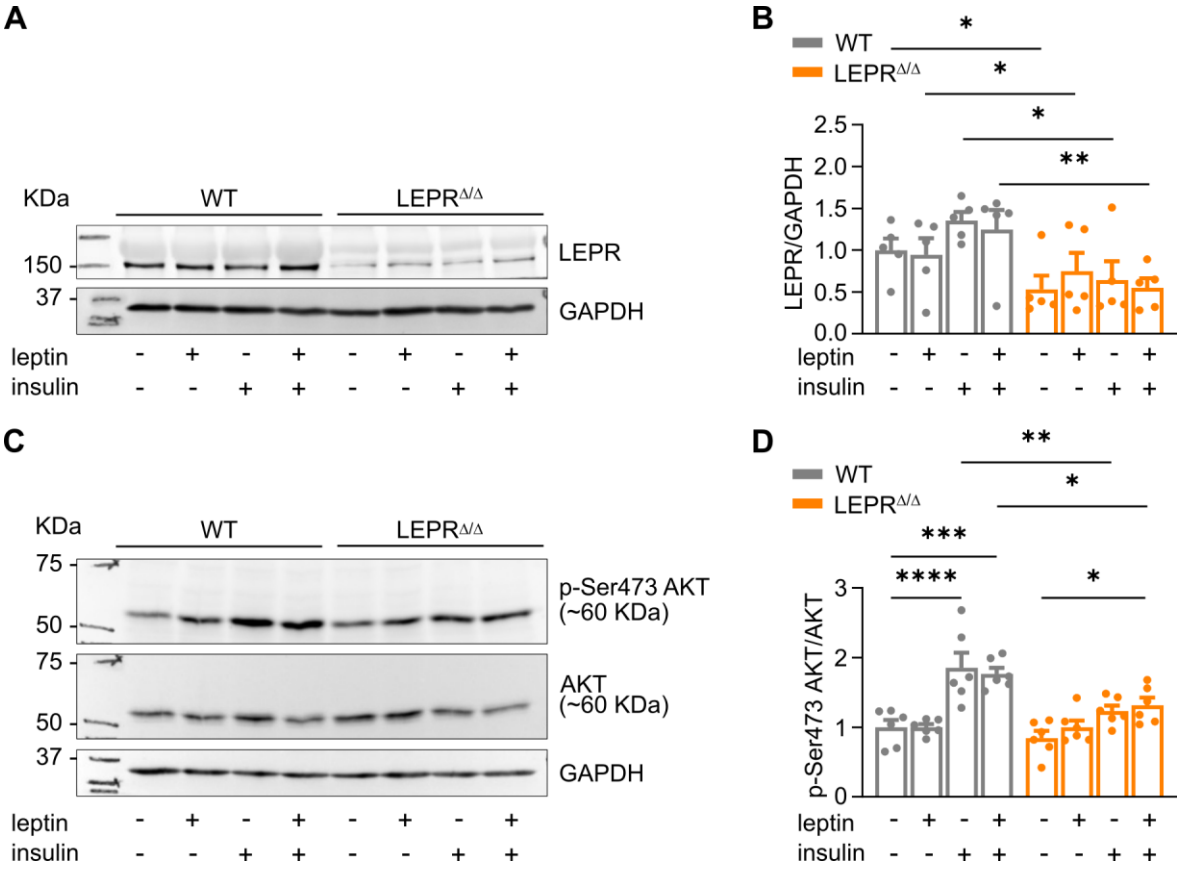

Figure 26. Insulin signalling activation in WT- and LEPR$^{\Delta/\Delta}$-iPSC-CMs upon acute stimulation with insulin, and leptin, and their co-stimulation in F2 medium. (A, B) Representative western blots and quantification of LEPR in WT- and LEPR$^{\Delta/\Delta}$-iPSC-CMs cultured in F2 medium upon acute stimulation with leptin (1.24 nM), insulin (50 nM) and their combination. Protein levels were normalized to GAPDH (WT F2: n = 5; LEPR$^{\Delta/\Delta}$ F2: n = 5). *P < 0.05; **P < 0.01 leptin-, insulin- or leptin and insulin-stimulated WT *vs.* non-stimulated WT; leptin-, insulin- or leptin and insulin-stimulated LEPR$^{\Delta/\Delta}$ *vs.* non-stimulated LEPR$^{\Delta/\Delta}$; LEPR$^{\Delta/\Delta}$ *vs.* WT by using the two-way ANOVA with the Šídák's multiple comparison test. (C, D) Representative western blots and quantification of changes in the phosphorylation of AKT (Ser473) in WT- and LEPR$^{\Delta/\Delta}$-iPSC-CMs cultured in F2 medium upon acute stimulation with leptin (1.24 nM), insulin (50 nM) and their combination. Protein levels were normalized to total AKT (WT F2: n = 6; LEPR$^{\Delta/\Delta}$ F2: n = 6). *P < 0.05; **P < 0.01; ***P < 0.001; ****P < 0.0001 leptin-, insulin- or leptin and insulin-stimulated WT *vs.* non-stimulated WT; leptin-, insulin- or leptin and insulin-stimulated LEPR$^{\Delta/\Delta}$ *vs.* non-stimulated LEPR$^{\Delta/\Delta}$; LEPR$^{\Delta/\Delta}$ *vs.* WT by using the two-way ANOVA with the Šídák's multiple comparison test. WT- and LEPR$^{\Delta/\Delta}$-iPSC-CMs were starved overnight prior to stimulation.

4.4 Alterations of metabolic flexibility in LEPR$^{\Delta/\Delta}$-iPSC-CMs

4.4.1 Expression of metabolic markers in WT- and LEPR$^{\Delta/\Delta}$-iPSC-CMs

To assess the metabolic phenotype of WT- and LEPR$^{\Delta/\Delta}$-iPSC-CMs maintained in B27 and F2 medium, the expression of genes involved in the uptake and metabolism of glucose and fatty acids was analysed. In WT-iPSC-CMs, mRNA expression of the glucose transporters *GLUT-1* (Fig. 27A) and *GLUT-4* (Fig. 27B) was significantly higher when cultured in F2 medium when compared with B27 medium. While the expression of the fatty acid

transporter *CD36* was comparable in WT-iPSC-CMs cultured in B27 and F2 medium (Fig. 27C), the expression of another fatty acid transporter *CPT1-B* encoding an integral outer mitochondrial membrane protein was enhanced in WT-iPSC-CMs cultured in F2 compared to B27 medium (Fig. 27D). In LEPR$^{\Delta/\Delta}$-iPSC-CMs, only slight increases in *GLUT-1* and *GLUT-4* were observed when cultured in F2 medium compared with B27 medium (Fig. 27A, B) whereas *CD36* expression was similar in these two media (Fig. 27C). Similar to WT-iPSC-CMs, significantly higher *CPT1-B* expression was observed in LEPR$^{\Delta/\Delta}$-iPSC-CMs cultured in F2 medium compared to those in B27 medium (Fig. 27D). Notably, *GLUT-1, GLUT-4* and *CD36* expression was slightly lower but *CPT1-B* expression was slightly higher in LEPR$^{\Delta/\Delta}$-iPSC-CMs compared to WT-iPSC-CMs when cultured in F2 medium (Fig. 27), suggesting that LEPR loss of function in iPSC-CMs may influence the uptake and metabolism of glucose and fatty acids.

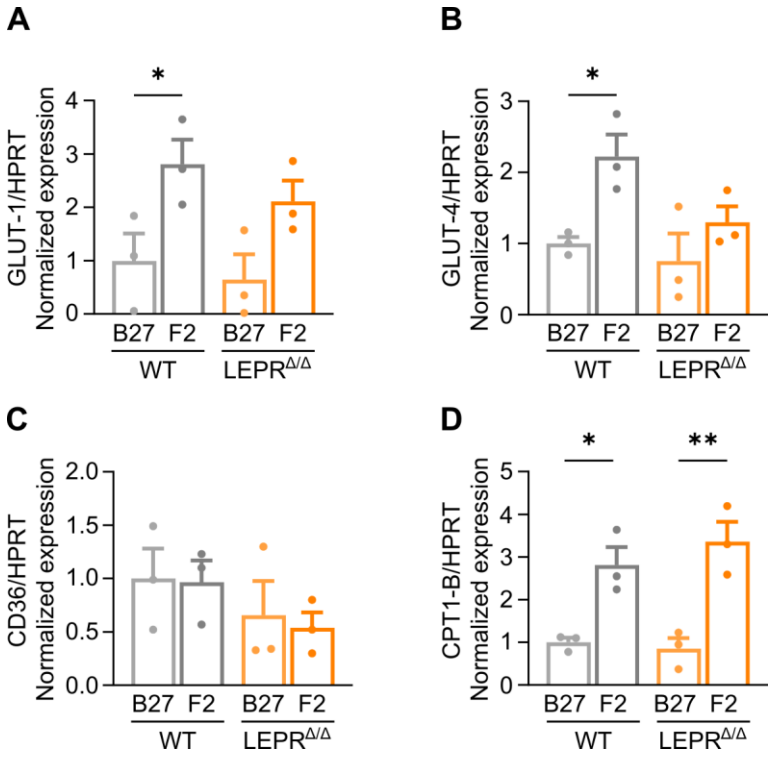

Figure 27. mRNA expression of metabolic markers in WT- and LEPR$^{\Delta/\Delta}$-iPSC-CMs in B27 and F2 medium. Direct comparison of (A) *GLUT-1,* (B) *GLUT-4,* (C) *CD36,* and (D) *CPT1-B* expression in WT- and LEPR$^{\Delta/\Delta}$-iPSC-CMs cultured in B27 or F2 medium (WT B27: n = 3; LEPR$^{\Delta/\Delta}$ B27: n = 3; WT F2: n = 3; LEPR$^{\Delta/\Delta}$ F2: n = 3). mRNA levels were normalized to *HPRT*. *P < 0.05; **P < 0.01 LEPR$^{\Delta/\Delta}$ *vs.* WT for B27 and F2 as well as B27 *vs.* F2 for WT and LEPR$^{\Delta/\Delta}$ by using the two-way ANOVA with the Šídák's multiple comparisons test.

Another important player in CM energy homeostasis is AMPK, which is known to regulate glucose and fatty acid uptake and oxidation when AMP/ATP ratio is high (Bairwa *et al.*,

2016). AMPK phosphorylation (Thr172) levels were comparable in WT-iPSC-CMs cultured in B27 and F2 medium, while AMPK activation was significantly lower in LEPR$^{\Delta/\Delta}$-iPSC-CMs in F2 medium compared to those cultivated in B27 medium (Fig. 28A, B). Moreover, significantly higher AMPK activation was shown in LEPR$^{\Delta/\Delta}$-iPSC-CMs compared to WT-iPSC-CMs in B27 medium (Fig. 28A, B), but slightly lower in LEPR$^{\Delta/\Delta}$-iPSC-CMs compared to WT-iPSC-CMs in F2 medium (Fig. 28A, B).

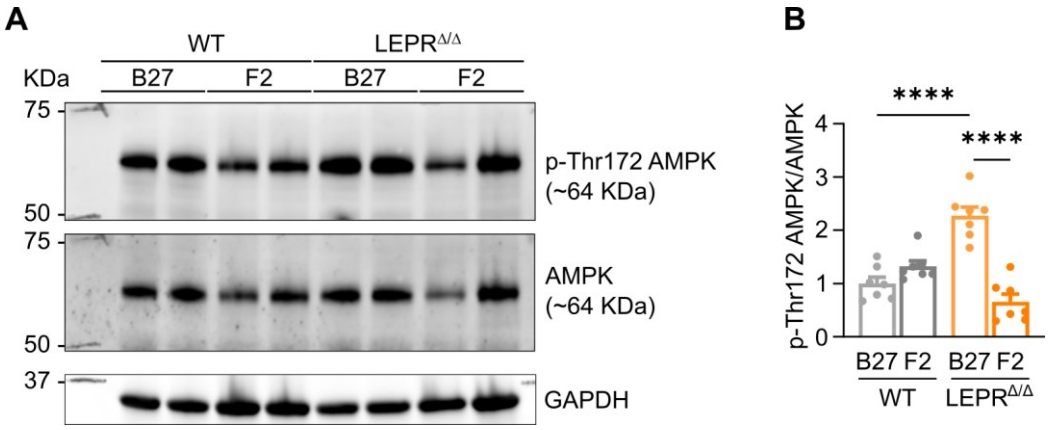

Figure 28. Phosphorylation of AMPK in WT- and LEPR$^{\Delta/\Delta}$-iPSC-CMs in B27 and F2 medium. (A, B) Representative western blots and quantification of changes in AMPK phosphorylation (Thr172) in WT- and LEPR$^{\Delta/\Delta}$-iPSC-CMs cultured in B27 or F2 medium (WT B27: n = 7; LEPR$^{\Delta/\Delta}$ B27: n = 7; WT F2: n = 7; LEPR$^{\Delta/\Delta}$ F2: n = 7). Phosphorylated AMPK levels were normalized to total AMPK. ****P < 0.0001 LEPR$^{\Delta/\Delta}$ *vs.* WT for B27 and F2 as well as B27 *vs.* F2 for WT and LEPR$^{\Delta/\Delta}$ by using the two-way ANOVA with the Šídák's multiple comparisons test.

4.4.2 Changes in mitochondrial function of LEPR$^{\Delta/\Delta}$-iPSC-CMs

To gain further insights into the relationship between the LEPR loss of function and metabolic flexibility in iPSC-CMs, changes in mitochondrial respiration were evaluated in both WT- and LEPR$^{\Delta/\Delta}$-iPSC-CMs in B27 and F2 medium (Fig. 29). The metabolic status of WT-iPSC-CMs cultured under F2 medium was first compared to conventional B27 culture condition (Fig. 29A). No significant changes in basal respiration (Fig. 29C), ATP production (Fig. 29F), proton leak (Fig. 29G) and non-mitochondrial oxygen consumption (Fig. 29H) were found, but 2-fold higher maximal and spare respiration rates (Fig. 29D, E), as quantified by OCR using the Seahorse analyser, were observed in WT-iPSC-CMs cultured in F2 medium compared to those in B27 medium. For LEPR$^{\Delta/\Delta}$-iPSC-CMs (Fig. 29B), cultivation in F2 medium led to increased basal respiration (Fig. 29C), and ATP production (Fig. 29F) compared to B27 medium, which is different from WT-iPSC-CMs. Similar to WT-iPSC-CMs, LEPR$^{\Delta/\Delta}$-iPSC-CMs revealed 1.5-fold higher maximal and spare respiration rates in F2 medium compared to B27 medium (Fig. 29D, E), but no changes in proton leak

(Fig. 29G), and non-mitochondrial respiration level (Fig. 29H). Interestingly, LEPR$^{\Delta/\Delta}$-iPSC-CMs cultured in B27 demonstrated significantly lower basal respiration (Fig. 29C) and ATP production (Fig. 29F) compared to WT-iPSC-CMs under the same condition whereas no differences were observed in terms of other parameters (Fig. 29D, E, G, H). Importantly, in the presence of fatty acids (under the F2 condition), LEPR$^{\Delta/\Delta}$-iPSC-CMs had significantly lower maximal and spare respiration rates than WT-iPSC-CMs (Fig. 29D, E), while proton leak and non-mitochondrial oxygen consumption were comparable in WT and LEPR$^{\Delta/\Delta}$-iPSC-CMs (Fig. 29G, H).

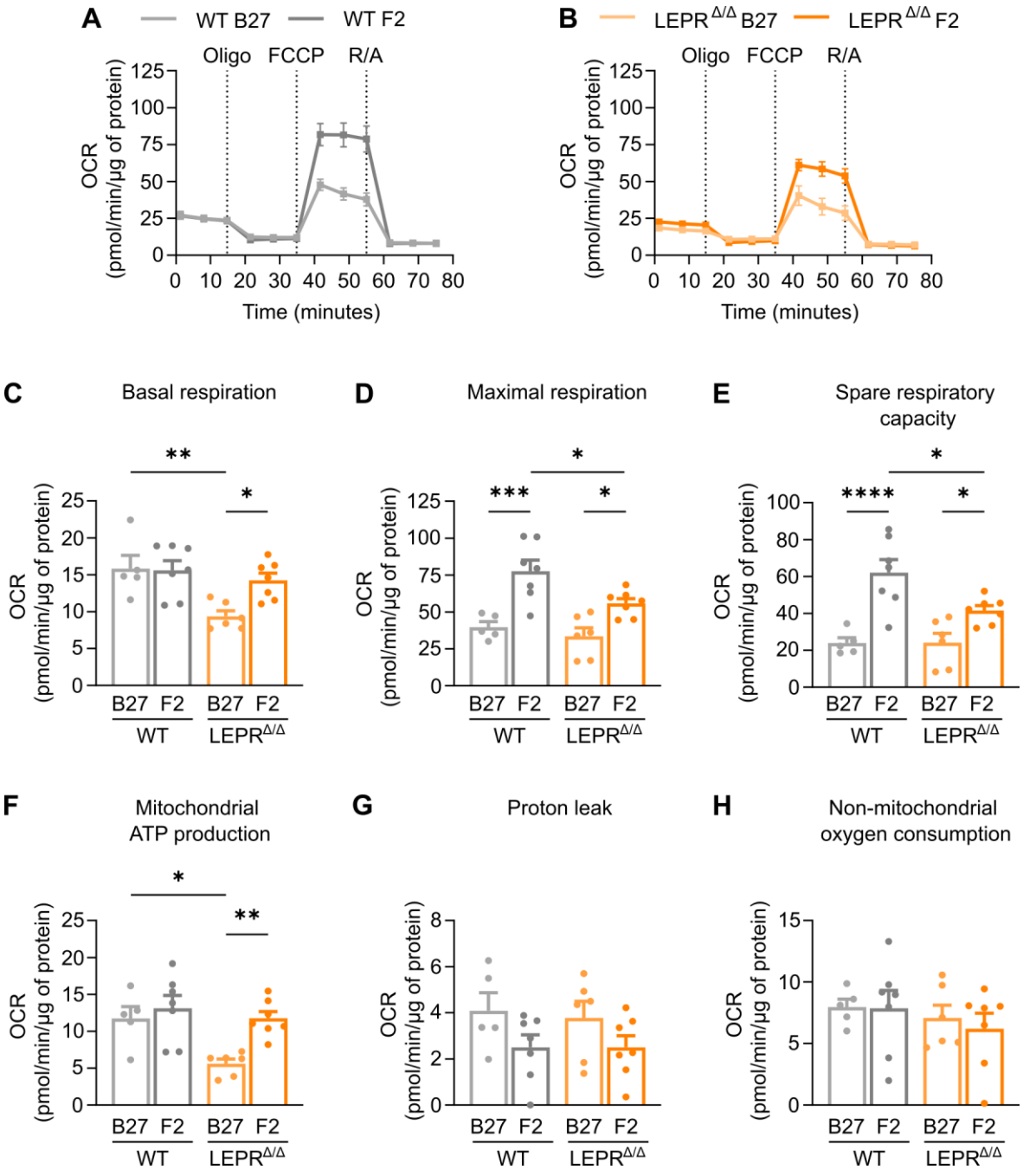

Figure 29. Effect of loss of function of LEPR on mitochondrial respiratory function in iPSC-CMs in B27 and F2 medium. (A, B) Changes in the mitochondrial respiration by assessment of the real-time oxygen consumption rate (OCR) of WT- (A) and LEPR$^{\Delta/\Delta}$-iPSC-CMs (B) cultured in B27 or F2 medium in response to treatment with oligomycin (Oligo), carbonyl cyanide-4-(trifluoromethoxy)phenylhydrazone (FCCP), and rotenone/antimycin A (R/A). (C-H) Quantitative analyses of the calculated parameters for basal respiration (C), maximal respiration (D), spare respiratory capacity (E), mitochondrial ATP production (F), proton leak (G), and non-mitochondrial oxygen consumption (H). Each data point represents an OCR measurement performed in at least three different wells of a 96-well plate (WT B27: n = 5; LEPR$^{\Delta/\Delta}$ B27: n = 6; WT F2: n = 7; LEPR$^{\Delta/\Delta}$ F2: n = 7). *P < 0.05; **P < 0.01; ***P < 0.001; ****P < 0.0001 LEPR$^{\Delta/\Delta}$ *vs.* WT for B27 and F2 as well as B27 *vs.* F2 for WT and LEPR$^{\Delta/\Delta}$ by using the two-way ANOVA with the Šídák's multiple comparisons test.

4.4.3 Changes in glycolytic function in LEPR$^{\Delta/\Delta}$-iPSC-CMs

To further evaluate LEPR role in glycolysis in iPSC-CMs in the presence of glucose and fatty acids as energy substrates, the ECAR was used to assess glycolytic parameters using the glycolysis stress test (Fig. 30). No significant changes in glycolysis were found, in both WT- and LEPR$^{\Delta/\Delta}$-iPSC-CMs in B27 or F2 medium (Fig. 30) Importantly, ECAR rose in both WT- and LEPR$^{\Delta/\Delta}$-iPSC-CMs in B27 and F2 medium after blocking of mitochondrial ATP synthase and shutting down oxidative phosphorylation with oligomycin, which is used to measure “glycolytic capacity” (Fig 30A, D). However, the maximum amount of glycolysis that the cells can acutely perform (glycolytic capacity) is significantly higher only in WT- but not in LEPR$^{\Delta/\Delta}$-iPSC-CMs in F2 compared to B27 medium (Fig. 30C). Interestingly, glycolytic reserve was increased in both WT- and LEPR$^{\Delta/\Delta}$-iPSC-CMs cultured in F2 compared to B27 medium, respectively (Fig. 30E), but slightly higher in WT-iPSC-CMs than in LEPR$^{\Delta/\Delta}$-iPSC-CMs under the F2 condition (Fig. 30E). Non-glycolytic acidification was increased in WT- and only slightly in LEPR$^{\Delta/\Delta}$-iPSC-CMs in B27 or F2 medium (Fig. 30F).

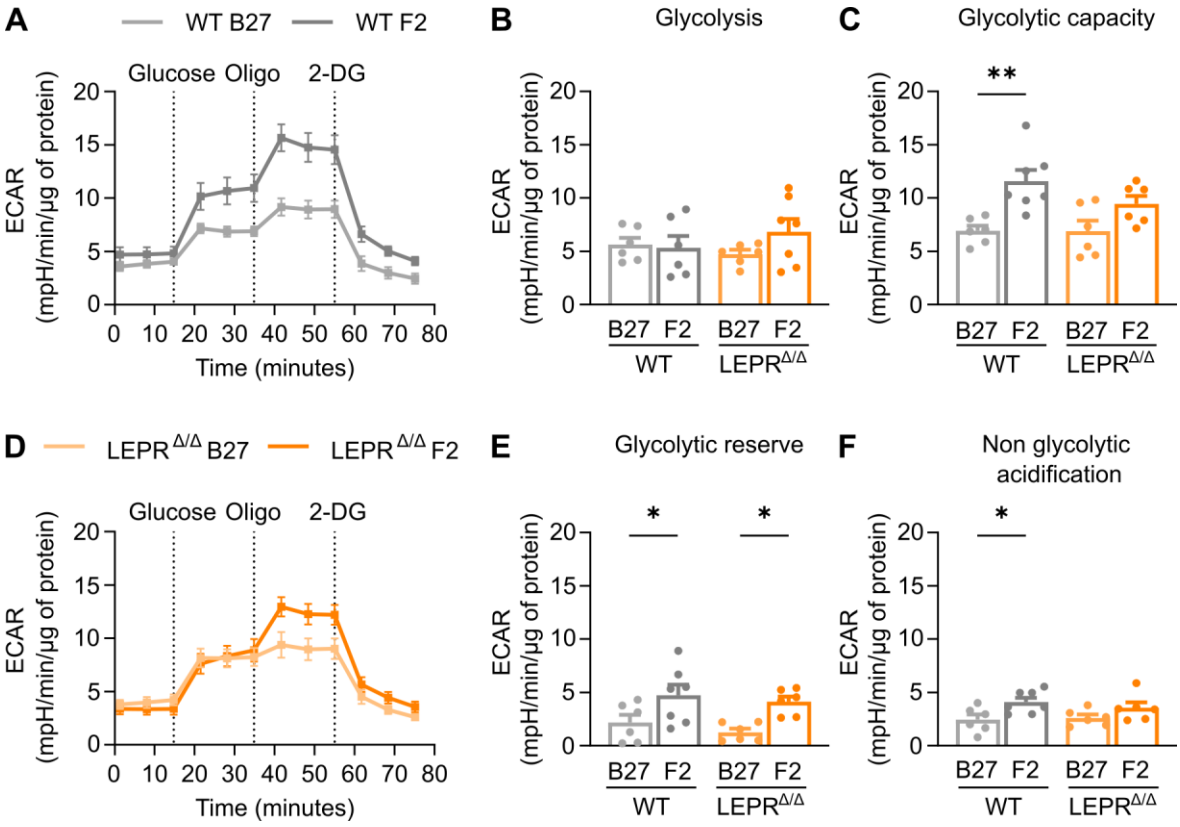

Figure 30. Glycolytic function in WT- and LEPR$^{\Delta/\Delta}$-iPSC-CMs in B27 and F2 medium. (A, D) Changes in the glycolytic function by assessment of the extracellular acidification rate (ECAR) of WT- (A) and LEPR$^{\Delta/\Delta}$-iPSC-CMs (D) cultured in B27 or F2 medium in response to treatment with glucose, oligomycin (Oligo), and 2-deoxy-D-glucose (2-DG). (B, C, E, F) Quantitative analyses of the calculated parameters for glycolysis (B), glycolytic capacity (C), glycolytic reserve (E), non glycolytic

acidification (F). Each data point represents an ECAR measurement performed in at least three different wells of a 96-well plate (WT B27: n = 6; LEPR$^{\Delta/\Delta}$ B27: n = 6; WT F2: n = 7; LEPR$^{\Delta/\Delta}$ F2: n = 6). *P < 0.05; **P < 0.01 LEPR$^{\Delta/\Delta}$ *vs.* WT for B27 and F2 as well as B27 *vs.* F2 for WT and LEPR$^{\Delta/\Delta}$ by using the two-way ANOVA with the Šídák's multiple comparisons test.

To assess the glycolytic intermediate enrichments in WT- and LEPR$^{\Delta/\Delta}$-iPSC-CMs in the presence of glucose as well as the effect of hormone stimulations, ^{13}C-isotope-assisted glucose metabolic flux was analysed with the stimulation of leptin (1.24 nM), insulin (10 nM) or their combination for 1-, 2- and 3-hours, respectively. Following the addition of [U-$^{13}C_6$] glucose, the time-dependent incorporation of ^{13}C-label into the intermediates of glycolysis was measured. The atomic percent excess (APE) was calculated following natural abundance correction (Alves *et al.*, 2015). In the presence of glucose, WT-iPSC-CMs (Fig. 31A) showed a faster glycolytic process than LEPR$^{\Delta/\Delta}$-iPSC-CMs (Fig. 32A), as demonstrated by ^{13}C-label transfer from [U-$^{13}C_6$] glucose to [U-$^{13}C_3$] pyruvate.

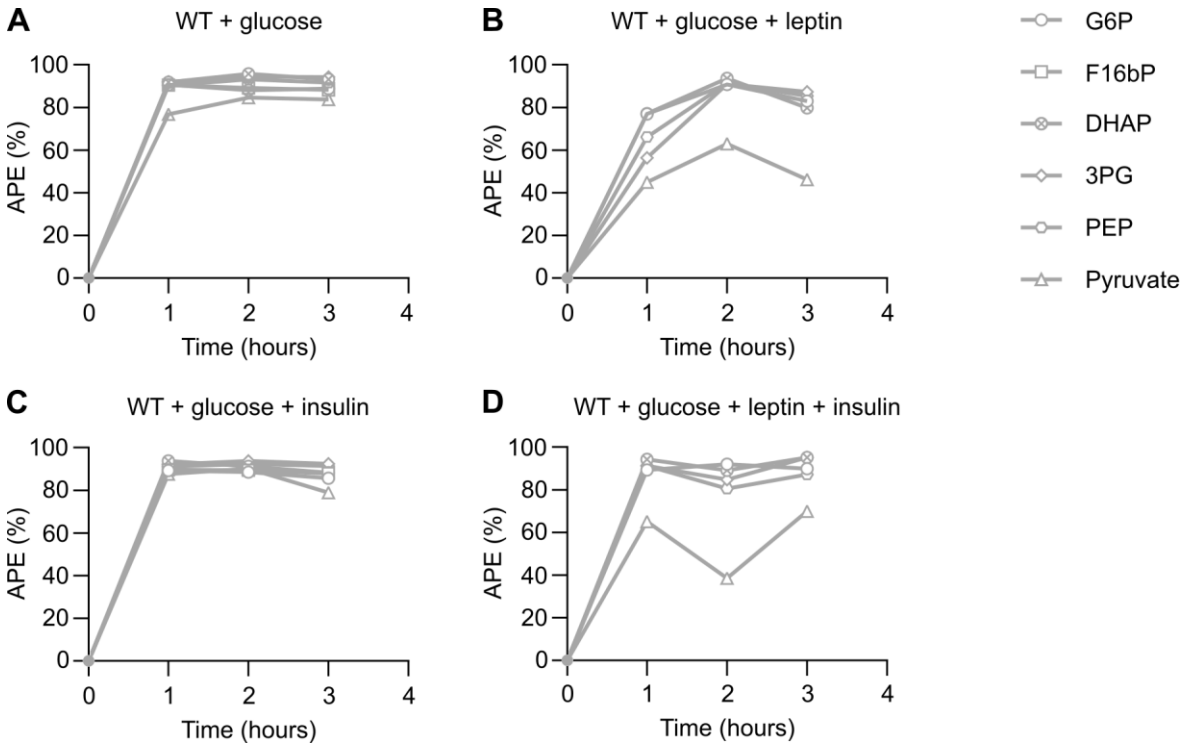

Figure 31. Time-dependent incorporation of ^{13}C-label into the intermediates of glycolysis in WT-iPSC-CMs. (A-D) Time-course of ^{13}C-labelling (1-3 hours) in WT-iPSC-CMs stimulated with leptin (1.24 nM; B), insulin (10 nM; C) or co-stimulated (D) in B27 medium. Curves indicate the metabolic intermediates contributing to glycolysis: glucose 6-phosphate (G6P), fructose 1,6-bisphosphate (F16bP), dihydroxyacetone phosphate (DHAP), 3-phosphoglyceric acid (3PG), phosphoenolpyruvate (PEP), pyruvate.

Nearly all glycolytic intermediates analysed (except pyruvate) approached steady state (>90% APE) within 1 hour in WT-iPSC-CMs (Fig. 31A) whereas only G6P and 3PG approached

steady state (>90% APE) within 1 hour in LEPR$^{\Delta/\Delta}$-iPSC-CMs (Fig. 32A). Moreover, whereas 70% and 80% of ^{13}C-label transfer occurred from phosphoenolpyruvate (PEP) to pyruvate in WT-iPSC-CMs in the presence of [U-$^{13}C_6$] glucose for 1 and 2 hours (Fig. 31A), respectively, only 50% and 50% of ^{13}C-label transfer from PEP to pyruvate in LEPR$^{\Delta/\Delta}$-iPSC-CMs at the same conditions (Fig. 32A), indicating slower glycolysis in non-stimulated LEPR$^{\Delta/\Delta}$-iPSC-CMs compared to WT-iPSC-CMs. Importantly, the insulin stimulation resulted in the acceleration of ^{13}C-label transfer from PEP to pyruvate in both WT- (Fig. 31C) and LEPR$^{\Delta/\Delta}$-iPSC-CMs (Fig. 32C) when compared to their respective non-stimulated groups (Figs. 31A, 32A). In particular, the ^{13}C-label transfer was faster in WT-iPSC-CMs after the insulin stimulation compared to LEPR$^{\Delta/\Delta}$-iPSC-CMs (Figs. 31C, 32C). On the contrary, the leptin stimulation in WT-iPSC-CMs led to slower glycolysis when compared to the non-stimulated group, as demonstrated by the clear discrimination of the curves and by the slower slopes of label accumulations in different intermediates representing the glycolytic metabolic intermediates (Fig. 31A, B).

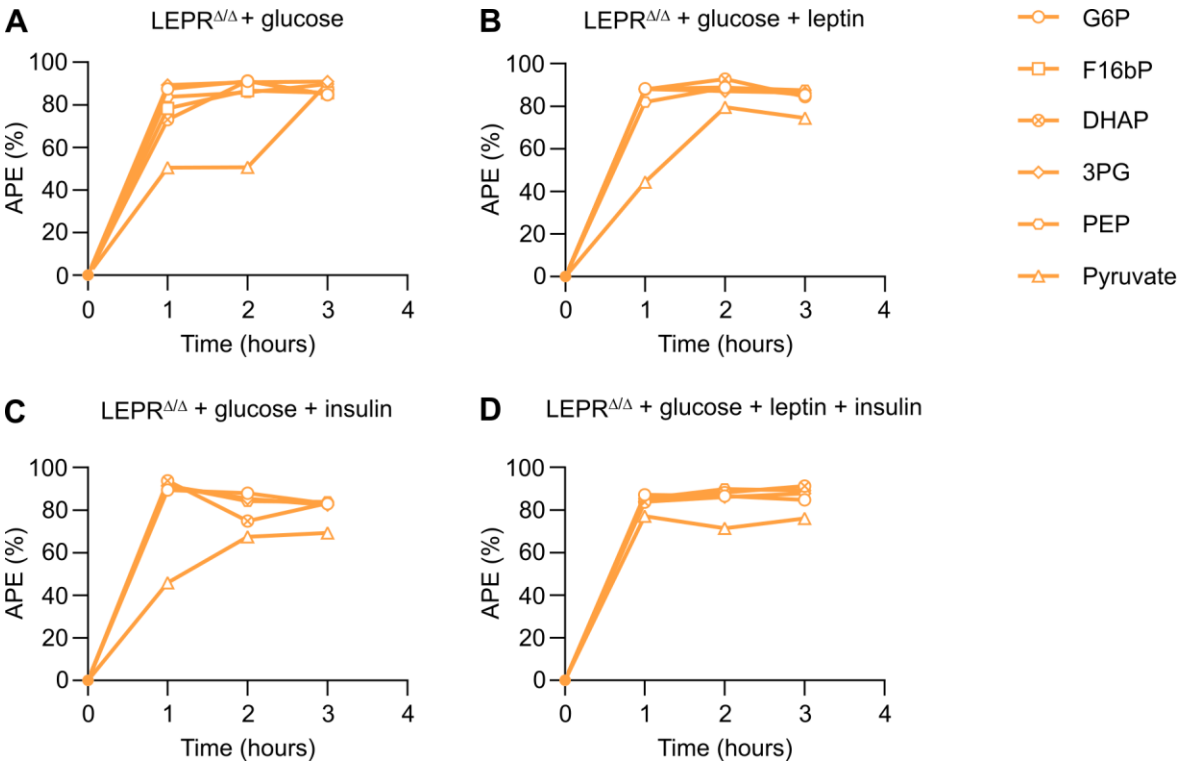

Figure 32. Time-dependent incorporation of ^{13}C-label into the intermediates of glycolysis in LEPR$^{\Delta/\Delta}$-iPSC-CMs. (A-D) Time-course of ^{13}C-labeling (1-3 hours) in LEPR$^{\Delta/\Delta}$-iPSC-CMs stimulated with leptin (1.24 nM; B), insulin (10 nM; C) or co-stimulated (D). Curves indicate the metabolic intermediates contributing to glycolysis: glucose 6-phosphate (G6P), fructose 1,6-bisphosphate (F16bP), dihydroxyacetone phosphate (DHAP), 3-phosphoglyceric acid (3PG), phosphoenolpyruvate (PEP), pyruvate.

Notably, no leptin effect was appreciated in LEPR$^{\Delta/\Delta}$-iPSC-CMs upon the leptin stimulation (Fig. 32A, B), indicating the loss of function of LEPR in LEPR$^{\Delta/\Delta}$-iPSC-CMs. Moreover, in WT-iPSC-CMs co-stimulated with insulin and leptin revealed that leptin might influence the effect of insulin, showing slower glycolysis compared to the insulin-stimulated WT group (Fig. 31C, D), however, the leptin and insulin co-stimulation in LEPR$^{\Delta/\Delta}$-iPSC-CMs demonstrated similar results to the insulin stimulation (Fig. 32C, D). Furthermore, upon the leptin stimulation, reduced ^{13}C-label transfer from the precursors to the subsequent products become more evident at the late step of glycolysis in WT-iPSC-CMs as shown in Fig. 33A, C for G6P and PEP, while the same was not possible to be observed in LEPR$^{\Delta/\Delta}$-iPSC-CMs under the same conditions (Fig. 33B, D). These data indicate the interaction of insulin and leptin signalling in glucose metabolism in WT-iPSC-CMs and loss of function of LEPR in LEPR$^{\Delta/\Delta}$-iPSC-CMs impacting glucose metabolism.

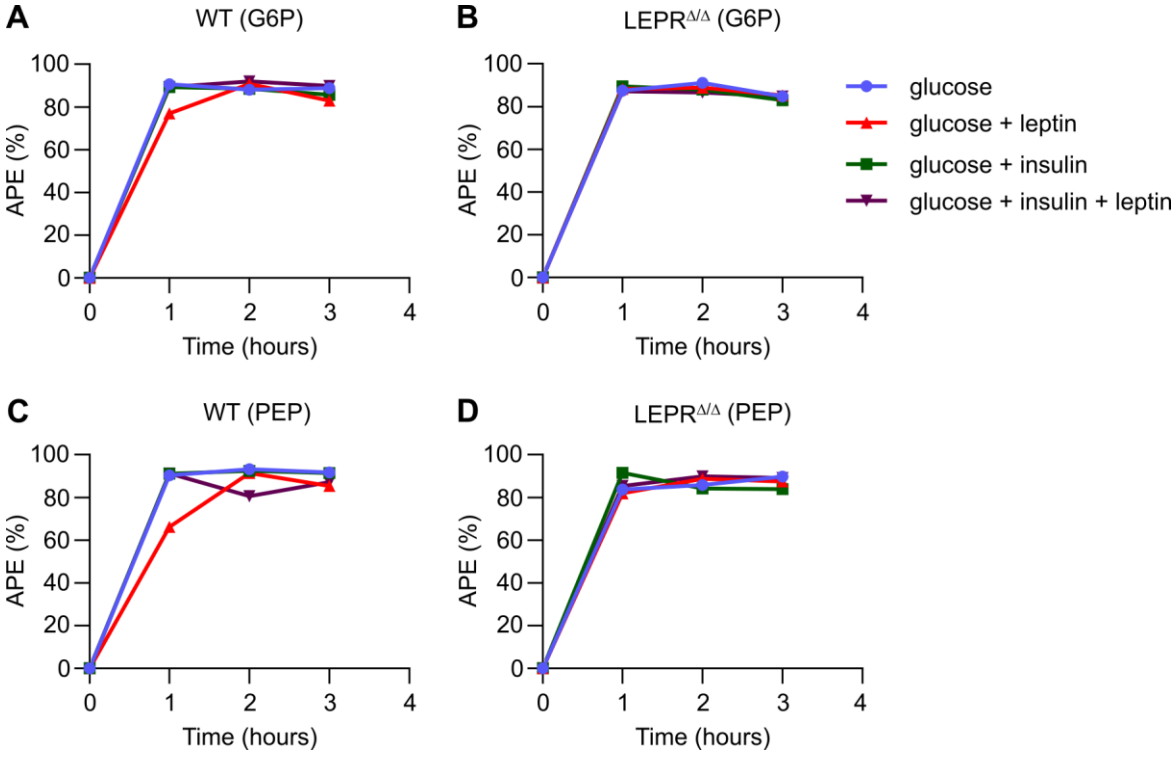

Figure 33. Time-dependent incorporation of ^{13}C-label into the intermediates of glycolysis in WT- and LEPR$^{\Delta/\Delta}$-iPSC-CMs. (A-D) Time-course of glucose 6-phosphate (G6P), and phosphoenolpyruvate (PEP) (1-3 hours) in WT- and LEPR$^{\Delta/\Delta}$-iPSC-CMs stimulated with leptin (1.24 nM), insulin (10 nM) or co-stimulated in B27 medium.

As a summary, lower expression levels of LEPR mRNA and protein were found in LEPR$^{\Delta/\Delta}$-iPSC-CMs. Physiological culture medium with the presence of glucose and fatty acids as energy substrates at physiological concentrations (F2 medium) improved downstream

LEPR pathway activation in WT-iPSC-CMs, while loss of function of LEPR in LEPR$^{\Delta/\Delta}$-iPSC-CMs resulted in no activation of JAK2 after leptin stimulation, independent of medium conditions. Insulin signalling activation was not altered in LEPR$^{\Delta/\Delta}$-iPSC-CMs in B27 medium. However, LEPR$^{\Delta/\Delta}$-iPSC-CMs showed reduced AKT phosphorylation and lower expression of *GLUT-1 and GLUT-4* in F2 medium compared to WT-iPSC-CMs, revealing an important LEPR role in the regulation of insulin pathway under physiological conditions. AMPK phosphorylation was enhanced in LEPR$^{\Delta/\Delta}$-iPSC-CMs in B27 but decreased in F2, when compared to WT-iPSC-CMs under the same conditions, indicating that LEPR$^{\Delta/\Delta}$-iPSC-CMs suffer energy stress under B27 condition and increased fatty acid supply under physiological F2 conditions reduces the energy stress. This is supported by the improved mitochondrial respiration and glycolytic capacity observed in both WT- and LEPR$^{\Delta/\Delta}$-iPSC-CMs in F2 compared to B27 culture conditions. Loss of function of LEPR in LEPR$^{\Delta/\Delta}$-iPSC-CMs was further evidenced by the lack of response to leptin in glycolysis, while WT-iPSC-CMs exhibited a delayed incorporation of ^{13}C-label into the intermediates of glycolysis.

4.5 Long-term effects of leptin under (patho)physiological conditions

The results shown above in this thesis suggest a role of leptin in CM metabolism, however it remains elusive whether loss of function of LEPR determines the metabolic shift, such as the decrease in glucose metabolism and increase in fatty acid oxidation. To shed light on this open question, we further studied the impact of long-term treatment with leptin (4 weeks) at physiological (1.24 nM) or pathophysiological levels (up to 100-fold) on iPSC-CMs. F3+ medium enriched in fatty acids, high insulin (700 nM), high leptin (100 nM), and high glucose (11 mM) was used to mimic the condition known in patients with diabetic cardiomyopathy, while F2 medium with the addition of low leptin (1.24 nM) was used as physiological medium.

4.5.1 Changes in LEPR signalling activation in WT- and LEPR$^{\Delta/\Delta}$-iPSC-CMs under different metabolic conditions

First, LEPR expression was studied in both WT- and LEPR$^{\Delta/\Delta}$-iPSC-CMs under the different metabolic conditions. Slightly lower expression of LEPR in LEPR$^{\Delta/\Delta}$-iPSC-CMs was observed when compared to WT-iPSC-CMs under the different conditions (Fig. 34A, B). To understand whether long-term culture with leptin at low or high concentrations induces changes in LEPR signalling activation, phosphorylation of JAK2 was analysed. Slightly increased JAK2 phosphorylation was observed in WT-iPSC-CMs in the presence of leptin at the low concentration (F2+) compared to WT-iPSC-CMs in the absence of leptin (F2). Importantly, JAK2 activation was inhibited in WT-iPSC-CMs in F3+ medium with high leptin

concentration, indicating that long-term cultivation of WT-iPSC-CMs with high leptin concentration led to the desensitization of LEPR and the impaired LEPR signalling. Furthermore, LEPR$^{\Delta/\Delta}$-iPSC-CMs showed no leptin-dependent JAK2 phosphorylation as observed in WT-iPSC-CMs in F2+ medium, which confirms the absence of functional LEPR (Fig. 34C, D).

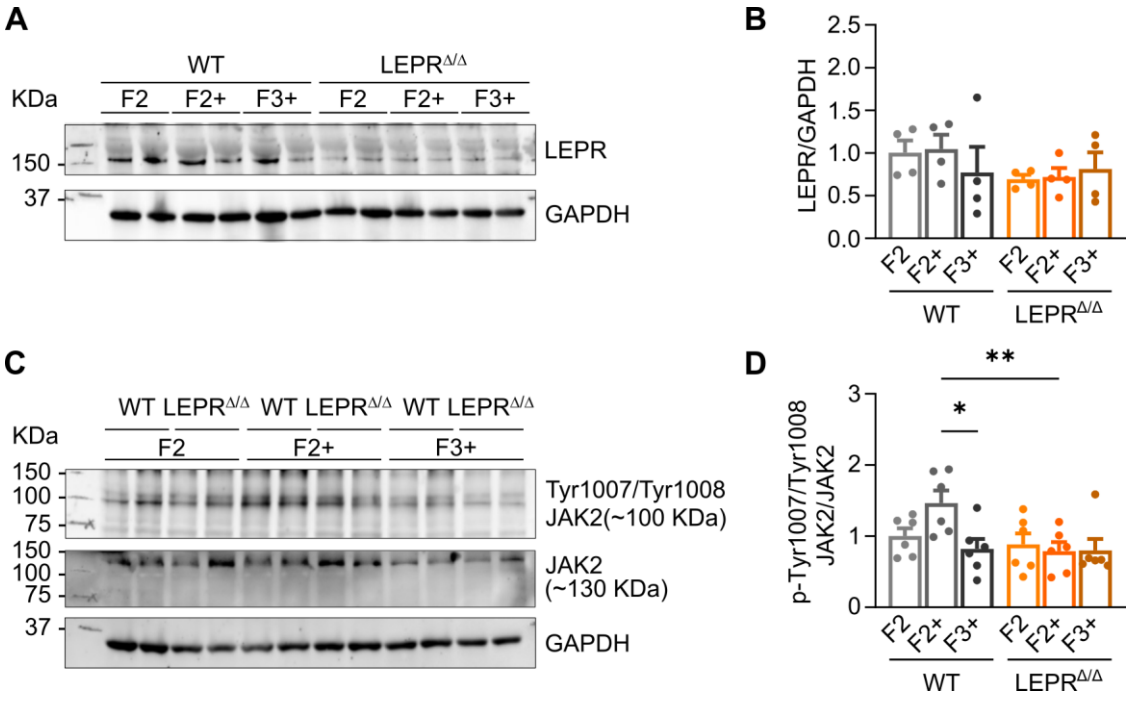

Figure 34. LEPR signalling activation in WT- and LEPR$^{\Delta/\Delta}$-iPSC-CMs in F2, F2+ or F3+ medium. (A, B) Representative western blots and quantification of LEPR in WT- and LEPR$^{\Delta/\Delta}$-iPSC-CMs cultured in F2, F2+ or F3+ medium (WT F2: n = 4; WT F2+: n = 4; WT F3+: n = 4; LEPR$^{\Delta/\Delta}$ F2: n = 4; LEPR$^{\Delta/\Delta}$ F2+: n = 4; LEPR$^{\Delta/\Delta}$ F3+: n = 4). (C, D) Representative western blots and quantification of changes in JAK2 phosphorylation (Tyr1007/1008) in WT- and LEPR$^{\Delta/\Delta}$-iPSC-CMs cultured in F2, F2+ or F3+ medium (WT F2: n = 6; WT F2+: n = 6; WT F3+: n = 6; LEPR$^{\Delta/\Delta}$ F2: n = 6; LEPR$^{\Delta/\Delta}$ F2+: n = 6; LEPR$^{\Delta/\Delta}$ F3+: n = 6). *P < 0.05; **P < 0.01 LEPR$^{\Delta/\Delta}$ *vs.* WT for F2, F2+ and F3+ as well as F2 *vs.* F2+, F3+ *vs.* F2, F2+ *vs.* F3+ for WT and LEPR$^{\Delta/\Delta}$ by using the two-way ANOVA with the Šídák's multiple comparisons test.

4.5.2 Long-term leptin effects on expression of metabolic markers

The alteration of cardiac function in diabetic patients occurs through different mechanisms, such as decreased glucose transport and carbohydrate oxidation and increase in fatty acid utilisation. Cardiac glucose metabolism is compromised at several points in patients with T2DM: glucose uptake, glycolysis and intramitochondrial pyruvate oxidation (Lopaschuk, 2002). To study the metabolic phenotype of WT- and LEPR$^{\Delta/\Delta}$-iPSC-CMs maintained in F2, F2+ or F3+ medium, the gene expression profiles were analysed. A tendency for reduced *GLUT-4* gene expression was observed in WT-iPSC-CMs cultured in medium with low (F2+)

and high (F3+) leptin concentration compared to WT-iPSC-CMs cultured in the absence of leptin (F2). Interestingly, expression levels of the *GLUT-4* gene in LEPR$^{\Delta/\Delta}$-iPSC-CMs cultured in F2, F2+ or F3+ were comparable to that of WT-iPSC-CMs in F3+ medium (Fig. 35B). No significant differences in *GLUT-1* expression were detected in WT- and LEPR$^{\Delta/\Delta}$-iPSC-CMs under different metabolic conditions, but slight lower levels were seen in LEPR$^{\Delta/\Delta}$-iPSC-CMs than in WT-iPSC-CMs (Fig. 35A). A tendency for increased *CD36* expression was observed in WT-iPSC-CMs in F2+ compared to F2 medium, which was coupled with higher *CPT1-B* expression under the same conditions (Fig. 35C, D). On the other hand, the diabetic condition (F3+) resulted in increased *CPT1-B* expression in WT-iPSC-CMs compared to those in F2, whereas *CD36* expression was comparable, suggesting higher consumption of fatty acids despite of lower fatty acid import in WT-iPSC-CMs in F3+ medium. Similar to WT-iPSC-CMs in the F3+ condition, LEPR$^{\Delta/\Delta}$-iPSC-CMs in F3+ revealed enhanced *CPT1-B* expression compared to LEPR$^{\Delta/\Delta}$-iPSC-CMs cultured in the absence of leptin (F2) (Fig. 35C, D).

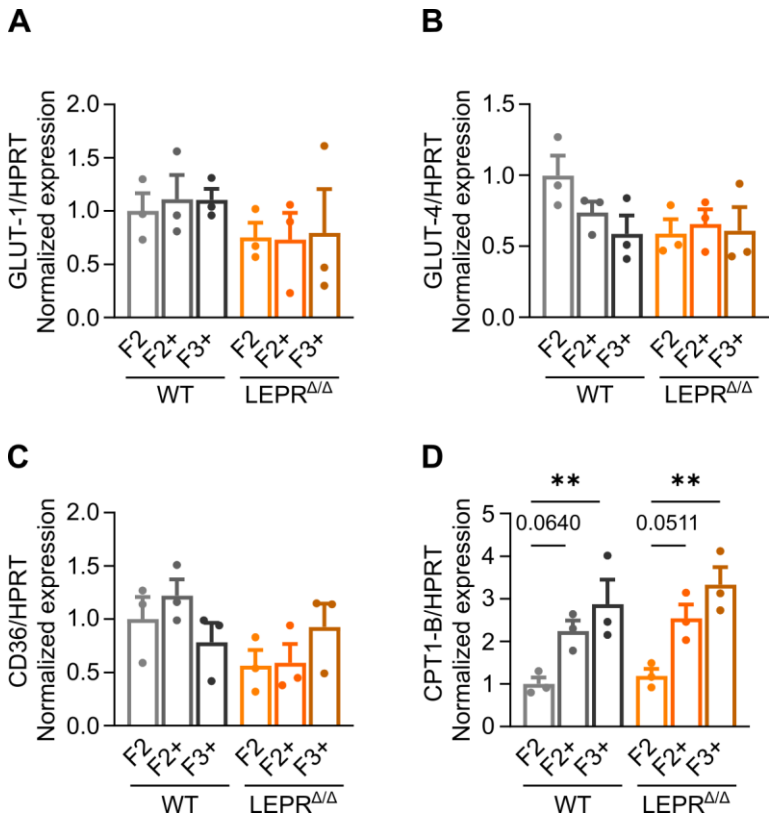

Figure 35. mRNA expression levels of metabolic markers in WT- and LEPR$^{\Delta/\Delta}$-iPSC-CMs in F2, F2+ or F3+ medium. Direct comparison of (A) *GLUT-1,* (B) *GLUT-4,* (C) *CD36,* and (D) *CPT1-B* expression in WT- and LEPR$^{\Delta/\Delta}$-iPSC-CMs cultured in F2, F2+ or F3+ medium (WT F2: n = 3; LEPR$^{\Delta/\Delta}$ F2: n = 3; WT F2+: n = 3; LEPR$^{\Delta/\Delta}$ F2+: n = 3; WT F3+: n = 3; LEPR$^{\Delta/\Delta}$ F3+: n = 3). mRNA levels were normalized to *HPRT*. **P < 0.01 LEPR$^{\Delta/\Delta}$ *vs.* WT for F2, F2+ and F3+ as well as F2 *vs.* F2+, F3+ *vs.*

F2, F2+ *vs.* F3+ for WT and LEPR$^{\Delta/\Delta}$ by using the two-way ANOVA with the Šídák's multiple comparisons test.

To further study fatty acid utilization in LEPR$^{\Delta/\Delta}$-iPSC-CMs under diabetic conditions, AMPK phosphorylation was explored. WT-iPSC-CMs presented enhanced AMPK phosphorylation in F3+ medium compared to those in F2 medium. LEPR$^{\Delta/\Delta}$-iPSC-CMs revealed high AMPK phosphorylation in F2 and F2+ medium (Fig. 36A, B). In addition, LEPR$^{\Delta/\Delta}$-iPSC-CMs showed slightly lower AMPK phosphorylation compared to WT-iPSC-CMs under the diabetic condition (F3+) (Fig. 36A, B).

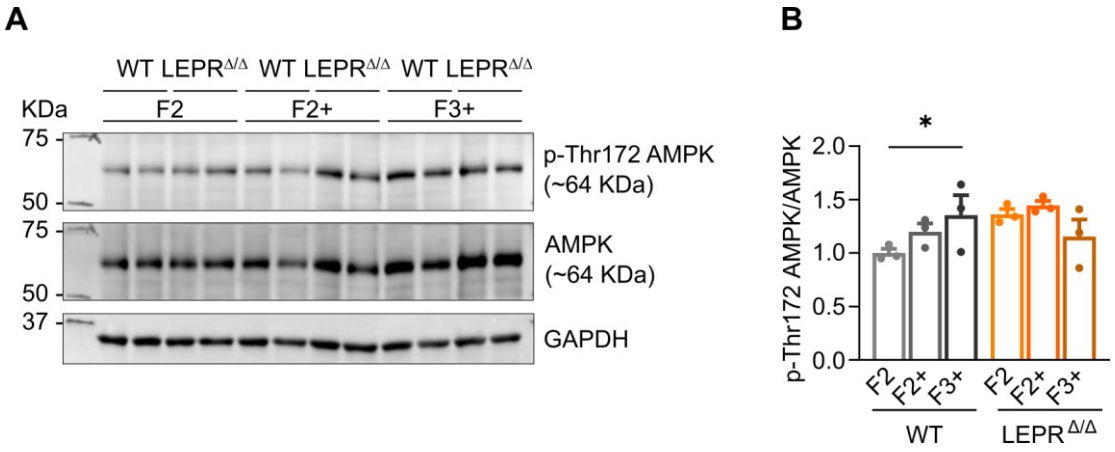

Figure 36. Effects of long-term treatment with leptin on AMPK phosphorylation in WT- and LEPR$^{\Delta/\Delta}$-iPSC-CMs. (A, B) Representative western blots and quantification of changes in AMPK phosphorylation (Thr172) in WT- and LEPR$^{\Delta/\Delta}$-iPSC-CMs cultured in F2, F2+, or F3+ medium (WT F2: n = 3; LEPR$^{\Delta/\Delta}$ F2: n = 3; WT F2+: n = 3; LEPR$^{\Delta/\Delta}$ F2+: n = 3; WT F3+: n = 3; LEPR$^{\Delta/\Delta}$ F3+: n = 3). Protein levels were normalized to total AMPK. *P < 0.05 LEPR$^{\Delta/\Delta}$ *vs.* WT for F2, F2+ and F3+ as well as F2 *vs.* F2+, F3+ *vs.* F2, F2+ *vs.* F3+ for WT and LEPR$^{\Delta/\Delta}$ by using the two-way ANOVA with the Šídák's multiple comparisons test.

4.5.3 Changes in mitochondrial function under different medium conditions

The shift of cardiac energy substrate consumption from glucose to fatty acid oxidation, occurring in the diabetic heart, is essential to ensure continuous ATP generation to maintain cardiac function, however, this chronical maladaptation leads to decreased energetic reserves and cardiac efficiency (Nagoshi *et al.*, 2011). As shown in Fig. 37, WT-iPSC-CMs cultured in F2+ or F3+ did not result in significant changes in mitochondrial oxygen consumption compared with F2, suggesting the preservation of mitochondrial function regardless of the different metabolic conditions. For LEPR$^{\Delta/\Delta}$-iPSC-CMs, cultivation in F2+ medium led to the decrease in basal respiration and ATP production (Fig. 37D, G), while no significant differences were observed in maximal respiration and spare respiratory capacity compared to F2 medium (Fig. 37E, F). On the contrary, LEPR$^{\Delta/\Delta}$-iPSC-CMs in F3+ medium

revealed slightly higher maximal respiration (Fig. 37E) and significantly higher spare respiratory capacity compared to F2 medium (Fig. 37F), and significantly increased in maximal respiration and spare respiratory capacity compared to F2+ medium (Fig. 37E, F). In general, LEPR$^{\Delta/\Delta}$-iPSC-CMs revealed reduced mitochondrial function when compared to WT-iPSC-CMs under different metabolic conditions, as demonstrated by lower basal respiration, maximal respiration, spare respiratory capacity, and mitochondrial ATP production in different medium conditions. Proton leak and non-mitochondrial oxygen consumption were comparable in WT and LEPR$^{\Delta/\Delta}$-iPSC-CMs when cultured in F2, F2+ or F3+ medium (Fig. 37H, I).

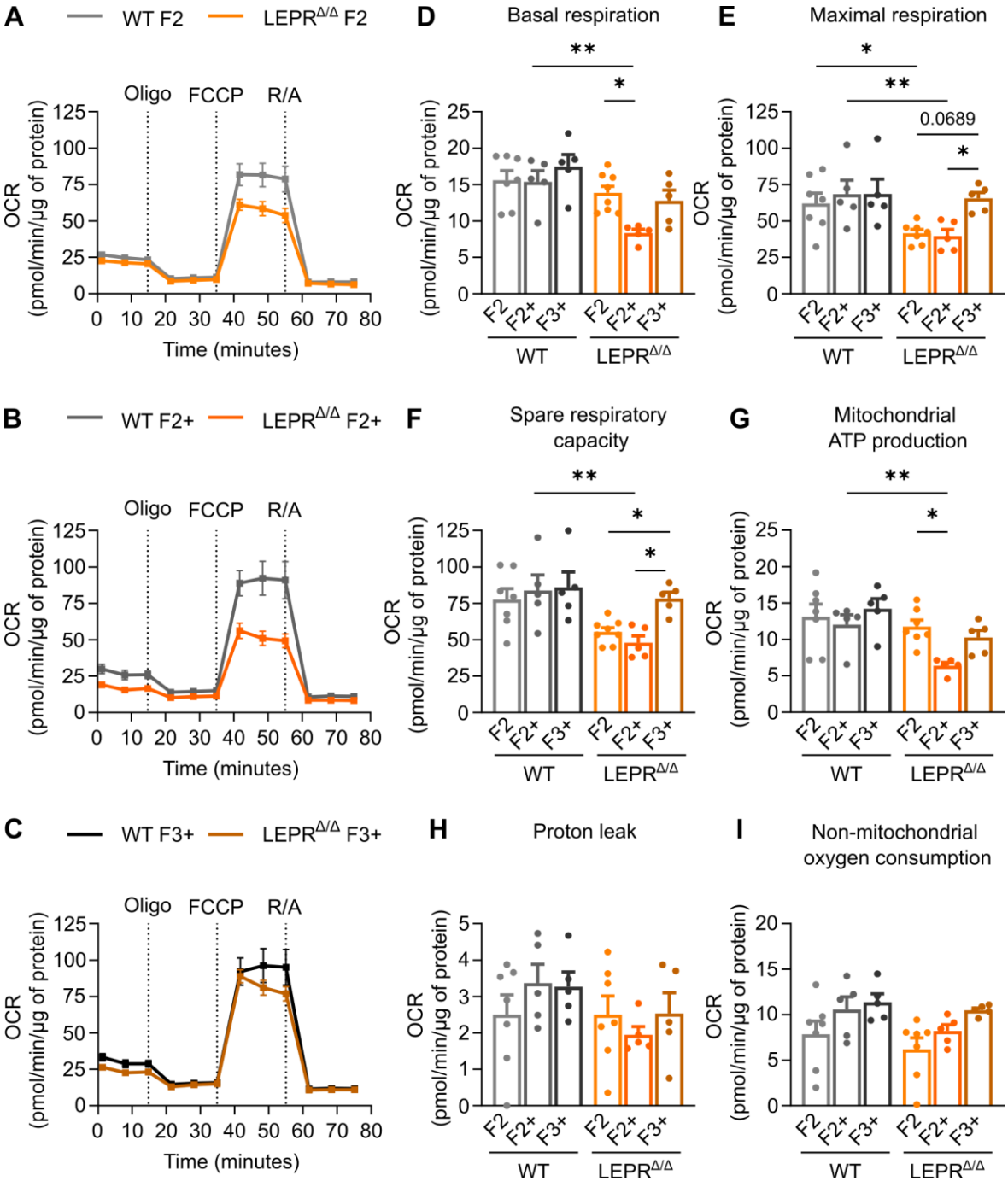

Figure 37. Changes in mitochondrial respiratory function in WT- and LEPR$^{\Delta/\Delta}$-iPSC-CMs in F2, F2+ or F3+ medium. (A-C) Changes in the mitochondrial respiration by assessment of the real-time oxygen consumption rate (OCR) of WT- and LEPR$^{\Delta/\Delta}$-iPSC-CMs cultured in F2 (A), F2+ (B) or F3+ (C) medium in response to treatment with oligomycin (Oligo), carbonyl cyanide-4-(trifluoromethoxy)phenylhydrazone (FCCP), and rotenone/antimycin A (R/A). (D-I) Quantitative analyses of the calculated parameters for basal respiration (D), maximal respiration (E), spare respiratory capacity (F), mitochondrial ATP production (G), proton leak (H), and non-mitochondrial oxygen consumption (I). Each data point represents an OCR measurement performed in at least three different wells of a 96-well plate (WT F2: n = 7; LEPR$^{\Delta/\Delta}$ F2: n = 7; WT F2+: n = 5; LEPR$^{\Delta/\Delta}$ F2+: n = 5; WT F3+: n = 5; LEPR$^{\Delta/\Delta}$ F3+: n = 5). *P < 0.05; **P < 0.01 LEPR$^{\Delta/\Delta}$ *vs.* WT for F2, F2+ and F3+ as well as F2 *vs.* F2+, F3+ *vs.* F2, F2+ *vs.* F3+ for WT and LEPR$^{\Delta/\Delta}$ by using the two-way ANOVA with the Šídák's multiple comparisons test.

4.5.4 Changes in glycolytic capacity under different metabolic conditions

Patients with T2DM have high plasma levels and myocardial uptake of fatty acids. High levels of circulating fatty acids and their increased oxidation are primarily responsible for the inhibition of both glycolysis and glucose oxidation in the heart (Nagoshi *et al.*, 2011). To get further insight into the use of glucose in WT- and $LEPR^{\Delta/\Delta}$-iPSC-CMs under different metabolic conditions, glycolytic parameters was assessed using the Seahorse analyser. Although a slight decrease in glycolysis and glycolytic capacity was observed in WT-iPSC-CMs cultured in F2+ and F3+ medium compared to the F2 medium, no significant difference was identified in these parameters (Fig. 38D, E). Glycolysis was significantly lower in $LEPR^{\Delta/\Delta}$-iPSC-CMs in F2+ and F3+ medium, compared to $LEPR^{\Delta/\Delta}$-iPSC-CMs in F2 medium, indicating reduced glucose oxidation in the presence of leptin (Fig. 38D, E). Furthermore, $LEPR^{\Delta/\Delta}$-iPSC-CMs in F3+ showed lower glycolytic capacity not only compared to those in F2 medium but also compared to WT-iPSC-CMs under the same conditions, suggesting that metabolic conditions result in greater impact in $LEPR^{\Delta/\Delta}$-iPSC-CMs compared to WT groups (Fig. 38E). Both WT- and $LEPR^{\Delta/\Delta}$-iPSC-CMs cultured in F2+ and F3+ compared to F2 medium showed no difference in glycolytic reserve (Fig. 38F). Moreover, there are slight decreases in non-glycolytic acidification in both WT- and $LEPR^{\Delta/\Delta}$-iPSC-CMs cultured in F2+ and F3+ compared to F2, suggesting reduced ECAR caused by processes other than glycolysis in the presence of leptin (Fig. 38G).

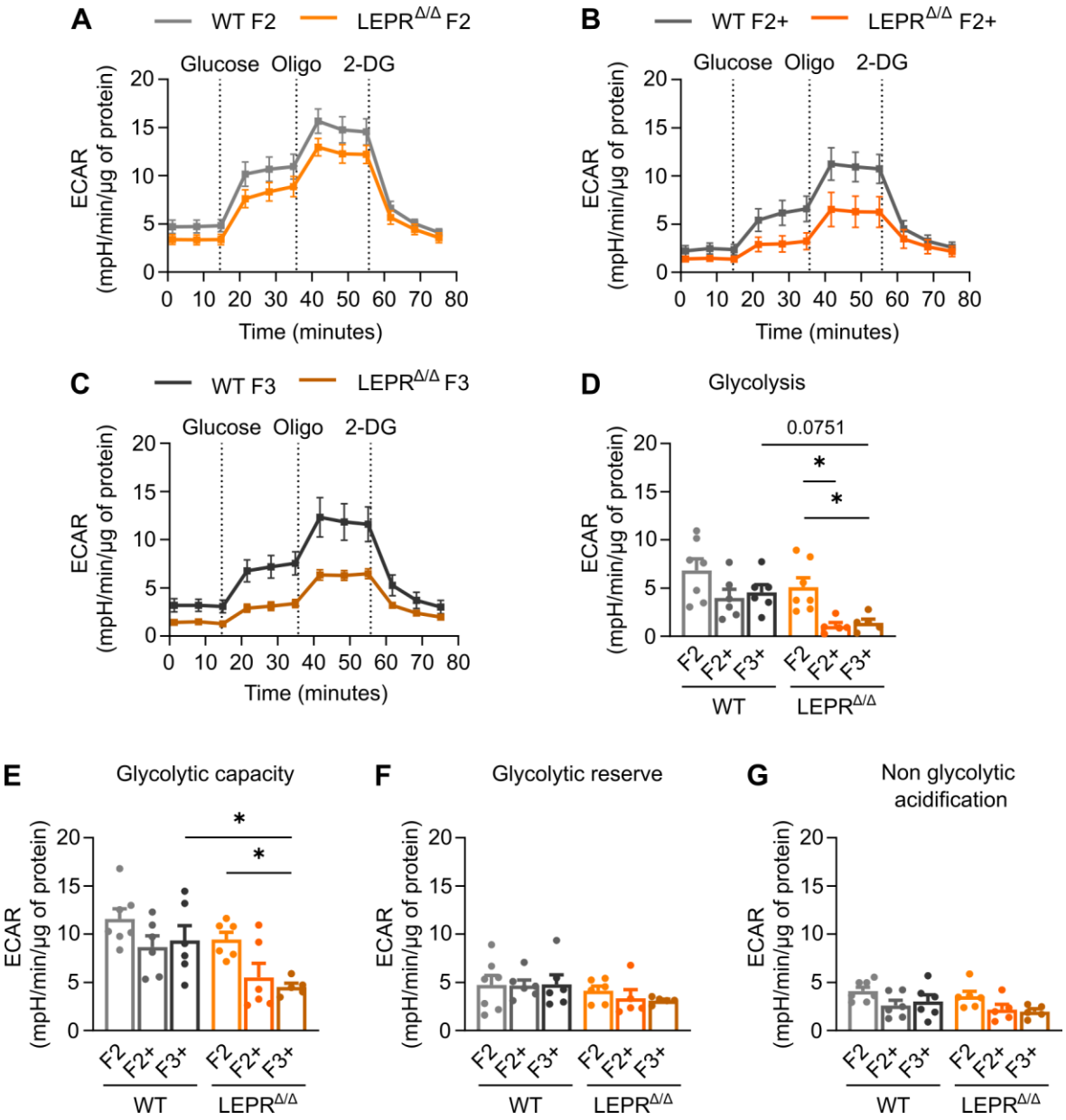

Figure 38. Changes in glycolytic function in WT- and LEPR$^{\Delta/\Delta}$-iPSC-CMs in F2, F2+ or F3+ medium. (A-C) Changes in the glycolytic function by assessment of the extracellular acidification rate (ECAR) of WT and LEPR$^{\Delta/\Delta}$-iPSC-CMs cultured in F2 (A), F2+ (B) or F3+ (C) medium in response to treatment with glucose, oligomycin (Oligo), and 2-deoxyglucose (2-DG). (D-G) Quantitative analyses of the calculated parameters for glycolysis (D), glycolytic capacity (E), glycolytic reserve (F), and non glycolytic acidification (G). Each data point represents an ECAR measurement performed in at least three different wells of a 96-well plate (WT F2: n = 7; LEPR$^{\Delta/\Delta}$ F2: n = 6; WT F2+: n = 6; LEPR$^{\Delta/\Delta}$ F2+: n = 5; WT F3+: n = 6; LEPR$^{\Delta/\Delta}$ F3+: n = 5). *P < 0.05 LEPR$^{\Delta/\Delta}$ *vs.* WT for F2, F2+ and F3+ as well as F2 *vs.* F2+, F3+ *vs.* F2, F2+ *vs.* F3+ for WT and LEPR$^{\Delta/\Delta}$ by using the two-way ANOVA with the Šídák's multiple comparisons test.

4.5.5 Changes in lipid droplet accumulation under different conditions

One of the characteristic pathological features of hearts from obese and diabetic individuals is the accumulation of lipid droplets in CMs, which is also found in *db/db* mice. The

accumulation of lipid droplets can promote lipotoxicity and decrease cardiac function (Hall *et al.*, 2014; Sharma *et al.*, 2004). Interestingly, the loss of LEPR function in LEPR$^{\Delta/\Delta}$-iPSC-CMs led to reduced lipid accumulation, as compared to the WT groups under the same metabolic conditions (F2+ or F3+), suggesting an increased lipid oxidation (Fig. 39A, B).

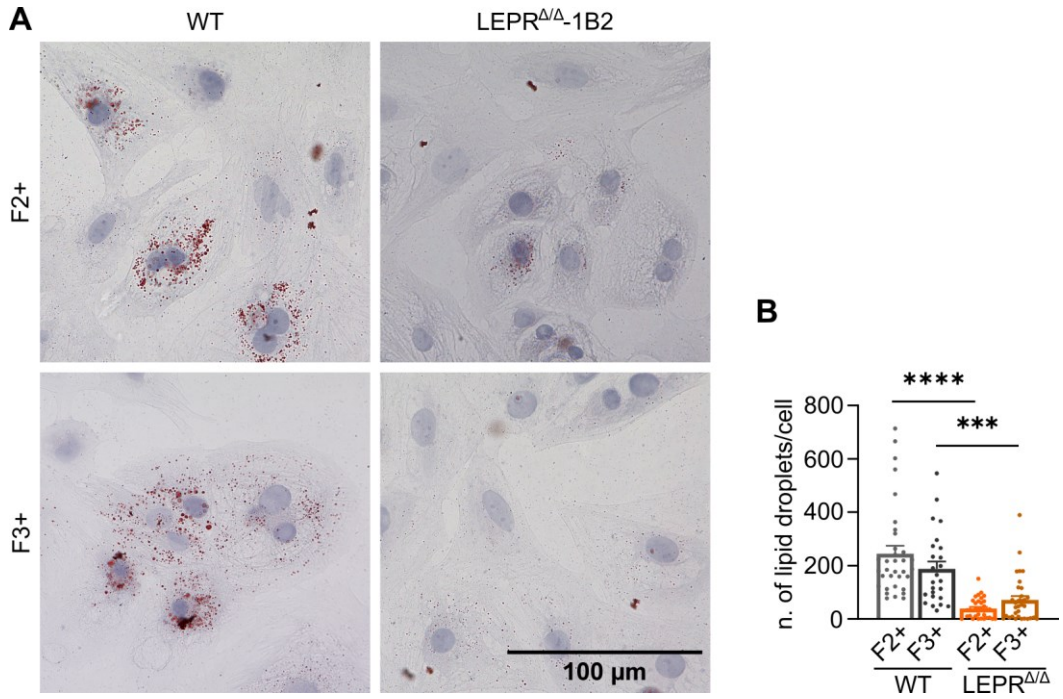

Figure 39. Lipid droplet accumulation in WT- and LEPR$^{\Delta/\Delta}$-iPSC-CMs in F2+ or F3+ medium. (A, B) Representative images (A) and quantification of changes in lipid droplet accumulation (B) in WT- and LEPR$^{\Delta/\Delta}$-iPSC-CMs in F2+ and F3+ medium, using Oil-Red-O-staining. In total, 25-34 CMs were analysed for each group (WT F2+: n = 34; LEPR$^{\Delta/\Delta}$ F2+: n = 25; WT F3+: n = 34; LEPR$^{\Delta/\Delta}$ F3+: n =33. ***P < 0.001; ****P < 0.0001 LEPR$^{\Delta/\Delta}$ *vs.* WT for F2+ and F3+ as well as F3+ *vs.* F2+ for WT and LEPR$^{\Delta/\Delta}$ by using the two-way ANOVA with the Šídák's multiple comparisons test. Nuclei were stained with haematoxylin. Scale bar: 100 µm.

5 Discussion

Diabetic cardiomyopathy is one of the major causes of disease-related death in patients with T2DM. Both insulin and leptin resistance are the hallmarks of obesity-related T2DM. In the cardiovascular system, leptin resistance or leptin signalling deficiency results in impaired response of the heart to metabolic stress conditions, leading to the risk increase of cardiac dysfunction and heart failure. In last three decades, the role of leptin in the regulation of food intake and energy expenditure in the hypothalamus has been well studied. However, it is largely unclear whether leptin and LEPR signalling play a direct role in the progression of CM dysfunction in patients with obesity-related T2DM. Animal studies using leptin- and Lepr-deficient rodents have helped to increase our knowledge of the underlying molecular and pathophysiological mechanisms of obese- and T2DM-associated metabolic and cardiovascular diseases. However, there are substantial differences between the animal models used so far and the phenotypes of patients with obesity or T2DM, which make data interpretation challenging (Poetsch *et al.*, 2020).

Disease modelling using human iPSCs combined with the CRISPR/Cas9 technique allows us to study and better understand abnormal LEPR signalling in CMs *in vitro*, which could be essential for the obesity- and T2DM-associated cardio-metabolic remodeling processes. In this study, *LEPR* expression was found already in iPSCs, and expression levels were not significantly different during iPSC-CM differentiation and maturation. On the contrary, no LEPR protein expression was observed during early cardiac development but was detected at the last stages of iPSC-CM maturation. Using CRISPR/Cas9 gene-editing technology, two $LEPR^{\Delta/\Delta}$-iPSC lines mimicking a LEPR mutation known in an early-onset obesity patient were successfully generated. $LEPR^{\Delta/\Delta}$-iPSCs were able to differentiate into spontaneously beating CMs and no difference was observed in cardiac differentiation efficiency when compared to WT-iPSCs. Lower *LEPR* mRNA levels were found in $LEPR^{\Delta/\Delta}$-iPSCs and during CM differentiation and maturation, which corresponded to lower LEPR protein expression. Changes in LEPR activation were demonstrated by leptin-dependent JAK2 phosphorylation in WT-iPSC-CMs cultured in physiological (F2) medium. Loss of function of LEPR in $LEPR^{\Delta/\Delta}$-iPSC-CMs resulted in no activation of JAK2 regardless of culture medium conditions. Although no differences were observed in the insulin pathway activation when WT- and $LEPR^{\Delta/\Delta}$-iPSC-CMs were cultured in B27 medium, a LEPR relevant role in the regulation of the insulin pathway was demonstrated by slightly lower *GLUT-1* and *GLUT-4* expression in $LEPR^{\Delta/\Delta}$-iPSC-CMs compared to WT-iPSC-CMs in F2 medium, which was in line with the decreased insulin-dependent AKT phosphorylation. One of the important findings of this study is that the medium conditions used for culturing iPSC-CMs are critical

for studying leptin and insulin signalling in iPSC-CMs. Fatty acids supplied in F2 medium improved energy metabolism in both WT- and LEPR$^{\Delta/\Delta}$-iPSC-CMs compared to B27 medium. When LEPR$^{\Delta/\Delta}$-iPSC-CMs cultured in B27 medium without fatty acid supply led increased AMPK activation, lower mitochondrial respiration and glycolytic capacity compared to WT-iPSC-CMs under the same conditions, indicating functional leptin signalling is essential for energy metabolism of iPSC-CMs. Long-term culture of WT-iPSC-CMs in the presence of 1.24 nM leptin (F2+) slightly increased the JAK2 activation, while long-term culture with 100 nM leptin (F3+) led to desensitization of LEPR and subsequently impaired leptin signalling. Metabolic flexibility was not altered in WT-iPSC-CMs under different medium conditions, although the higher *CPT1-B* expression, AMPK activation and lower lipid accumulation were observed in WT-iPSC-CMs when cultured in F3+ compared to F2 or F2+, indicating increased fatty acid consumption under high leptin conditions. Increased reliance on fatty acids as energy substrate in LEPR$^{\Delta/\Delta}$-iPSC-CMs in F3+ medium was demonstrated by higher *CPT1-B* expression, higher oxygen consumption rate, and lower lipid accumulation compared to F2 or F2+ medium, accompanied by the inefficient use of glucose in LEPR$^{\Delta/\Delta}$-iPSC-CMs in F3+ by decreased glycolysis and glycolytic capacity compared to F2 medium and to WT-iPSC-CMs under the same condition.

5.1 LEPR expression during cardiac development

So far, the importance of Lepr during embryogenesis has been mainly investigated in animal models. Pioneering studies by Hoggard and colleagues using in situ hybridisation and immunocytochemistry revealed that leptin and its receptor Lepr were expressed at both mRNA and protein levels in the placenta and in a restricted number of tissues, mainly bones and cartilage in the developing murine foetus at E14.5 (Hoggard *et al.*, 1997). In addition, *Lepr* transcripts were detected from E12.5 on in several tissues including the neural tissue and mesoderm-derived tissues, suggesting an important role of leptin during the growth and development of the murine foetus (Camand *et al.*, 2002; Hoggard *et al.*, 1997). However, no *Lepr* mRNA or protein expression was identified in the heart of the murine fetus (Hoggard *et al.*, 1997). These studies suggest that leptin and Lepr may not be required for early development of the heart in the mouse. To my best knowledge, there is no data available in terms of leptin and LEPR expression during human early development so far. In the current study, *LEPR* mRNA expression was observed during early cardiac differentiation of human iPSCs and in iPSC-CMs. However, LEPR protein expression was detected exclusively in iPSC-CMs at late stages. Moreover, LEPR$^{\Delta/\Delta}$-iPSCs were able to differentiate into spontaneously beating CMs, indicating loss of function of LEPR does not affect the

initiation of cardiac differentiation and the CM lineage commitment. In addition, the efficiency of CM differentiation is also not altered, as demonstrated by the comparable efficiency of cTNT-positive cells at day 60 in WT- and LEPR$^{\Delta/\Delta}$-iPSC-CMs. These data indicate that leptin and LEPR signalling are not required in the early steps of cardiac development. Although Lepr was not detected in the mouse fetus, *Lepr* transcripts and protein expression were found in adult mouse CMs (Lollmann *et al.*, 1997). Interestingly, leptin and LEPR expression was increased more than 4 folds in the failing human heart, suggesting the leptin and LEPR signalling plays an important role during disease progression and cardiac remodeling (McGaffin *et al.*, 2009).

5.2 CRISPR/Cas9 genome edited iPSCs with LEPR mutations for the study of LEPR function in the human system

The molecular mechanisms by which the leptin-LEPR signalling pathway contributes to obese- and T2DM-associated metabolic and cardiovascular diseases are controversially discussed in the literature. To unravel LEPR role in human CMs, a specific LEPR mutation known in early-onset obesity patients was generated in iPSCs using CRISPR/Cas9 genome editing in this study. CRISPR/Cas9-mediated gene editing in iPSCs hold a great potential to dissect the contribution of a gene/protein to function and represents a screening platform for drug development and therapy (Han & Entcheva, 2023). In this study, the gRNA was designed to specifically target the region of LEPR in which a mutation (c.2396-1G>T) was found in a Pakistan child of 1.5 years. The patient presented early onset obesity with BMI (31.9 kg/m^2), high serum leptin concentration (76.8 ng/ml) and increased insulin (19.0 µIU/ml) levels, making the patient at high risk of insulin resistance and diabetes development (Saeed *et al.*, 2014). The mutation found in the patient is localized in the LEPR FNIII subdomain which is part of the extracellular domain and can orientate the cytoplasmic tails in a manner that favors LEPR signalling, making this region indispensable for LEPR activation (Fong *et al.*, 1998; Zabeau *et al.*, 2005). In this study, two inCas9-iPSC lines with doxycycline inducible Cas9 were used and the efficiency of gRNA transfection into these two lines was very high as evaluated by fluorescence microscopy. Moreover, sequencing data from CRISPR/Cas9-edited clones show that the protocol used here is very efficient for introducing indel mutations into human iPSCs through the NHEJ repair mechanism. Some of the edited clones revealed the *LEPR* exon 17 skipping or the formation of a LEPR truncated protein. The clones 1B2 and 1E6 presented a homologous insertion of “A” in *LEPR* exon 17 (c.2396insA), leading to a reading frameshift and a formation of a PTC (D799Efs*7) as demonstrated by gDNA and cDNA Sanger sequencing analysis. Since the

truncated protein formed lacks transmembrane and cytoplasmic domains, which are important for LEPR signalling transduction, LEPR is successfully knocked out in these two iPSC lines (LEPR$^{\Delta/\Delta}$-iPSCs) using the CRISPR/Cas9 gene-editing technology, which could be used to study the role of LEPR in human pluripotent stem cells as well as in different iPSC-differentiated cells, including neurons and CMs.

So far, most of the studies on LEPR in stem cells have not fully addressed mechanistically whether and how LEPR directly regulates stem cell functions. However, it has been shown that *LEPR* is important for the maintenance of the pluripotent stem cell state in iPSCs generated from *db/db* mice, which exhibited significantly lowered protein levels of the pluripotency markers OCT4 and NANOG, suggesting a role of LEPR in regulating pluripotency-associated genes (Gupta *et al.*, 2020). Whilst *OCT4* and *NANOG* mRNA levels were not evaluated in this study, OCT4 and SOX4 were detectable by immunofluorescence microscopy in generated human LEPR$^{\Delta/\Delta}$-iPSCs, which retained stem cell morphology and pluripotency. To further characterize LEPR$^{\Delta/\Delta}$-iPSCs, LEPR mRNA and protein expression levels were evaluated in LEPR$^{\Delta/\Delta}$-iPSCs. Lower *LEPR* gene expression was observed in LEPR$^{\Delta/\Delta}$-iPSCs compared to WT-iPSCs. However, no protein expression was detected either in WT- or LEPR$^{\Delta/\Delta}$-iPSCs. These findings suggest that leptin and LEPR signalling may not play an important role in human iPSCs, however, further detail studies should be performed in terms of expression of pluripotent markers as well as the metabolic changes in LEPR$^{\Delta/\Delta}$-iPSCs.

5.3 Medium conditions are important for studying leptin and insulin signalling in iPSC-CMs

It is known that leptin directly acts on peripheral tissues to regulate energy metabolism (Ceddia *et al.*, 2002), however very little is known about its ability to modulate cardiac metabolism. Increase in myocardial fatty acid utilization and decrease in glucose utilization, which are observed in animal models with *Lepr* deficiency, could be accounted for the secondary effects of the resulting obesity and diabetes or by centrally mediated leptin effects (Abel *et al.*, 2008).

In this study, LEPR expression and JAK2 phosphorylation were investigated in both WT- and LEPR$^{\Delta/\Delta}$-iPSC-CMs cultured in B27 or F2 medium. B27 medium contains high glucose and high insulin, which is a routine medium in cardiogenic differentiation protocols used worldwide. F2 medium is supplemented with glucose and insulin at lower concentrations and fatty acids, which was generated in our lab. We found that JAK2 phosphorylation was significantly lower in LEPR$^{\Delta/\Delta}$-iPSC-CMs in both B27 and F2 medium compared to those in

the WT groups under the same conditions, indicating impaired LEPR signalling. To further demonstrate LEPR loss of function in LEPR$^{\Delta/\Delta}$-iPSC-CMs, WT- and LEPR$^{\Delta/\Delta}$-iPSC-CMs were starved overnight and acutely stimulated with 1.24 nM leptin for 5- 10- or 15-min. However, acute leptin stimulation showed no effect on JAK2 phosphorylation either in LEPR$^{\Delta/\Delta}$- or in WT-iPSC-CMs cultured in B27 medium. The most striking finding in this part is that 15-min leptin treatment of WT-iPSC-CMs cultured in F2 medium resulted in increased JAK2 phosphorylation, while leptin treatment for 5- 10- or 15-min did not result in change of JAK2 phosphorylation in LEPR$^{\Delta/\Delta}$-iPSC-CMs under the same condition, indicating loss of function of LEPR in this cell line. These results suggest that culture medium conditions play a key role in the regulation of CM metabolism. Despite the glucose-based B27 medium is widely used in cardiogenic differentiation protocols, this medium has some limitations given by the glucose-rich and the lipid-poor (<10 µM total lipids) medium conditions (Yang *et al.*, 2019). The newly developed F2 medium with glucose and oxidative substrate levels adapted to the metabolic needs of CMs in a more physiological concentration range is more suitable for studying the leptin-LEPR signalling in iPSC-CMs.

Human plasma leptin concentration is about 3 to 16 ng/ml (0.18 to 1 nM) and usually less than 100 ng/ml (6.2 nM) under physiological conditions (Jensen *et al.*, 1999), however, the concentration and the stimulation time used to unravel the role of leptin in CMs are inconstant in different studies. Treatment with 500 nM leptin for 15 min increased phosphorylation of STAT3 in adult rat ventricular CMs (Wold *et al.*, 2002), while in neonatal rat CMs 50 ng/ml leptin treatment for 15 min was sufficient to induce STAT3 activation (Abe *et al.*, 2007). Increased STAT3 phosphorylation was also shown in perfused rat heart with 1.9 nM leptin for 40 min (Sharma *et al.*, 2009). Little is known about LEPR activation in human CMs. A previous study showed that 6 nM leptin stimulation for 10 min induced JAK2 phosphorylation in human ventricular myocytes isolated from biopsies of children undergoing surgical repair of tetralogy of Fallot (Madani *et al.*, 2006). To compare these data with our findings, it is necessary to keep in mind that CMs isolated from rats or children with tetralogy of Fallot were cultivated only shortly in medium containing high glucose and 10% FBS before leptin stimulation. The findings in this thesis reveal that leptin under physiological concentration range can activate the downstream signalling of LEPR in WT-iPSC-CMs only cultured in the physiological medium condition for a long period. These results imply that physiological medium containing glucose and fatty acids represents a fundamental parameter to study leptin role in CMs.

LEPR regulates many intracellular signalling pathways mediated by insulin receptor (IR), including regulation of AKT (Sweeney, 2002). Thus, there is clearly potential for a crosstalk

between leptin and insulin intracellular signalling. Previous studies showed that treatment with 3.1 nM leptin for 15 min increased AKT phosphorylation in neonatal rat CMs (Zeidan *et al.*, 2011), however, no additive or inhibitory effect of leptin on insulin-stimulated AKT phosphorylation was observed in HL-1 cells incubated with 60 nM leptin for 1 or 24 hours or co-incubated with insulin (100 nM, 10 min) (Palanivel *et al.*, 2006). In the present study, a time-course for 5- 10- 15 min of 50 nM insulin stimulation was performed in WT-iPSC-CMs cultured in F2 medium, demonstrating a small increase in AKT phosphorylation upon 10 min insulin stimulation. Leptin (1.24 nM), insulin (50 nM) or leptin and insulin co-stimulation showed no effect on LEPR expression between $LEPR^{\Delta/\Delta}$-iPSC-CMs and WT-iPSC-CMs under B27 medium, while lower LEPR expression was found in $LEPR^{\Delta/\Delta}$-iPSC-CMs compared to WT-iPSC-CMs upon the same stimulation cultivated under F2 medium. Leptin treatment alone (1.24 nM; 10 min) showed no significant changes in AKT phosphorylation either in $LEPR^{\Delta/\Delta}$- or in WT-iPSC-CMs in B27 or F2 medium, in line with the study conducted by Palanivel (Palanivel *et al.*, 2006). Insulin-dependent phosphorylation of AKT was enhanced in both WT- and $LEPR^{\Delta/\Delta}$-iPSC-CMs in B27 and F2 medium, and a significant increase in AKT phosphorylation was also observed with leptin and insulin co-stimulation in WT- and $LEPR^{\Delta/\Delta}$-iPSC-CMs in B27 and F2 medium, indicating the insulin signalling pathway activation in both groups of iPSC-CMs. Interestingly, although no difference in AKT phosphorylation were observed between non-stimulated $LEPR^{\Delta/\Delta}$-iPSC-CMs and WT-iPSC-CMs, insulin effect on AKT phosphorylation in $LEPR^{\Delta/\Delta}$-iPSC-CMs was less pronounced compared to WT-iPSC-CMs upon insulin or insulin and leptin co-stimulation in F2 medium, supporting the hypothesis of lower insulin sensitivity or impaired insulin signalling in $LEPR^{\Delta/\Delta}$-iPSC-CMs in the presence of fatty acids in the culture medium. Taken together, in this study, leptin does not play a direct role in AKT phosphorylation, although it may contribute to the glucose utilisation in WT-iPSC-CMs. Moreover, the findings in this thesis indicate that the lack of JAK2 activation in $LEPR^{\Delta/\Delta}$-iPSC-CMs is concomitant with the decrease of insulin sensitivity, suggesting that the effect of leptin on glucose metabolism is impaired in $LEPR^{\Delta/\Delta}$-iPSC-CMs in F2 medium.

5.4 Reduced metabolic flexibility in $LEPR^{\Delta/\Delta}$-iPSC-CMs

As mentioned in the Introduction section, during early cardiac development, glycolysis is the major source of energy. As CMs mature and become terminally differentiated, mitochondrial oxidative capacity enhances. In this study, F2 medium significantly increased the OCR linked to the maximal respiration and spare respiration capacity in WT-iPSC-CMs, mimicking the enhanced mitochondrial oxidative capacity in matured CMs. Glycolytic

capacity, glycolytic reserve and non glycolytic acidification were also significantly higher in WT-iPSC-CMs in F2 medium compared to the B27 medium. These results are consistent with previous studies demonstrating the enhanced iPSC-CM maturation in lipid-enriched medium conditions (Feyen *et al.*, 2020; Yang *et al.*, 2019). Furthermore, WT-iPSC-CMs in F2 medium showed higher expression levels of genes encoding glucose transporters (*GLUT-1, GLUT-4*) and fatty acids transporter (*CPT1-B*) while no difference was observed in *CD36* expression compared to WT-iPSC-CMs cultured in B27 medium, indicating a shift toward adult CM phenotype in WT-iPSC-CMs when cultured in F2 medium. Moreover, current study provides a comprehensive assessment of the alterations of metabolic flexibility in LEPR$^{\Delta/\Delta}$-iPSC-CMs compared to WT-iPSC-CMs. It has been reported that metabolic modulation to sustain glucose utilization by perinatal overexpression of the glucose transporter GLUT-4 prevented cardiac dysfunction in *db/db* mice (Belke *et al.*, 2000; Semeniuk *et al.*, 2002). In this study, LEPR$^{\Delta/\Delta}$-iPSC-CMs showed no difference in *GLUT-1*, *GLUT-4*, *CD36* and *CPT1-B* expression compared to WT-iPSC-CMs cultured in B27 medium. However, culture of WT- and LEPR$^{\Delta/\Delta}$-iPSC-CMs in F2 medium demonstrated lower, although not significant, *GLUT-4* expression in LEPR$^{\Delta/\Delta}$-iPSC-CMs compared to WT-iPSC-CMs, suggesting again the importance of a physiological medium condition to reveal the metabolic profile of LEPR$^{\Delta/\Delta}$-iPSC-CMs. Further study should be performed to investigate whether lower *GLUT-4* mRNA level correspond to lower GLUT-4 protein expression and translocation to the membrane with consequent lower glucose uptake in LEPR$^{\Delta/\Delta}$-iPSC-CMs. Under intracellular glucose shortage, which results in energy deficiency, AMPK directly senses the increase in AMP/ATP and ADP/ATP ratios, leading to its activation (Bairwa *et al.*, 2016), which is in line with the increased AMPK phosphorylation found when LEPR$^{\Delta/\Delta}$-iPSC-CMs in B27 medium with glucose at high concentration were compared to WT-iPSC-CMs under the same condition. Therefore, these results indicate that there is a lower intracellular energy level in LEPR$^{\Delta/\Delta}$-iPSC-CMs compared to the WT group, pointing out the inability of LEPR$^{\Delta/\Delta}$-iPSC-CMs to adequately use glucose as an energy source. These findings are supported by the lower basal respiration and mitochondrial ATP synthesis found in LEPR$^{\Delta/\Delta}$-iPSC-CMs compared to WT-iPSC-CMs under B27 medium, which indicate impaired mitochondrial function. Culturing LEPR$^{\Delta/\Delta}$-iPSC-CMs in F2 medium containing glucose and fatty acids partially restored their energy balance, as demonstrated by comparable levels of basal respiration and mitochondrial ATP production with WT-iPSC-CMs, although maximal respiration and spare respiratory capacity were still lower in LEPR$^{\Delta/\Delta}$-iPSC-CMs compared to the WT group under the same condition. The inability of LEPR$^{\Delta/\Delta}$-iPSC-CMs to efficiently utilise glucose as an energy

substrate was further suggested by ECAR-related glycolytic capacity, which was slightly lower in LEPR$^{\Delta/\Delta}$-iPSC-CMs cultured under the F2 medium compared to WT-iPSC-CMs in the same medium. These data confirm the hypothesis of lower glucose consumption in LEPR$^{\Delta/\Delta}$-iPSC-CMs, although improved glycolysis, glycolytic capacity and glycolytic reserve were observed in LEPR$^{\Delta/\Delta}$-iPSC-CMs cultured in F2 medium compared to the same group in B27 medium.

In addition, study of glycolytic fluxes in LEPR$^{\Delta/\Delta}$-iPSC-CMs demonstrated reduced ^{13}C-label transfer from phosphoenolpyruvate (PEP) to pyruvate compared to WT-iPSC-CMs in B27 medium, indicating slowed glycolysis. WT-iPSC-CMs incubated with leptin showed slower glycolysis when compared to their respective non-stimulated group, revealing leptin as a critical player in glucose homeostasis already at the early step of glycolysis, while no leptin effect was appreciated in LEPR$^{\Delta/\Delta}$-iPSC-CMs upon leptin stimulation. In previous studies, leptin has been shown to have no effect on glucose uptake or metabolism in HL-1 murine CMs (Palanivel *et al.*, 2006) and no effect on glucose oxidation in Sprague Dawley isolated working rat hearts (Atkinson *et al.*, 2002). Similarly, intravenous or intracerebroventricular infusion of leptin in mice had no effect on cardiac glucose uptake (Kamohara *et al.*, 1997). In contrast to these findings, however, a study of Langendorff-perfused Sprague Dawley rat hearts showed that leptin stimulated glucose uptake (Haap *et al.*, 2003). Moreover, a reduction in glucose (and lactate) metabolism has been described even before the onset of hyperglycaemia in Zucker rats (Golfman *et al.*, 2005; Wang *et al.*, 2005) which is in line with the findings in this study, showing reduced glycolysis in LEPR$^{\Delta/\Delta}$-iPSC-CMs. To assess the role of leptin in the regulation of glycolytic fluxes, further studies under physiological and pathophysiological medium conditions will be needed.

5.5 Direct effect of leptin on energy metabolism in iPSC-CMs

So far, it is largely unknown whether leptin plays a direct role in energy metabolism in CMs. To study this, low leptin concentration (1.24 nM) was applied to WT-iPSC-CMs in F2 medium for 4 weeks to mimic the physiological condition (F2+). As shown in this study as well as by other data in the lab, WT-iPSC-CMs cultured in F2 medium revealed improved maturation not only in energy metabolism but also in electrophysiological and functional parameters. Consistent with the results obtained under B27 and F2 culture conditions, LEPR expression was found to be slightly lower in LEPR$^{\Delta/\Delta}$-iPSC-CMs compared to the WT group under F2+, indicating no changes in LEPR expression in response to long-term treatment with leptin at physiological concentration. Culturing WT-iPSC-CMs under F2+ medium resulted in an increased, although not significant, JAK2 activation, implying leptin-

dependent regulation of downstream LEPR pathway. On the contrary, LEPR$^{\Delta/\Delta}$-iPSC-CMs in F2+ medium showed abrogated JAK2 activation demonstrating no leptin effect.

Fatty acid oxidation is highly regulated by the AMPK pathway. AMPK phosphorylates ACC and inhibits the ACC activity. This reduces malonyl CoA synthesis, activating CPT1-B and thereby increasing mitochondrial import and oxidation of long-chain acyl-CoA fatty acids (Kahn *et al.*, 2005). A previous study showed that leptin activated cardiac fatty acid metabolism in isolated working Sprague-Dawley rat hearts independent of the activation of the AMPK-ACC-malonyl CoA axis (Atkinson *et al.*, 2002). However, another study conducted in WT CMs from perfused rat hearts demonstrated the leptin-dependent AMPK activation and CD36 translocation to the membrane for stimulating fatty acid uptake to enhance fatty acid oxidation (Momken *et al.*, 2017). The differences observed in the previous studies might be a result of different tissue or cells studied and different experimental conditions. Whereas the whole heart tissue was used in the study by Atkinson et al., isolated CMs were investigated in the study conducted by Momken and colleagues. In the current study, a trend for an increase in AMPK phosphorylation in WT-iPSC-CMs under F2+ was observed, indicating a possible leptin effect. In addition, culturing WT-iPSC-CMs in F2+ medium led to slightly increased *CD36* and *CPT1-B* expression compared to F2 medium. However, mitochondrial oxygen consumption in WT-iPSC-CMs did not differ in the presence or absence of leptin. Further experiments should be performed to study the fatty acid uptake and lipid droplet accumulation in WT-iPSC-CMs in the presence or absence of long-term treatment with leptin at physiological concentration.

Interestingly, WT-iPSC-CMs showed no difference in *GLUT-1* expression when cultured in F2+ medium, while a trend for a decrease in *GLUT-4* expression was observed compared to WT-iPSC-CMs in F2 medium. Since GLUT-1 and GLUT-4 are the insulin-independent or -dependent glucose transporters, respectively, these data suggest that leptin may interact with insulin regulating *GLUT-4* expression and glucose uptake. In this study a direct role of leptin in decreasing glucose uptake and consumption is further demonstrated by slightly decreased glycolysis and glycolytic capacity when WT-iPSC-CMs are cultured in the presence of leptin at physiological concentration. These data differed from the *ex-vivo* study using Sprague Dawley rat hearts perfused in the working mode with both glucose and palmitate, showing that rates of glucose oxidation were unaffected by the presence of leptin (60 ng/ml) for 60 min (Atkinson *et al.*, 2002). The reason for these differences may again due to different tissue or cells used in different studies and different experimental conditions (for example, time period with leptin treatment). In LEPR$^{\Delta/\Delta}$-iPSC-CMs, no difference was observed in *CD36* expression and AMPK activation in the presence or absence of leptin, at

physiological concentration, but slightly higher *CPT1-B* expression in the presence of low leptin. However, lower basal respiration, maximal respiration, spare respiratory capacity, and ATP production were observed in LEPR$^{\Delta/\Delta}$-iPSC-CMs in F2+ compared to WT-iPSC-CMs under the same condition. These differences are more pronounced when compared with those in the absence of leptin, suggesting leptin plays a role in lower mitochondrial respiration in LEPR$^{\Delta/\Delta}$-iPSC-CMs independent of the activation of LEPR and AMPK. Lower lipid accumulation was detected in in LEPR$^{\Delta/\Delta}$-iPSC-CMs compared to WT-iPSC-CMs in F2+ medium, which may suggest an increased lipid oxidation in the absence of a functional LEPR, however, the fatty acid uptake and lipid droplet accumulation in LEPR$^{\Delta/\Delta}$-iPSC-CMs in the presence or absence of long-term treatment with leptin at physiological concentration need to be further investigated. Culturing of LEPR$^{\Delta/\Delta}$-iPSC-CMs in F2+ medium demonstrated no difference in the expression of *GLUT-1* and *GLUT-4,* compared to F2 medium, however significant decrease in glycolysis was observed in LEPR$^{\Delta/\Delta}$-iPSC-CMs in F2+ medium compared to the F2, suggesting lower glucose consumption in the presence of leptin. In the future, the effect of long-term leptin treatment on glucose uptake in LEPR$^{\Delta/\Delta}$-iPSC-CMs should be studied.

Taken together, these findings indicate that leptin has a direct role in regulating fatty acid and glucose metabolism via the activation of JAK2 and AMPK in WT-iPSC-CMs. Loss of function of LEPR results in the blunted activation of JAK2 and AMPK and the alterations in fatty acid and glucose metabolism in LEPR$^{\Delta/\Delta}$-iPSC-CMs. However, there is an effect of long-term treatment with leptin on glucose and fatty acid metabolism in LEPR$^{\Delta/\Delta}$-iPSC-CMs, which is independent of the activation of LEPR and AMPK and cannot be explained by the published data available in the literature.

5.6 Effect of pathophysiological culture condition on metabolic flexibility in iPSC-CMs

Altered myocardial substrate and energy metabolism play a critical role in diabetic cardiomyopathy development (Lopaschuk, 2002; Young *et al.*, 2002). As mentioned in the Introduction part, T2DM is characterized by reduced glucose metabolism and enhanced fatty acid metabolism (Belke *et al.*, 2000; Boudina & Abel, 2007; Buchanan *et al.*, 2005). This study provides the first comprehensive assessment of long-term culture of CMs with leptin under pathophysiological conditions in a human-based CM model. In this study, high leptin (100 nM), high insulin (700 nM) and high glucose (11 mM) were used in the cultivation of WT- and LEPR$^{\Delta/\Delta}$-iPSC-CMs in F3+ medium for 4 weeks to mimic the hyperleptinemia,

hyperinsulinemia and hyperglycaemia which are conditions known in patients with obesity-associated T2DM.

Similar to leptin receptor resistance known in obesity-related T2DM patients, desensitization of LEPR was achieved by diabetic-like culture condition as demonstrated by the blunted JAK2 activation in WT-iPSC-CMs in F3+ medium with high leptin concentration. Considering the diabetic condition studied in the animal model, the myocardial activity of AMPK was significantly elevated in mice fed a high-fat diet for 1.5 and 3 weeks, most likely due to increased leptin levels (Park *et al.*, 2005). These findings are in line with the data in the current study showing that WT-iPSC-CMs cultured in F3+ medium displayed the increased AMPK phosphorylation. LEPR$^{\Delta/\Delta}$-iPSC-CMs cultured in F3+ medium showed slightly reduced AMPK phosphorylation compared to F2 medium, which is in line with previous studies reporting the decrease in cardiac function and blunted AMPK activation in *db/db* mice (Li *et al.*, 2010), or in mice with CM-specific deletion of *Lepr* (*Lepr*−/−), demonstrating impaired energy production via AMPK and mTOR signalling (Hall *et al.*, 2012). Importantly, culturing of WT-iPSC-CMs in F3+ medium induced higher *CPT1-B* expression compared to F2 medium, indicating that the pathophysiological condition (high insulin, high leptin, and high glucose) induces the expression of *CPT1-B* at the mRNA level. Increased *CPT1-B* expression is also found in LEPR$^{\Delta/\Delta}$-iPSC-CMs in F3+ medium compared to the same group under F2 medium. These findings suggest that high levels of leptin and insulin may affect fatty acid oxidation. Further studies should be performed to investigate whether higher *CPT1-B* expression at the mRNA level is associated with higher protein expression and higher fatty acid uptake and oxidation in WT- and LEPR$^{\Delta/\Delta}$-iPSC-CMs under pathophysiological conditions.

CD36 is present in cellular vesicles and can be translocated to the cell membrane rapidly by muscle contraction or AMPK activation (van de Weijer *et al.*, 2011). In the current study, long-term culture of WT-iPSC-CMs with high concentration of leptin in F3+ medium showed no effect on *CD36* expression compared to F2 medium. However, *CD36* expression was slightly higher in LEPR$^{\Delta/\Delta}$-iPSC-CMs in F3+ compared to F2. Previous studies demonstrated that *CD36* mRNA levels were increased but total expression of CD36 protein was unchanged in obesity and diabetes, however, permanent translocation of CD36 to the cell membrane seemed to occur in leptin receptor deficient animal models (Carley & Severson, 2005; Coort *et al.*, 2004). Further studies are needed to evaluate the role of leptin in CD36 protein expression and translocation to the membrane in both WT- and LEPR$^{\Delta/\Delta}$-iPSC-CMs under diabetic conditions to figure out the changes in fatty acid uptake. In T2DM patients a marked increase in cardiac fatty acid oxidation has been reported (Karwi *et al.*, 2021). In

db/db mice alterations in substrate metabolism were paralleled by a decreased contractility eventually leading to cardiomyopathy (Boudina *et al.*, 2007). In this study, WT-iPSC-CMs maintain substrate flexibility under diabetic conditions, as shown by no difference in mitochondrial oxygen consumption rate in WT-iPSC-CMs in F3+ compared to F2 medium. On the contrary, $LEPR^{\Delta/\Delta}$-iPSC-CMs cultured in F3+ medium showed increased OCR compared to F2 medium, as demonstrated by slightly augmented maximal respiration, and significantly increased spare respiratory capacity.

In addition, *Lepr*-deficient animals show elevated triglyceride levels and lipid accumulation in the myocardium that may promote lipotoxicity (Sharma *et al.*, 2004; Zhou *et al.*, 2000). However, in this study lipid accumulation was reduced in $LEPR^{\Delta/\Delta}$-iPSC-CMs cultured under F3+ medium compared to WT-iPSC-CMs under the same metabolic conditions. These results might be attributed to the increase fatty acid oxidation observed by increased cardiac oxygen consumption in WT-iPSC-CMs and in $LEPR^{\Delta/\Delta}$-iPSC-CMs. Another explanation could be that the fatty acids supplied to the culture is lower in this study than fatty acids available in the blood system of patients with obesity-related T2DM. Moreover, by performing Oil-Red-O-staining different lipid species within lipid droplets cannot be distinguished. In fact, Oil-Red-O-staining stains only the most hydrophobic and neutral lipids (triglycerides, diacylglycerols, and cholesterol esters), whereas polar lipids (phospholipids, sphingolipids, and ceramides) are not stained. Therefore, although lower lipid accumulation in $LEPR^{\Delta/\Delta}$-iPSC-CMs are observed compared to WT-iPSC-CMs under pathophysiological conditions, further investigations are needed to determine the nature of the lipids. For example, elevated intracellular palmitate can promote apoptosis through *de novo* ceramide formation with deleterious consequences on cellular function (Carley & Severson, 2005; Hickson-Bick *et al.*, 2000).

Increased reliance of the heart on fatty acids in the diabetic heart has a detrimental effect on cardiac efficiency and worsens the energy status in diabetes, mainly through inhibiting cardiac glucose oxidation (Karwi *et al.*, 2021). In mice fed a high-fat diet after 1.5 and 3 weeks, myocardial levels of GLUT-4 are reduced, and it is accompanied by reduced insulin signalling (Park *et al.*, 2005). In line with these previous studies, although no difference in *GLUT-1* expression was observed in WT-iPSC-CMs cultured in diabetic-like (F3+) medium, a tendency of lower expression of insulin-dependent glucose transporter *GLUT-4* was showed compared to F2 medium. However, no effect of long-term treatment with high concentration of leptin on both *GLUT-1* and *GLUT-4* expression was observed in $LEPR^{\Delta/\Delta}$-iPSC-CMs. These data suggest that leptin-mediated signalling interacts with the insulin signalling to regulate *GLUT-4* expression in WT-iPSC-CMs, but loss of function of LEPR

leads to the disturbance of their interaction and no changes in *GLUT-4* expression in LEPR$^{\Delta/\Delta}$-iPSC-CMs. Slightly lower *GLUT-1* expression was observed in LEPR$^{\Delta/\Delta}$-iPSC-CMs when compared to WT-iPSC-CMs in F3+ medium, while no difference was observed in *GLUT-4* expression in LEPR$^{\Delta/\Delta}$-iPSC-CMs compared to WT-iPSC-CMs in F3+ medium, supporting the hypothesis of lower glucose uptake in the absence of a functional LEPR in CMs.

Similar to the condition known in T2DM patients, LEPR$^{\Delta/\Delta}$-iPSC-CMs demonstrated lower ECAR related glycolysis and glycolytic capacity when cultured in F3+ medium compared to F2 medium, which points out the decrease in glucose consumption after long-term treatment with high concentration of leptin. Moreover, decreased glycolytic capacity was observed in LEPR$^{\Delta/\Delta}$-iPSC-CMs compared to WT-iPSC-CMs under diabetic condition, which emphasise the incapability to use efficiently glucose caused by the lack of LEPR function. However, pathophysiological culture condition (F3+) did not affect the glycolytic function of WT-iPSC-CMs when compared to the F2+ condition, suggesting that the glucose utilisation is not altered in WT-iPSC-CMs in F3+ medium. The effect of long-term treatment with high leptin concentration on glucose uptake in WT- and LEPR$^{\Delta/\Delta}$-iPSC-CMs should be further investigated in future studies. Based on these results, in LEPR$^{\Delta/\Delta}$-iPSC-CMs fatty acid oxidation is increased while carbohydrate oxidation is decreased under pathophysiological medium condition (F3+), as previously shown in *db/db* mice or T2DM patients. This mechanism might reduce cardiac energy efficiency and flexibility, and thereby may contribute to cardiomyopathy development.

5.7 Conclusions and future perspectives

In this study, iPSC disease models were used to investigate the LEPR expression and function in (WT)-iPSC-CMs and LEPR$^{\Delta/\Delta}$-iPSC-CMs. Physiological (F2+) and pathophysiological (F3+) medium conditions were applied to (WT)-iPSC-CMs and LEPR$^{\Delta/\Delta}$-iPSC-CMs to investigate leptin role in cardiac metabolism. The results reveal that i) LEPR is important in the maturation of (WT)-iPSC-CMs; ii) culture medium condition including physiological range of insulin, glucose and fatty acid are fundamental to study the leptin role in iPSC-CM metabolism; and iii) loss of LEPR resulted in low intracellular energy level and inefficient use of glucose in iPSC-CMs.

These results provide evidence for the hypotheses that leptin plays a direct role in CMs, and under physiological conditions, plays a beneficial role in cardiac metabolism by participating in glucose homeostasis, and that loss of LEPR function under diabetic conditions contributes to the development of diabetic cardiomyopathy. Certainly, there are

also limitations to this work. One limitation is the use of AlbuMax and KOSR in F2, F2+ and F3+ media, given their complex composition of various nutrients. Although different fatty acids such as palmitic acid and linoleic acids have been shown to promote maturation of iPSC-CMs (Correia *et al.*, 2017; Yang *et al.*, 2019), we are not able to distinguish between the lipids or lipid combination which has the most prominent effect on CM maturation. A second limitation in this study is the absence of a specific antibody for LEPR which could demonstrate the presence of truncated protein of LEPR in $LEPR^{\Delta/\Delta}$-iPSC-CMs, although LEPR cDNA sequencing data show a formation of a premature stop codon. Amino acid sequencing of LEPR protein could provide more information about the LEPR truncated protein in $LEPR^{\Delta/\Delta}$-iPSC-CMs. Besides these limitations, further studies should be performed to investigate function of different LEPR isoforms in iPSC-CMs. The most well studied LEPR isoform is the OBR-b, however OB-Ra, OB-Rb, and OB-Re were identified in mouse heart homogenates (Purdham *et al.*, 2004), therefore a potential role of these isoform should be further studied in the iPSC-based human cardiac system.

Given the different regulation of metabolic markers (*GLUT-1*, *GLUT-4*, *CD36* and *CPT1-B*) in $LEPR^{\Delta/\Delta}$-iPSC-CMs compared to WT-iPSC-CMs, fractionation of subcellular proteins to assess protein localization and enrichment from specific cellular compartments should be conducted to discover the regulation of these genes at the protein level. Furthermore, to discriminate the effect of leptin under pathophysiological condition from the effect of insulin and glucose, the generation of a medium with fatty acids, high glucose and high insulin will provide further knowledge regarding the contribution of leptin in diabetic cardiomyopathy development. Additionally, mass spectrometry-based phosphoproteomics could help to further understand how leptin regulates cardiac metabolism, and to figure out the specific proteins responsible for the metabolic switch between glucose and fatty acid consumption under physiological and pathophysiological conditions. This is important for the development of new therapeutic approaches for diabetes and diabetic cardiomyopathy.

6 Summary

Background and aims: Leptin resistance or leptin signalling deficiency are associated with increased risk of diabetic cardiomyopathy and heart failure, which is a leading cause of obesity- and diabetes type 2 (T2DM)-related morbidity and mortality. Various metabolic disturbances are involved in this pathogenesis, such as elevated glucose and fatty acid levels, insulin resistance and altered myocardial substrate utilization. Rodent models provided useful insights into the underlying molecular mechanisms of obese- and T2DM-associated cardiometabolic diseases, however, they cannot fully recapitulate the disease phenotype of obese or T2DM patients. The aims of this study were to study the effect of leptin receptor (LEPR) mutations on the leptin-mediated signalling pathways in human cardiomyocytes, and to investigate glucose and fatty acid metabolism in the heart under (patho)physiological conditions.

Methods and results: To study the role of LEPR in human cardiomyocytes (CMs), human induced pluripotent stem cell-derived cardiomyocytes (iPSC-CMs) were used as a model. In the first part of this study, LEPR expression and function was investigated in wild type (WT)-iPSC-CMs by PCR and Western Blot. LEPR protein expression was almost not detectable in iPSCs and during early cardiac differentiation stages, however mRNA *LEPR* expression was comparable in the different steps of cardiac development. Importantly, LEPR protein expression was observed in WT-iPSC-CMs at the maturation stages, indicating that LEPR plays an important role in matured CMs. Thanks to CRISPR/Cas9 technology, LEPR mutations were introduced into iPSCs. Among the several clones obtained, 1B2 $LEPR^{\Delta/\Delta}$-iPSC line was fully characterized and showed normal capacity to differentiate into spontaneously beating CMs. Although the B27 medium represents a well-established medium to cultivate iPSC-CMs, it has limitations for studying CM metabolism due to its high concentration of insulin and glucose, but low concentration of fatty acids. Physiological medium condition (F2) including physiological range of glucose, insulin and fatty acids was found to be fundamental to study LEPR signalling pathway in iPSC-CMs. Western blot analysis showed functional LEPR downstream pathway activation in WT-iPSC-CMs, while the absence of LEPR function was demonstrated in $LEPR^{\Delta/\Delta}$-iPSC-CMs cultured in F2 medium. Moreover, improved medium condition, offered by the F2 medium, ameliorates insulin sensitivity as result of increased insulin-dependent AKT phosphorylation in WT-iPSC-CMs, while loss of LEPR function was associated with downregulation of insulin pathway activation. Additionally, leptin direct effect was observed on the regulation of glucose metabolism in WT-iPSC-CMs by reducing glycolytic fluxes, which was not observed in $LEPR^{\Delta/\Delta}$-iPSC-CMs, as measured by ^{13}C-isotope-assisted glucose metabolic flux. These

data indicate that the signalling interaction between insulin and leptin is important in regulation of glucose metabolism and is abolished in LEPR$^{\Delta/\Delta}$-iPSC-CMs. The matured WT-iPSC-CMs in F2 medium display adult CM-like metabolic phenotype such as enhanced mitochondrial respiration and glycolytic function, as measured by Seahorse analyser, compared to the same group cultured in the B27 medium. The mutation generated in LEPR$^{\Delta/\Delta}$-iPSC-CMs caused an “energy starvation” status which led to increased AMPK phosphorylation compared to the WT group in B27 medium, which was associated with lower mitochondrial oxygen consumption rate (OCR) linked basal respiration and ATP production. In the next part of this study, the long-term leptin treatment of iPSC-CMs under physiological medium conditions in the presence of physiological range of insulin, glucose, and fatty acids (F2+) influenced LEPR downstream pathway activation such as JAK2 and AMPK suggesting a leptin-dependent role in fatty acid uptake and oxidation in WT-iPSC-CMs. On the contrary, leptin did not affect JAK2 and AMPK activation in LEPR$^{\Delta/\Delta}$-iPSC-CMs. Culturing of (WT)-iPSC-CMs in F2+ medium demonstrated no significant difference in mitochondrial oxygen consumption, while slightly lower glycolysis and glycolytic capacity was observed. However, a leptin effect on fatty acid and glucose metabolism was observed in LEPR$^{\Delta/\Delta}$-iPSC-CMs, which is independent from LEPR downstream regulation. To study the effect of high leptin levels, a medium mimicking some of the diabetic hallmarks, such as high glucose, high insulin, and high leptin levels, was used. Metabolic flexibility was observed in WT-iPSC-CMs in F3+ medium as showed by no difference in mitochondrial function in WT-iPSC-CMs in the presence or absence of high leptin. In contrast, LEPR$^{\Delta/\Delta}$-iPSC-CMs in F3+ medium demostrated higher OCR compared to F2 medium, which is accompanied by lower glycolysis and glycolytic capacity, indicating the incapability of LEPR$^{\Delta/\Delta}$-iPSC-CMs to use glucose as energy source, as measured by Seahorse analysis.

Conclusion and outlook: Taken together, this study demonstrates the importance of leptin and LEPR at the late stage of CM maturation and the fundamental role of metabolic medium condition including physiological range of glucose and fatty acid to study the role of leptin in iPSC-CMs. In addition, LEPR$^{\Delta/\Delta}$-iPSC-CMs in diabetic condition (F3+) represent a suitable model to investigate leptin-dependent cardiac metabolism, resulting in increased mitochondrial oxygen consumption and decreased glycolytic function, resembling the condition known in obesity-related T2DM patients. Further studies should focus on the regulation of the metabolic switch between glucose and fatty acid utilization in the absence of a functional LEPR. Understanding the contribution of leptin/LEPR signalling in human CM metabolism will shed light on novel therapeutic approaches to treat diabetic cardiomyopathy.

7 Zusammenfassung

Wissenschaftlicher Hintergrund und Ziele: Leptinresistenz oder Störungen des Leptinsignalweges gehen mit einem erhöhten Risiko für die Entwicklung diabetischer Kardiomyopathie und Herzinsuffizienz einher, welche unter den häufigsten Ursachen für Morbidität und Mortalität von Patienten mit Adipositas- und Typ 2 Diabetes (T2DM) sind. Verschiedene metabolische Dysregulationen sind mit diesem Krankheitsbild verbunden, beispielsweise erhöhte Blutzuckerwerte und Blutfette, Insulinresistenz sowie ein gestörter myokardialer Stoffwechsel. Obgleich mittels Mausmodellen wertvolle Erkenntnisse über die zugrunde liegenden molekularen Mechanismen dieser kardiometabolischen Krankheiten gewonnen werden konnte, sind diese Modelle nicht in der Lage die komplexen Krankheitsbilder zu rekapitulieren, die in Patienten mit Adipositas bzw. Typ-2 Diabetes vorliegen. Aus diesem Grund bestand das Ziel dieser Arbeit darin, den Effekt von Mutationen im Leptinrezeptors (LEPR) auf die Signalantwort des Rezeptors in humanen Kardiomyozyten zu untersuchen und den Glukose- und Fettsäuremetabolismus des Herzens unter pathophysiologischen Bedingungen zu charakterisieren.

Methoden und Ergebnisse: Um die Rolle des LEPR im humanen Kardiomyozyten näher zu erforschen, wurden, aus humanen induzierten pluripotenten Stammzellen differenzierte Kardiomyozyten (iPS-KM), als Modellsystem eingesetzt. Zunächst wurde die Expression und Funktion des LEPR in Wildtyp (WT-)-iPS-KM mittels PCR und Western Blot untersucht. Eine Expression des LEPR auf Proteinebene war nahezu undetektierbar in iPS-Zellen vor der Differenzierung sowie in den frühen kardialen Phasen des Differenzierungsprozesses, während die mRNA des LEPR während der Differenzierung nachgewiesen werden konnte. Nach abgeschlossener Differenzierung konnte eine robuste Proteinexpression des LEPR in WT-iPS-KM nachgewiesen werden, was auf eine wichtige Rolle für die Reifung der Kardiomyozyten hindeutet. Mittels CRISPR-Cas9 Geneditierung wurden Mutationen in das LEPR-Gen in iPS-Zellen eingebracht. Unter verschiedenen Klonen wurde die 1B2 $LEPR^{\Delta/\Delta}$-iPS-Linie zur weiteren Charakterisierung ausgewählt und aus diesen iPS erfolgreich iPS-KM differenziert. Die Zusammensetzung des, zur Kultivierung von iPS-KM weit verbreiteten, B27-Standardmediums brachte einige Limitationen für die geplanten Studien mit sich, insbesondere die hohen Konzentrationen von Glukose und Insulin sowie die geringen Level von Fettsäuren. Daher wurde ein spezielles Maturierungsmedium (F2-Medium) verwendet, welches physiologische Konzentrationen von Glukose, Insulin und Fettsäuren enthält. Die Ergebnisse dieser Studien zeigen, dass die physiologische Zusammensetzung des Mediums von fundamentaler Wichtigkeit für die Untersuchungen des LEPR-Signalwegs sind. Während die die Aktivierung nachgeschalteter Effektorproteine des LEPR in WT-iPS-

KM nachgewiesen werden konnte, zeigten LEPR$^{\Delta/\Delta}$-iPS-KM, die in F2-Medium kultiviert wurden, keine LEPR-Signalantwort. Die Kultivierung im optimierten F2-Medium führte weiterhin zur verbesserten Insulinsensitivität in WT-iPS-KM, die anhand einer insulin-induzierten AKT-Phosphorylierung nachgewiesen wurde, während in LEPR$^{\Delta/\Delta}$-iPS-KM eine deutlich schwächere Aktivierung des Insulinsignalwegs beobachtet wurde. In Untersuchungen des Glukosemetabolismus mittels ^{13}C-isotopenmarkierter Glukose konnte zudem ein direkter Effekt von Leptin auf den Glukosemetabolismus, anhand der Reduzierung des glykolytischen Fluxes, in WT-iPS-KM gezeigt werden, der in LEPR$^{\Delta/\Delta}$-iPS-KM nicht beobachtet werden konnte. Diese Ergebnisse deuten darauf hin, dass die Wechselwirkung zwischen Insulin- und Leptinsignalwegen für die Regulation des Glukosemetabolismus maßgeblich ist und diese Interaktion durch den Knockout des Leptinrezeptors in den LEPR$^{\Delta/\Delta}$-iPS-KM nicht mehr vorhanden ist. Die Kultivierung von WT-iPS-KM in F2-Medium führt, im direkten Vergleich zu Zellen in B27-Medium, zur Ausprägung eines, adulten Kardiomyozyten ähnlicherem metabolischen Phänotyp, was anhand einer gesteigerten mitochondrialen Zellatmung und verbesserter glykolytischer Funktionalität mittels Seahorse-Experimenten gezeigt wurde. In LEPR$^{\Delta/\Delta}$-iPS-KM wurde ein währenddessen „Energiemangelzustand“ beobachtet, welcher mit einem gesteigerten AMPK-Phosphorylierungslevel, verringertem mitochondrialem Sauerstoffverbrauch und reduzierter ATP-Produktion im Vergleich zu WT-iPS-KM in B27-Medium einherging.

In weiteren Studien dieser Arbeit wurde nachgewiesen, dass die Langzeitbehandlung der iPS-KM mit einer physiologischen Leptinkonzentration in Gegenwart der physiologischer Konzentrationen von Insulin, Glukose und Fettsäuren (F2+-Medium) die Aktivierung von JAK2 und AMPK im LEPR Signalweg beeinflusst. Diese Ergebnisse deuten auf eine Rolle von Leptin für die Aufnahme und die Verstoffwechselung von Fettsäuren in WT-iPS-KM hin. Im Gegensatz dazu hatte die Leptin-Langzeitbehandlung keinen Einfluss auf die JAK2 und AMPK-Aktivierung in LEPR$^{\Delta/\Delta}$-iPS-KM. In Bezug auf WT-iPS-KM in F2+-Medium wurden keine signifikanten Veränderungen im mitochondrialen Sauerstoffverbrauch festgestellt, während die Glykolyseaktivität und glykolytische Kapazität leicht vermindert waren. Für LEPR$^{\Delta/\Delta}$-iPS-KM wurde in Effekt der Leptinbehandlung mit F2+-Medium sowohl auf den Fettsäurestoffwechsel, als auch auf den Glukosemetabolismus beobachtet, welcher unabhängig vom klassischen LEPR-Signalweg war.

Der Einfluss hoher Leptinlevel wurde einem Medium (F3+-Medium) untersucht, welches Charakteristika von Diabetes-Patienten, wie hohe Glukosekonzentrationen, hohe Insulinkonzentrationen sowie hohe Leptinkonzentrationen, wiederspiegelt. Hohe Leptinkonzentrationen hatten keinen Einfluss auf die mitochondriale Funktion und

Glykolyseaktivität in WT-iPS-KM, was auf eine intakte metabolische Flexibilität der Zellen hindeutet. Im Gegensatz dazu wiesen $LEPR^{\Delta/\Delta}$-iPS-KM, die in F3+-Medium kultiviert wurden, einen höherer Sauerstoffverbrauch im Vergleich zu Kultivierung in F2-Medium auf, was ebenso mit einer verringerten Glykolyseaktivität und glykolytischen Kapazität einherging. Dies weist darauf hin, dass in $LEPR^{\Delta/\Delta}$-iPS-KM eine Störung in der Nutzung von Glukose als Energiesubstrat vorliegt und die metabolische Flexibilität maßgeblich eingeschränkt ist.

Schlussfolgerung und Ausblick: Zusammengefasst liefert diese Studie entscheidende Hinweise auf eine hohe Relevanz von Leptin und dem LEPR für Kardiomyozyten in späteren Entwicklungs- bzw. Reifestadien und die kritische Bedeutung von komplexen Kulturmedien mit physiologischen Konzentrationen von Glukose und Fettsäuren, um den Einfluss von Leptin auf iPS-KM zu untersuchen. Weiterhin wurde nachgewiesen, dass $LEPR^{\Delta/\Delta}$-iPS-KM die in einem Diabetes-simulierenden Medium kultiviert werden, ein geeignetes Modellsystem zur Untersuchung der Auswirkung von Leptin auf den kardialen Stoffwechse repräsentieren, welche mit erhöhtem mitochondrialer Zellatmung und verminderter glykolytischer Funktion einhergeht und somit die Situation in adipösen T2DM-Patienten widerspiegelt. Weitergehende Studien fokussieren sich auf die Regulation des Umschaltens zwischen Glukose- und Fettsäurestoffwechsel in $LEPR^{\Delta/\Delta}$-iPS-KM ohne funktionellen LEPR. Das daraus resultierende, tiefere Verständnis des Leptin-Leptinrezeptor Signalwegs in humanen Kardiomyozyten soll Ansatzpunkte zur Entwicklung neuer Therapien für diabetische Kardiomyopathie liefern.

8 References

Abe, Y., Ono, K., Kawamura, T., Wada, H., Kita, T., Shimatsu, A., & Hasegawa, K. (2007). Leptin induces elongation of cardiac myocytes and causes eccentric left ventricular dilatation with compensation. *Am J Physiol Heart Circ Physiol, 292*(5), H2387-2396.

Abel, E. D. (2004). Glucose transport in the heart. *Front Biosci, 9*, 201-215.

Abel, E. D., Litwin, S. E., & Sweeney, G. (2008). Cardiac remodeling in obesity. *Physiol Rev, 88*(2), 389-419.

Ahrén, B., Larsson, H., Wilhelmsson, C., Näsman, B., & Olsson, T. (1997). Regulation of circulating leptin in humans. *Endocrine, 7*(1), 1-8.

Alves, T. C., Pongratz, R. L., Zhao, X., Yarborough, O., Sereda, S., Shirihai, O., Cline, G. W., Mason, G., & Kibbey, R. G. (2015). Integrated, Step-Wise, Mass-Isotopomeric Flux Analysis of the TCA Cycle. *Cell Metab, 22*(5), 936-947.

Aponte, Y., Atasoy, D., & Sternson, S. M. (2011). AGRP neurons are sufficient to orchestrate feeding behavior rapidly and without training. *Nature Neuroscience, 14*(3), 351-355.

Atkinson, L. L., Fischer, M. A., & Lopaschuk, G. D. (2002). Leptin activates cardiac fatty acid oxidation independent of changes in the AMP-activated protein kinase-acetyl-CoA carboxylase-malonyl-CoA axis. *J Biol Chem, 277*(33), 29424-29430.

Avendano, G. F., Agarwal, R. K., Bashey, R. I., Lyons, M. M., Soni, B. J., Jyothirmayi, G. N., & Regan, T. J. (1999). Effects of glucose intolerance on myocardial function and collagen-linked glycation. *Diabetes, 48*(7), 1443-1447.

Awan, M. M., & Saggerson, E. D. (1993). Malonyl-CoA metabolism in cardiac myocytes and its relevance to the control of fatty acid oxidation. *Biochemical Journal, 295*(1), 61-66.

Bairwa, S. C., Parajuli, N., & Dyck, J. R. (2016). The role of AMPK in cardiomyocyte health and survival. *Biochim Biophys Acta, 1862*(12), 2199-2210.

Balland, E., Chen, W., Dodd, G. T., Conductier, G., Coppari, R., Tiganis, T., & Cowley, M. A. (2019). Leptin Signaling in the Arcuate Nucleus Reduces Insulin's Capacity to Suppress Hepatic Glucose Production in Obese Mice. *Cell Rep, 26*(2), 346-355 e343.

Barouch, L. A., Gao, D., Chen, L., Miller, K. L., Xu, W., Phan, A. C., Kittleson, M. M., Minhas, K. M., Berkowitz, D. E., Wei, C., & Hare, J. M. (2006). Cardiac myocyte apoptosis is associated with increased DNA damage and decreased survival in murine models of obesity. *Circulation Research, 98*(1), 119-124.

Barrangou, R., Fremaux, C., Deveau, H., Richards, M., Boyaval, P., Moineau, S., Romero, D. A., & Horvath, P. (2007). CRISPR provides acquired resistance against viruses in prokaryotes. *Science, 315*(5819), 1709-1712.

Batho, C. A. P., Mills, R. J., & Hudson, J. E. (2020). Metabolic Regulation of Human Pluripotent Stem Cell-Derived Cardiomyocyte Maturation. *Curr Cardiol Rep, 22*(8), 73.

Belke, D. D., Larsen, T. S., Gibbs, E. M., & Severson, D. L. (2000). Altered metabolism causes cardiac dysfunction in perfused hearts from diabetic (db/db) mice. *Am J Physiol Endocrinol Metab, 279*(5), E1104-1113.

Belke, D. D., Swanson, E. A., & Dillmann, W. H. (2004). Decreased sarcoplasmic reticulum activity and contractility in diabetic db/db mouse heart. *Diabetes, 53*(12), 3201-3208.

Belouzard, S., Delcroix, D., & Rouille, Y. (2004). Low levels of expression of leptin receptor at the cell surface result from constitutive endocytosis and intracellular retention in the biosynthetic pathway. *Journal of Biological Chemistry, 279*(27), 28499-28508.

Ben Jehuda, R., Shemer, Y., & Binah, O. (2018). Genome Editing in Induced Pluripotent Stem Cells using CRISPR/Cas9. *Stem Cell Reviews and Reports, 14*(3), 323-336.

Berglund, E. D., Vianna, C. R., Donato, J., Jr., Kim, M. H., Chuang, J.-C., Lee, C. E., Lauzon, D. A., Lin, P., Brule, L. J., Scott, M. M., Coppari, R., & Elmquist, J. K. (2012). Direct leptin action on POMC neurons regulates glucose homeostasis and hepatic insulin sensitivity in mice. *The Journal of Clinical Investigation, 122*(3), 1000-1009.

Bjorbaek, C., Buchholz, R. M., Davis, S. M., Bates, S. H., Pierroz, D. D., Gu, H., Neel, B. G., Myers, M. G., Jr., & Flier, J. S. (2001). Divergent roles of SHP-2 in ERK activation by leptin receptors. *Journal of Biological Chemistry, 276*(7), 4747-4755.

Bluemke, D. A., Kronmal, R. A., Lima, J. A. C., Liu, K., Olson, J., Burke, G. L., & Folsom, A. R. (2008). The Relationship of Left Ventricular Mass and Geometry to Incident Cardiovascular Events: The MESA (Multi-Ethnic Study of Atherosclerosis) Study. *Journal of the American College of Cardiology, 52*(25), 2148-2155.

Boudina, S., & Abel, E. D. (2007). Diabetic cardiomyopathy revisited. *Circulation, 115*(25), 3213-3223.

Boudina, S., Sena, S., Theobald, H., Sheng, X., Wright, J. J., Hu, X. X., Aziz, S., Johnson, J. I., Bugger, H., Zaha, V. G., & Abel, E. D. (2007). Mitochondrial energetics in the heart in obesity-related diabetes: direct evidence for increased uncoupled respiration and activation of uncoupling proteins. *Diabetes, 56*(10), 2457-2466.

Buchanan, J., Mazumder, P. K., Hu, P., Chakrabarti, G., Roberts, M. W., Yun, U. J., Cooksey, R. C., Litwin, S. E., & Abel, E. D. (2005). Reduced cardiac efficiency and altered substrate metabolism precedes the onset of hyperglycemia and contractile dysfunction in two mouse models of insulin resistance and obesity. *Endocrinology, 146*(12), 5341-5349.

Bugger, H., & Abel, E. D. (2010). Mitochondria in the diabetic heart. *Cardiovascular Research, 88*(2), 229-240.

Camand, O., Turban, S., Abitbol, M., & Guerre-Millo, M. (2002). Embryonic expression of the leptin receptor gene in mesoderm-derived tissues. *C R Biol, 325*(2), 77-87.

Carley, A. N., Semeniuk, L. M., Shimoni, Y., Aasum, E., Larsen, T. S., Berger, J. P., & Severson, D. L. (2004). Treatment of type 2 diabetic db/db mice with a novel PPARγ agonist improves cardiac metabolism but not contractile function. *American Journal of Physiology-Endocrinology and Metabolism, 286*(3), E449-E455.

Carley, A. N., & Severson, D. L. (2005). Fatty acid metabolism is enhanced in type 2 diabetic hearts. *Biochim Biophys Acta, 1734*(2), 112-126.

Caro, J. F., Kolaczynski, J. W., Nyce, M. R., Ohannesian, J. P., Opentanova, I., Goldman, W. H., Lynn, R. B., Zhang, P. L., Sinha, M. K., & Considine, R. V. (1996). Decreased cerebrospinal-fluid/serum leptin ratio in obesity: a possible mechanism for leptin resistance. *Lancet, 348*(9021), 159-161.

Ceddia, R. B., Koistinen, H. A., Zierath, J. R., & Sweeney, G. (2002). Analysis of paradoxical observations on the association between leptin and insulin resistance. *FASEB J, 16*(10), 1163-1176.

Christensen, A. A., & Gannon, M. (2019). The Beta Cell in Type 2 Diabetes. *Current Diabetes Reports, 19*(9), 81.

Christoffersen, C., Bollano, E., Lindegaard, M. L., Bartels, E. D., Goetze, J. P., Andersen, C. B., & Nielsen, L. B. (2003). Cardiac lipid accumulation associated with diastolic dysfunction in obese mice. *Endocrinology, 144*(8), 3483-3490.

Claret, M., & Schneeberger, M. (2012). Recent Insights into the Role of Hypothalamic AMPK Signaling Cascade upon Metabolic Control. *Frontiers in Neuroscience, 6*.

Clement, K., Vaisse, C., Lahlou, N., Cabrol, S., Pelloux, V., Cassuto, D., Gourmelen, M., Dina, C., Chambaz, J., Lacorte, J. M., Basdevant, A., Bougneres, P., Lebouc, Y., Froguel, P., & Guy-Grand, B. (1998). A mutation in the human leptin receptor gene causes obesity and pituitary dysfunction. *Nature, 392*(6674), 398-401.

Clemmensen, C., Chabenne, J., Finan, B., Sullivan, L., Fischer, K., Kuchler, D., Sehrer, L., Ograjsek, T., Hofmann, S. M., Schriever, S. C., Pfluger, P. T., Pinkstaff, J., Tschop, M. H., Dimarchi, R., & Muller, T. D. (2014). GLP-1/glucagon coagonism restores

leptin responsiveness in obese mice chronically maintained on an obesogenic diet. *Diabetes, 63*(4), 1422-1427.

Cooper, R. H., Randle, P. J., & Denton, R. M. (1975). Stimulation of phosphorylation and inactivation of pyruvate dehydrogenase by physiological inhibitors of the pyruvate dehydrogenase reaction. *Nature, 257*(5529), 808-809.

Coort, S. L., Hasselbaink, D. M., Koonen, D. P., Willems, J., Coumans, W. A., Chabowski, A., van der Vusse, G. J., Bonen, A., Glatz, J. F., & Luiken, J. J. (2004). Enhanced sarcolemmal FAT/CD36 content and triacylglycerol storage in cardiac myocytes from obese zucker rats. *Diabetes, 53*(7), 1655-1663.

Correia, C., Koshkin, A., Duarte, P., Hu, D., Teixeira, A., Domian, I., Serra, M., & Alves, P. M. (2017). Distinct carbon sources affect structural and functional maturation of cardiomyocytes derived from human pluripotent stem cells. *Sci Rep, 7*(1), 8590.

Cyganek, L., Tiburcy, M., Sekeres, K., Gerstenberg, K., Bohnenberger, H., Lenz, C., Henze, S., Stauske, M., Salinas, G., Zimmermann, W. H., Hasenfuss, G., & Guan, K. (2018). Deep phenotyping of human induced pluripotent stem cell-derived atrial and ventricular cardiomyocytes. *JCI Insight, 3*(12).

D'Souza, A., Howarth, F. C., Yanni, J., Dobryznski, H., Boyett, M. R., Adeghate, E., Bidasee, K. R., & Singh, J. (2011). Left ventricle structural remodelling in the prediabetic Goto–Kakizaki rat. *Experimental Physiology, 96*(9), 875-888.

de Wert, G., & Mummery, C. (2003). Human embryonic stem cells: research, ethics and policy. *Hum Reprod, 18*(4), 672-682.

Deinsberger, J., Reisinger, D., & Weber, B. (2020). Global trends in clinical trials involving pluripotent stem cells: a systematic multi-database analysis. *npj Regenerative Medicine, 5*(1), 15.

Deltcheva, E., Chylinski, K., Sharma, C. M., Gonzales, K., Chao, Y., Pirzada, Z. A., Eckert, M. R., Vogel, J., & Charpentier, E. (2011). CRISPR RNA maturation by trans-encoded small RNA and host factor RNase III. *Nature, 471*(7340), 602-607.

Deshpande, A. D., Harris-Hayes, M., & Schootman, M. (2008). Epidemiology of Diabetes and Diabetes-Related Complications. *Physical Therapy, 88*(11), 1254-1264.

Ding, Q., Regan, Stephanie N., Xia, Y., Oostrom, Leoníe A., Cowan, Chad A., & Musunuru, K. (2013). Enhanced Efficiency of Human Pluripotent Stem Cell Genome Editing through Replacing TALENs with CRISPRs. *Cell Stem Cell, 12*(4), 393-394.

Doenst, T., Nguyen, T. D., & Abel, E. D. (2013). Cardiac metabolism in heart failure: implications beyond ATP production. *Circulation Research, 113*(6), 709-724.

Domae, K., Miyagawa, S., Yoshikawa, Y., Fukushima, S., Hata, H., Saito, S., Kainuma, S., Kashiyama, N., Iseoka, H., Ito, E., Harada, A., Takeda, M., Sakata, Y., Toda, K., Pak, K., Yamada, T., & Sawa, Y. (2021). Clinical Outcomes of Autologous Stem Cell-Patch Implantation for Patients With Heart Failure With Nonischemic Dilated Cardiomyopathy. *J Am Heart Assoc, 10*(13), e008649.

Drawnel, F. M., Boccardo, S., Prummer, M., Delobel, F., Graff, A., Weber, M., Gerard, R., Badi, L., Kam-Thong, T., Bu, L., Jiang, X., Hoflack, J. C., Kiialainen, A., Jeworutzki, E., Aoyama, N., Carlson, C., Burcin, M., Gromo, G., Boehringer, M., Stahlberg, H., Hall, B. J., Magnone, M. C., Kolaja, K., Chien, K. R., Bailly, J., & Iacone, R. (2014). Disease modeling and phenotypic drug screening for diabetic cardiomyopathy using human induced pluripotent stem cells. *Cell Rep, 9*(3), 810-821.

Dunn, S. L., Bjornholm, M., Bates, S. H., Chen, Z., Seifert, M., & Myers, M. G., Jr. (2005). Feedback inhibition of leptin receptor/Jak2 signaling via Tyr1138 of the leptin receptor and suppressor of cytokine signaling 3. *Molecular Endocrinology, 19*(4), 925-938.

Eguchi, M., Liu, Y., Shin, E. J., & Sweeney, G. (2008). Leptin protects H9c2 rat cardiomyocytes from H2O2-induced apoptosis. *The FEBS Journal, 275*(12), 3136-3144.

Ellis, J. M., Mentock, S. M., Depetrillo, M. A., Koves, T. R., Sen, S., Watkins, S. M., Muoio, D. M., Cline, G. W., Taegtmeyer, H., Shulman, G. I., Willis, M. S., & Coleman, R. A. (2011). Mouse cardiac acyl coenzyme a synthetase 1 deficiency impairs Fatty Acid oxidation and induces cardiac hypertrophy. *Molecular and Cellular Biology, 31*(6), 1252-1262.

Elmquist, J. K., Bjorbaek, C., Ahima, R. S., Flier, J. S., & Saper, C. B. (1998). Distributions of leptin receptor mRNA isoforms in the rat brain. *Journal of Comparative Neurology, 395*(4), 535-547.

Farooqi, I. S., Jebb, S. A., Langmack, G., Lawrence, E., Cheetham, C. H., Prentice, A. M., Hughes, I. A., McCamish, M. A., & O'Rahilly, S. (1999). Effects of recombinant leptin therapy in a child with congenital leptin deficiency. *New England Journal of Medicine, 341*(12), 879-884.

Farooqi, I. S., & O'Rahilly, S. (2009). Leptin: a pivotal regulator of human energy homeostasis. *The American Journal of Clinical Nutrition, 89*(3), 980S-984S.

Farooqi, I. S., Wangensteen, T., Collins, S., Kimber, W., Matarese, G., Keogh, J. M., Lank, E., Bottomley, B., Lopez-Fernandez, J., Ferraz-Amaro, I., Dattani, M. T., Ercan, O., Myhre, A. G., Retterstol, L., Stanhope, R., Edge, J. A., McKenzie, S., Lessan, N., Ghodsi, M., De Rosa, V., Perna, F., Fontana, S., Barroso, I., Undlien, D. E., & O'Rahilly, S. (2007). Clinical and molecular genetic spectrum of congenital deficiency of the leptin receptor. *N Engl J Med, 356*(3), 237-247.

Fei, H., Okano, H. J., Li, C., Lee, G. H., Zhao, C., Darnell, R., & Friedman, J. M. (1997). Anatomic localization of alternatively spliced leptin receptors (Ob-R) in mouse brain and other tissues. *Proceedings of the National Academy of Sciences, 94*(13), 7001-7005.

Feyen, D. A. M., McKeithan, W. L., Bruyneel, A. A. N., Spiering, S., Hormann, L., Ulmer, B., Zhang, H., Briganti, F., Schweizer, M., Hegyi, B., Liao, Z., Polonen, R. P., Ginsburg, K. S., Lam, C. K., Serrano, R., Wahlquist, C., Kreymerman, A., Vu, M., Amatya, P. L., Behrens, C. S., Ranjbarvaziri, S., Maas, R. G. C., Greenhaw, M., Bernstein, D., Wu, J. C., Bers, D. M., Eschenhagen, T., Metallo, C. M., & Mercola, M. (2020). Metabolic Maturation Media Improve Physiological Function of Human iPSC-Derived Cardiomyocytes. *Cell Rep, 32*(3), 107925.

Field, A. E., Coakley, E. H., Must, A., Spadano, J. L., Laird, N., Dietz, W. H., Rimm, E., & Colditz, G. A. (2001). Impact of overweight on the risk of developing common chronic diseases during a 10-year period. *Archives of Internal Medicine, 161*(13), 1581-1586.

Fong, T. M., Huang, R. R., Tota, M. R., Mao, C., Smith, T., Varnerin, J., Karpitskiy, V. V., Krause, J. E., & Van der Ploeg, L. H. (1998). Localization of leptin binding domain in the leptin receptor. *Mol Pharmacol, 53*(2), 234-240.

Ford, E. S., Williamson, D. F., & Liu, S. (1997). Weight change and diabetes incidence: findings from a national cohort of US adults. *American Journal of Epidemiology, 146*(3), 214-222.

Frederich, R. C., Hamann, A., Anderson, S., Löllmann, B., Lowell, B. B., & Flier, J. S. (1995). Leptin levels reflect body lipid content in mice: Evidence for diet-induced resistance to leptin action. *Nature Medicine, 1*(12), 1311-1314.

Funakoshi, S., Fernandes, I., Mastikhina, O., Wilkinson, D., Tran, T., Dhahri, W., Mazine, A., Yang, D., Burnett, B., Lee, J., Protze, S., Bader, G. D., Nunes, S. S., Laflamme, M., & Keller, G. (2021). Generation of mature compact ventricular cardiomyocytes from human pluripotent stem cells. *Nature Communications, 12*(1).

Galicia-Garcia, U., Benito-Vicente, A., Jebari, S., Larrea-Sebal, A., Siddiqi, H., Uribe, K. B., Ostolaza, H., & Martin, C. (2020). Pathophysiology of Type 2 Diabetes Mellitus. *Int J Mol Sci, 21*(17).

Garland, P. B., Randle, P. J., & Newsholme, E. A. (1963). Citrate as an Intermediary in the Inhibition of Phosphofructokinase in Rat Heart Muscle by Fatty Acids, Ketone Bodies, Pyruvate, Diabetes, and Starvation. *Nature, 200*(4902), 169-170.

Ge, H., Huang, L., Pourbahrami, T., & Li, C. (2002). Generation of soluble leptin receptor by ectodomain shedding of membrane-spanning receptors in vitro and in vivo. *Journal of Biological Chemistry, 277*(48), 45898-45903.

Geraets, I. M. E., Chanda, D., van Tienen, F. H. J., van den Wijngaard, A., Kamps, R., Neumann, D., Liu, Y., Glatz, J. F. C., Luiken, J., & Nabben, M. (2018). Human embryonic stem cell-derived cardiomyocytes as an in vitro model to study cardiac insulin resistance. *Biochim Biophys Acta Mol Basis Dis, 1864*(5 Pt B), 1960-1967.

Golfman, L. S., Wilson, C. R., Sharma, S., Burgmaier, M., Young, M. E., Guthrie, P. H., Van Arsdall, M., Adrogue, J. V., Brown, K. K., & Taegtmeyer, H. (2005). Activation of PPARgamma enhances myocardial glucose oxidation and improves contractile function in isolated working hearts of ZDF rats. *Am J Physiol Endocrinol Metab, 289*(2), E328-336.

Gong, Y., Ishida-Takahashi, R., Villanueva, E. C., Fingar, D. C., Munzberg, H., & Myers, M. G., Jr. (2007). The long form of the leptin receptor regulates STAT5 and ribosomal protein S6 via alternate mechanisms. *Journal of Biological Chemistry, 282*(42), 31019-31027.

Gonzalez, F., Zhu, Z., Shi, Z. D., Lelli, K., Verma, N., Li, Q. V., & Huangfu, D. (2014). An iCRISPR platform for rapid, multiplexable, and inducible genome editing in human pluripotent stem cells. *Cell Stem Cell, 15*(2), 215-226.

Göttingen, U. M. C. (2019a). UMGi014-C. Retrieved from https://hpscreg.eu/cell-line/UMGi014-C

Göttingen, U. M. C. (2019b). UMGi020-B. Retrieved from https://hpscreg.eu/cell-line/UMGi020-B

Graneli, C., Hicks, R., Brolen, G., Synnergren, J., & Sartipy, P. (2019). Diabetic Cardiomyopathy Modelling Using Induced Pluripotent Stem Cell Derived Cardiomyocytes: Recent Advances and Emerging Models. *Stem Cell Rev Rep, 15*(1), 13-22.

Griffen, S. C., Wang, J., & German, M. S. (2001). A genetic defect in β-cell gene expression segregates independently from the fa locus in the ZDF rat. *Diabetes, 50*(1), 63-68.

Groot, P. H. E., Scholte, H. R., & Hülsmann, W. C. (1976). Fatty Acid Activation: Specificity, Localization, and Function. In R. Paoletti & D. Kritchevsky (Eds.), *Advances in Lipid Research* (Vol. 14, pp. 75-126): Elsevier.

Gruzdeva, O., Borodkina, D., Uchasova, E., Dyleva, Y., & Barbarash, O. (2019). Leptin resistance: underlying mechanisms and diagnosis. *Diabetes Metab Syndr Obes, 12*, 191-198.

Gupta, M. K., Vethe, H., Softic, S., Rao, T. N., Wagh, V., Shirakawa, J., Barsnes, H., Vaudel, M., Takatani, T., Kahraman, S., Sakaguchi, M., Martinez, R., Hu, J., Bjorlykke, Y., Raeder, H., & Kulkarni, R. N. (2020). Leptin Receptor Signaling Regulates Protein Synthesis Pathways and Neuronal Differentiation in Pluripotent Stem Cells. *Stem Cell Reports, 15*(5), 1067-1079.

Haap, M., Houdali, B., Maerker, E., Renn, W., Machicao, F., Hoffmeister, H. M., Haring, H. U., & Rett, K. (2003). Insulin-like effect of low-dose leptin on glucose transport in Langendorff rat hearts. *Exp Clin Endocrinol Diabetes, 111*(3), 139-145.

Habets, D. D., Coumans, W. A., Voshol, P. J., den Boer, M. A., Febbraio, M., Bonen, A., Glatz, J. F., & Luiken, J. J. (2007). AMPK-mediated increase in myocardial long-chain fatty acid uptake critically depends on sarcolemmal CD36. *Biochemical and Biophysical Research Communications, 355*(1), 204-210.

Haffner, S. M., Miettinen, H., Mykkänen, L., Karhapää, P., Rainwater, D. L., & Laakso, M. (1997). Leptin concentrations and insulin sensitivity in normoglycemic men. *International Journal of Obesity, 21*(5), 393-399.

Hafstad, A. D., Khalid, A. M., How, O. J., Larsen, T. S., & Aasum, E. (2007). Glucose and insulin improve cardiac efficiency and postischemic functional recovery in perfused hearts from type 2 diabetic (db/db) mice. *American Journal of Physiology-Endocrinology and Metabolism, 292*(5), E1288-E1294.

Hall, M. E., Harmancey, R., & Stec, D. E. (2015). Lean heart: Role of leptin in cardiac hypertrophy and metabolism. *World J Cardiol, 7*(9), 511-524.

Hall, M. E., Maready, M. W., Hall, J. E., & Stec, D. E. (2014). Rescue of cardiac leptin receptors in db/db mice prevents myocardial triglyceride accumulation. *Am J Physiol Endocrinol Metab, 307*(3), E316-325.

Hall, M. E., Smith, G., Hall, J. E., & Stec, D. E. (2012). Cardiomyocyte-specific deletion of leptin receptors causes lethal heart failure in Cre-recombinase-mediated cardiotoxicity. *Am J Physiol Regul Integr Comp Physiol, 303*(12), R1241-1250.

Han, J. L., & Entcheva, E. (2023). Gene Modulation with CRISPR-based Tools in Human iPSC-Cardiomyocytes. *Stem Cell Rev Rep*, 1-20.

Hardie, D. G., & Carling, D. (1997). The AMP-Activated Protein Kinase. *European Journal of Biochemistry, 246*(2), 259-273.

Harmancey, R., Lam, T. N., Lubrano, G. M., Guthrie, P. H., Vela, D., & Taegtmeyer, H. (2012). Insulin resistance improves metabolic and contractile efficiency in stressed rat heart. *The FASEB Journal, 26*(8), 3118-3126.

Hekerman, P., Zeidler, J., Bamberg-Lemper, S., Knobelspies, H., Lavens, D., Tavernier, J., Joost, H. G., & Becker, W. (2005). Pleiotropy of leptin receptor signalling is defined by distinct roles of the intracellular tyrosines. *The FEBS Journal, 272*(1), 109-119.

Hickson-Bick, D. L., Buja, L. M., & McMillin, J. B. (2000). Palmitate-mediated alterations in the fatty acid metabolism of rat neonatal cardiac myocytes. *J Mol Cell Cardiol, 32*(3), 511-519.

Hoggard, N., Hunter, L., Duncan, J. S., Williams, L. M., Trayhurn, P., & Mercer, J. G. (1997). Leptin and leptin receptor mRNA and protein expression in the murine fetus and placenta. *Proc Natl Acad Sci U S A, 94*(20), 11073-11078.

Hornung, F., Rogal, J., Loskill, P., Loffler, B., & Deinhardt-Emmer, S. (2021). The Inflammatory Profile of Obesity and the Role on Pulmonary Bacterial and Viral Infections. *International Journal of Molecular Sciences, 22*(7), 3456.

Hou, N., Luo, M. S., Liu, S. M., Zhang, H. N., Xiao, Q., Sun, P., Zhang, G. S., Luo, J. D., & Chen, M. S. (2010). Leptin induces hypertrophy through activating the peroxisome proliferator-activated receptor alpha pathway in cultured neonatal rat cardiomyocytes. *Clinical and Experimental Pharmacology and Physiology, 37*(11), 1087-1095.

Huang, L., Wang, Z., & Li, C. (2001). Modulation of circulating leptin levels by its soluble receptor. *Journal of Biological Chemistry, 276*(9), 6343-6349.

Huo, L., Gamber, K., Greeley, S., Silva, J., Huntoon, N., Leng, X. H., & Bjorbaek, C. (2009). Leptin-dependent control of glucose balance and locomotor activity by POMC neurons. *Cell Metab, 9*(6), 537-547.

Ingalls, A. M., Dickie, M. M., & Snell, G. D. (1950). Obese, a new mutation in the house mouse. *Journal of Heredity, 41*(12), 317-318.

Ishino, Y., Shinagawa, H., Makino, K., Amemura, M., & Nakata, A. (1987). Nucleotide sequence of the iap gene, responsible for alkaline phosphatase isozyme conversion in Escherichia coli, and identification of the gene product. *Journal of bacteriology, 169*(12), 5429-5433.

Itzhaki, I., Maizels, L., Huber, I., Zwi-Dantsis, L., Caspi, O., Winterstern, A., Feldman, O., Gepstein, A., Arbel, G., Hammerman, H., Boulos, M., & Gepstein, L. (2011). Modelling the long QT syndrome with induced pluripotent stem cells. *Nature, 471*(7337), 225-229.

Jang, Y. Y., & Ye, Z. (2016). Gene correction in patient-specific iPSCs for therapy development and disease modeling. *Human Genetics, 135*(9), 1041-1058.

Jensen, M. D., Hensrud, D., O'Brien, P. C., & Nielsen, S. (1999). Collection and interpretation of plasma leptin concentration data in humans. *Obes Res, 7*(3), 241-245.

Jia, G., DeMarco, V. G., & Sowers, J. R. (2016). Insulin resistance and hyperinsulinaemia in diabetic cardiomyopathy. *Nature Reviews Endocrinology, 12*(3), 144-153.

Jia, G., Hill, M. A., & Sowers, J. R. (2018). Diabetic Cardiomyopathy. *Circulation Research, 122*(4), 624-638.

Jiang, F., & Doudna, J. A. (2017). CRISPR–Cas9 Structures and Mechanisms. *Annual Review of Biophysics, 46*(1), 505-529.

Jiang, Y., Hoenisch, R. C., Chang, Y., Bao, X., Cameron, C. E., & Lian, X. L. (2022). Robust genome and RNA editing via CRISPR nucleases in PiggyBac systems. *Bioactive Materials, 14*, 313-320.

Kahn, B. B., Alquier, T., Carling, D., & Hardie, D. G. (2005). AMP-activated protein kinase: ancient energy gauge provides clues to modern understanding of metabolism. *Cell Metab, 1*(1), 15-25.

Kamohara, S., Burcelin, R., Halaas, J. L., Friedman, J. M., & Charron, M. J. (1997). Acute stimulation of glucose metabolism in mice by leptin treatment. *Nature, 389*(6649), 374-377.

Karwi, Q. G., Sun, Q., & Lopaschuk, G. D. (2021). The Contribution of Cardiac Fatty Acid Oxidation to Diabetic Cardiomyopathy Severity. *Cells, 10*(11).

Kastin, A. J., Pan, W., Maness, L. M., Koletsky, R. J., & Ernsberger, P. (1999). Decreased transport of leptin across the blood-brain barrier in rats lacking the short form of the leptin receptor. *Peptides, 20*(12), 1449-1453.

Kaszubska, W., Falls, H. D., Schaefer, V. G., Haasch, D., Frost, L., Hessler, P., Kroeger, P. E., White, D. W., Jirousek, M. R., & Trevillyan, J. M. (2002). Protein tyrosine phosphatase 1B negatively regulates leptin signaling in a hypothalamic cell line. *Molecular and Cellular Endocrinology, 195*(1), 109-118.

Kerbey, A. L., Randle, P. J., Cooper, R. H., Whitehouse, S., Pask, H. T., & Denton, R. M. (1976). Regulation of pyruvate dehydrogenase in rat heart. Mechanism of regulation of proportions of dephosphorylated and phosphorylated enzyme by oxidation of fatty acids and ketone bodies and of effects of diabetes: role of coenzyme A, acetyl-coenzyme A and reduced and oxidized nicotinamide-adenine dinucleotide. *Biochemical Journal, 154*(2), 327-348.

Kieffer, T. J., & Habener, J. F. (2000). The adipoinsular axis: effects of leptin on pancreatic β-cells. *American Journal of Physiology-Endocrinology and Metabolism, 278*(1), E1-E14.

Kielar, D., Clark, J. S. C., Ciechanowicz, A., Kurzawski, G., Sulikowski, T., & Naruszewicz, M. (1998). Leptin receptor isoforms expressed in human adipose tissue. *Metabolism, 47*(7), 844-847.

Kim, J. D., Leyva, S., & Diano, S. (2014). Hormonal regulation of the hypothalamic melanocortin system. *Frontiers in Physiology, 5*.

Kim, J. Y., Nam, Y., Rim, Y. A., & Ju, J. H. (2022). Review of the Current Trends in Clinical Trials Involving Induced Pluripotent Stem Cells. *Stem Cell Rev Rep, 18*(1), 142-154.

Krashes, M. J., Koda, S., Ye, C., Rogan, S. C., Adams, A. C., Cusher, D. S., Maratos-Flier, E., Roth, B. L., & Lowell, B. B. (2011). Rapid, reversible activation of AgRP neurons drives feeding behavior in mice. *The Journal of Clinical Investigation, 121*(4), 1424-1428.

Kumar, R., Yong, Q. C., Thomas, C. M., & Baker, K. M. (2012). Intracardiac intracellular angiotensin system in diabetes. *American Journal of Physiology-Regulatory, Integrative and Comparative Physiology, 302*(5), R510-R517.

Kurdi, M., & Booz, G. W. (2011). New take on the role of angiotensin II in cardiac hypertrophy and fibrosis. *Hypertension, 57*(6), 1034-1038.

Lee, G. H., Proenca, R., Montez, J. M., Carroll, K. M., Darvishzadeh, J. G., Lee, J. I., & Friedman, J. M. (1996). Abnormal splicing of the leptin receptor in diabetic mice. *Nature, 379*(6566), 632-635.

Lee, J., Liu, J., Feng, X., Salazar Hernandez, M. A., Mucka, P., Ibi, D., Choi, J. W., & Ozcan, U. (2016). Withaferin A is a leptin sensitizer with strong antidiabetic properties in mice. *Nature Medicine, 22*(9), 1023-1032.

Lee, Y., Wang, M. Y., Kakuma, T., Wang, Z. W., Babcock, E., McCorkle, K., Higa, M., Zhou, Y. T., & Unger, R. H. (2001). Liporegulation in diet-induced obesity. The antisteatotic role of hyperleptinemia. *J Biol Chem, 276*(8), 5629-5635.

Levelt, E., Gulsin, G., Neubauer, S., & McCann, G. P. (2018). MECHANISMS IN ENDOCRINOLOGY: Diabetic cardiomyopathy: pathophysiology and potential metabolic interventions state of the art review. *Eur J Endocrinol, 178*(4), R127-R139.

Li, K., Wang, G., Andersen, T., Zhou, P., & Pu, W. T. (2014). Optimization of Genome Engineering Approaches with the CRISPR/Cas9 System. *PLOS ONE, 9*(8), e105779.

Li, M. A., Turner, D. J., Ning, Z., Yusa, K., Liang, Q., Eckert, S., Rad, L., Fitzgerald, T. W., Craig, N. L., & Bradley, A. (2011). Mobilization of giant piggyBac transposons in the mouse genome. *Nucleic Acids Research, 39*(22), e148-e148.

Li, S., Pan, H., Tan, C., Sun, Y., Song, Y., Zhang, X., Yang, W., Wang, X., Li, D., Dai, Y., Ma, Q., Xu, C., Zhu, X., Kang, L., Fu, Y., Xu, X., Shu, J., Zhou, N., Han, F., Qin, D., Huang, W., Liu, Z., & Yan, Q. (2018). Mitochondrial Dysfunctions Contribute to Hypertrophic Cardiomyopathy in Patient iPSC-Derived Cardiomyocytes with MT-RNR2 Mutation. *Stem Cell Reports, 10*(3), 808-821.

Li, W., Stauske, M., Luo, X., Wagner, S., Vollrath, M., Mehnert, C. S., Schubert, M., Cyganek, L., Chen, S., Hasheminasab, S. M., Wulf, G., El-Armouche, A., Maier, L. S., Hasenfuss, G., & Guan, K. (2020). Disease Phenotypes and Mechanisms of iPSC-Derived Cardiomyocytes From Brugada Syndrome Patients With a Loss-of-Function SCN5A Mutation. *Front Cell Dev Biol, 8*, 592893.

Li, Y. J., Wang, P. H., Chen, C., Zou, M. H., & Wang, D. W. (2010). Improvement of mechanical heart function by trimetazidine in db/db mice. *Acta Pharmacol Sin, 31*(5), 560-569.

Liang, P., Sallam, K., Wu, H., Li, Y., Itzhaki, I., Garg, P., Zhang, Y., Vermglinchan, V., Lan, F., Gu, M., Gong, T., Zhuge, Y., He, C., Ebert, A. D., Sanchez-Freire, V., Churko, J., Hu, S., Sharma, A., Lam, C. K., Scheinman, M. M., Bers, D. M., & Wu, J. C. (2016). Patient-Specific and Genome-Edited Induced Pluripotent Stem Cell-Derived Cardiomyocytes Elucidate Single-Cell Phenotype of Brugada Syndrome. *J Am Coll Cardiol, 68*(19), 2086-2096.

Liedtke, A. J., DeMaison, L., Eggleston, A. M., Cohen, L. M., & Nellis, S. H. (1988). Changes in substrate metabolism and effects of excess fatty acids in reperfused myocardium. *Circulation Research, 62*(3), 535-542.

Lindström, P. (2007). The physiology of obese-hyperglycemic mice [ob/ob mice]. *The Scientific World Journal 7*, 666-685.

Liu, J., Lee, J., Salazar Hernandez, M. A., Mazitschek, R., & Ozcan, U. (2015). Treatment of obesity with celastrol. *Cell, 161*(5), 999-1011.

Lollmann, B., Gruninger, S., Stricker-Krongrad, A., & Chiesi, M. (1997). Detection and quantification of the leptin receptor splice variants Ob-Ra, b, and, e in different mouse tissues. *Biochem Biophys Res Commun, 238*(2), 648-652.

Lopaschuk, G. D. (2001). Malonyl Coa Control of Fatty Acid Oxidation in the Diabetic Rat Heart. In A. Angel, N. Dhalla, G. Pierce, & P. Singal (Eds.), *Diabetes and Cardiovascular Disease: Etiology, Treatment, and Outcomes* (pp. 155-165). Boston, MA: Springer US.

Lopaschuk, G. D. (2002). Metabolic abnormalities in the diabetic heart. *Heart Fail Rev, 7*(2), 149-159.

Lopaschuk, G. D., & Jaswal, J. S. (2010). Energy metabolic phenotype of the cardiomyocyte during development, differentiation, and postnatal maturation. *J Cardiovasc Pharmacol, 56*(2), 130-140.

Lopaschuk, G. D., & Stanley, W. C. (1997). Glucose metabolism in the ischemic heart. *Circulation, 95*(2), 313-315.

Lopaschuk, G. D., Ussher, J. R., Folmes, C. D. L., Jaswal, J. S., & Stanley, W. C. (2010). Myocardial Fatty Acid Metabolism in Health and Disease. *Physiological Reviews, 90*(1), 207-258.

Lopez, C. A., Al-Siddiqi, H., Purnama, U., Iftekhar, S., Bruyneel, A. A. N., Kerr, M., Nazir, R., da Luz Sousa Fialho, M., Malandraki-Miller, S., Alonaizan, R., Kermani, F., Heather, L. C., Czernuszka, J., & Carr, C. A. (2007). Clinical and molecular genetic spectrum of congenital deficiency of the leptin receptor. *New England Journal of Medicine, 356*(3), 237-247.

Lourenco, A. P., Leite-Moreira, A. F., Balligand, J. L., Bauersachs, J., Dawson, D., de Boer, R. A., de Windt, L. J., Falcao-Pires, I., Fontes-Carvalho, R., Franz, S., Giacca, M., Hilfiker-Kleiner, D., Hirsch, E., Maack, C., Mayr, M., Pieske, B., Thum, T., Tocchetti, C. G., Brutsaert, D. L., & Heymans, S. (2018). An integrative translational approach to study heart failure with preserved ejection fraction: a position paper from the Working Group on Myocardial Function of the European Society of Cardiology. *European Journal of Heart Failure, 20*(2), 216-227.

Luiken, J. J., Coort, S. L., Willems, J., Coumans, W. A., Bonen, A., van der Vusse, G. J., & Glatz, J. F. (2003). Contraction-induced fatty acid translocase/CD36 translocation in rat cardiac myocytes is mediated through AMP-activated protein kinase signaling. *Diabetes, 52*(7), 1627-1634.

Luiken, J. J., Koonen, D. P., Willems, J., Zorzano, A., Becker, C., Fischer, Y., Tandon, N. N., Van Der Vusse, G. J., Bonen, A., & Glatz, J. F. (2002). Insulin stimulates long-chain fatty acid utilization by rat cardiac myocytes through cellular redistribution of FAT/CD36. *Diabetes, 51*(10), 3113-3119.

Madani, S., De Girolamo, S., Munoz, D. M., Li, R. K., & Sweeney, G. (2006). Direct effects of leptin on size and extracellular matrix components of human pediatric ventricular myocytes. *Cardiovasc Res, 69*(3), 716-725.

Mali, P., Yang, L., Esvelt, K. M., Aach, J., Guell, M., DiCarlo, J. E., Norville, J. E., & Church, G. M. (2013). RNA-guided human genome engineering via Cas9. *Science, 339*(6121), 823-826.

Mandavia, C. H., Aroor, A. R., Demarco, V. G., & Sowers, J. R. (2013). Molecular and metabolic mechanisms of cardiac dysfunction in diabetes. *Life Sci, 92*(11), 601-608.

Marraffini, L. A., & Sontheimer, E. J. (2008). CRISPR interference limits horizontal gene transfer in staphylococci by targeting DNA. *Science, 322*(5909), 1843-1845.

McGaffin, K. R., Zou, B., McTiernan, C. F., & O'Donnell, C. P. (2009). Leptin attenuates cardiac apoptosis after chronic ischaemic injury. *Cardiovasc Res, 83*(2), 313-324.

Mercer, J. G., Hoggard, N., Williams, L. M., Lawrence, C. B., Hannah, L. T., & Trayhurn, P. (1996). Localization of leptin receptor mRNA and the long form splice variant (Ob-Rb) in mouse hypothalamus and adjacent brain regions by in situ hybridization. *FEBS Letters, 387*(2-3), 113-116.

Mercer, J. G., Moar, K. M., Hoggard, N., Strosberg, A. D., Froguel, P., & Bailleul, B. (2000). B219/OB-R 5'-UTR and leptin receptor gene-related protein gene expression in mouse brain and placenta: tissue-specific leptin receptor promoter activity. *Journal of Neuroendocrinology, 12*(7), 649-655.

Mishra, T., & Rath, P. (2005). Diabetic cardiomyopathy: evidences, pathophysiology, and therapeutic considerations. *Journal, Indian Academy of Clinical Medicine, 6*(4), 313.

Mittendorfer, B., Horowitz, J. F., DePaoli, A. M., McCamish, M. A., Patterson, B. W., & Klein, S. (2011). Recombinant Human Leptin Treatment Does Not Improve Insulin Action in Obese Subjects With Type 2 Diabetes. *Diabetes, 60*(5), 1474-1477.

Mizushige, K., Yao, L., Noma, T., Kiyomoto, H., Yu, Y., Hosomi, N., Ohmori, K., & Matsuo, H. (2000). Alteration in left ventricular diastolic filling and accumulation of myocardial collagen at insulin-resistant prediabetic stage of a type II diabetic rat model. *Circulation, 101*(8), 899-907.

Momken, I., Chabowski, A., Dirkx, E., Nabben, M., Jain, S. S., McFarlan, J. T., Glatz, J. F., Luiken, J. J., & Bonen, A. (2017). A new leptin-mediated mechanism for stimulating fatty acid oxidation: a pivotal role for sarcolemmal FAT/CD36. *Biochem J, 474*(1), 149-162.

Moon, H. S., Matarese, G., Brennan, A. M., Chamberland, J. P., Liu, X., Fiorenza, C. G., Mylvaganam, G. H., Abanni, L., Carbone, F., Williams, C. J., De Paoli, A. M., Schneider, B. E., & Mantzoros, C. S. (2011). Efficacy of metreleptin in obese patients with type 2 diabetes: cellular and molecular pathways underlying leptin tolerance. *Diabetes, 60*(6), 1647-1656.

Moretti, A., Laugwitz, K. L., Dorn, T., Sinnecker, D., & Mummery, C. (2013). Pluripotent stem cell models of human heart disease. *Cold Spring Harb Perspect Med, 3*(11).

Mueckler, M. (1994). Facilitative glucose transporters. *European Journal of Biochemistry, 219*(3), 713-725.

Muller, T. D., Sullivan, L. M., Habegger, K., Yi, C. X., Kabra, D., Grant, E., Ottaway, N., Krishna, R., Holland, J., Hembree, J., Perez-Tilve, D., Pfluger, P. T., DeGuzman, M. J., Siladi, M. E., Kraynov, V. S., Axelrod, D. W., DiMarchi, R., Pinkstaff, J. K., & Tschop, M. H. (2012). Restoration of leptin responsiveness in diet-induced obese mice using an optimized leptin analog in combination with exendin-4 or FGF21. *Journal of Peptide Science, 18*(6), 383-393.

Myers, M. G., Jr., Heymsfield, S. B., Haft, C., Kahn, B. B., Laughlin, M., Leibel, R. L., Tschop, M. H., & Yanovski, J. A. (2012). Challenges and opportunities of defining clinical leptin resistance. *Cell Metab, 15*(2), 150-156.

Nagoshi, T., Yoshimura, M., Rosano, G. M., Lopaschuk, G. D., & Mochizuki, S. (2011). Optimization of cardiac metabolism in heart failure. *Curr Pharm Des, 17*(35), 3846-3853.

Nakashima, K., Narazaki, M., & Taga, T. (1997). Leptin receptor (OB-R) oligomerizes with itself but not with its closely related cytokine signal transducer gp130. *FEBS Letters, 403*(1), 79-82.

Narsinh, K. H., Jia, F., Robbins, R. C., Kay, M. A., Longaker, M. T., & Wu, J. C. (2011). Generation of adult human induced pluripotent stem cells using nonviral minicircle DNA vectors. *Nat Protoc, 6*(1), 78-88.

Neely, J. R., & Morgan, H. E. (1974). Relationship between carbohydrate and lipid metabolism and the energy balance of heart muscle. *Annual Review of Physiology, 36*(1), 413-459.

Nerbonne, J. M. (2004). Studying cardiac arrhythmias in the mouse--a reasonable model for probing mechanisms? *Trends Cardiovasc Med, 14*(3), 83-93.

Nishina, P. M., Naggert, J. K., Verstuyft, J., & Paigen, B. (1994). Atherosclerosis in genetically obese mice: the mutants obese, diabetes, fat, tubby, and lethal yellow. *Metabolism, 43*(5), 554-558.

Nunziata, A., Funcke, J. B., Borck, G., von Schnurbein, J., Brandt, S., Lennerz, B., Moepps, B., Gierschik, P., Fischer-Posovszky, P., & Wabitsch, M. (2018). Functional and Phenotypic Characteristics of Human Leptin Receptor Mutations. *Journal of the Endocrine Society, 3*(1), 27-41.

Okita, K., Hong, H., Takahashi, K., & Yamanaka, S. (2010). Generation of mouse-induced pluripotent stem cells with plasmid vectors. *Nat Protoc, 5*(3), 418-428.

Orfali, K. A., Fryer, L. G., Holness, M. J., & Sugden, M. C. (1993). Long-term regulation of pyruvate dehydrogenase kinase by high-fat feeding. Experiments in vivo and in cultured cardiomyocytes. *FEBS Letters, 336*(3), 501-505.

Palanivel, R., Eguchi, M., Shuralyova, I., Coe, I., & Sweeney, G. (2006). Distinct effects of short- and long-term leptin treatment on glucose and fatty acid uptake and metabolism in HL-1 cardiomyocytes. *Metabolism, 55*(8), 1067-1075.

Parikh, S. S., Blackwell, D. J., Gomez-Hurtado, N., Frisk, M., Wang, L., Kim, K., Dahl, C. P., Fiane, A., Tonnessen, T., Kryshtal, D. O., Louch, W. E., & Knollmann, B. C. (2017). Thyroid and Glucocorticoid Hormones Promote Functional T-Tubule Development in Human-Induced Pluripotent Stem Cell-Derived Cardiomyocytes. *Circ Res, 121*(12), 1323-1330.

Park, M. A., Jung, H. S., & Slukvin, I. (2018). Genetic Engineering of Human Pluripotent Stem Cells Using PiggyBac Transposon System. *Current Protocols in Stem Cell Biology, 47*(1), e63.

Park, S. J., Zhang, D., Qi, Y., Li, Y., Lee, K. Y., Bezzerides, V. J., Yang, P., Xia, S., Kim, S. L., Liu, X., Lu, F., Pasqualini, F. S., Campbell, P. H., Geva, J., Roberts, A. E., Kleber, A. G., Abrams, D. J., Pu, W. T., & Parker, K. K. (2019). Insights Into the Pathogenesis of Catecholaminergic Polymorphic Ventricular Tachycardia From Engineered Human Heart Tissue. *Circulation, 140*(5), 390-404.

Park, S. Y., Cho, Y. R., Kim, H. J., Higashimori, T., Danton, C., Lee, M. K., Dey, A., Rothermel, B., Kim, Y. B., Kalinowski, A., Russell, K. S., & Kim, J. K. (2005). Unraveling the temporal pattern of diet-induced insulin resistance in individual organs and cardiac dysfunction in C57BL/6 mice. *Diabetes, 54*(12), 3530-3540.

Pascual, F., & Coleman, R. A. (2016). Fuel availability and fate in cardiac metabolism: A tale of two substrates. *Biochimica et Biophysica Acta (BBA) - Molecular and Cell Biology of Lipids, 1861*(10), 1425-1433.

Paul, D. S., Grevengoed, T. J., Pascual, F., Ellis, J. M., Willis, M. S., & Coleman, R. A. (2014). Deficiency of cardiac Acyl-CoA synthetase-1 induces diastolic dysfunction, but pathologic hypertrophy is reversed by rapamycin. *Biochimica et Biophysica Acta (BBA) - Molecular and Cell Biology of Lipids, 1841*(6), 880-887.

Paz-Filho, G., Mastronardi, C., Wong, M. L., & Licinio, J. (2012). Leptin therapy, insulin sensitivity, and glucose homeostasis. *Indian J Endocrinol Metab, 16*(Suppl 3), S549-555.

Pereira, L., Matthes, J., Schuster, I., Valdivia, H. H., Herzig, S., Richard, S., & Gomez, A. M. (2006). Mechanisms of [Ca2+]i Transient Decrease in Cardiomyopathy of db/db Type 2 Diabetic Mice. *Diabetes, 55*(3), 608-615.

Petrie, J. R., Guzik, T. J., & Touyz, R. M. (2018). Diabetes, Hypertension, and Cardiovascular Disease: Clinical Insights and Vascular Mechanisms. *Canadian Journal of Cardiology, 34*(5), 575-584.

Pinieiro, R., Iglesias, M. J., Eiras, S., Vinuela, J., Lago, F., & Gonzalez-Juanatey, J. R. (2005). Leptin does not induce hypertrophy, cell cycle alterations, or production of MCP-1 in cultured rat and mouse cardiomyocytes. *Endocrine Research, 31*(4), 375-386.

Poetsch, M. S., Strano, A., & Guan, K. (2020). Role of Leptin in Cardiovascular Diseases. *Front Endocrinol (Lausanne), 11*, 354.

Poetsch, M. S., Strano, A., & Guan, K. (2022). Human Induced Pluripotent Stem Cells: From Cell Origin, Genomic Stability, and Epigenetic Memory to Translational Medicine. *Stem Cells, 40*(6), 546-555.

Purdham, D. M., Zou, M. X., Rajapurohitam, V., & Karmazyn, M. (2004). Rat heart is a site of leptin production and action. *Am J Physiol Heart Circ Physiol, 287*(6), H2877-2884.

Rahmouni, K., Sigmund, C. D., Haynes, W. G., & Mark, A. L. (2009). Hypothalamic ERK mediates the anorectic and thermogenic sympathetic effects of leptin. *Diabetes, 58*(3), 536-542.

Rajapurohitam, V., Gan, X. T., Kirshenbaum, L. A., & Karmazyn, M. (2003). The Obesity-Associated Peptide Leptin Induces Hypertrophy in Neonatal Rat Ventricular Myocytes. *Circulation Research, 93*(4), 277-279.

Ran, F. A., Hsu, P. D., Wright, J., Agarwala, V., Scott, D. A., & Zhang, F. (2013). Genome engineering using the CRISPR-Cas9 system. *Nature Protocols, 8*(11), 2281-2308.

Randle, P., Newsholme, E., & Garland, P. (1964). Regulation of glucose uptake by muscle. 8. Effects of fatty acids, ketone bodies and pyruvate, and of alloxan-diabetes and starvation, on the uptake and metabolic fate of glucose in rat heart and diaphragm muscles. *Biochemical Journal, 93*(3), 652-665.

Randolph, L. N., Bao, X., Zhou, C., & Lian, X. (2017). An all-in-one, Tet-On 3G inducible PiggyBac system for human pluripotent stem cells and derivatives. *Scientific Reports, 7*(1), 1549.

Regan, T. J. (1983). Congestive heart failure in the diabetic. *Annual review of medicine, 34*(1), 161-168.

Ren, D., Li, M., Duan, C., & Rui, L. (2005). Identification of SH2-B as a key regulator of leptin sensitivity, energy balance, and body weight in mice. *Cell Metabolism, 2*(2), 95-104.

Rider, O. J., Cox, P., Tyler, D., Clarke, K., & Neubauer, S. (2013). Myocardial substrate metabolism in obesity. *International Journal of Obesity, 37*(7), 972-979.

Roden, M., & Shulman, G. I. (2019). The integrative biology of type 2 diabetes. *Nature, 576*(7785), 51-60.

Rodrigues, B., Cam, M. C., & McNeill, J. H. (1998). Metabolic disturbances in diabetic cardiomyopathy. *Molecular and Cellular Biochemistry, 180*, 53-57.

Rose, H., Hennecke, T., & Kammermeier, H. (1990). Sarcolemmal fatty acid transfer in isolated cardiomyocytes governed by albumin/membrane-lipid partition. *Journal of Molecular and Cellular Cardiology, 22*(8), 883-892.

Rostovskaya, M., Fu, J., Obst, M., Baer, I., Weidlich, S., Wang, H., Smith, A. J., Anastassiadis, K., & Stewart, A. F. (2012). Transposon-mediated BAC transgenesis in human ES cells. *Nucleic Acids Research, 40*(19), e150-e150.

Roth, J. D., Roland, B. L., Cole, R. L., Trevaskis, J. L., Weyer, C., Koda, J. E., Anderson, C. M., Parkes, D. G., & Baron, A. D. (2008). Leptin responsiveness restored by amylin agonism in diet-induced obesity: Evidence from nonclinical and clinical studies. *Proceedings of the National Academy of Sciences, 105*(20), 7257-7262.

Rowe, R. G., & Daley, G. Q. (2019). Induced pluripotent stem cells in disease modelling and drug discovery. *Nature Reviews Genetics, 20*(7), 377-388.

Russell, R. R., 3rd, Bergeron, R., Shulman, G. I., & Young, L. H. (1999). Translocation of myocardial GLUT-4 and increased glucose uptake through activation of AMPK by AICAR. *American Journal of Physiology - Heart and Circulatory Physiology, 277*(2 46-2), H643-H649.

Russell, R. R., 3rd, Yin, R., Caplan, M. J., Hu, X., Ren, J., Shulman, G. I., Sinusas, A. J., & Young, L. H. (1998). Additive effects of hyperinsulinemia and ischemia on myocardial GLUT1 and GLUT4 translocation in vivo. *Circulation, 98*(20), 2180-2186.

Saddik, M., Gamble, J., Witters, L. A., & Lopaschuk, G. D. (1993). Acetyl-CoA carboxylase regulation of fatty acid oxidation in the heart. *Journal of Biological Chemistry, 268*(34), 25836-25845.

Saeed, S., Bonnefond, A., Manzoor, J., Philippe, J., Durand, E., Arshad, M., Sand, O., Butt, T. A., Falchi, M., Arslan, M., & Froguel, P. (2014). Novel LEPR mutations in obese Pakistani children identified by PCR-based enrichment and next generation sequencing. *Obesity (Silver Spring), 22*(4), 1112-1117.

Saeed, S., Bonnefond, A., Manzoor, J., Shabbir, F., Ayesha, H., Philippe, J., Durand, E., Crouch, H., Sand, O., Ali, M., Butt, T., Rathore, A. W., Falchi, M., Arslan, M., & Froguel, P. (2015). Genetic variants in LEP, LEPR, and MC4R explain 30% of

severe obesity in children from a consanguineous population. *Obesity (Silver Spring), 23*(8), 1687-1695.

Schocken, D. D., Benjamin, E. J., Fonarow, G. C., Krumholz, H. M., Levy, D., Mensah, G. A., Narula, J., Shor, E. S., Young, J. B., & Hong, Y. (2008). Prevention of Heart Failure. *Circulation, 117*(19), 2544-2565.

Schwartz, M. W., Seeley, R. J., Campfield, L. A., Burn, P., & Baskin, D. G. (1996). Identification of targets of leptin action in rat hypothalamus. *The Journal of Clinical Investigation, 98*(5), 1101-1106.

Schwenk, R. W., Luiken, J. J., Bonen, A., & Glatz, J. F. (2008). Regulation of sarcolemmal glucose and fatty acid transporters in cardiac disease. *Cardiovascular Research, 79*(2), 249-258.

Semeniuk, L. M., Kryski, A. J., & Severson, D. L. (2002). Echocardiographic assessment of cardiac function in diabetic db/db and transgenic db/db-hGLUT4 mice. *Am J Physiol Heart Circ Physiol, 283*(3), H976-982.

Seron, K., Couturier, C., Belouzard, S., Bacart, J., Monte, D., Corset, L., Bocquet, O., Dam, J., Vauthier, V., Lecoeur, C., Bailleul, B., Hoflack, B., Froguel, P., Jockers, R., & Rouille, Y. (2011). Endospanins regulate a postinternalization step of the leptin receptor endocytic pathway. *Journal of Biological Chemistry, 286*(20), 17968-17981.

Seufert, J. (2004). Leptin effects on pancreatic beta-cell gene expression and function. *Diabetes, 53 Suppl 1*, S152-S158.

Seufert, J., Kieffer, T. J., & Habener, J. F. (1999). Leptin inhibits insulin gene transcription and reverses hyperinsulinemia in leptin-deficient ob/ob mice. *Proceedings of the National Academy of Sciences, 96*(2), 674-679.

Shah, D., Virtanen, L., Prajapati, C., Kiamehr, M., Gullmets, J., West, G., Kreutzer, J., Pekkanen-Mattila, M., Helio, T., Kallio, P., Taimen, P., & Aalto-Setala, K. (2019). Modeling of LMNA-Related Dilated Cardiomyopathy Using Human Induced Pluripotent Stem Cells. *Cells, 8*(6).

Shanks, N., Greek, R., & Greek, J. (2009). Are animal models predictive for humans? *Philos Ethics Humanit Med, 4*, 2.

Sharma, S., Adrogue, J. V., Golfman, L., Uray, I., Lemm, J., Youker, K., Noon, G. P., Frazier, O. H., & Taegtmeyer, H. (2004). Intramyocardial lipid accumulation in the failing human heart resembles the lipotoxic rat heart. *FASEB J, 18*(14), 1692-1700.

Sharma, V., Mustafa, S., Patel, N., Wambolt, R., Allard, M. F., & McNeill, J. H. (2009). Stimulation of cardiac fatty acid oxidation by leptin is mediated by a nitric oxide-p38 MAPK-dependent mechanism. *Eur J Pharmacol, 617*(1-3), 113-117.

Shen, S., Sewanan, L. R., Shao, S., Halder, S. S., Stankey, P., Li, X., & Campbell, S. G. (2022). Physiological calcium combined with electrical pacing accelerates maturation of human engineered heart tissue. *Stem Cell Reports, 17*(9), 2037-2049.

Shin, E. J., Schram, K., Zheng, X. L., & Sweeney, G. (2009). Leptin attenuates hypoxia/reoxygenation-induced activation of the intrinsic pathway of apoptosis in rat H9c2 cells. *Journal of Cellular Physiology, 221*(2), 490-497.

Shinnawi, R., Shaheen, N., Huber, I., Shiti, A., Arbel, G., Gepstein, A., Ballan, N., Setter, N., Tijsen, A. J., Borggrefe, M., & Gepstein, L. (2019). Modeling Reentry in the Short QT Syndrome With Human-Induced Pluripotent Stem Cell-Derived Cardiac Cell Sheets. *J Am Coll Cardiol, 73*(18), 2310-2324.

Sinha, M. K., Ohannesian, J. P., Heiman, M. L., Kriauciunas, A., Stephens, T. W., Magosin, S., Marco, C., & Caro, J. F. (1996). Nocturnal rise of leptin in lean, obese, and non-insulin-dependent diabetes mellitus subjects. *J Clin Invest, 97*(5), 1344-1347.

Smith, C. C., Mocanu, M. M., Davidson, S. M., Wynne, A. M., Simpkin, J. C., & Yellon, D. M. (2006). Leptin, the obesity-associated hormone, exhibits direct cardioprotective effects. *British Journal of Pharmacology, 149*(1), 5-13.

Sousa Fialho, M. D. L., Purnama, U., Dennis, K., Montes Aparicio, C. N., Castro-Guarda, M., Massourides, E., Tyler, D. J., Carr, C. A., & Heather, L. C. (2021). Activation of

HIF1alpha Rescues the Hypoxic Response and Reverses Metabolic Dysfunction in the Diabetic Heart. *Diabetes, 70*(11), 2518-2531.

Stemmer, M., Thumberger, T., Del Sol Keyer, M., Wittbrodt, J., & Mateo, J. L. (2015). CCTop: An Intuitive, Flexible and Reliable CRISPR/Cas9 Target Prediction Tool. *PLoS One, 10*(4), e0124633.

Sun, H., Saeedi, P., Karuranga, S., Pinkepank, M., Ogurtsova, K., Duncan, B. B., Stein, C., Basit, A., Chan, J. C. N., Mbanya, J. C., Pavkov, M. E., Ramachandaran, A., Wild, S. H., James, S., Herman, W. H., Zhang, P., Bommer, C., Kuo, S., Boyko, E. J., & Magliano, D. J. (2022). IDF Diabetes Atlas: Global, regional and country-level diabetes prevalence estimates for 2021 and projections for 2045. *Diabetes Res Clin Pract, 183*, 109119.

Sweeney, G. (2002). Leptin signalling. *Cell Signal, 14*(8), 655-663.

Taegtmeyer, H. (1985). Carbohydrate interconversions and energy production. *Circulation, 72*(5 Pt 2), IV1-8.

Takahashi, K., Tanabe, K., Ohnuki, M., Narita, M., Ichisaka, T., Tomoda, K., & Yamanaka, S. (2007). Induction of pluripotent stem cells from adult human fibroblasts by defined factors. *Cell, 131*(5), 861-872.

Takahashi, K., & Yamanaka, S. (2006). Induction of pluripotent stem cells from mouse embryonic and adult fibroblast cultures by defined factors. *Cell, 126*(4), 663-676.

Tartaglia, L. A., Dembski, M., Weng, X., Deng, N., Culpepper, J., Devos, R., Richards, G. J., Campfield, L. A., Clark, F. T., Deeds, J., Muir, C., Sanker, S., Moriarty, A., Moore, K. J., Smutko, J. S., Mays, G. G., Wool, E. A., Monroe, C. A., & Tepper, R. I. (1995). Identification and expression cloning of a leptin receptor, OB-R. *Cell, 83*(7), 1263-1271.

Tritos, N. A., Manning, W. J., & Danias, P. G. (2004). Role of Leptin in the Development of Cardiac Hypertrophy in Experimental Animals and Humans. *Circulation, 109*(7), e67-e67.

Turner, B., Williams, S., Taichman, D., & Vijan, S. (2010). Type 2 Diabetes. *Annals of Internal Medicine, 152*(5), ITC3-1.

Unger, R. H., Clark, G. O., Scherer, P. E., & Orci, L. (2010). Lipid homeostasis, lipotoxicity and the metabolic syndrome. *Biochim Biophys Acta, 1801*(3), 209-214.

Uotani, S., Bjorbaek, C., Tornoe, J., & Flier, J. S. (1999). Functional properties of leptin receptor isoforms: internalization and degradation of leptin and ligand-induced receptor downregulation. *Diabetes, 48*(2), 279-286.

Vallerie, S. N., & Bornfeldt, K. E. (2015). Metabolic Flexibility and Dysfunction in Cardiovascular Cells. *Arterioscler Thromb Vasc Biol, 35*(9), e37-42.

van de Weijer, T., Schrauwen-Hinderling, V. B., & Schrauwen, P. (2011). Lipotoxicity in type 2 diabetic cardiomyopathy. *Cardiovasc Res, 92*(1), 10-18.

Van den Bergh, A., Flameng, W., & Herijgers, P. (2006). Type II diabetic mice exhibit contractile dysfunction but maintain cardiac output by favourable loading conditions. *Eur J Heart Fail, 8*(8), 777-783.

van der Vusse, G. J., Glatz, J. F., Stam, H. C., & Reneman, R. S. (1992). Fatty acid homeostasis in the normoxic and ischemic heart. *Physiol Rev, 72*(4), 881-940.

van der Vusse, G. J., van Bilsen, M., & Glatz, J. F. (2000). Cardiac fatty acid uptake and transport in health and disease. *Cardiovasc Res, 45*(2), 279-293.

Velic, A., Laturnus, D., Chhoun, J., Zheng, S., Epstein, P., & Carlson, E. (2013). Diabetic basement membrane thickening does not occur in myocardial capillaries of transgenic mice when metallothionein is overexpressed in cardiac myocyt. *The Anatomical Record, 296*(3), 480-487.

Vincent, H. K., Powers, S. K., Dirks, A. J., & Scarpace, P. J. (2001). Mechanism for obesity-induced increase in myocardial lipid peroxidation. *International Journal of Obesity, 25*(3), 378-388.

Voulgari, C., Papadogiannis, D., & Tentolouris, N. (2010). Diabetic cardiomyopathy: from the pathophysiology of the cardiac myocytes to current diagnosis and management strategies. *Vasc Health Risk Manag, 6*, 883-903.

Wang, B., Charukeshi Chandrasekera, P., & J Pippin, J. (2014). Leptin-and leptin receptor-deficient rodent models: relevance for human type 2 diabetes. *Current diabetes reviews, 10*(2), 131-145.

Wang, G., Yang, L., Grishin, D., Rios, X., Ye, L. Y., Hu, Y., Li, K., Zhang, D., Church, G. M., & Pu, W. T. (2017). Efficient, footprint-free human iPSC genome editing by consolidation of Cas9/CRISPR and piggyBac technologies. *Nat Protoc, 12*(1), 88-103.

Wang, P., Lloyd, S. G., Zeng, H., Bonen, A., & Chatham, J. C. (2005). Impact of altered substrate utilization on cardiac function in isolated hearts from Zucker diabetic fatty rats. *Am J Physiol Heart Circ Physiol, 288*(5), H2102-2110.

Warren, L., Manos, P. D., Ahfeldt, T., Loh, Y. H., Li, H., Lau, F., Ebina, W., Mandal, P. K., Smith, Z. D., Meissner, A., Daley, G. Q., Brack, A. S., Collins, J. J., Cowan, C., Schlaeger, T. M., & Rossi, D. J. (2010). Highly efficient reprogramming to pluripotency and directed differentiation of human cells with synthetic modified mRNA. *Cell Stem Cell, 7*(5), 618-630.

Waterson, M. J., & Horvath, T. L. (2015). Neuronal Regulation of Energy Homeostasis: Beyond the Hypothalamus and Feeding. *Cell Metabolism, 22*(6), 962-970.

Watson, R. T., & Pessin, J. E. (2006). Bridging the GAP between insulin signaling and GLUT4 translocation. *Trends in Biochemical Sciences, 31*(4), 215-222.

Way, K. J., Isshiki, K., Suzuma, K., Yokota, T., Zvagelsky, D., Schoen, F. J., Sandusky, G. E., Pechous, P. A., Vlahos, C. J., Wakasaki, H., & King, G. L. (2002). Expression of connective tissue growth factor is increased in injured myocardium associated with protein kinase C beta2 activation and diabetes. *Diabetes, 51*(9), 2709-2718.

Westermann, D., Rutschow, S., Jager, S., Linderer, A., Anker, S., Riad, A., Unger, T., Schultheiss, H. P., Pauschinger, M., & Tschope, C. (2007). Contributions of Inflammation and Cardiac Matrix Metalloproteinase Activity to Cardiac Failure in Diabetic Cardiomyopathy: The Role of Angiotensin Type 1 Receptor Antagonism. *Diabetes, 56*(3), 641-646.

Wheeler, T. J., Fell, R. D., & Hauck, M. A. (1994). Translocation of two glucose transporters in heart: effects of rotenone, uncouplers, workload, palmitate, insulin and anoxia. *Biochimica et Biophysica Acta (BBA) - Biomembranes, 1196*(2), 191-200.

WHO. (2021). World Health Organization, Obesity and overweight. [Updated: 09.06.2021, Retrieved: 25.04.2023] URL: https://www.who.int/news-room/fact-sheets/detail/obesity-and-overweight

Wold, L. E., Relling, D. P., Duan, J., Norby, F. L., & Ren, J. (2002). Abrogated leptin-induced cardiac contractile response in ventricular myocytes under spontaneous hypertension: role of Jak/STAT pathway. *Hypertension, 39*(1), 69-74.

Wondmkun, Y. T. (2020). Obesity, Insulin Resistance, and Type 2 Diabetes: Associations and Therapeutic Implications. *Diabetes Metab Syndr Obes, 13*, 3611-3616.

Woodard, L. E., & Wilson, M. H. (2015). piggyBac-ing models and new therapeutic strategies. *Trends in Biotechnology, 33*(9), 525-533.

Xu, F. P., Chen, M. S., Wang, Y. Z., Yi, Q., Lin, S. B., Chen, A. F., & Luo, J. D. (2004). Leptin induces hypertrophy via endothelin-1-reactive oxygen species pathway in cultured neonatal rat cardiomyocytes. *Circulation, 110*(10), 1269-1275.

Yang, W., Mills, J. A., Sullivan, S., Liu, Y., French, D. L., & Gadue, P. (2008). iPSC Reprogramming from Human Peripheral Blood Using Sendai Virus Mediated Gene Transfer. In *StemBook*. Cambridge (MA).

Yang, X., Rodriguez, M. L., Leonard, A., Sun, L., Fischer, K. A., Wang, Y., Ritterhoff, J., Zhao, L., Kolwicz, S. C., Jr., Pabon, L., Reinecke, H., Sniadecki, N. J., Tian, R., Ruohola-Baker, H., Xu, H., & Murry, C. E. (2019). Fatty Acids Enhance the

Maturation of Cardiomyocytes Derived from Human Pluripotent Stem Cells. *Stem Cell Reports, 13*(4), 657-668.

Young, M. E., McNulty, P., & Taegtmeyer, H. (2002). Adaptation and maladaptation of the heart in diabetes: Part II: potential mechanisms. *Circulation, 105*(15), 1861-1870.

Yu, J., Hu, K., Smuga-Otto, K., Tian, S., Stewart, R., Slukvin, II, & Thomson, J. A. (2009). Human induced pluripotent stem cells free of vector and transgene sequences. *Science, 324*(5928), 797-801.

Yu, J., Vodyanik, M. A., Smuga-Otto, K., Antosiewicz-Bourget, J., Frane, J. L., Tian, S., Nie, J., Jonsdottir, G. A., Ruotti, V., Stewart, R., Slukvin, II, & Thomson, J. A. (2007). Induced pluripotent stem cell lines derived from human somatic cells. *Science, 318*(5858), 1917-1920.

Yusa, K., Zhou, L., Li, M. A., Bradley, A., & Craig, N. L. (2011). A hyperactive piggyBac transposase for mammalian applications. *Proceedings of the National Academy of Sciences, 108*(4), 1531-1536.

Zabeau, L., Defeau, D., Iserentant, H., Vandekerckhove, J., Peelman, F., & Tavernier, J. (2005). Leptin receptor activation depends on critical cysteine residues in its fibronectin type III subdomains. *J Biol Chem, 280*(24), 22632-22640.

Zeidan, A., Hunter, J. C., Javadov, S., & Karmazyn, M. (2011). mTOR mediates RhoA-dependent leptin-induced cardiomyocyte hypertrophy. *Mol Cell Biochem, 352*(1-2), 99-108.

Zhan, C., Zhou, J., Feng, Q., Zhang, J. E., Lin, S., Bao, J., Wu, P., & Luo, M. (2013). Acute and long-term suppression of feeding behavior by POMC neurons in the brainstem and hypothalamus, respectively. *The Journal of Neuroscience, 33*(8), 3624-3632.

Zhang, Y., Proenca, R., Maffei, M., Barone, M., Leopold, L., & Friedman, J. M. (1994). Positional cloning of the mouse obese gene and its human homologue. *Nature, 372*(6505), 425-432.

Zhao, S., Zhu, Y., Schultz, R. D., Li, N., He, Z., Zhang, Z., Caron, A., Zhu, Q., Sun, K., Xiong, W., Deng, H., Sun, J., Deng, Y., Kim, M., Lee, C. E., Gordillo, R., Liu, T., Odle, A. K., Childs, G. V., Zhang, N., Kusminski, C. M., Elmquist, J. K., Williams, K. W., An, Z., & Scherer, P. E. (2019). Partial Leptin Reduction as an Insulin Sensitization and Weight Loss Strategy. *Cell Metab, 30*(4), 706-719 e706.

Zhou, H., Wu, S., Joo, J. Y., Zhu, S., Han, D. W., Lin, T., Trauger, S., Bien, G., Yao, S., Zhu, Y., Siuzdak, G., Scholer, H. R., Duan, L., & Ding, S. (2009). Generation of induced pluripotent stem cells using recombinant proteins. *Cell Stem Cell, 4*(5), 381-384.

Zhou, W., & Freed, C. R. (2009). Adenoviral gene delivery can reprogram human fibroblasts to induced pluripotent stem cells. *Stem Cells, 27*(11), 2667-2674.

Zhou, Y. T., Grayburn, P., Karim, A., Shimabukuro, M., Higa, M., Baetens, D., Orci, L., & Unger, R. H. (2000). Lipotoxic heart disease in obese rats: implications for human obesity. *Proc Natl Acad Sci U S A, 97*(4), 1784-1789.

Zimmet, P., Alberti, K. G., & Shaw, J. (2001). Global and societal implications of the diabetes epidemic. *Nature, 414*(6865), 782-787.

Zorzano, A., Sevilla, L., Camps, M., Becker, C., Meyer, J., Kammermeier, H., Munoz, P., Guma, A., Testar, X., Palacin, M., Blasi, J., & Fischer, Y. (1997). Regulation of glucose transport, and glucose transporters expression and trafficking in the heart: studies in cardiac myocytes. *The American Journal of Cardiology, 80*(3, Supplement 1), 65A-76A.

9 Acknowledgements

I would like to deeply thank all the people that express their support during my PhD journey. In particular, I would like to deeply thank my primary supervisor Prof. Dr. Kaomei Guan for her guide and supervision during these years. I am really grateful for all the suggestions, feedbacks, warm encouragements and advises especially during the difficult times.
My great appreciation goes also to my secondary supervisor from King's College Dr. Cynthia Andoniadou for her presence and very keen supervision despite the distance, the suggestions, and the very warm support. I also would like to thank Prof. Ali El-Armouche for the very interesting discussion during the Internal seminar. A particular thanks to my TAC committee members Prof. Barbara Ludwig and Prof. Ünal Coskun for the brainstorming and nice feedbacks during the TAC meeting, which were always helpful to get more insight about the project. I would like to thank Dr. Tiago Alves, for the nice collaboration, the great encouragement and for always having a door open for me. I am grateful that I had the opportunity to join the DIGS-BB and IRTG program for all the experiences, lectures, workshops, collaborations that made me grow as a scientist. Thank you to all the members from the Pharmacology and Toxicology Institute, a very big thank to Mareike for her presence, suggestions, great help and to be always there when I needed, to Ying for her huge help with the cell culture, for her kindness and true friendship, to Xiaojing to share with me so much knowledge about the cell culture and for the nice talks in the office, to Mario for the nice talks and for the discussions about the projects, to Susanne, Wener, Fatima, Konstanze, Jessie, Romy for their great kindness and availability during these years. Thank you to all the PhD students and friends with who I have shared my best and worst moments, this journey wouldn't have been the same without all of you. A special thanks is for my wonderful soul Julia with whom I have the best memories of these years. Thank you to my Italian Giulia, I am super glad you came to Dresden and of our beautiful friendship. Thanks to Filippo for all the nice coffee breaks in the good and bad moments. Thanks to Lorenzo for all the talks, you make me feel always at home. My gratitude goes to my family and especially to my parents that have always supported me in every decision, encouraged and believed in me with their immense love no matter how far we live apart. Last but not least, I would like to thank my beloved Federico for his daily support and encouragement, for making this journey lighter and colourful.

10 Declaration

Statements for the opening of doctorate proceedings

1. I herewith declare that I have produced this paper without the prohibited assistance of third parties and without making use of aids other than those specified; notions taken over directly or indirectly from other sources have been identified as such.
2. I received assistance from the following persons in conjunction with the selection and evaluation of materials and creation of the manuscript:

- Prof. Dr. rer. nat. Kaomei Guan

3. No further persons were involved in the intellectual creation of the presented work. I have in particular not taken recourse to the assistance of a commercial doctorate advisor. No third parties have received remuneration or payment in kind from me, neither directly nor indirectly, for work in connection with the contents of the presented thesis.
4. This paper has not previously been presented in identical or similar form to any other German or foreign examination board.
5. Contents of this thesis have been published in the following form:
    - Poetsch M. S.*, Strano A.*, & Guan K. (2020). Role of Leptin in Cardiovascular Diseases. *Front Endocrinol (Lausanne), 11*, 354. (*equal contribution)
    - Poetsch, M. S., Strano, A., & Guan, K. (2022). Human Induced Pluripotent Stem Cells: From Cell Origin, Genomic Stability, and Epigenetic Memory to Translational Medicine. *Stem Cells*, *40*(6), 546-555.
6. I confirm that I have not previously failed to complete doctorate proceedings successfully.
7. I confirm that I accept the Doctorate Regulations of the Faculty of Medicine Carl Gustav Carus of the Dresden University of Technology.
8. I have observed and complied with the Referencing Guide for Doctorate Theses of the Faculty of Medicine of the Dresden University of Technology.
9. I acknowledge the “Guidelines on the safeguarding of good scientific practice, the prevention of scientific misconduct and the handling of violations” of the Dresden University of Technology.

Dresden, (Anna Strano)

Statements on the observance of legal stipulations

I herewith confirm that the following currently applicable legal requirements have been observed in connection with my thesis:

☐ Favourable opinion of the Ethics Commission in case of clinical studies, epidemiological studies with personal references or contexts covered by the law on medical devices

- Votum der Ethikkommission an der TU Dresden: **EK 422092019** mit der Studie „Reprogrammierung somatischer Zellen in induzierte pluripotente Stammzellen für die Untersuchung von mono- und polygenetische bedingten Herz- und die damit verbundenen Erkrankungen“ (Antragsteller: Institut für Pharmakologie und Toxikologie, Prof. Dr. Kaomei Guan).

Case ref. no of the responsible Ethics Commission:

☐ Observance of the stipulations of animal welfare legislation

Case ref. no. of the approving authority for the project/participation: **does not apply**

☐ Observance of the stipulations of genetic engineering legislation/project number: **Az. 54-8452/46** (Az. 55-8811.72/46 bis11/2016)

☐ Observance of the data privacy rules of the Faculty of Medicine and University Clinic Carl Gustav Carus.

Dresden, (Anna Strano)